ISSN 1408-7073

RMZ

MATERIALS AND GEOENVIRONMENT

MATERIALI IN GEOOKOLJE

Volume 52 Letnik

Ljubljana, December 2005

No. 4 Št.

RMZ - Materials and Geoenvironment
RMZ - Materiali in geookolje

Old title: Rudarsko-metalurški zbornik (Mining and Metallurgy Quarterly),
ISSN 0035-9645, 1952-1997.

Is issued quarterly by the *Faculty of Natural Science and Engineering, Ljubljana,* the *Institute for Mining, Geotechnology and Environment Ljubljana* and *Premogovnik Velenje, Velenje.*
Izdaja *Naravoslovnotehniška fakulteta Univerze v Ljubljani* in *Inštitut za rudarstvo, geotehnologijo in okolje Ljubljana,* štirikrat letno.
Financially supported also by Ministry of Education, Science and Sport of Republic of Slovenia.
Pri financiranju revije sodeluje *Ministrstvo za šolstvo, znanost in šport Republike Slovenije.*

Editorial Office (Uredništvo):
Barbara Bohar Bobnar
Iztok Anželj
Nives Vukič
Digital Layout (Priprava za tisk):
Tomaž Sterniša s.p., Ljubljana
Print (Tisk): R-TISK d.o.o, Ljubljana

RMZ - Materials and Geoenvironment
Aškerčeva cesta 12, p.p. 312
1001 Ljubljana, R. Slovenija
Telefon: +386 (0)1 470 45 00
Telefaks: +386 (0)1 470 45 60

Indexation bases of RMZ-M&G: CA SEARCH-Chemical Abstracts, METADEX, GeoRef, Energy Science and Technology, PASCAL. Main of 23 bases registrated
Baze v katerih je RMZ-M&G indeksiran: CA SEARCH-Chemical Abstracts, METADEX, GeoRef, Energy Science and Technology, PASCAL. Najpomembnejši med 23 registriranimi

Naklada 700 izvodov. Printed in 700 copies.
Letna naroč za posameznike: 4.000,00 SIT, za inštitucije: 8.000,00 SIT
Yearly subscribtion 20 EUR, institutions 40 EUR

Tekoči račun pri Novi Ljubljanski banki, d.d. Ljubljana:
UJP 01100-6030708186
Davčna številka: 24405388

ISSN 1408-7073

RMZ - MATERIALS AND GEOENVIRONMENT

PERIODICAL FOR MINING, METALLURGY AND GEOLOGY

RMZ - MATERIALI IN GEOOKOLJE

REVIJA ZA RUDARSTVO, METALURGIJO IN GEOLOGIJO

RMZ-M&G, Vol. 52, No. 4 pp. 661-825 (2005)

Ljubljana, December 2005

Historical Review

More than 80 years have passed since in 1919 the University Ljubljana in Slovenia was founded. Technical fields were joint in the School of Engineering that included the Geologic and Mining Division while the Metallurgy Division was established in 1939 only. Today the Departments of Geology, Mining and Geotechnology, Materials and Metallurgy are part of the Faculty of Natural Sciences and Engineering, University of Ljubljana.

Before War II the members of the Mining Section together with the Association of Yugoslav Mining and Metallurgy Engineers began to publish the summaries of their research and studies in their technical periodical Rudarski zbornik (Mining Proceedings). Three volumes of Rudarski zbornik (1937, 1938 and 1939) were published. The War interrupted the publication and not untill 1952 the first number of the new journal Rudarsko-metalurški zbornik - RMZ (Mining and Metallurgy Quarterly) has been published by the Division of Mining and Metallurgy, University of Ljubljana. Later the journal has been regularly published quarterly by the Departments of Geology, Mining and Geotechnology, Materials and Metallurgy, and the Institute for Mining, Geotechnology and Environment.

On the meeting of the Advisory and the Editorial Board on May 22nd 1998 Rudarsko-metalurški zbornik has been renamed into "RMZ - Materials and Geoenvironment (RMZ - Materiali in Geookolje)" or shortly RMZ - M&G.

RMZ - M&G is managed by an international advisory and editorial board and is exchanged with other world-known periodicals. All the papers are reviewed by the corresponding professionals and experts.

RMZ - M&G is the only scientific and professional periodical in Slovenia, which is published in the same form nearly 50 years. It incorporates the scientific and professional topics in geology, mining, and geotechnology, in materials and in metallurgy.

The wide range of topics inside the geosciences are wellcome to be published in the RMZ - Materials and Geoenvironment. Research results in geology, hydrogeology, mining, geotechnology, materials, metallurgy, natural and antropogenic pollution of environment, biogeochemistry are proposed fields of work which the journal will handle. RMZ - M&G is co-issued and co-financed by the Faculty of Natural Sciences and Engineering Ljubljana, and the Institute for Mining, Geotechnology and Environment Ljubljana. In addition it is financially suported also by the Ministry of Education Science and Sport of Slovenian Government.

Editor in chief

Table of Contents - Kazalo

Simulation of microbiological pollution in the unsaturated zone of karstified limestone aquifers – tracing with bacteriophages

Mihael Bricelj[1], Barbara Čenčur Curk[2]

[1]NIB – National Institute of Biology, Slovenia; mihael.bricelj@nib.si
[2]IRGO - Institute for Mining, Geotechnology and Environment, Slovenia;
E-mail: barbara.cencur@irgo.si

Received: June 30, 2005 **Accepted**: November 24, 2005

Abstract: The purpose of the research was to study the infiltration and migration of health-hazardous human viruses, such as enteroviruses, in the unsaturated zone of fractured and karstified rock, since these rocks present important aquifers in Slovenia. As a possible model for behavior of health-hazardous viruses, we used the salmonella bacteriophage P22H5. After injection, bacteriophages remain in the fractures (channels) and microfracture systems of the unsaturated zone and are rinsed by subsequent larger precipitation events even up to several months after the injection. The field experiments have shown different flow patterns depending on the fractured rock structure. In the research area some fast conduits (large fractures or faults) exist where water runs faster than in the total conductive part of the rock. On the other hand the tracer delay in microfracture system areas was observed.

Key words: pollutant transport, fractured and karstified rocks, bacteriophage, experimental field site, Sinji Vrh (Slovenia)

Introduction

The purpose of the research was to study the infiltration and migration of health-hazardous human viruses, such as enteroviruses, in the unsaturated zone of fractured and karstified rock, since these rocks present important aquifers in Slovenia. As a possible model for the behavior of health-hazardous viruses, salmonella bacteriophage P22H5 was used. Phages have served as useful models for the behavior of human enteric viruses in water treatment processes, groundwater viral transport, inactivation and attachment studies on various subsurfaces, because of their similarity to enteric viruses in structure, size, and resistance to inactivation (Hedberg & Osterholm, 1993; Harvey & Ryan, 2004). Better knowledge of the pollutant transport and persistence of tracer in environment enables us to determine vulnerability and define protected areas for drinking water resources.

The bacteriophage P22H5 is a virulent mutant that propagates in mouse typhoid fever bacteria *Salmonella typhimurium* and rarely occurs in waters (Seeley, 1982). From previous tracing experiments (Bricelj, 1986) it is well known that coliphages are a common constituent of faecally polluted waters and for this reason are not a suitable

Scientific paper

tracer, especially in the case of very high dilutions of the tracer, when a high or low background of coliphages may interfere with the tracer curve. The phage tracer P22H5 was injected at ten locations in 14 tracer experiments in running water and into the unsaturated zone in a karstic area where no background of phages for its host bacteria were present (BRICELJ, 2003).

The tracer experiment was carried out in the subsurface zone, since microbial activity is assumed to be most active in the upper parts of the unsaturated zone.

EXPERIMENTAL FIELD SITE SINJI VRH

A tracer experiment with bacteriophages was performed on the experimental field site Sinji Vrh (ČENČUR CURK, 1997), Slovenia. It is located in the unsaturated zone of fractured and karstified Jurassic limestone at the edge of the Trnovski Gozd plateau (mean altitude 900 m a.s.l.), which is an overthrust of carbonate rock over Eocene flysch (Fig. 1). The subvertical Avče fault with a Dinaric direction NW-SE and several parallel faults cross this territory. These faults are interwoven with numerous connecting faults extending in the general direction N-S.

Their intensity varies from open wide fractured zones to crushed and broken zones (JANEŽ, 1997). The groundwater horizon lies extremely deep and appears on the surface at the lowest point of the impermeable flysh border (Fig. 1) at altitudes between 219 and 235 m as the karstic Hubelj spring. Its catchment area is estimated to about 50 km^2 with an average annual precipitation of 2450 mm (TRČEK, 2003).

The experimental field site Sinji Vrh presents a 340 m long artificial research tunnel, 5 to 25 m below the surface (Fig. 1). An agro-meteorological station has been installed on the surface near the tunnel entrance, where precipitation, evaporation, air temperature, air moisture, solar radiation, wind speed and direction (both at two levels) are continuously measured. A tracer experiment area (Fig. 1) was chosen close to the tunnel entrance on the north-western part. The main dip direction of fractures is NNE-SSW with subvertical dip because of the location of the area within a crushed zone of Avče fault. In the broken zone the tunnel is supported by concrete (Fig. 1). The Jurassic limestone of the tracer experiment area is composed of 99 % calcite and has a south-westerly dip direction and a gentle dip (of 5° to 30°). The unsaturated fractured and karstified limestone has a negligible matrix porosity and very high fracture density with some greater conduits (VESELIČ & ČENČUR CURK, 2001).

The injection hole was drilled through the soil cover in order to avoid tracer retardation because of sorption. A special construction for collecting water penetrating through the rock was developed. The water seeping from the ceiling of the research tunnel is gathered in 1.5 m long segments (MP1 - MP10; Fig. 1) with a gathering surface of 2.2 m^2.

MATERIAL AND METHODS

Bacteriophage P22H5 and salmonella mouse typhoid fever bacteria NIB22 (LT2 w.t. strain) were obtained from Dr. Miklavž Grabnar, Department of Molecular Biology, Biotechnical Faculty, University of Ljubljana.

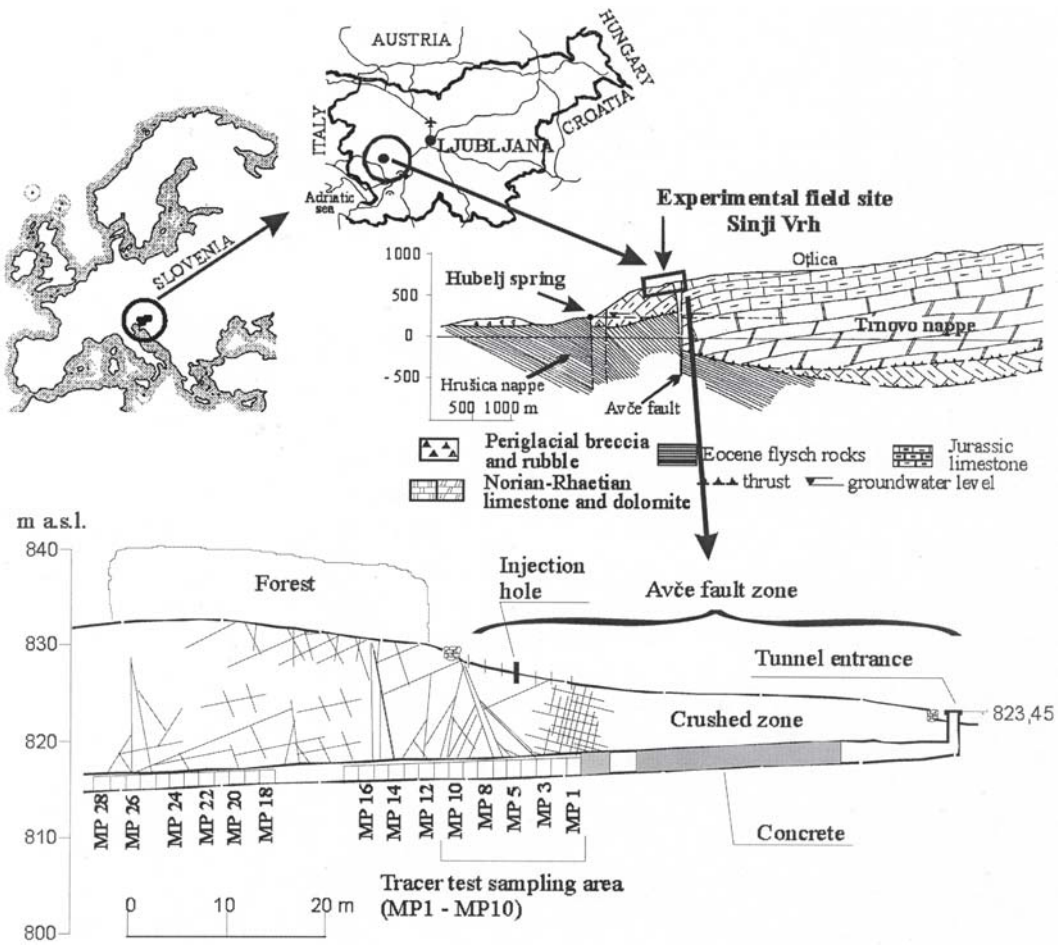

Figure 1. Location of the experimental field site Sinji Vrh (EFS Sinji Vrh) with geological cross section of Trnovo plateau (Janež, 1997; Veselič et al., 2001). Below: Longitudinal section of the EFS Sinji Vrh with tracer tests area and tracer test sampling points in the research tunnel: MP1 – MP10 (after Veselič and Čenčur Curk, 2001).

The propagation of phages to obtain crude bacteriophage lysates was done by the method described in dissertation thesis of Bricelj (1994). The nutrient media Brain Heart Infusion Broth and Nutrient Agar were from Biolife, Milano. Water samples and phage suspensions were tested for viable phages (plaque forming units - pfu) according to the agar layer method of Adams (1966), using host bacteria as the indicator strains.

On 29th September 2003 10.4 liters of tracing solution, composed of 11 tracers (salts, fluorescent dyes, deuterium, micro spheres and bacteriophage), was poured in 10 minutes into the new drilled borehole to the depth of 0.9 m. There were 1.2E+15 plaque forming units (pfu) of bacteriophage P22H5 as a part of tracer cocktail. It should be pointed out, that the phage concentration in injected tracing solution was calculated to

predicted concentration at measuring points from the microfracture system, since there is slower flow with higher dispersion of the tracer. Because of that an overdose is reached in fast pathways such as MP4 and MP5 (see structure on Figure 1 below).

RESULTS

The phage tracer appeared first at sampling point five (MP5) after 4.1 days with the peak value of 3.1 E+09 pfu/ml (Fig. 2, Table 1 and Table 2). One day later a positive result was obtained at MP4, the phage appeared with the peak value of 1.1 E+08 pfu/ml.

The tracer appeared at all sampling points within 22 days. Peak values occurred at the time of appearance at MP2 and MP8. At MP3 the tracer appeared after 8 days, but the peak value was not reached until 50 days. At the furthest sampling points from the injection hole (MP1, MP2 and MP9, MP10) the peak values were within the lowest pfu values (Fig. 2).

The first sampling campaign was completed in September 2004, after about one year (Fig. 2): at MP4 after 324 days and at MP5 after 347 days. At that time, there were still 4.2E+02 pfu/ml in MP4 and 9.8E+02 pfu/ml in MP5 in ml of water sample. Unfortunately the samples were not taken in October and November 2004, since at that time were some significant precipitation events. In winter there were no samples due to freezing of the ground and snow cover. The first water, seeping through the system, was obtained after snow melting at the end of March 2005. After 591 days (May 2005) of collecting the samples there

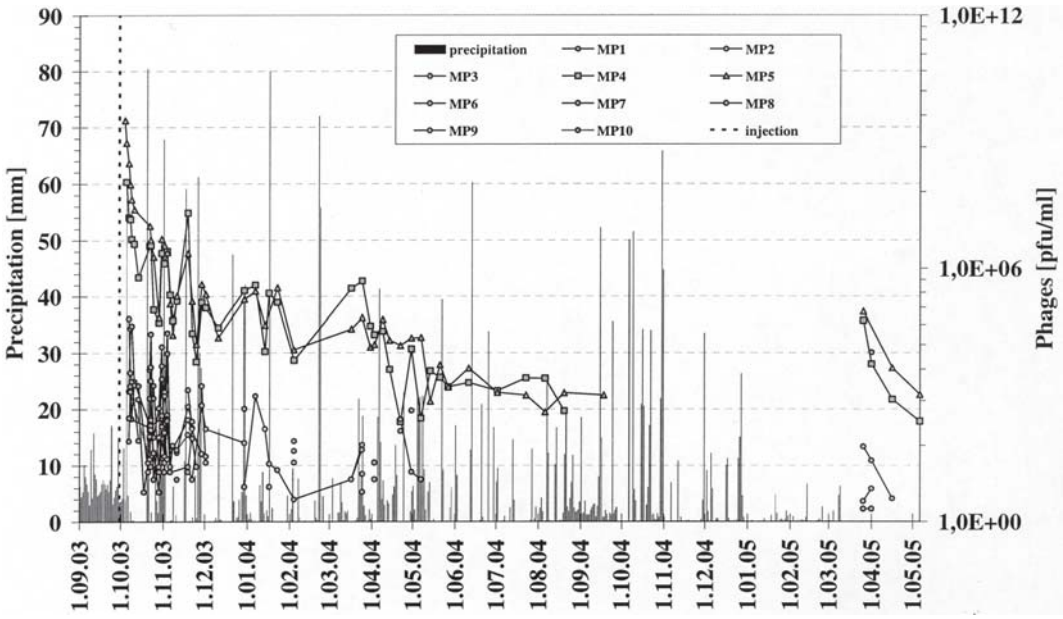

Figure 2. The presence of bacteriophage P22H5 at sampling points MP1- MP10. The concentrations in MP1 – M3 and MP6 – MP10 are grouped below and marked alike. They are depicted only for comparison with MP4 and MP5.

were positive results at MP4, MP5 and MP6 with the following concentrations: 9.5E+01, 6.2E+02 and 2.0E+00 pfu/ml, respectively (Fig. 2). The sampling of water is still going on, but with lower frequency. The recovery value was calculated only for MP4 and MP5 and was 0.95 % of the injected quantity at both sampling points (0.04 % for MP4 and 0.91 % for MP5).

The results of appearance of the phage tracer, the appearance of peak values and time of the last sample containing phage tracer at different sampling points are summarized in Table 1. Table 2 presents time sequence of the phage tracer appearance at sampling points.

Discussion

After the injection of bacteriophages, they remain in the fractures (channels) and microfracture systems of the unsaturated zone and are rinsed by subsequent larger precipitation events even up to year and a half after the injection. Some authors refer that the edges in subsurface structures could be one of the principal causes of charge heterogeneity. Such conditions could permit that negatively charged bacteriophages attach to otherwise repulsive surfaces, especially if the edges of crystals are oppositely charged (Bickmore et al., 2002; Flynn et al., 2004).

The results from Sinji Vrh have shown that the unsaturated zone in the fractured and karstified rocks plays an important role in pollution retardation and storage. The rinsing of pollutants to deeper parts of the karst aquifer depends on the saturation rate of the soil and the unsaturated zone (precipitation events). The field experiments have shown different flow patterns depending on the fractured rock

Table 1. Appearance and presence of the phage tracer at MP1 to MP10. The time is in days and quantity of phages in plaque forming units (pfu) in ml of sample.

sampling point	appearance of tracer	peak value	appearance of peak value	Last sample containing phages (last positive result)
	days	pfu/ml	days	days
MP1	7	2.1E+03	11	63
MP 2	7	2.9E+02	7	63
MP 3	22	5.7E+02	50	550
MP 4	5	1.1E+08	5	591
MP 5	4	3.1E+09	4	591
MP 6	8	4.3E+04	11	591
MP 7	13	1.4E+04	31	550
MP 8	7	6.5E+04	7	550
MP 9	22	1.7E+03	25	214
MP 10	8	4.9E+03	40	177

Table 2. Time sequence of the phage tracer appearance at measuring points.

days	measuring point
4	MP 5
5	MP 4
7	MP 2
7	MP 8
11	MP1
11	MP 6
25	MP 9
31	MP 7
40	MP 10
50	MP 3

structure. In the research area some fast conduits (large fractures or faults) exist where water runs faster than in the total conductive part of the rock, as in the case of MP4 and MP5. Tracer delay in microfracture system areas was also observed, especially at MP3, MP7, MP9 and MP10 (see Fig. 1 and 2). At these points the appearance of the peak value was delayed for 50, 31, 25 and 40 days respectively. A very low recovery rate is due to the dispersion of the tracer in directions where it could not be sampled and the decay of tracer, dependent upon removal mechanisms such as filtration, sedimentation and irreversible adsorption (SINTON ET AL., 1997).

Recent research with bacteriophages MS2 (ZHUANG ET AL., 2003), PRD1 (BLANFORD ET AL., 2005) and T7 (FLYNN ET AL., 2004) is much more concerned with breakthrough percentage, recovery calculations of peak values of tracer curve, kinetics of virus surface inactivation and analytical models than with the longevity of phages in environment. Some notions on persistence of phages in the environment are referred by DEBORDE ET AL., 2003, for the phages MS2 and PRD1 in floodplain aquifer. The breakthrough curves of phages contained

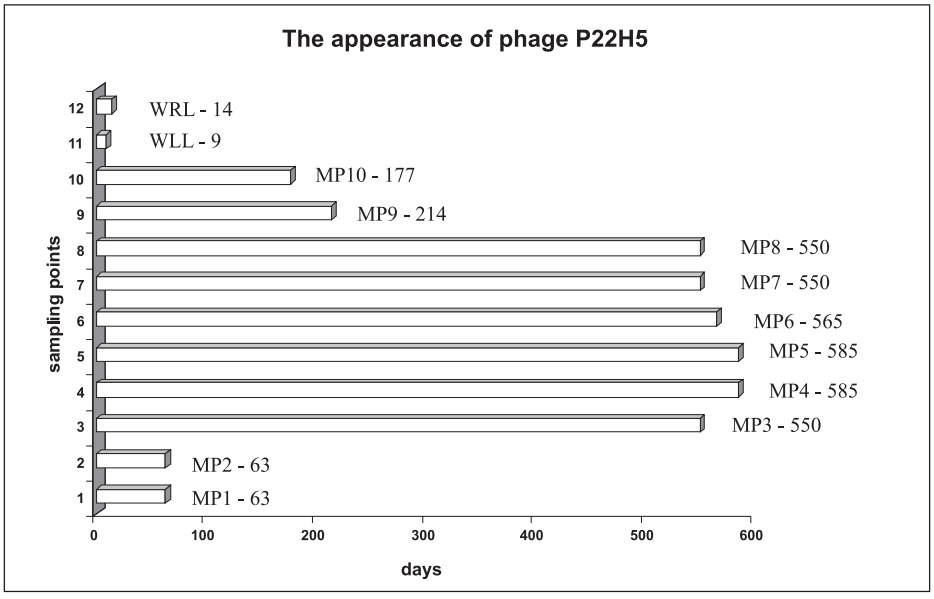

Figure 3. The presence of bacteriophage P22H5 at the sampling points MP1 – MP10 in Sinji Vrh. The sampling points WRL and WLD, represent the percolation of phage tracer through right (WRL) and left (WLL) soil lysimeter at Wagna experimental field near Graz.

long tails, so the slow releases of phages have been observed over a period of more than six months. There is need for further research of mechanisms of phage persistence in the environment and health-related significance of the mechanisms of such processes.

The results were compared (Fig. 2) with the results from tracer tests in soil and gravel at the Wagna lysimeter station (Austria). The phage tracer was very quickly eliminated from the water trickling through 1 m soil and 0.5 m gravel and positive results were concluded after nine or fourteen days respectively, in the left and right lysimeter (WLL and WRL). The results in the lysimeter are consistent with the findings of Van Elsas et al., 1991 and Powelson et al., 1991 and Van Cuyk et al., 2001.

References

Adams, M.H. (1959): Bacteriophages, Methods of Study of Bacterial Viruses., 443-522. *Interscience Publishers*, New York.

Bickmore, B.R., Nagy, K.L., Sandlin, P.E., Carter T.S. (2002): Quantifying surface areas of clays by atomic force microscopy. *Am. Mineral*. Vol. 87, No. 5-6, pp. 780-783.

Blanford, W.J., Brusseau, M.L., Yeh, T.C.J., Gerba, C.P., Harvey, R. (2005): Influence of water chemistry and travel distance on bacteriophage PRD-1 transport in a sandy aquifer. *Water Research*; Vol. 39, No. 11, pp. 2345-2357.

Bricelj, M., Kosi, G., Vrhovšek, D. (1986): Tracing with Salmonella-phage P22H5. *Steir. Beitr. Z. Hydrologie* Vol. 37/38, pp. 296-271.

Bricelj, M. (1994): Underground Water Tracing with the Phages of Salmonella typhimurium. *Dissertation Thesis*, University of Ljubljana, Biotechnical faculty, Department of Biology, 113 p.

Bricelj, M. (2003): Microbial Tracers in Groundwater Research. *RMZ – Materials and Geoenvironment* Vol. 50, No. 1, pp. 67-70.

Deborde, D.C., Woessner, W.W., Kiley, Q.T., Ball, P. (1999): Rapid transport of viruses in a floodplain aquifer. *Water research* Vol. 33, No. 10, pp. 2229-2238.

Čenčur Curk, B. (1997): Experimental field sites as a basis for the study of solute transport in the vadose zone of karstified rock. *Acta hydrotechnica* Vol. 15/20, 1-111.

Bricelj. M, Čenčur Curk. B. (2005): Bacteriophage transport in the unsaturated zone of karstified limestone aquifers. Proceedings of the conference "Karst 2005", in press

Flynn, R., Cornaton, F., Hunkeler, D., Rossi, P. (2004): Bacteriophage transport through a finning-upwards sedimentary sequence; laboratory experiments and stimulation. *Journal of Contaminant Hydrology* Vol. 74, pp. 231-252.

Harvey, R.W., Ryan, J.N. (2004): Use of PRD1 bacteriophage in groundwater viral transport, inactivation, and attachment studies. *FEMS Microbiology Ecology* Vol. 42, pp. 3-16.

Hedberg, C.W., Osterholm. M.T. (1993): Outbreaks of Foodborne and Waterborne Viral Gastroenteritis. *Clinical Microbiology Reviews* Vol. 6, 199-210.

Janež, J. (1997): Geological structure and hydrogeological position of the Hubelj spring. In: Karst hydrogeological investigations in south-western Slovenia. *Acta carsologica* , Vol. XXVI, No. 1, 82-86.

Powelson, D.K., Simpson, J.R., Gerba, .CP. (1991): Effect of organic matter on virus transport in unsaturated flow. *Applied and Environmental Microbiology*. Vol. 57, No. 8, pp. 2192-2196.

Seeley, N.D., Primrose, S.B. (1982): The Isolation of the Bacteriophage from the Environment. *Journal of Applied Microbiology* Vol. 53, pp. 1-17.

Sinton, L.W., Finlay, R.K., Pang, L., Scott, D.M. (1997): Transport of bacteria and bacteriophages in irrigated effluent into and through and alluvial gravel aquifer. *Water, Air and Soil Pollution* Vol. 98, No. 1-2,.17-42.

Trček, B. (2003): Epikarst zone and the karst aquifer behaviour: a case study of the Hubelj catchment, Slovenia. Ljubljana. *Geološki zavod Slovenije,* 1-100.

VAN CUYK, S, SIEGRIST, R., LIGAN, A., MASSON, S., FISCHER, E., FIGUEROA, L. (2001): Hydraulic and purification behaviours and their interactions during wastewater treatment in soil infiltration system. *Water Research* Vol. 35, No. 4, pp. 953–964.

VAN-ELSAS, J.D., TREVORS, J.T., VAN-OVERBEEK, L.S. (1991): Influence of soil properties on the vertical movement of genetically-marked Pseudomonas fluorescens through large soil microcosms. *Biology and Fertility of Soils* Vol. 10, No. 4, pp. 249-255.

VESELIČ, M., ČENČUR CURK, B. (2001): Test studies of flow and solute transport in the unsaturated fractured and karstified rock on the experimental field site Sinji Vrh, Slovenia. In: *New approaches characterizing groundwater flow*, Seiler & Wohnlich (eds), Balkema, Lisse, pp. 211-214.

VESELIČ, M., ČENČUR CURK, B., TRČEK, B. (2001): Experimental field site Sinji Vrh. In: Tracers in the unsaturated zone = Markierungsstoffe in der ungesättigten Zone, Berg et al. (eds), *Beitraege zur Hydrogeologie* Vol. 52, pp. 45-60.

Comparative Analysis of Single Well Aquifer Test Methods on the Mill Tailing Site of Boršt Žirovski vrh, Slovenija

Primerjalna analiza metod obdelave hidravličnih poizkusov v črpanem vodnjaku na odlagališču hidrometalurške jalovine Boršt, Žirovski vrh, Slovenija

Jože Ratej, Mihael Brenčič

Geological Survey of Slovenia, Dimičeva 14, 1000 Ljubljana, Slovenia;
E-mail: joze.ratej@geo-zs.si, mbrencic@geo-zs.si

Received: June 02, 2005 **Accepted**: November 24, 2005

Abstract: Several aquifer tests were performed during hydrogeological investigations on mill tailings Boršt of uranium mine Žirovski vrh and large data set was generated. These results were used for comparative study of several analytical models for hydraulic test evaluation and for comparison of the results provided by them. In the present paper, methods of Jacob (Cooper & Jacob, 1967), Papadopulos et al. (1967), Theis (1935), Hvorslev (1951) and Cooper et al. (1967) are compared. In most cases the highest values are obtained by Papadopulos method. In some cases results of Hvorslev and Cooper method are up to two and a half decades lower than results of other three methods. This is mostly due to long duration of pumping. The critical values of pumping times, where results of different slug test and pumping test methods coincide, were also defined.

Izvleček: Med hidrogeološkimi raziskavami na odlagališču hidrometalurške jalovine Boršt rudnika urana Žirovski vrh je bilo izvedenih več hidravličnih poizkusov, na podlagi katerih smo dobili velik nabor podatkov. Le-te smo uporabili za primerjalno analizo več analitičnih modelov za obdelavo hidravličnih testov. Med seboj smo primerjali metode Jacoba (Cooper & Jacob, 1967), Papadopulos-a et al. (1967), Theis-a (1935), Hvorslev-a (1951) in Cooper-ja et al. (1967). V večini primerov smo najvišje rezultate dobili s Papadopulosovo metodo. V nekaterih primerih so bili rezultati Hvorsleva in Cooperja za dve in pol dekade nižji od rezultatov ostalih metod, kar je v glavnem posledica trajanja črpanja. Opredelili smo tudi t.i. "kritične čase", torej tiste čase trajanja črpanja, ob katerih se rezultati različnih metod še razmeroma skladajo.

Keywords: comparative analysis, slug test, pumping test, single well test
Ključne besede: primerjalna analiza, impulzni poizkus, črpalni poizkus, poizkus na črpanem vodnjaku

Scientific paper

INTRODUCTION

During in-situ hydrogeological tests, a large number of factors affect the final outcome and only the obvious ones can be included in analytical models in order to ensure its relative simplicity. With comparative analysis one tries to assess analytical models with respect to their behavior in certain conditions, their resilience toward unexpected factor influences, and their ability to obtain representative results. Potential sources of error are usually related to local variation in permeability, leakage through pipe fittings and between pipe and adjacent soil, undetected impervious boundary close to the test, hydraulic fracturing by excessive differences in water heads, soil remolding or clogging or uprising during the test, and time lag in the piezometric responses (CHAPUIS, 1990). In addition, errors can arise from the selection of analytical model.

During hydrogeological investigations on mill tailings Boršt of uranium mine Žirovski vrh (50 km W of Ljubljana) several pumping and slug tests were performed and large data set was generated. The characterization by hydraulic tests was made with the aim to define hydraulic permeability of the mill tailings and bedrock. These results were later used for hydrological balance calculations and groundwater numerical modeling of the mill tailings, which is positioned on large landslide.

The large data set gives us opportunity to study several analytical tests for hydraulic test evaluation and to compare the results provided by them. In the present paper, methods of Jacob (COOPER & JACOB, 1967), PAPADOPULOS ET AL. (1967), THEIS (1935), HVORSLEV (1951) and COOPER ET AL. (1967) are compared.

Previous studies on the subject of comparative analysis of aquifer test methods have mostly discussed relations between different slug test methods, since they are the cheapest and therefore the most widely used methods for field evaluation of hydraulic conductivity. HERZOG & MORSE (1994) and HERZOG (1994) compared methods of HVORSLEV (1951), COOPER (1967) and NGUYEN & PINDER (1984), and pointed out the importance of using several methods for calculating hydraulic conductivity, since no method can be applied at all times and employing of other methods is needed. MACE (1999) compared methods of HERBERT & KITCHING (1981), BARKER & HERBERT (1989), HVORSLEV (1951), BOUWER & RICE (1976) and COOPER (1967) method for slug tests in large-diameter, hand-dug wells. He suggests that due to substantial well storage considerable pumping time may be required to lower the water level to the desired position. However, this shouldn't affect the calculation result provided that recovery time is considerably longer than pumping time.

The relations between HVORLEV's (1951) and COOPER's (1967) model has been discussed by CHIRLIN (1989), who provides a rather assertive statement that for slug-tests the method of Cooper gives correct values of hydraulic conductivity, and Hvorslev's result deviate from the these real values due to neglecting aquifer storativity. In contrast, CHAPUIS ET AL. (1990), CHAPUIS (1998) and CHAPUIS & CHENAF (2002) provides several independent proofs (mathematical, physical, numerical and experimental), that the theory

of Cooper et al. (1967) does not adequately represent slug-test conditions and thus can not give values of T and S.

Karanth & Prakash (1988) studied the relations between slug tests and pump tests. They indicate that transmissivity values obtained by those two methods vary mostly within a factor of three, except for pump-test transmissivity values less than 1.16×10^{-4} m^2/s.

Methods

Construction of boreholes

On the mill tailing site Boršt and its surroundings 21 new boreholes have been installed between May and October 2003. They were organized in two groups to determine the values of hydraulic conductivity of hydrometallurgical tailing as well as the bedrock that forms the base of tailings. The depths of piezometers ranged from 5 to 25 m and from 26 to 105 m, respectively.

After the drilling, every well was rinsed with clean water and then activated with the air-lift method. Activation took place until clean water flew out of the well, which was hard to achieve because in most cases dirtiness of water was a consequence of mud rinsing of hydrometallurgical tailings instead of drilling residue removal. No filter packs were installed in any of the piezometers.

Shallow piezometers are equipped with cemented ϕ168 mm wide surface casing and have plastic inner casing PVC-U DN 100, slot 0.75 mm. Usually this casing goes up to 3 m in the base of the aquifer, where a plug and a sink are installed as well. Deep piezometers are installed in the same manner as the shallow ones with the exception of piezometers number 3, 4 and 5 (Table 1), which have one additional inner casing and piezometer number 12, which has two additional cemented inner casings due to its greater depth.

Pumping well performance

In all 20 piezometers, hydraulic tests were performed between 4th of September and 4th of November 2003 and were interrupted by heavy rain in the mean time.

In all wells saturated thickness wasn't big enough to create a sufficient pressure head drop to develop test correctly. In addition, a large part of the material deposited in Boršt has relatively low permeability and consequently wells have very low yield (less than 0,1 l/s). Therefore, regular pumping tests weren't feasible in most of the wells, since the pump's lower limit of operation is approximately at discharges 1-2 dcl/s. Improvised slug tests were performed instead. Wells were pumped at a middle rate, which was defined on the basis of previous hydrogeological interpretation. So, basic condition for slug tests, water being removed from the well nearly instantaneously, was satisfied and drawdown response wasn't damaged. Such tests enabled the use of slug test methods as well as pumping test methods, since they satisfied all conditions for the two methods.

Prior to testing pressure probes connected to automatic data loggers were inserted in the pumping well plus in other boreholes in its vicinity. Selection of probes with sensitivities

that ranged from 1 to 3 bars depended on expected maximal drawdown (10-30 m). Time intervals between measurements were constant throughout the test but they varied between the tests from 1 to 24 seconds and were adjusted according to the duration of measurement and the expected rate of water level lowering. After a couple of tests it proved that there were no water level changes detected in the adjacent wells, therefore, we continued with testing with only one probe.

Due to absence of water level change in the wells adjacent to the pumping well we had to limit our selection of analytical methods to those that describe single-well tests (i.e. tests that don't use any other piezometer for water level changes observation except the pumping well itself). Some of those methods were primarily developed for ordinary pumping tests with one or more piezometers (JACOB's (1967) and THEIS's (1935) methods), but can also be used for single-well tests provided that certain additional assumptions and conditions are met.

Analytical methods

All methods discussed can not be applied to all performed tests in the same degree of reliance, since each method has different underlying assumption. Therefore, differences in basic conditions and assumptions that have to be satisfied for models to be successfully applied are presented in the following section as well as the governing equations.

Models

In this paper, methods of Jacob (COOPER & JACOB, 1967), PAPADOPULOS (1967), Theis (1935), HVORSLEV (1951) and COOPER (1967) are compared. These methods were selected while they are the most used in engineering practice. They assume boundary conditions that in most cases can reasonably be met in the field. Methods differ from one another in the given solution to the partial differential equation of groundwater flow as well as in their underlying assumptions. The later are incorporated, since field conditions in real world are way too complicated to be described with relatively simple analytical equations, therefore, certain assumptions and conditions have to be met to reduce the practical problem to mathematical constraints. Only some of them underlie all discussed methods, what leads to differences in results arising from the very fundaments of the application.

Methods of Jacob, Papadopulos and Theis presume that (a) the well is pumped at a constant rate, whereas Hvorslev's and Cooper's methods suppose that (b) the water is added into or removed from the well instantaneously. In order to satisfy both conditions, improvised tests were performed where the wells were pumped at a *constant rate* (a) for a *short time* (b). If the pumping times are too long (longer than some critical time) empirical data doesn't coincide with the slug test model. According to MACE (1999), pumping times shorter than one day do not affect the performance of slug tests. However, in case of Boršt, these critical times were proved to be much shorter, about 30 – 90 minutes.

All five methods count for the storage in the well either by using only late time data in calculations or by incorporating this consideration directly in the type curves. On the other hand, Hvorslev method assumes

incompressible water and soil, which in other words means that it does not count for storage in the aquifer as oppose to other methods discussed. As a consequence of this assumption flow toward the well is to be quasi-stationary by the Hvorslev theory, while in other methods flow is described as non-stationary. In addition, Hvorslev's model doesn't presume the penetration of entire aquifer and is in all less rigorous than other methods.

Governing equations
The general equation of groundwater flow

$$\frac{\partial^2 s}{\partial r^2} + \frac{1}{r}\frac{\partial s}{\partial r} = \frac{S}{T}\frac{\partial s}{\partial t} \tag{1}$$

was among the presented authors first solved by THEIS (1935), who produced the following equation, derived from analogy between groundwater flow and conduction of heat:

$$s = \frac{Q}{4\pi KD}\int_0^{\infty}\frac{e^{-y}dy}{y} = \frac{Q}{4\pi KD}W(u) \tag{2}$$

where

$$W(u) = -0.5772 - \ln u + u - \frac{u^2}{2.2!} + \frac{u^3}{3.3!} - \frac{u^4}{4.4!}\ldots, \text{ where } u = \frac{r^2 S}{4KDt} \tag{3}$$

This equation was derived for fully penetrating pumping wells in homogeneous and isotropic non-leaky confined aquifers. An approximation u < 0.01 by Jacob is then applied to this equation, so that the terms beyond ln *u* in equation (3) become so small that they can be neglected. The equation for recovery data is then rewritten as:

$$K = \frac{2{,}30Q}{4\pi D\Delta s'} \tag{4}$$

and

$$t, t' > \frac{25r_c^2}{KD} \tag{5}$$

where t is the time since pumping started and t' is the time since cessation of pumping, Δs' is change of head per one log cycle of time on semi-log plot s vs. t/t' (t/t' on the logarithmic scale).

The most frequently used method for pumping tests, namely the Jacob (COOPER & JACOB, 1946) method is also based on the presented approximation of Theis's formula (2), except that it's applicable to drawdown data. The later can be simplified to give the following equation for calculating hydraulic conductivity from pumping test data:

$$K = \frac{2{,}30Q}{4\pi D\Delta s} \tag{6}$$

where Δs is change of head per one log cycle of time on semi-log plot s vs. t (t on the logarithmic scale). An additional assumption for single well test should be satisfied:

$$t > \frac{25r_c^2}{KD} \tag{7}$$

The most widely used method for slug tests has to be that of HVORSLEV (1951), and is based on the following equation, derived for fully penetrating well in a confined aquifer, where a quasi-stationary flow and incompressible water and soil (i.e. zero aquifer storage) are assumed:

$$K = \frac{A}{\Delta tF}\ln\frac{h_1}{h_2} \tag{8}$$

where A is the cross-sectional area of the well, l is the length of the tested portion, h_1 and h_2 are two values of water elevation in the well at the end and at the beginning of time interval Δt, and F is the shape factor that equals:

$$F = \frac{2\pi l}{\ln(\frac{l}{r_w})} \tag{9}$$

Hvorslev presented numerous such factors for different geometries. Among those, the shape factor for cased hole and uncased or perforated extension into aquifer of finite thickness was selected and used in our calculations.

PAPADOPULOS ET AL. (1967) suggested a solution developed directly for single well pumping tests. It is based on a large-diameter wells method, where well storage cannot be neglected. The governing equation for this method is:

$$K = \frac{Q}{4\pi Ds_w}F(u_w,\alpha,\rho) \tag{10}$$

where

$$F(u_w,\alpha,\rho) = \frac{8\alpha}{\pi}\int_0^\infty \frac{C(\beta)}{D(\beta)\beta^2}d\beta \tag{11}$$

$$C(\beta)=\left[1-\exp\left(-\beta^2\frac{\rho^2}{4u}\right)\right]\left[J_0(\beta\rho)A(\beta)-Y_0(\beta\rho)B(\beta)\right] \tag{12}$$

$$A(\beta)=\beta Y_0(\beta)-2\alpha Y_1(\beta) \tag{13}$$

$$B(\beta)=\beta J_0(\beta)-2\alpha J_1(\beta) \tag{14}$$

$$D(\beta)=\left[A(\beta)\right]^2+\left[B(\beta)\right]^2 \tag{15}$$

$$u_w=\frac{r_{ew}^2S}{4KDt}\ ,\ \alpha=\frac{r_{ew}^2S}{r_c^2},\ \text{and}\ \rho=\frac{r}{r_w} \tag{16}$$

K represents hydraulic conductivity, Q is pumping rate, D is aquifer thickness, s_w is drawdown in the well, r_{ew} is effective radius of screened part of the well, r_c is radius of the unscreened part of the well, where the water is changing, t is time since pumping started, and F is well function, which is represented by the type curves and J_0 (and Y_0) and Y_1 are zero-order and first-order Bessel functions of the first and second kind, respectively.

Cooper et al. (1967) presented also another overlapping graphs solution for slug tests. It is based on the following equation:

$$\frac{h_t}{h_0}=F(\alpha,\beta) \tag{17}$$

where

$$\alpha=\frac{r_{ew}^2S}{r_c^2}\quad \beta=\frac{KDt}{r_c^2}\quad h_0=\frac{V}{\pi r_c^2} \tag{18}$$

h_0 is the initial water elevation in the well, h_t is the water elevation at time t, b is the dimensionless time, V is the volume of water added to the well, and F(a,b) is the well function which is represented with a set of type curves (Figure 1, left) and is described by the equation.

$$F(\alpha,\beta)=\frac{8\alpha}{\pi^2}\int_0^\infty\frac{\exp(-\beta u^2/\alpha)}{uf(u,\alpha)}du \tag{19}$$

where

$$f(u,\alpha)=[uJ_0(u)-2\alpha J_1(u)]^2+[uY_0(u)-2\alpha Y_1(u)]^2 \tag{20}$$

and $J_0(u)$, $J_1(u)$, $Y_0(u)$, $Y_1(u)$ – are zero-order and first-order Bessel functions of the first and second kind.

Data processing

In general, there are two types of numerical data processing, that both base on regression principle (methods will further be addressed only by the leading author). Curve fitting methods Papadopulos and Cooper try to find best possible fit between empirical data and type curves. They read four parameters (two in each graph) that enable the calculation of hydraulic conductivity of the aquifer (Figure 1, left). Straight-line methods Jacob, Theis and Hvorslev derive the drawdown equation with certain operations and/or simplifications to the form that yields a straight-line graph (Figure 1, right). The slope of the line and its intersection with the ordinate axis facilitate the computation of aquifer parameters.

To define the subjective factor which is always present when applying different methods to aquifer test data, a short description of data segment selection criteria is given here. For drawdown data, the early time data doesn't coincide with the Jacob model, which is a consequence of the well-bore storage. Therefore, only late time data (later than approximately 2 – 5 minutes after the start of the pumping) was used for calculation. Similarly, first part of the recovery data was excluded from the calculation as well. Results obtained from this part of recovery data are erroneous because water rises faster than normally due to water coming back from the pipe to the well after the cessation of pumping. After this water returns, the recovery data should correspond to the Theis, Hvorslev and Cooper models.

However, the subjective factor remains, since curve-matching as well as straight line matching processes were done solely by visually estimating the position of the best fit, and it was not quantified by the least-squares error function.

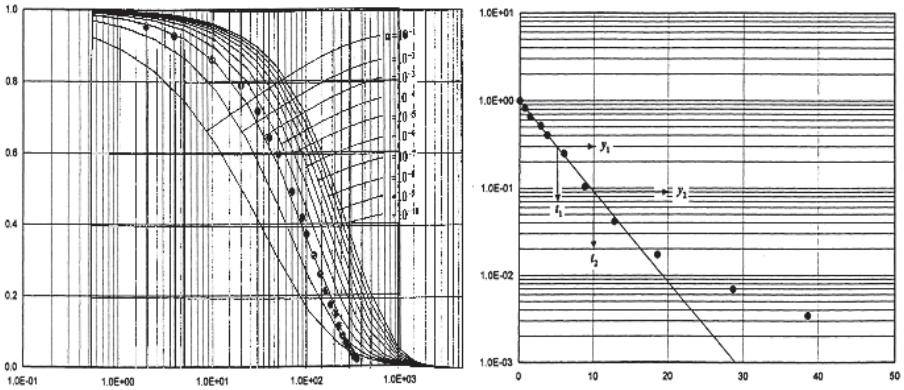

Figure 1. Data processing - left: Curve-fitting Cooper method; right: Straight-line Hvorslev method (BATU, 1998)

Slika 1. Obdelava podatkov - levo: Prilagajanje tipskim krivuljam pri Cooperjevi metodi; desno: Metoda Hvorsleva s premico (BATU; 1998)

Results and discussion

Field results

The calculation of hydraulic conductivity values from aquifer tests on Boršt site gave the following results as presented in Table 1. As can bee seen from this table not all the methods could be applied to all tests. In cases number 15 and 17 to 20, slug tests with addition of water were performed, so the first three methods were inapplicable. Nevertheless, these cases were included in the analysis because of the study of the relationship between Hvorslev and Cooper method. In case number 14 the experimental data couldn't be fitted with sufficient certainty to type curves in Papadopulos method.

Since no "real" values of hydraulic conductivity are available, we can only compare these results relatively towards one another and thus their rank numbers are given in the brackets for each test.

Ranks of the hydraulic conductivity values for several cases show some typical arrangements (Figure 3). It is evident that in almost all cases the highest or at least second highest values are obtained by Papadopulos method. Moreover, cases number 1, 3, 4, 6, 8, 11 and 16 exhibit additional similarities. Results of Hvorslev and Cooper method are up to two and a half decades lower than results of other three methods. Among those two, Hvorslev's method results are usually somewhat higher than those of Cooper's

Table 1. Hydraulic conductivity values and their ranks for 20 aquifer tests in Boršt, Žirovski vrh (1 – 12: deep piezometers; 13 – 20: shallow piezometers)
Tabela 1. Vrednosti koeficientov prepustnosti in njihovi rangi za 20 hidravličnih testov na Borštu (1 – 12: globoki piezometri; 13 – 20: plitvi piezometri)

Well No.	K_{Jacob}	$K_{Papadopulos}$	K_{Theis}	$K_{Hvorslev}$	K_{Cooper}
1	6.38E-06 (1)	4.41E-06 (2)	1.84E-06 (3)	3.64E-07 (5)	4.30E-07 (4)
2	8.11E-07 (4)	1.75E-06 (2)	2.58E-06 (1)	7.06E-07 (5)	1.02E-06 (3)
3	6.46E-08 (4)	2.70E-07 (1)	2.15E-07 (2)	1.25E-07 (3)	2.58E-08 (5)
4	5.65E-07 (2)	8.11E-07 (1)	5.35E-07 (3)	1.40E-08 (4)	1.03E-09 (5)
5	6.62E-08 (5)	1.85E-07 (1)	8.28E-08 (3)	7.77E-08 (4)	1.63E-07 (2)
6	2.25E-06 (2)	3.66E-06 (1)	5.03E-07 (3)	6.51E-08 (5)	7.58E-08 (4)
7	4.82E-08 (3)	2.04E-08 (5)	4.42E-08 (4)	9.75E-08 (2)	1.42E-07 (1)
8	3.62E-07 (2)	3.72E-07 (1)	1.72E-07 (3)	1.31E-07 (4)	4.37E-08 (5)
9	1.43E-07 (5)	3.74E-07 (2)	1.76E-07 (4)	2.21E-07 (3)	5.09E-07 (1)
10	4.06E-07 (4)	5.55E-07 (2)	3.40E-07 (5)	4.12E-07 (3)	7.27E-07 (1)
11	7.63E-08 (2)	9.11E-08 (1)	2.79E-08 (3)	2.75E-09 (4)	1.23E-09 (5)
12	8.32E-07 (3)	2.90E-06 (1)	6.59E-07 (4)	3.69E-07 (5)	1.20E-06 (2)
13	8.42E-06 (4)	3.01E-06 (5)	5.46E-05 (2)	1.18E-04 (1)	5.10E-05 (3)
14	4.67E-05 (1)		1.30E-05 (4)	2.27E-05 (3)	4.50E-05 (2)
15				5.85E-07 (2)	7.41E-07 (1)
16	1.22E-05 (3)	5.14E-05 (1)	4.91E-05 (2)	4.02E-06 (4)	1.52E-06 (5)
17				4.43E-05 (2)	7.44E-05 (1)
18				6.72E-05 (2)	1.45E-04 (1)
19				1.49E-05 (2)	7.09E-05 (1)
20				1.23E-07 (2)	1.71E-07 (1)

method. Results of Theis and Jacob methods are in between Hvorslev and Cooper method results of one side and Papadopulos method values on the other. In addition, Jacob method gives a bit higher values than Theis model.

Differences between tests can also be noticed on the scatter point graphs, where pumping test method is plotted against slug test method. They are most evident in the relationship between Jacob and Hvorslev method, which are believed to be the most resilient and straight forward solutions among pumping and slug test methods, respectively. Most of the cases coincide with the equal values line, except in some cases, which fall on a line parallel to the equal values line and where results of Jacob are greater than values of Hvorslev.

Differences in results also occur between method that use drawdown data (Jacob, Papadopulos) and those that use recovery data (Theis, Hvorslev, Cooper). Nevertheless, they can only be observed where pumping times were short, otherwise they are blurred by the differences between the pumping and slug test. Overall, the recovery results show greater variability in values than those calculated from drawdown data.

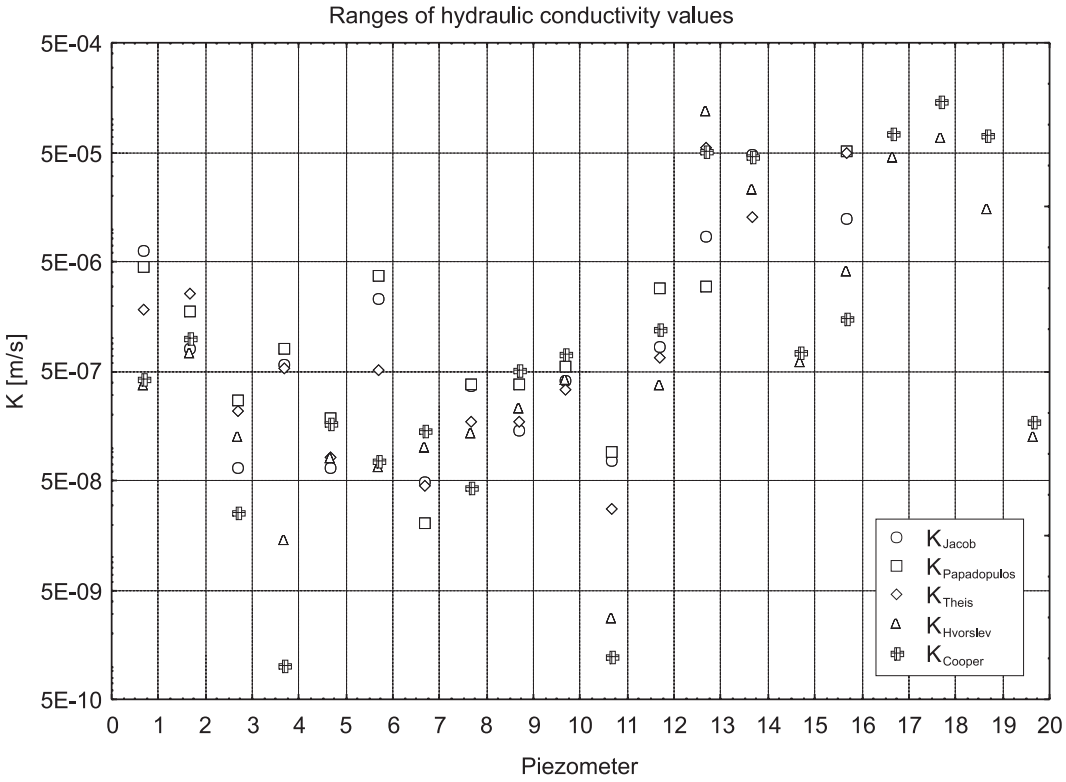

Figure 2. Ranges of results obtained by methods of JACOB ET AL. (1946), PAPADOPULOS ET AL. (1967), THEIS (1935), HVORSLEV (1951) and COOPER ET AL. (1967)
Slika 2. Razponi dobljenih vrednosti po metodah JACOBA ET AL. (1946), PAPADOPULOSA ET AL. (1967), THEISA (1935), HVORSLEVA (1951) in COOPERJA ET AL. (1967)

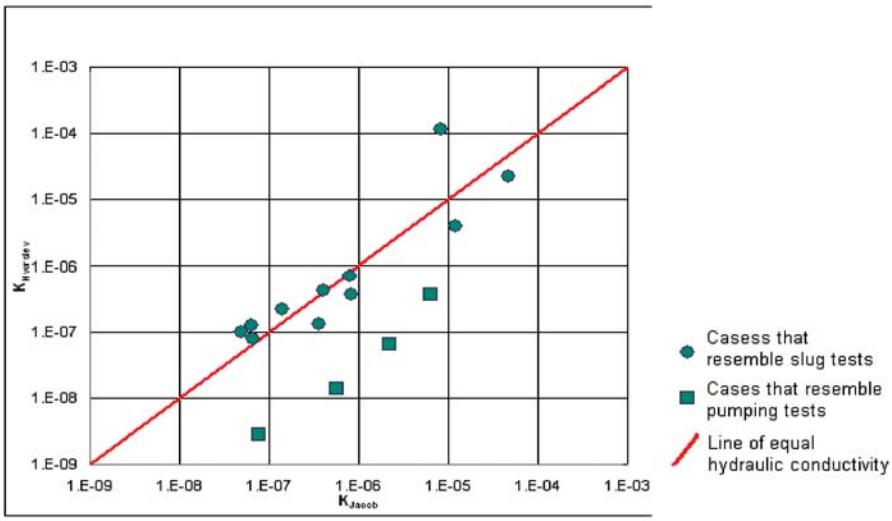

Figure 3. Relation between hydraulic conductivity values of Jacob and Hvorslev method
Slika 3. Razmerje med koeficienti prepustnosti po Jacobovi metodi in metodi Hvorsleva

In Table 2 correlations between results from different analitical models are presented. The most profound relation among the pairs of five discussed methods in case of Boršt is that of the two slug test methods – Hvorslev and Cooper. Somewhat lower are the correlations between the three pumping test methods. In general, pumping test methods do not correlate with slug test methods at such high degree.

Discussion

Results obtained by using different methods for calculation of hydraulic conductivity from aquifer tests showed a clear separation between tests with longer pumping times and those with shorter pumping timer. A term of "critical time" was introduced to distinguish between the two types of tests which describes the longest time of pumping at which slug tests methods can be employed and the results of these methods don't diverge significantly from those of pumping test methods. Critical time was only determined approximately. MACE (1999) showed that the instant addition/removal of water condition is quite flexible and can be extended to one whole day of pumping. However, this doesn't prove to be the case in aquifer tests on mill

Table 2. Correlations between results from different analitical models
Tabela 2. Korelacije med rezultati različnih metod

R	K_{Jacob}	$K_{Papadopulos}$	K_{Theis}	$K_{Hvorslev}$	K_{Cooper}
K_{Jacob}	1				
$K_{Papadopulos}$	0.92	1			
K_{Theis}	0.90	0.86	1		
$K_{Hvorslev}$	0.66	0.57	0.84	1	
K_{Cooper}	0.54	0.47*	0.68	0.93	1

*statistically insignificant

tailing of Boršt. Differences in results start to appear in tests with pumping times longer than half an hour, and the longer the pumping time, the greater the distinction between pumping and slug test method results. To be precise, in such cases slug test methods underestimate hydraulic conductivity values by as much as two orders of magnitude.

Differences between "pumping" and "slug" tests can be seen in typical arrangements of ranks of the hydraulic conductivity values as described in previous section. Such typical arrangement is associated largely to those cases that resemble pumping tests more than slug tests, namely cases number 1, 3, 4, 6, 8, 11 and 16. Moreover, cases of pumping times longer than "critical time" can be further distinguished from other cases as can be seen in Figure 5. "Pumping" test cases (number 1, 4, 6, 11) are the ones that diverge from the line of equal hydraulic conductivity towards the pumping test method axis, whereas "slug" test cases coincide well with this line. This shows that the results of these five methods can only be compared when a slug test was performed, and that the instant addition/removal of water condition is the most rigorous and thus the key condition to be satisfied in this matter.

Furthermore, systematic differences seem to appear between Theis's recovery method for pumping tests and Hvorslev's method for slug-tests. Since both are straight-line methods a clear separation between straight and non-straight line portion of the recovery data can be defined (i.e. the point where experimental data start to concur with the model) in data processing procedure. It is apparent, that in cases when our improvised aquifer test resembles slug test in higher degree than pumping test, the experimental data coincides with Hvorslev's model earlier than with Theis's model. On the other hand, field data falls in Theis's model earlier, in cases with longer pumping times when performed test resembles pumping test.

As a remark, KARANTH & PRAKASH (1988) showed that with decreasing values of hydraulic conductivity the transmissivity values of slug tests exceed values of pumping test. Since similar trends, but less extent, have been noted in this study using different methods on the same set of aquifer test data, we can conclude that a part of the slug-pumping test relationship arises solely from model structure.

Discrepancies between method that use drawdown data (Jacob, Papadopulos) and those that use recovery data (Theis, Hvorslev, Cooper) are a consequence of a couple technical facts. Firstly, not fully developed wells where activation of the well took place during the pumping resulted in lower values from drawdown data, and secondly, presence of well clogging with the fine-grained hydrometallurgical tailing which resulted in lower values from recovery data. Although these differences are small compared to the pumping/slug test differences, they add to the importance of model selection. The greater variability in results from recovery data also implies that well development is in fact an important factor.

Somewhat higher results can also be obtained by Papadopulos method as can be seen in Table 1. This is due to many cases when experimental values coincide with the straight portion of the type curves, where ambiguous results are usually gathered. This

portion of type curves represent the water being pumped from wellbore storage and is employed in cases of small well diameter and/or short pumping times as it was the case in Boršt. Nothing similar can be observed with the other curve-fitting method – Jacob method doesn't account for the wellbore storage and thus doesn't have such straight portions of type curves and the experimental and theoretic graphs can only be adjusted toward one another on x-axis.

Since results of Hvorslev's method are as rule lower than those of any other method a reason for this was sought as well. Lower values could be a consequence of the difference between pumping and slug test conditions with respect to Jacob's, Papadopulos's and Theis's method on one hand, and the fact that it does not account for the aquifer storage with respect to Cooper's model on the other. Namely, after the depression due to pumping is formed, the Hvorslev model assumes that the water must fill the gaps between the soil particles in the drained portion of the aquifer, whereas storage accounting Cooper model requires additional water to compensate for the aquifer storage. Consequently, water in Cooper's model should flow to the well slower than in Hvorslev's model, resulting in higher values of hydraulic conductivity using the Cooper's model given that the actual flow to the well used for calculation is in fact unique and therefore the same for both cases.

In addition, the difference between the Cooper and Hvorslev results in case of Boršt varies with the order of magnitude of the hydraulic conductivity. Since those methods could be applied to most performed tests and thus produced more results, we get a more thorough insight in their correlation. Figure 6 shows that in more permeable materials, results of Cooper exceed those of Hvorslev,

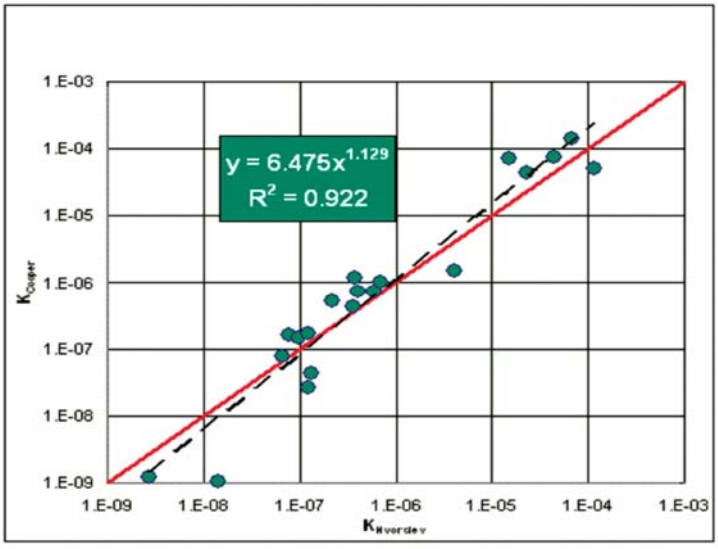

Figure 4. Relation between hydraulic conductivity values of Hvorslev and Cooper method
Slika 4. Razmerje med koeficienti prepustnosti po metodi Hvorsleva in Cooperjevi metodi

whereas in low permeability sediments Hvorslev's model gives higher values. The similar phenomenon was noted by HYDER & BUTLER (1995), who noted that results of Bouwer and Rice, which can at this point be addressed as adequate to the Hvorslev method, overestimate hydraulic conductivity in clay-rich formations. The best agreement between the two models can be found in the interval $1x10^{-7}$ and $1x10^{-6}$ m/s. This confirms the systematic difference between the two methods. Hvorslev's method is quasi 3-dimensional because of incorporation of shape factor, while Cooper's method is 2-dimensional. For coarse-grained sediments one must therefore estimate the importance of vertical flow to select the correct analysis method (HERZOG, 1994).

CONCLUSIONS

The comparative analysis of single well aquifer test methods in Boršt Žirovski vrh showed, that methods of JACOB ET AL. (1946), PAPADOPULOS ET AL. (1967) and THEIS (1935) for pumping tests give significantly different results than methods of HVORSLEV (1951) and COOPER ET AL. (1967) in cases when aquifer tests resembled pumping tests in higher degree than slug tests. Values were comparable in cases when times of pumping were shorter than "critical times", which were ascertained at about 30 minutes in case of Boršt. That shows that time of pumping is the key factor in this matter and that this is the most rigorous condition in case of Boršt, which is also the most easily removable one from technical point of view.

The present comparative analysis shows that the question of determination of hydraulic conductivity isn't trivial in the interpretative sense, because the final result highly depends on the analytical model selection. Despite unique properties of existing aquifers, differences between models lead to ambiguous result, which implies that thorough knowledge of models and their boundary conditions is needed in aquifer permeability characterization.

POVZETEK

Primerjalna analiza metod obdelave hidravličnih poizkusov v črpanem vodnjaku na odlagališču hidrometalurške jalovine Boršt, Žirovski vrh, Slovenija

Med hidrogeološkimi raziskavami na odlagališču hidrometalurške jalovine Boršt Rudnika urana Žirovski vrh je bilo izvedenih več črpalnih in nalivalnih poizkusov, na podlagi katerih je bil pridobljen velik nabor podatkov. Raziskave so bile opravljene za potrebe opredelitve koeficientov prepustnosti hidrometalurške jalovine in podlage. Opazovalne vrtine so bile izvrtane med majem in oktobrom leta 2003. Globine vrtin, ki so izvedene v hidrometalurški jalovini znašajo med 5 in 25 m, vrtine izvedene v karnijski podlagi, sestavljeni iz cordevolskih apnencev in dolomita ter julsko-tuvalskih klastičnih kamnin, pa so globoke med 26 in 105 m.

Debelina omočenega sloja se od vrtine do vrtine spreminja. Zaradi relativno slabe prepustnosti testiranih območij, debelina omočenega dela ni bila dovolj velika, da bi lahko s črpanjem ustvarili zadostno tlačno razliko med vodonosnikom in nivojem vode v črpalni vrtini, kar bi omogočilo ustrezen potek poizkusa. Ob tem sta določene prilagoditve terjali tudi slaba prepustnost in

posledično nizka izdatnost črpalnih vrtin. Vrtine smo tako na podlagi predhodne hidrogeološke interpretacije črpali z majhno količino. S tem smo dobili uporabne podatke o znižanju nivoja podzemne vode v vodnjaku kakor tudi uporabne podatke o dvigu nivoja za obdelavo z metodami za impulzne poizkuse.

Pridobljene podatke smo uporabili za primerjalno analizo več analitičnih modelov za obdelavo hidravličnih testov. Med seboj smo primerjali tiste metode, ki obravnavajo poizkuse na črpalnih vodnjakih (t.i. single-well testi). Tako smo primerjali metode Jacoba (Cooper & Jacob, 1967), Papadopulosa et al. (1967), Theisa (1935), Hvorsleva (1951) in Cooperja et al. (1967).

Vsaka od metod ima lastne robne pogoje, kar zahteva izpolnitev določenih predpostavk. Ujemanje oz. neujemanje teoretičnih modelov z dejanskim stanjem na terenu ima za posledico razlike v rezultatih med metodami. Obravnavane metode se med seboj ločijo tudi po načinu obdelave podatkov. Tako poznamo dva postopka numerične obdelave podatkov, ki se oba naslanjata na izračun regresije – (1) s prekrivanjem teoretičnih in empiričnih podatkov ter (2) s pomočjo trendne premice.

Na podlagi obdelave smo dobili rezultate, ki jih prikazuje Tabela 1. Ker "dejanski" podatki o prepustnosti niso na voljo, smo pridobljene koeficiente prepustnosti lahko primerjali le relativno. Posamezne koeficiente prepustnosti smo razvrstili glede na ostale vrednosti, ki so bile zabeležene v isti opazovalni vrtini in jim pripisali rang. Ti kažejo, da v večini primerov dobimo najvišje koeficiente prepustnosti s Papadopulosovo metodo.

V nekaterih primerih so koeficienti prepustnosti izračunani z metodami po Hvorslevu in Cooperju za dve in pol dekadi nižji od rezultatov ostalih metod, kar je v glavnem posledica trajanja črpanja. Opredelili smo tudi t.i. "kritične čase", torej tiste čase trajanja črpanja, ob katerih se rezultati različnih metod še razmeroma skladajo. Ti so v primeru Boršta med 30 in 90 minutami in so specifični za to območje. Za primerjavo lahko podamo primer s severnega Teksasa, ki ga navaja Mace (1999), v katerem črpalni časi, krajši od enega dneva naj ne bi vplivali na kvaliteto impulznega poizkusa. Efekt predolgega črpanja prikazuje Slika 3, kjer so v točkastem diagramu prikazani koeficienti prepustnosti po Jacobu proti koeficientom prepustnosti Hvorsleva. Večina rezultatov (krogi) se razporedi vzdolž premice z naklonom 1 in presečiščem 0, nekatere vrednosti (kvadrati) pa padejo na premico z enakim naklonom, ki je zamaknjena proti osi Hvorsleva. S krogi so ponazorjeni tisti poizkusi, ki so po dolžini črpanja bolj podobni impulznim poizkusom, s kvadrati pa tisti poizkusi, ki so bolj podobni črpalnim poizkusom.

Primerjalna analiza med rezultati je pokazala, da je čas črpanja ključni dejavnik in da lahko primerljive rezultate na območju Boršta dobimo pri črpalnih poizkusih, ki niso daljši od 30 minut. Hkrati se je izkazalo, da vprašanje opredelitve koeficienta prepustnosti v interpretativnem smislu ni trivialno, saj je končni rezultat v veliki meri odvisen od izbrane metode obdelave. Tako kljub enoznačnemu stanju v naravi razlike med robnimi pogoji posameznih metod vodijo do dvoumnih rezultatov, zaradi česar je za pravilno karakterizacijo hidravlične prepustnosti potrebno temeljito poznavanje modelov in pogojev njihove uporabe.

REFERENCES

BARKER, J.A., HERBERT, R. (1989): Nomograms for the analysis of recovery tests on large-diameter wells. Quarterly Journal of Engineering Geology 22, pp. 151-158.

BATU, V. (1998): Aquifer Hydraulics: A Comprehensive Guide To Hydrogeologic Data Analysis. John Wiley & Sons, Inc., New York.

BOUWER, H., RICE, R.C. (1976): A slug test for determining hydraulic conductivity of unconfined aquifers with completely or partially penetrating wells: Water Resources Research, Vol. 12, No. 4, pp. 423-428.

CHAPUIS, R.P., SOULIE, M., & SAYEGH, G. (1990): Laboratory modeling of field permeability in cased boreholes. *Canadian Geotechnical Journal*, Vol. 27, pp. 647-658.

CHAPUIS, R.P. (1998): Overdamped slug test in monitoring wells: review of interpretation methods with mathematical, physical, and numerical analysis of storativity influence. *Canadian Geotechnical Journal*, Vol. 35, pp. 697-719.

CHAPUIS, R.P., CHENAF, D. (2002): Slug tests in a confined aquifer: experimental results in a large soil tank and numerical modeling. *Canadian Geotechnical Journal*, Vol. 39, pp. 14-21.

CHIRLIN, G.R. (1989): A Critique of the Hvorslev Method for Slug Test Analysis: The Fully Penetrating Well. *Ground Water Monitoring & Remediation*, 130-138.

COOPER, H.H., JACOB, C.E. (1946): A generalized graphical method for evaluating formation constants and summarizing well field history. *Amer. Geophys. Union Trans*., Vol. 27, pp. 526-534.

COOPER, H.H., BREDEHOEFT, J.D., PAPADOPULOS, S.S. (1967): Response of a finite diameter well to an instantaneous charge of water. *Water Resources Res*., Vol. 3, pp. 263-269.

HERBERT, R., KITCHING, R. (1981): Determination of aquifer parameters from large-diameter dug well pumping tests. *Ground Water 19*, pp. 593-599.

HERZOG, B.L. (1994): Slug tests for determining hydraulic conductivity of natural geologic deposits. In: Hydraulic conductivity and waste contaminant transport in soil, ASTM STP 1142, D.E. Daniel and S.J. Trautwein, Eds., *American Society for Testing and Materials*, Philadelphia.

HERZOG, B.L., MORSE, W.J. (1994): Comparison of Slug test methodologies for Determination of Hydraulic Conductivity in Fine-Grained Sediments. *Ground Water and Vadose Zone Monitoring*, ASTM STP 1053; D.M. Nielsen and A.I. Johnson, Eds., American Society for Testing and Materials, Philadelphia. pp. 152-164.

HVORSLEV, J.M. (1951): Time lag and soil permeability in ground – water observations. *Waterways Experiment Station Corps of Engineers*, U.S.ARMY, Vol. 36, 50 p.

HYDER, Z, BUTLER, J.J. (1995): Slug tests in unconfined formations: an assessment of the Bouwer and Rice technique. *Ground Water*, Vol. 33, no. 1, 16-22.

KARANTH, K.R., PRAKASH, V.S. (1988): A comparative study of transmissivity values obtained by slug-tests and pump-tests. *Journal Geological Society of India*, Vol. 32, pp. 244-248.

MACE, R.E. (1999): Estimation of hydraulic conductivity in large-diameter, hand-dug wells using slug-test methods. *Journal of Hydrology,* 219, pp. 34-45.

NGUYEN, V., PINDER, G.F. (1984): Direct Calculation of Aquifer Parameters in Slug Test Analysis. Groundwater Hydraulics, *Water Resources Monograph 9*. J. Rosensheim and G.D. Bennet, Eds., American Geophysical Union, pp. 222-239.

PAPADOPULOS, S.S. COOPER H.H. JR. (1967): Drawdown in a well of large diameter. *Water Resources Res*., Vol. 3, pp. 241-244.

PAPADOPULOS, S.S., J.D. BREDEHOEFT, COOPER, H.H. (1973): On the analysis of 'slug test' data. *Water Resources Res*., Vol. 9, pp. 1087-1089.

THEIS, C.V. (1935): The relation between the lowering of the piezometric surface and the rate and duration of the discharge of the well using groundwater storage. *Trans. Amer. Geophys. Union*, Vol. 16, pp. 519-524.

Investigations of flow system and solute transport at an urban lysimeter at Union Brewery, Ljubljana, Slovenia

Proučevanje tokovnega sistema in prenosa snovi v urbanem lizimetru Pivovarne Union, Ljubljana, Slovenija

Branka Trček

Geological Survey of Slovenia, Dimičeva 14, SI–1000 Ljubljana, Slovenia
E-mail: branka.trcek@geo-zs.si

Received: April 15, 2005 **Accepted**: November 24, 2005

Abstract: Investigations of flow system and solute transport have been undertaken at an urban lysimeter at Union Brewery, near the centre of Ljubljana, with the intention of monitoring and controlling the environmental impacts of industry and traffic on groundwater within a Pleistocene alluvial gravel aquifer. The physico-chemical and isotopic properties of sampled groundwater have already produced general information on the hydrodynamic functioning of the study area and on solute transport - the main flow components, the flow hierarchy and the environmental response to the flow system have been indicated. Two important flow types are identified - lateral and vertical flow. The former has an important role in groundwater protection, whilst the latter is the main influence on contaminant transport towards the aquifer saturated zone.

Izvleček: V urbanem lizimetru Pivovarne Union, v bližini centra Ljubljane, potekajo raziskave tokovnega sistema in prenosa snovi. Njihov glavni namen je, da se proučijo vplivi industrije in prometa na podzemno vodo pleistocenskega prodnega vodonosnika. Fizikalno-kemične in izotopske lastnosti vzorčene vode so opisale osnovne hidrodinamične lastnosti opazovanega sistema. Opozorile so na hierarhijo toka v nezasičeni coni vodonosnika in odziv okolja nanjo. Identificirani sta bili dve pomembni vrsti tokov - lateralni in hitri vertikalni tok. Lateralni tok ima veliko vlogo pri zaščiti vodnih virov pleistocenskega prodnega vodonosnika. Vloga hitrega vertikalnega toka je povsem nasprotna, saj je le-ta glavni faktor za prenos in širjenje onesnaženja proti zasičeni coni vodonosnika.

Key words: urban lysimeter, Pleistocene alluvial gravel aquifer, environmental impacts, flow and solute transport
Ključne besede: urbani lizimeter, pleistocenski aluvialni prodni vodonosnik, vplivi okolja, tok in prenos snovi

Scientific paper

INTRODUCTION

Groundwater from a Pleistocene alluvial gravel aquifer is becoming an increasingly important drinking water source for the Ljubljana area. It is also an invaluable water source for Union Brewery, which is located within an urbanised and industrialised area near the centre of Ljubljana and supplies quality groundwater from four production wells (Fig. 1). The managers of the brewery are aware that this water should be protected. Therefore, investigation of the environmental impacts of industry and traffic on groundwater of the Pleistocene alluvial gravel aquifer, have been undertaken. Flow and solute transport monitoring was conducted in numerous piezometers within the brewery and in its vicinity (some of them are illustrated in Figure 1), as well as at the lysimeter, which is a topic of this paper. The main goal of the piezometric monitoring is to investigate groundwater quality, whereas the main goal of the lysimeter monitoring is to study possible contamination in the vicinity of the brewery and with that to evaluate the role of the unsaturated zone in groundwater protection.

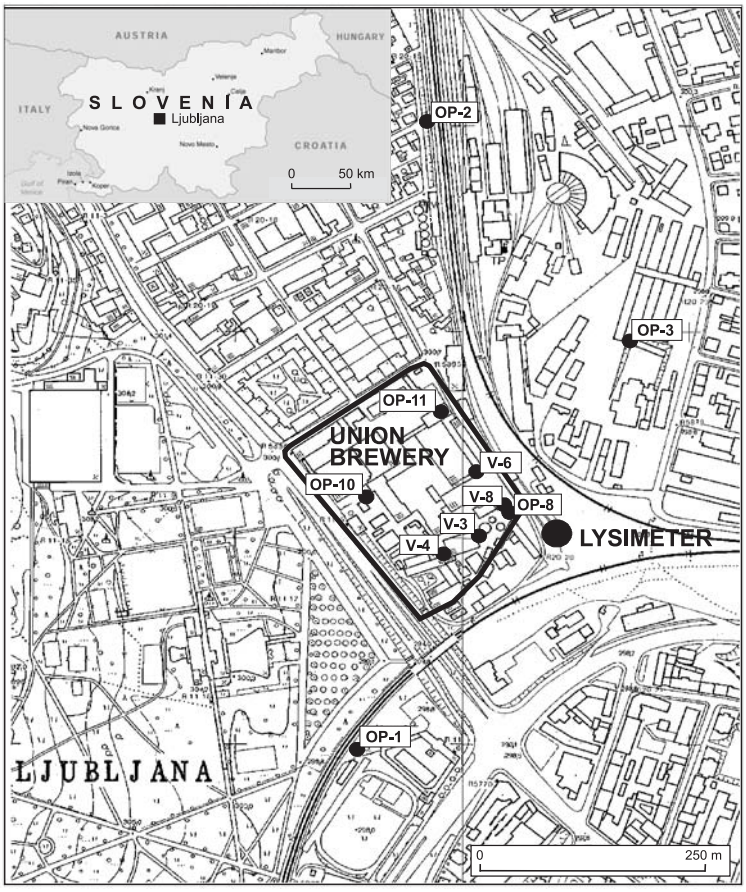

Figure 1. Study site (OP-x piezometer, V-x production well)
Slika 1. Raziskovalno območje (OP-x piezometer, V-x vodnjak)

Description of the study area

The urban lysimeter at Union Brewery was constructed (Juren et al., 2003) adjacent to the brewery (Fig. 1). It contains 42 boreholes – 36 on its right side, under industrial railway tracks and 6 on its left side, beneath the asphalt surface (Fig. 2). On the right side of the lysimeter the boreholes are up to 9.5 long and they are distributed in six columns (1-6) and six levels (I-VI) at depths of 0.3-4.0 m (Figs 2 and 3). On the left side of the lysimeter the boreholes are up to 2.5 m long and distributed in six columns (1-6) and three levels (I-III) at depths of 0.60-1.80 m.

The boreholes penetrate four layers: sandy gravel, silt-sandy gravel, clayey silt-sandy silt with gravel grains and gravel with sand and silt. The upper three layers are artificial, whereas the fourth layer consists of river deposits. A detailed geological cross-section of the ends of the boreholes on the right wall of the lysimeter is presented in Figure 3.

The lysimeter was equipped with a UMS recording and sampling system (Juren et al., 2003). Tensiometers, TDR probes and suction cups were installed at the ends of boreholes.

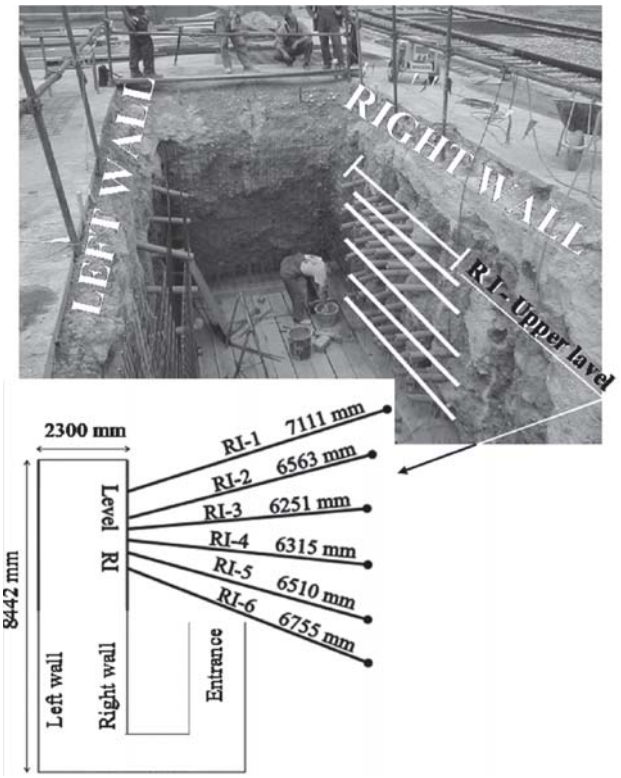

Figure 2. Lysimeter construction with the projection of the upper right level boreholes (modified after Juren et al., 2003)
Slika 2. Kostrukcija lizimetra z načrtom vrtin na zgornjem desnem nivoju (prirejeno po Juren et al., 2003)

METHODS AND TECHNIQUES

Monitoring of flow and solute transport processes in the lysimeter commenced in June 2003. During the first year of research, continuous measurement of water balance and of physico-chemical water parameters (pH and electroconductivity) were carried out to obtain basic information on the study area. In addition, monthly water sampling for analysis of the $\delta^{18}O$ and $\delta^{2}H$ isotopic composition was undertaken to obtain additional information about mixing processes and groundwater residence times in the unsaturated zone.

Groundwater was sampled with suction cups. A total of 18 sampling points were established on the right side of the lyimeter: RI-1 to RI-3, RII-1 to RII-3, etc. (Fig. 3), whereas on the left side of the lysimeter only 3 sampling points were established: LI-4, LII-5 and LIII-6. In addition, precipitation was sampled near the entrance to the lysimeter.

Groundwater was sampled and preserved based upon the method described by CLARK & FRITZ (1997). The characteristics of the isotopic composition of natural substances are described in numerous publications (e.g. CLARK & FRITZ, 1997; KENDALL & MCDONNELL, 1998; PEZDIČ, 1999).
The $\delta^{18}O$ composition is expressed relative to the standard SMOW (Standard Mean Ocean Water), conventionally reported in terms of a relative value δ, expressed with equation

$$\delta_x\ (‰) = (R_x/R_{st} - 1)1000 \qquad (1)$$

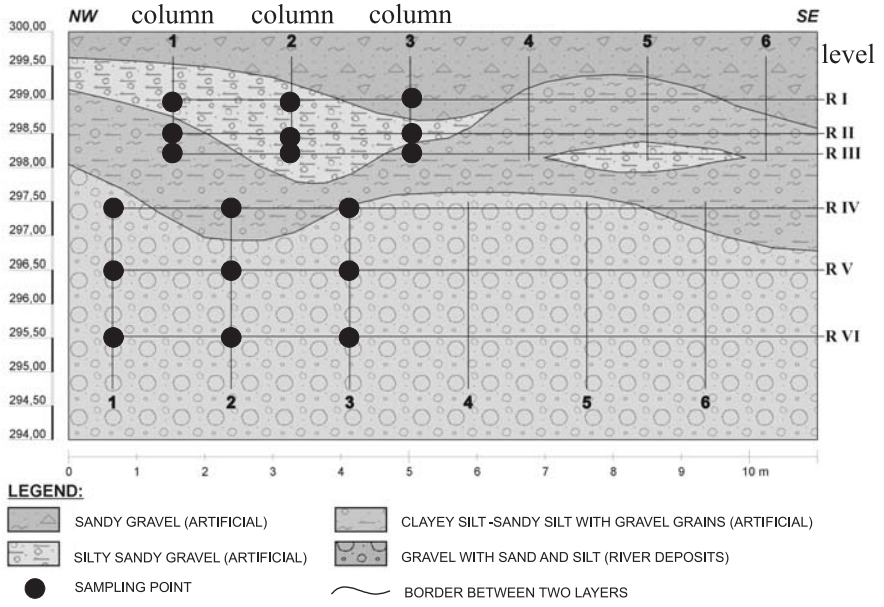

Figure 3. Geological cross-section of the right side of the lysimeter at the end of boreholes, with sampling points indicated (modified after JUREN ET AL., 2003)
Slika 3. Geološki prerez s konca vrtin na desni strani lizimetra z označenimi vzorčnimi mesti (prirejeno po JUREN IN SOD., 2003)

where R_x is the isotope ratio (e.g. $^{18}O/^{16}O$) in the substance X, R_{st} is the isotope ratio in the corresponding international standard substance, and δ is expressed in parts per thousand.

Water samples were analysed for $\delta^{18}O$ in the isotope laboratory at the GSF-Institute of Groundwater Ecology in Neuherberg (Germany), with a standard analytical error of ± 0.05 ‰.

Results

The water balance for the lysimeter sampling points during the first phase of the research is presented in Table 1. There is an absence of data for sampling points RIII-2 and RIII-3 for the first part of the monitoring period, because a proper measuring system was only established in April 2004. Nevertheless, it can be observed in Table 1 that these two sampling points discharged the highest volumes, and that on both, the right and left side of the lysimeter, the bulk of the water is discharged to sampling points on level III. It is important to note that a low discharge occurs under the asphalt surface (LIII-6, since none of the other sampling points did yield any drainage water at that period).

Figure 3 illustrates that the sampling points on level III are located near the contact between two structurally different layers: silty-sandy gravel and underlying clayey silty-sandy silt with gravel grains. The hydraulic conductivity of the upper layer is higher than that of the lower layer. Therefore it is presumed that the greater volumes discharged from level III result from the development of a lateral flow component. Figures 4 and 5 demonstrate that the discharges of level III are strongly dependent on precipitation levels and intensity. Figure 5 also indicates the occurrence of vertical flow from level III, which results in increased volume of discharge from sampling points

Table 1. Water balance of lysimeter sampling points
Tabela 1. Vodna bilanca vzorčnih mest v lizimetru

	Volume (ml)													Vol.(mm)
	RII 1	RV 1	RI 2	RII 2	RIII 2	RIV 2	RVI 2	RI 3	RIII 3	RIV 3	RV 3	RVI 3	LIII 6	Precipi-tation
10.7.03	280	340	86	41		70	19	455		110	45	160	5	57.7
27.8.03	385	490	38	45		95	38	370		45	65	38		71.6
17.9.03	175	175	21	20		50		220			40		38	44.5
16.10.03	380	200	110	24		890	29	190		100	24	40	37	110.7
12.11.03	190	180	100	20		60	55	180			20	30		121.4
9.12.03	190		60	20		60		120					20	73.8
20.1.04	280		20			80		90						150.3
17.2.04	180	10	35	20		48		25		27	7	7	10	12.7
25.3.04	230	30	190			50		40				35	20	122.5
15.4.04	420		110		49936	620			75580	40			25	94.3
12.5.04	190	23	25	27	79590	40		20	92550		20	35	5	64.8
15.6.04	520	10	30	20	76880	510		110	136210	50	20	30	25	83.1
13.7.04	210	40	100	20	81140	50		150	125330		30	30	15	133.0
11.8.04	220	25	80	22	89320	70			132530		70	50	20	89.2
total volume	3420	1485	825	237		2573	141	1820		372	241	375	185	1007.4

at the lower levels, particularly from RIV-2 (Oct. 2003, Apr. and Jun. 2004).

Statistical characteristics of the electroconductivity of sampled water are presented in the form of boxplots range from 180 to 615 µS/cm (Fig. 6).

Significantly higher values were recorded on the left side of the lysimeter - up to 4000 µS/cm. These most probably result from winter contamination.

Lowest electroconductivity values in the lysimeter are connected with levels I and II (Fig. 6 and 7), whereas highest values are connected with level III (Fig. 6 and 7), not with lower levels, which reflects the important role of the lateral flow component near this level. On the other hand, Figure 7 also illustrates when and where the vertical flow component dominated. Vertical breakthrough of water from level III into level IV is particularly highlighted for April 04.

Boxplots of the $\delta^{18}O$ isotopic composition of sampled water (precipitation and groundwater) are presented in Figure 8. Precipitation values range between -4.1 and -15.2 ‰ with a mean value of -8.9 ‰. Groundwater values vary between -4.5 and -14.7 ‰, whilst the means of single sampling points are between -8 and -10.7 ‰. The means that as well as the spread of $\delta^{18}O$ for the various lysimeter sampling points differ significantly. These differences most probably reflect different residence times of the seepage water. Comparison with precipitation indicates that the ranges of groundwater for the upper two levels (I, II and III) are highest, reflecting the intensive groundwater dynamics and short residence times. On the other hand, the range of groundwater values for the lower levels (IV, V and VI) are relatively small, which reflects less intensive dynamics and longer residence times.

The $\delta^{18}O$ characteristics of the sampled water are also illustrated in Figures 9 and 10, which

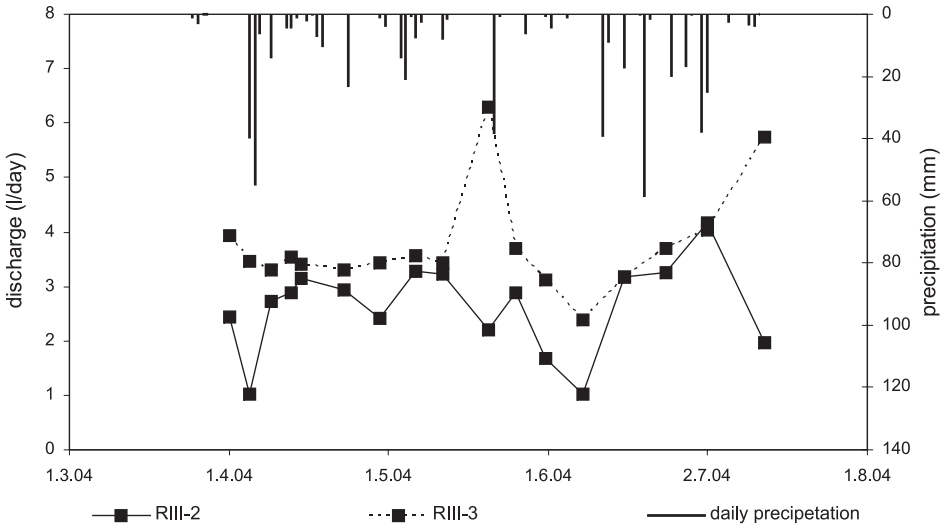

Figure 4. Daily discharge collected at lysimeter sampling points RIII-2 and RIII-3
Slika 4. Dnevni pritoki, zbrani v vzorčnih mestih RIII-2 in RIII-3

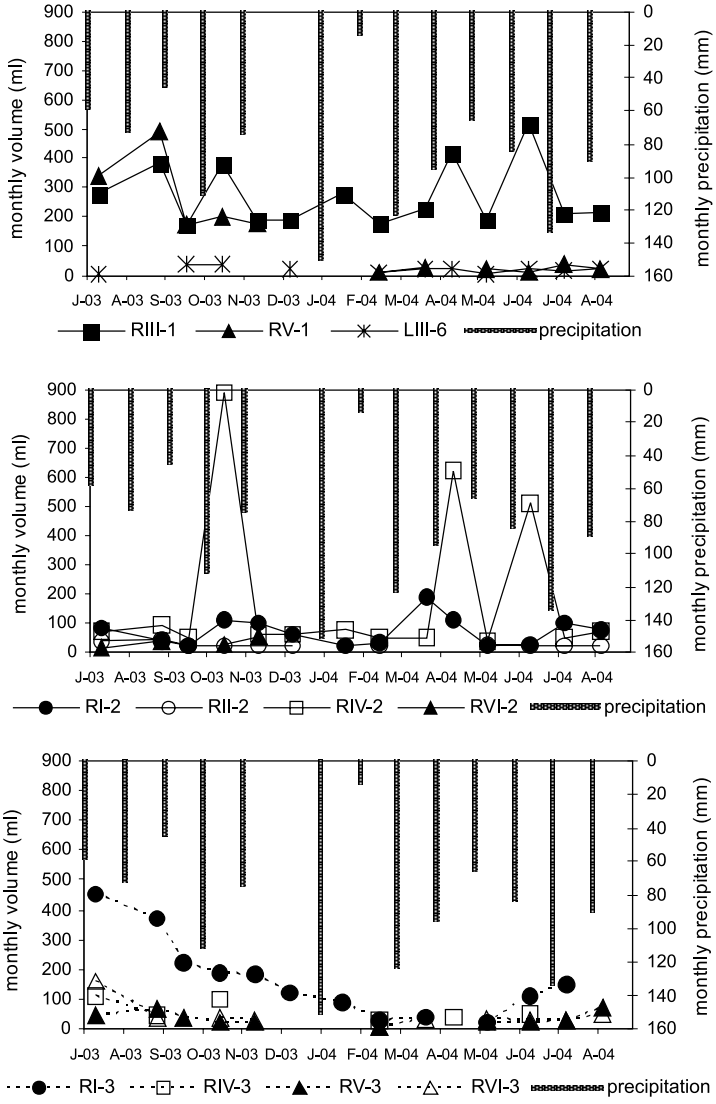

Figure 5. Monthly water volumes collected at lysimeter sampling points.
Slika 5. Mesečna količina vode, zbrana v vzorčnih mestih lizimetra

present the parameter time-trends for groundwater of the upper and lower lysimeter levels, respectively.

Comparison of $\delta^{18}O$ trends in precipitation and groundwater in Figures 9 and 10 demonstrates that variations in this parameter are much more attenuated in the lysimeter lower levels, which probably reflects longer groundwater average residence time. Peak values in both figures indicate vertical flow and solute transport in the aquifer during the main hydrological events, i.e. October 2003 and April 2004. For example, in April 2004, precipitation pushed low $\delta^{18}O$ water into the lower lysimeter levels (Fig. 10). It is

presumed that these values may have resulted from snowmelt. The influences of snowmelt may be observed in the lysimeter upper levels one month earlier (Fig. 9).

DISCUSSION AND CONCLUSIONS

Results of the first phase of the research at the Union Brewery lysimeter has produced general information on the hydrodynamic functioning of the study area and on solute transport. Synthesis of one-year of monitoring data has revealed the basic characteristics of flow and solute/ contaminant transport, since the main flow components, the flow hierarchy and the environmental response to the flow system are all indicated. Two important flow types were identified - lateral and vertical flow. Lateral flow has an important role in the protection of groundwater of the Pleistocene

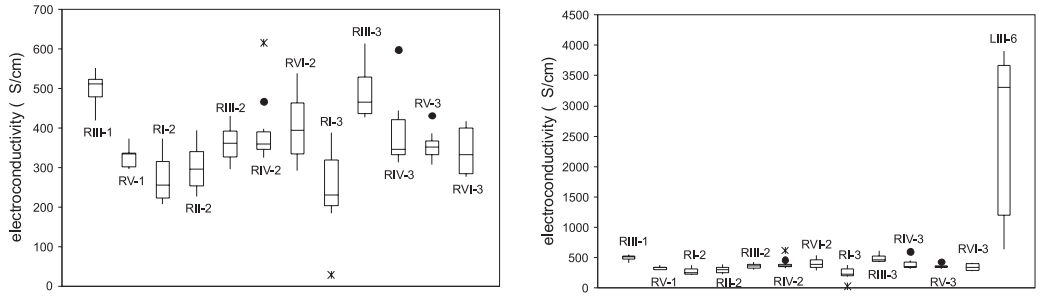

Figure 6. Boxplots of electroconductivity values for water sampled on the right and left side of the lysimeter beneath the industrial railway tracks and the asphalt surface respectively
Slika 6. Škatlasti diagrami električne prevodnosti v vodi, vzorčeni na levi in desni strani lizimetra

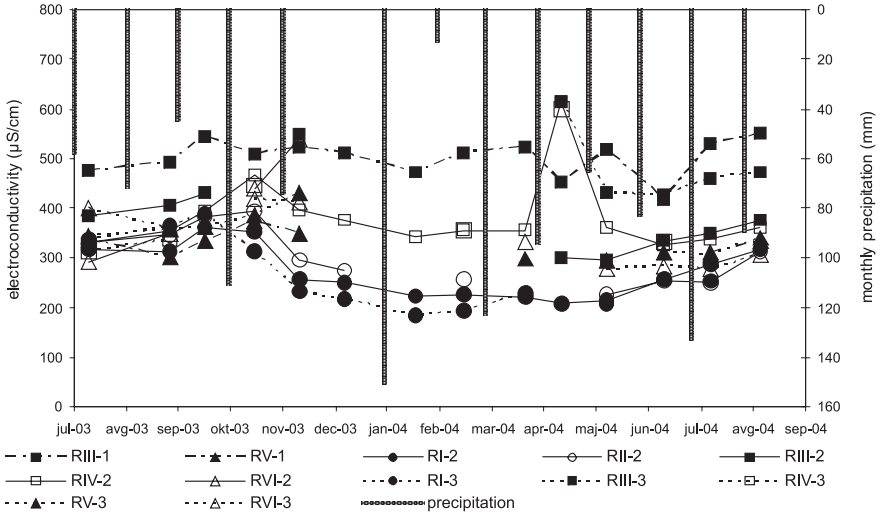

Figure 7. Time-trend plot of electroconductivity values for water sampled on the right side of the lysimeter beneath the industrial railway tracks
Slika 7. Časovno nihanje električne prevodnosti v vodi, vzorčeni na desni strani lizimetra

alluvial gravel aquifer. However, the role of vertical flow is quite the opposite, because it is the main factor controlling contaminant transport towards the aquifer saturated zone. Hence, investigation of the occurrence and frequency of rapid recharge events represents one of the main themes of the next research phase. With this regard, the monitoring of chlorides, of heavy metals and of herbicides has been established at the beginning of 2005 and the first tracing test was undertaken at the end of March 2005.

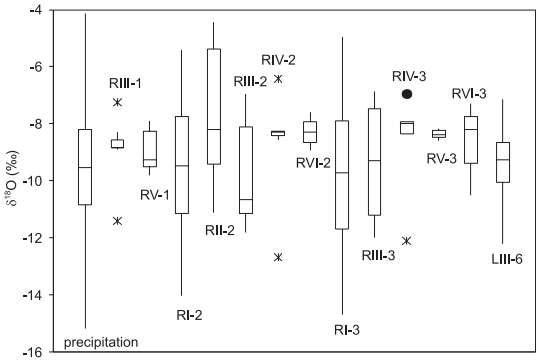

Figure 8. Box plots of $\delta^{18}O$ values in sampled water
Slika 8. Škatlasti diagram $\delta^{18}O$ vzorčene vode

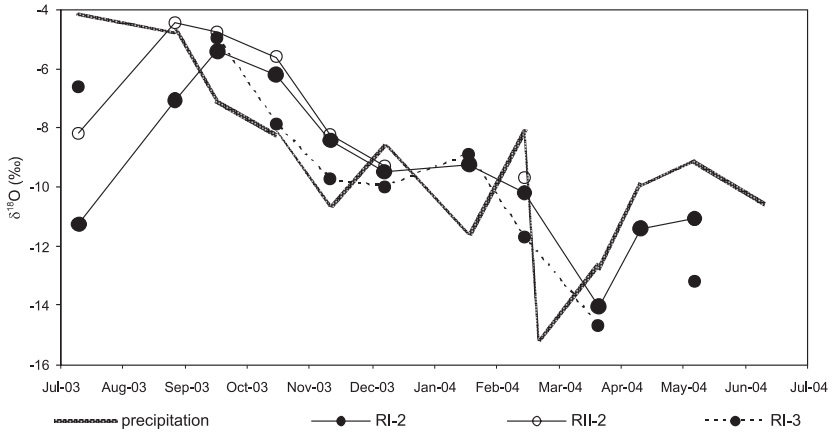

Figure 9. Time-trend plot of $\delta^{18}O$ values in water sampled from the lysimeter upper levels
Slika 9. Časovno nihanje $\delta^{18}O$ v vodi, vzorčeni v zgornjih nivojih lizimetra

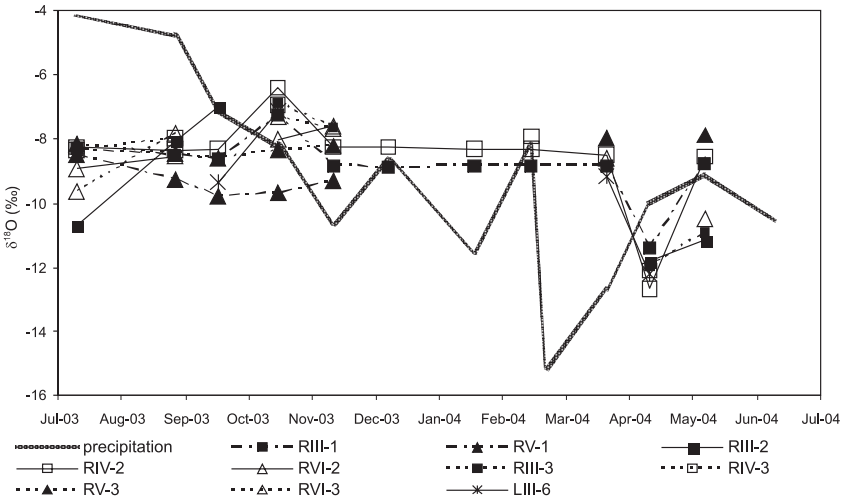

Figure 10. Time-trend plot of $\delta^{18}O$ values in water sampled from the lysimeter lower levels
Slika 10. Časovno nihanje $\delta^{18}O$ v vodi, vzorčeni v spodnjih nivojih lizimetra

POVZETEK

Proučevanje tokovnega sistema in prenosa snovi v urbanem lizimetru Pivovarne Union, Ljubljana, Slovenija

V urbanem lizimetru Pivovarne Union (sl. 1 in 2) potekajo raziskave toka in prenosa snovi v nezasičeni coni pleistocenskega prodnega vodonosnika (sl. 3), ki je vse pomembnejši vir pitne vode, ne le za Pivovarno Union, ampak tudi za mesto Ljubljana. Glavni cilj raziskav je študij vplivov industrije in prometa na omenjen vodonosnik, ki omogoča, da se prouči možnost onesnaženja virov podzemne vode na območju Pivovarne Union ter oceni vlogo nezasičene cone pri njihovi zaščiti.

V prvi raziskovalni fazi so se izvajale tedenske meritve vodne bilance in osnovnih fizikalno-kemičnih parametrov vode, poleg tega pa je potekalo tudi mesečno vzorčenje vode za analizo izotopske sestave kisika ($\delta^{18}O$).

V lizimetru se je vzorčila voda s pomočjo keramičnih svečk. 18 svečk je vgrajenih na koncu vrtin, na desni strani lizimetra (RI-1 do RI-6, RII-1 do RII-6 itd.), ki leži pod industrijskimi železniškimi tiri, 3 pa so vgrajene v vrtine na levi strani lizimetra (LI-4, LII-5 in LIII-6), ki leži pod asfaltnim območjem (sl. 2 in 3). Geološki prerez na sliki 3 kaže, da vrtine predirajo štiri različne plasti, vzorčna mesta pa so razporejena v 3 kolone in 6 nivojev na globinah 0,3-4 m.

Za prvo raziskovalno leto je prikazana vodna bilanca vzorčnih mest lizimetra v tabeli 1 ter na slikah 4 in 5. Pretoki vzorčnih mest so močno odvisni od količine in intenzivnosti padavin (sl. 4 in 5), iz tabele pa je mogoče razbrati, da največja količina vode priteka v vzorčna mesta na nivoju III. Predvideva se, da je to posledica razvoja lateralne komponente toka v bližini kontakta med dvema plastema z različno strukturo ter, posledično, različno hidravlično prevodnostjo (sl. 3). Na sliki 5 je mogoče opaziti

tudi pojavljanje vertikalnega toka iz nivoja III v nižja območja – povečana količina vode v vzorčnih mestih nižjih nivojev, zlasti na nivoju IV (oktober 2003, april in junij 2004).

Lastnosti električne prevodnosti vzorčenih vod so prikazene na slikah 6 in 7. V lizimetru so najnižje vrednosti parametra vezane na nivoja I in II, medtem ko so najvišje vrednosti vezane na nivo III in ne na nižje nivoje, kar odseva pomembno vlogo lateralne komponente toka v bližini nivoja III. Po drugi strani pa slika 7, ki prikazuje časovno nihanje električne prevodnosti v vzorčenih vodah, kaže, kdaj in kje je bilo izrazito vertikalno napajanja spodnjih nivojih lizimetra (oktobra 2003 in aprila 2004).

Lastnosti $\delta^{18}O$ so ilustrirane na slikah 8, 9 in 10. Glede na padavine imajo vode zgornjih nivojev lizimetra (I, II in III) največje razpone vrednosti, kar odseva intenzivno dinamiko in s tem kratek zadrževalni čas. Nihanje parametra je veliko bolj dušeno v spodnjem delu lizimetra (IV, V in VI), kar odseva manj intenzivno dinamiko in daljši zadrževalni čas. Na slikah 9 in 10 je treba pozornost nameniti odstopanjem od običajnih trendov. Le-ta opozarjajo na vertikalni tok in prenos snovi v vodonosniku med glavnimi hidrološki dogodki - oktobra 2003 in aprila 2004. Aprila 2004 so npr. padavine izpodrinile v spodnji del lizimetra vodo, ki je bila izotopsko osiromašena (sl. 10), kar je mogoče pripisati topljenju snega. Primerjava slik 9 in 10 kaže, da je vpliv topljenja snega opazen v zgornjem delu lizimetra že mesec prej.

Rezultati prve faze raziskav v urbanem lizimetru Pivovarne Union so opisali osnovne lastnosti toka in prenosa snovi v opazovanem okolju. Opozorili so na hierarhijo toka v nezasičeni coni vodonosnika in odziv okolja nanjo. Identificirani sta bili dve pomembni vrsti tokov - lateralni in hitri vertikalni tok. Lateralni tok ima pomebno vlogo pri zaščiti podzemnih vodnih virov pleistocenskega prodnega vodonosnika. Vloga vertikalnega toka je povsem nasprotna, saj je le-ta glavni faktor za prenos in širjenje onesnaženja proti zasičeni coni vodonosnika. Glede na to, je glavna tema druge raziskovalne faze proučevanje hitrega vertikalnega napajanja. V ta namen se je vzpostavil na začetku leta 2005 monitoring kloridov, težkih kovin in herbicidov, konec marca 2005 pa se je izvedel prvi sledilni poskus.

References

Berg, W., Čenčur Curk, B., Frank, J., Feichtinger, F., Nützmann, G., Papesch, W., Rajner, V., Rank, D., Schneider, S., Seiler, K.P., Steiner, K.H., Stenitzer, E., Stichler, W., Trček, B., Vargay, Z., Veselič, M., Zojer, H. (2001):Tracers in the unsaturated zone. *Steir. Beitr. Hydrogeol.*: 52, pp. 1-102.

Burgman, J.O., Calles, B., Westman, F. (1987): Conclusions from a ten year study of oxygen-18 in precipitation and runoff in Sweden. In: Publication of IAEA Symposium 299 on Isotope techniques in Water Resources Development. *IAEA,* Vienna, pp. 579-590.

Clark, I.D. and Fritz, P. (1997): Environmental Isotopes in Hydrogeology. *Lewis Publishershers,* New York, 311 p.

FANK, J., RAMSPACHER P., ZOJER, H. (2001): Art der Sickerwassergewinnung und Ergebnisinterpretation. In: Bericht der BAL über die Lysimetertagung, Gumpenstein, 16-17 April 1991. *BAL, Gumpenstein,* pp. 55-62.

HELSEL, D.R. & HIRSCH, R.M. (1992): Statistical Methods in Water Resources, *Elsevier*, Amsterdam, 522 p.

JUREN, A., PREGL, M., VESELIČ, M. (2003): Project of an urban lysimeter at the Union brewery, Ljubljana, Slovenia. *RMZ-Materials and Geoenvironment.* 50/3, pp. 153-156.

KENDALL, C. & MCDONELL, J.J. (1998): Isotope tracers in catchment hydrology, *Elsevier*, Amsterdam, 722 p.

KLOTZ, D., SEILER, K.P., SCHEUNERT, I., SCHROLL, R. (1999): Die Lysimeteranlagen des GSF-Forschungscentrums fuer Umwelt und Gesundheit. In: Bericht uber die 8. *Lysimetertagung. BAL, Gumpenstein*, pp. 157-160.

NIMMO, J.R. (2002): What Measurable Properties Can Predict Preferential Flow? In: Proc. of 17th World Congress of Soil Science, Bangkok, 14-21 Augut 2002. *International Union of Soil Science*, Bankog.

PEZDIČ, J. (1999): Isotopes and geochemical processes, University book, *Faculty of natural sciences, Department of geology*, Ljubljana, , 269 p.

RAIMER, D., BERTHIER, E., ANDRIEU, H. (2003): Development and results of an urban lysimeter. *Geophysical Research Abstracts*. 5, pp. 37-92.

SEILER, K.P., LOEWENSTERN, S., SCHNEIDER, S. (2000): The role of by-pass and matrix flow in the unsaturated zone for the groundwater protection. In: SILILO ET AL. (eds.), Groundwater: Past Achivements and Future Challeng. *Balkema*, Rotterdam, pp. 43-76.

TRČEK, B. (2003): Epikarst zone and the karst aquifer behaviour, a case study of the Hubelj catchment, Slovenia, *Geološki zavod Slovenije,* Ljubljana, 100 p.

Vpliv mineralne sestave in strukture na obstojnost apnencev kot naravnega kamna

The weathering durability of limestones as a function of their mineral composition and texture

Simona Jarc, Breda Mirtič

Oddelek za geologijo, NTF, Univerza v Ljubljani, Aškerčeva 12, Ljubljana, Slovenija;
E-mail: simona.jarc@ntfgeo.uni-lj.si

Received: October 17, 2004 **Accepted**: November 24, 2005

Izvleček: Določali smo vpliv mineralne sestave nekaterih vrst slovenskih apnencev na njihovo uporabno vrednost. Vzorci so bili izbrani iz nekaterih aktivnih in občasno delujočih kamnolomov apnenca: iz Hotavelj, Lesnega Brda, Drenovega Griča in Lipice. Odvzeti so bili vzorci sveže kamnine in že prepereli vzorci iz opuščenih delov kamnoloma, ki so bili okoli trideset let izpostavljeni vremenskim pogojem in delovanju različnih organizmov. Mineralna sestava je bila določena s pomočjo rentgenske difrakcije in vrstičnega elektronskega mikroskopa. S primerjavo površin svežih in že nekoliko preperelih vzorcev smo opazovali učinke preperevanja; predvsem gre za raztapljanje kamnine, vpliv insolacije in delovanja organizmov. Pogosto se različni načini preperevanja prepletajo in so medsebojno odvisni, tako da njihovih učinkov ne moremo razlikovati. Obstojnost kamnine je odvisna predvsem od strukture apnenca, ki jo pogojujeta način nastanka in vrsta diagenetskih procesov, in ne toliko od same mineralne sestave.

Abstract: The influence of the mineral composition on weathering durability of some Slovenian building limestones has been investigated. Samples were taken from some active or occasionally active quarries: Hotavlje, Lesno Brdo, Drenov Grič and Lipica. The comparison between fresh limestone samples and about 30 years weathered samples was made. The mineral composition was determined by X-ray diffraction and scanning electron microscope. The combine effects of weathering, such as dissolution, insolation and biological activity, have been documented. The weathering durability is above all the result of limestone texture, therefore the origin and diagenetic processes play more important role than mineral composition itself.

Ključne besede: apnenec, mineralna sestava, vrstični elektronski mikroskop (SEM), preperevanje
Key words: limestone, mineral composition, scanning electron microscope (SEM), weathering

Uvod

Kalcitne in dolomitne kamnine predstavljajo dobro desetino vseh sedimentnh kamnin (Morse & Mackenzie, 1990), v Sloveniji pa zavzemajo karbonatne kamnine skoraj polovico ozemlja, samo apnenci okoli 35 % (Gams, 1974). Z apnenci se srečujemo praktično na vsakem koraku. Opazujemo jih v njihovem naravnem okolju ali pa kot gradbene in okrasne elemente, tu pa se nujno pojavi vprašanje njihove obstojnosti. Glavni

Scientific paper

dejavnik obstojnosti kamnine je njena sestava. Apnenci imajo enostavno kemično in mineralno sestavo, kljub temu pa obstajajo med njimi velike razlike v obstojnosti in uporabni vrednosti. Izbrani slovenski apnenci so razmeroma čisti; vsebujejo preko 91 mas.% $CaCO_3$.

Z elektronskim mikroskopom opazujemo obliko mineralov, strukturo, vezivo v kamninah veliko bolj natančno kot z optičnim mikroskopom. Omenjene lastnosti močno vplivajo na obstojnost kamnine. Elektronski mikroskop se zelo veliko uporablja prav za opazovanje preperelih površin kamnin (VILES & MOSES, 1998).

PREISKOVANE VRSTE APNENCEV

Apnenec iz Hotavelj je cordevolske starosti, izrazito pisan in mineralno nehomogen. Kamnino po Folku imenujemo intrabiomikrosparit (BILBIJA & GRIMŠIČAR, 1987, RAMOVŠ, 1987). Obarvanost hotaveljskega apnenca je posledica določenih primesi, to pomeni, da se kemična in mineralna sestava nekoliko spreminjata, zato smo poskušali dobiti čimbolj enakomerno obarvane vzorce apnenca. Ločili smo tri barvne različke: sivega (v nadaljevanju ga označujemo kot HS, rožnatega (HR) in rdečega (HRd). Zaradi pogostih leč ali plasti nekarbonatnega materiala v hotaveljskem apnencu smo le-te poskušali analizirati kot samostojni vzorec (HV).

Pisani apnenec z Lesnega Brda je po nastanku, starosti, sestavi in lastnostih skoraj enak hotaveljskemu (MIRTIČ ET AL, 1999). Tudi lesnobrdski apnenec je zelo pisan, od sive do rožnate barve, sivega različka je relativno manj, zato smo v preiskavah uporabili samo rožnati različek (LBRd). Črni karnijski apnenec z Drenovega Griča (vzorec DGC) je nekoliko mlajši od pisanega cordevolskega apnenca z Lesnega Brda.

V Lipici ločimo glede na velikost skeletnega drobirja dve vrsti apnenca, enotni in rožasti. V obeh primerih gre za rekristalizirana biomikritna apnenca zgornjekredne starosti, ki se razlikujeta v teksturi. To razlikovanje, ki ga uporabljajo v kamnarski industriji, smo ohranili: vzorec enotnega apnenca označujemo kot LiU, vzorec rožnatega apnenca kot LiF (JARC, 1996, JARC, 2000).

METODE DELA

Kemično analizo preiskovanih apnencev so opravili v laboratoriju ACME v Kanadi. Določili so količino SiO_2, Al_2O_3, Fe_2O_3, MgO, CaO, Na_2O, K_2O, TiO_2, P_2O_5, MnO, Cr_2O_3, Sr, žarilno izgubo (LOI – loss of ignition) z metodo induktivno vezane plazme emisijske spektrometrije (ICP-ES), celotni ogljik in žveplo pa z Leco (ACME, 1999). Za silikatno analizo so 0,2 g vzorca talili z 1,2 g $LiBO_2$ in raztopili v 100 ml 5 % HNO_3. Žarilno izgubo (LOI) so določili glede na spremembo mase vzorca po 1 uri žganja pri temperaturi 1000 °C. Rezultati kemične analize so v tabeli 1.

Difraktogrami vseh vzorcev so bili posneti na rentgenskem difraktometru Philips, na Oddelku za geologijo. Pogoji snemanja so bili naslednji: sevanje Cu_Ka, Ni filter, napetost 40 kV, tok 20 mA, hitrost snemanja 2,5°/minuto, območje snemanja 2q od 2° do 70°. Z metodo rentgenske difrakcije so bili v vzorcih določeni sledeči minerali:

Tabela 1. Kemična sestava vzorcev. Količine oksidov, žarilne izgube (LOI), ogljika in žvepla so v masnih odstotkih, stroncija v ppm.
Table 1. Chemical composition of investigated samples. All oxides, carbon, sulfur and loss of ignition content are in %, strontium in ppm.

	SiO_2	Al_2O_3	Fe_2O_3	MgO	CaO	Na_2O	K_2O	TiO_2	P_2O_5	MnO	Cr_2O_3	Sr	LOI	C/TOT	S/TOT
HS1	0,21	0,17	0,05	0,91	54,91	0,03	<0,04	0,01	0,04	0,02	0,004	101	43,6	11,8	0,01
HS1p	0,38	0,15	0,05	0,94	54,56	<0,01	<0,04	<0,01	0,02	0,02	0,004	100	43,7	11,4	0,01
HS2	0,31	0,17	0,07	0,69	55,42	0,02	0,04	0,01	0,03	0,02	0,003	98	43,2	11,7	0,01
HR1	1,12	0,48	0,21	0,67	53,85	0,04	0,12	0,01	0,05	0,03	0,002	96	43,4	11,6	0,01
HR2	1,33	0,64	0,24	0,62	54,03	0,02	0,19	0,02	0,04	0,03	0,001	95	43	11,4	0,01
HRd1	0,58	0,31	0,59	0,52	54,24	<0,01	0,06	0,01	0,04	0,05	0,006	99	43,6	11,3	0,01
HRd2	0,84	0,42	0,75	0,45	54,08	0,04	0,12	0,01	0,03	0,05	0,006	94	43,1	11,5	0,01
HRd2p	0,95	0,42	0,72	0,46	54,16	<0,01	0,12	<0,01	0,02	0,05	0,003	95	43,1	11,5	0,01
HRd3	0,83	0,42	0,79	0,47	54,49	0,01	0,1	0,01	0,01	0,05	0,001	96	42,9	11,8	0,01
HV1	17,29	8,36	5,91	5,09	29,75	0,03	3,07	0,18	0,05	0,08	0,01	59	30,2	7,61	0,01
HV2	18,44	8,77	6,09	4,78	28,96	0,01	3,26	0,19	0,07	0,08	0,01	55	29,4	7,07	0,03
LBRd1	1,26	0,77	0,29	0,42	54,00	0,03	0,12	0,04	0,08	0,01	0,003	133	42,9	11,2	0,01
LBRd2	1,66	0,99	0,34	0,44	53,82	0,02	0,18	0,04	0,01	0,01	0,005	110	42,5	11,4	0,01
DGC1	1,47	0,77	0,51	0,83	51,75	0,03	0,12	0,03	0,02	0,01	0,004	972	44,4	13,1	0,23
DGC2	1,73	0,88	0,82	0,77	51,00	0,05	0,11	0,04	0,01	0,01	0,002	1055	44,5	14,2	0,37
LiU1	<0,02	0,12	0,07	0,35	55,63	0,02	<0,04	0,01	0,01	<0,01	0,001	189	43,7	11,7	0,01
LiU2	0,02	0,1	0,1	0,3	55,96	0,01	0,04	0,02	0,03	<0,01	0,01	188	43,4	11,7	0,03
LiF1	<0,02	0,09	0,07	0,31	55,76	0,03	<0,04	0,01	0,03	<0,01	0,004	261	43,6	11,6	0,01
LiF2	<0,02	0,08	0,09	0,28	56,03	0,02	<0,04	<0,01	0,02	<0,01	0,006	220	43,4	11,7	0,04

- Hotavlje sivi (HS1, HS2): kalcit, dolomit, vermikulit, muskovit.
- Hotavlje rožnati (HR1, HR2): kalcit, muskovit.
- Hotavlje rdeči (HRd1, HRd2, HRd3): kalcit, muskovit, pirit, vermikulit.
- Hotavlje vložki (HV1, HV2): kalcit, klorit, hematit, dolomit, muskovit.
- Lesno Brdo (LBRd1, LBRd2): kalcit, klorit, muskovit.
- Drenov Grič (DGC1, DGC2): kalcit, klorit, kremen.
- Lipica enotni (LiU1, LiU2): kalcit, klorit.
- Lipica rožasti (LiF1, LiF2): kalcit, klorit.

Pripravo vzorcev in samo mikroskopiranje na vrstičnem elektronskem mikroskopu (SEM) smo opravili na Inštitutu Jožef Stefan. Vzorce smo spolirali z diamantno pasto granulacije 0,25 mm in jih naparili z grafitom. Na posameznih mestih smo s pomočjo odbitih elektronov skušali ugotoviti elementno sestavo.

Površine svežih in preperelih vzorcev smo opazovali s pomočjo sekundarnih elektronov. Prepereli vzorci so bili odvzeti na površini opuščenih delov kamnolomov, kjer so bili okoli 30 let izpostavljeni naravnim procesom preperevanja. Vzorcev nismo spolirali, predhodno smo jih samo ultrazvočno očistili, zvakumirali in naparili z grafitom in zlatom.

Rezultati in razprava

V **apnencu iz Hotavelj** prevladujejo euhedralna romboedrska zrna kalcita z gladkimi ploskvami, velikosti okoli 10 mm. Na posameznih mestih jih sekajo večje žile

in leče drobnozrnatega kalcita, glinenih mineralov, glinencev (ortoklaz in albit) ter pirita. Te minerale smo potrdili tudi z elementno analizo.

Sivi različek hotaveljskega apnenca ima največ MgO, ki pa kljub vsemu ne presega 1 mas.%, kar ustreza približno 0,6 mas.% magnezija (tabela 1). Z rentgensko difrakcijo smo zasledili tudi dolomit. Velikost kalcitnih sparitnih kristalov je v povprečju okoli 20 mm. Gre za zelo čist $CaCO_3$, ki vsebuje le okoli 0,36 mas.% magnezija. Količina magnezija je tako majhna, da ne moremo ugotoviti, ali je enakomerno razporejen v kalcitni rešetki ali je koncentriran na posamezna področja. Na redkih mestih opazimo več kot 100 mm velika sparitna zrna, ki niso homogena, vsebujejo nekoliko več magnezija (okoli 0,73 mas.%). Razporeditev z magnezijem bogatejših delov je popolnoma naključna čez celoten presek preiskovanega vzorca in jo lahko opazujemo le, če je sparitni kristal dovolj velik. Pri kristalih manjših dimenzij pa dobimo le povprečno količino magnezija (0,36 mas.%). Apnenec je malo porozen, gre za zaprto poroznost, pore pa dobimo na mejah posameznih sparitnih polj. Vzorec je zelo nehomogen. Takoj, ko je poroznost nekoliko večja, so v apnencu tudi glineni minerali. Z uporabljenimi metodami ne moremo ugotoviti načina nastanka glinenih mineralov: lahko predstavljajo netopne ostanke, nastale pri raztapljanju apnenca zaradi delovanja pornih in meteornih vod, ali so sekundarnega nastanka. Oblika por pa kaže, da litifikacija kamnine še ni popolna. Elementarna analiza glinenih mineralov pokaže natrij, magnezij, aluminij in silicij ter kisik (glinene minerale vermikulitove skupine je pokazala tudi rentgenska difrakcija); natančnejša kvalitativna analiza glinenega minerala je nemogoča, ker so kristali premajhni in okolica moti.

Analiza površine **rdečega hotaveljskega različka** pokaže, da je količina magnezija v celotnem vzorcu približno enaka (približno 0,27 mas.% Mg). Apnenec je, kljub majhni količini železa (0,33 mas.%), intenzivno obarvan. Rdeči različek hotaveljskega apnenca ima med vsemi vzorci največ Fe_2O_3 (tabela 1). Z rentgensko analizo smo ugotovili prisotnost pirita, vendar ga pod elektronskim mikroskopom nismo zasledili. Prav tako nismo opazili glinenih mineralov. Poleg karbonatnih mineralov pa so v vzorcu tudi nepravilno oblikovana, približno 70 mm velika kremenova zrna.

Glede na rezultate rentgenske difrakcije ima **rožnati različek hotaveljskega apnenca** najmanj pestro sestavo. Sparitni deli se menjavajo z bolj poroznimi in z magnezijem nekoliko bogatejšimi mikritnimi deli. Mikritni deli vzorca imajo tudi več drobnih glinenih mineralov (sestave magnezij, kalij, aluminij, silicij in kisik) in podolgovate kristale muskovita. Poleg omenjenih elementov je v vzorcu tudi železo, ki povzroča značilno obarvanost tega hotaveljskega različka. Sparitni deli pripadajo čistemu $CaCO_3$, magnezija ne zaznamo. Poleg kalcita in muskovita pa smo pod elektronskim mikroskopom opazili majhna, nekaj 10 mm velika, nepravilna kremenova zrna in večja, do 150 mm velika zrna kalijevega glinenca.

Opazovanje **vzorca HV** pod optičnim mikroskopom pokaže večja sparitna polja (800 mm) relativno čistega kalcita, ki so med seboj ločena z velikimi razpokami. Te so zapolnjene z glinenimi minerali, sekun-

darnim karbonatom in železovimi minerali. V sparitu dobimo nepravilno oblikovana zrna kremena (80 mm), podolgovata zrna muskovita in pirit. V vezivu prevladujejo glineni minerali, muskovit, veliko je tudi železa. Če elementarno analizo primerjamo z rezultati rentgenske difrakcije, je železo vezano na hematit, ki to vezivo značilno obarva. Poleg kalcitnih kristalov so v vzorcu tudi lepi kristali 900 mm velikega conarnega dolomita. Verjetno gre za poznodiagenetski dolomit. Conarnost ni rezultat različne sestave; razmerje magnezija in kalcija je povsod približno enako, 1:3. Razlika je torej v optični orientaciji dolomita. Sklepamo, da gre za sintaksialni dolomitni cement, ki je precipitiral v okolni prazni prostor, ki je nastal s predhodnim raztapljanjem $CaCO_3$ (Krinsley et al., 1998).

Opazovanje obrusov pokaže, da barvnih različkov **hotaveljskega apnenca** med seboj ne moremo ločiti. Izstopa le različek HV, kar pa je razumljivo, saj je tudi kemično in mineraloško popolnoma drugačen. Površina preperelega apnenca ima popolnoma drugačen videz (slika 1). Že pri majhni povečavi lahko opazimo pore, ki jih pri svežem vzorcu apnenca še nismo opazili. Nekatere pore imajo obliko kalcitnih zrn. V takšnih primerih so nastale pore lahko rezultat fizikalnega preperevanja: temperaturne razlike in zmrzali so razrahljale vezi med kristali, zrno pa je izpadlo. Močno je tudi biogeno preperevanje. Izrazito okrogle pore so nastale z vrtanjem organizmov v substrat. Gre torej za kombinacijo kemičnega, fizikalnega in biogenega preperevanja (Summerfield, 1994).

Naravne vode imajo navadno rahlo kisel do rahlo alkalen pH (Ford & Williams, 1994, Drever, 1997). V tem območju je raztapljanje omejeno predvsem s hitrostjo reakcij na površini trdne faze in ne toliko s hitrostjo izmenjave ionov med trdno fazo in

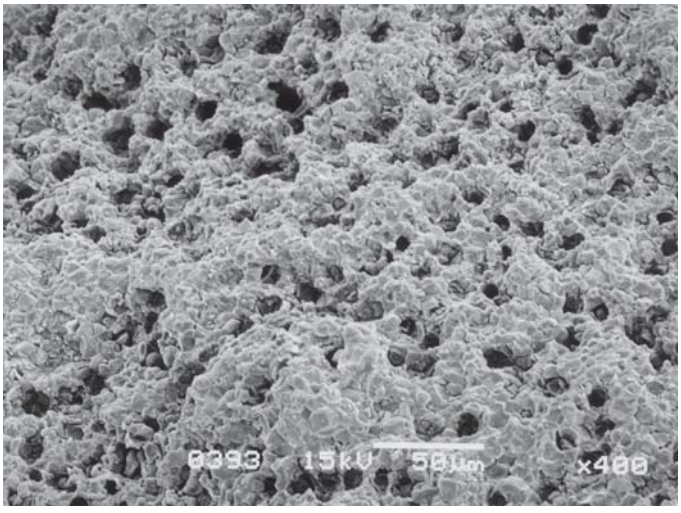

Slika 1. Preperela površina vzorca apnenca iz Hotavelj (HR). Izrazito okrogle pore so rezultat vrtanja organizmov.
Figure 1. Weathered surface of the Hotavlje limestone (HS). Rounded pores are the result of biogenic activity.

raztopino (MORSE, 1983). Kadar je raztapljanje odvisno predvsem od reakcij na površini, je rezultat povečan relief trdne faze. Raztapljanje v tem primeru poteka namreč samo na nekaterih mestih na površini. Na večjih kalcitnih kristalih lahko opazujemo primer takšnega raztapljanja vzdolž razkolnih ploskev (slika 2), ki predstavljajo mesta povečane reaktivnosti. Če pa je hitrost raztapljanja omejena s hitrostjo transporta izmenjave ionov med trdno fazo in okolno raztopino, torej z difuzijo, je navadno raztapljanje na površini bistveno hitrejše in enakomernejše, posledica je obljenje površine (BERNER, 1981, MORSE, 1983).

Primer selektivnega raztapljanja prikazuje slika 3. Površina večjega kalcitnega kristala ni ravna, temveč ima luskast videz. Tudi meje med posameznimi zrni so vse bolj izrazite, razpoke se širijo, obenem je močnejši vpliv fizikalnega preperevanja in končni učinek je izpad celega kalcitnega kristala, nastala pora ima obliko karbonatnega zrna. Elementna analiza je pokazala, da je v kalcitu tudi manjši delež magnezija. Kvantitativne analize sestave na nepoliranih vzorcih niso pravilne, saj so odboji elektronov tudi posledica reliefa in ne le elementne sestave. V obravnavanem primeru lahko govorimo le o kalcitu z manjšim deležem magnezija. Obenem z raztapljanjem prihaja tudi do obarjanja; na površini večjih kalcitnih zrn opazujemo drobne, pod 5 mm velike kristale kalcita.

Še večji je vpliv preperevanja na bolj mikritnem delu hotaveljskega apnenca; zaobljenost kristalov je večja, topografija je še izrazitejša. Mikrit ima večjo specifično površino kot sparit in je zato tudi bolj reaktiven. Topnost minerala narašča eksponencialno z njegovo specifično površino (MORSE & MACKENZIE, 1990). Drobni delci se raztapljajo drugače kot veliki, manjša zrna se lahko adhezivno vežejo na večja in tako preprečujejo njihovo raztapljanje (MACKENZIE ET AL., 1983). Zelo pomembna je tudi heterogenost velikosti

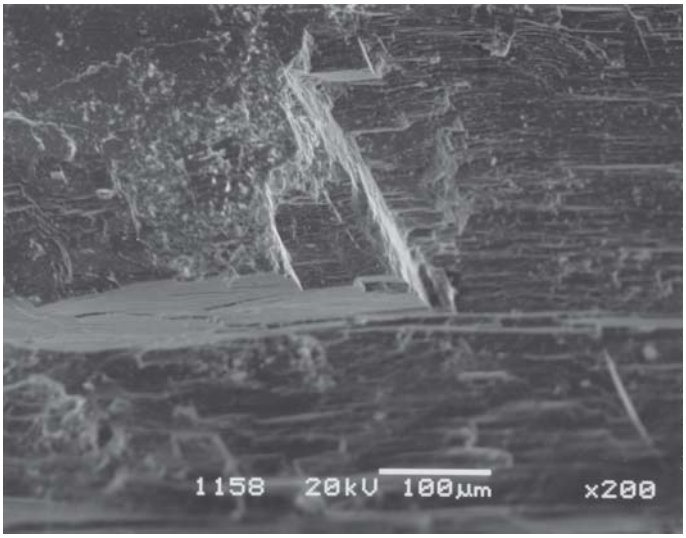

Slika 2. Raztapljanje vzdolž razkolnih ploskev (vzorec HV).
Figure 2. Dissolution on cleavage planes (sample HV).

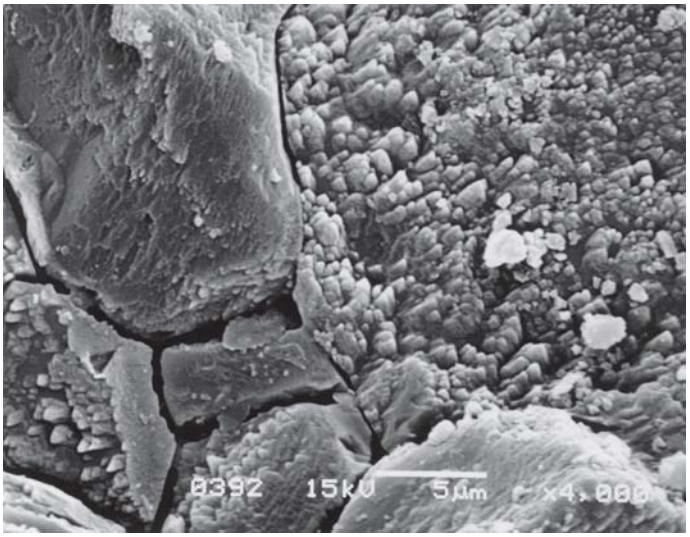

Slika 3. Večje kalcitno zrno ima luskast videz, ki je posledica selektivnega raztapljanja. Mikritni deli so bolj prizadeti in gradijo nižje dele površine (vzorec HS).
Figure 3. As a result of selective dissolution the surface of bigger calcitic grain is rough. Micrite is even more weathered and is found on concave parts of the sample (sample HS).

mineralnih zrn. Čim večje so razlike velikosti zrn v strukturi, hitreje poteka raztapljanje. Tako je biomikrit bolj topen kot čisti mikrit. Najbolj topni so biomikritni apnenci, hitrost raztapljanja pa se bistveno zmanjša, če jih sestavlja več kot 40 do 50 % sparita (Ford & Williams, 1994).

Obnašanje kamnine v vlažnem okolju je v splošnem določeno z mikrostrukturo, še posebej s strukturo por (Meng, 1992). Pri študiju preperevanja kamnin je pomembna t.i. efektivna velikost por (to so tiste pore, ki so pomembne za transport vode v kamnini). Voda povzroča tako kemijsko kot fizikalno razpadanje (Amoroso & Fassina, 1983). Kamnina, izpostavljena fizikalnemu razpadanju, je bolj podvržena tudi večjim kemičnim in biološkim spremembam, ker povečana površina in olajšan dostop zraku, vodi in drugim snovem, pomeni intenzivnejše kemične reakcije. Velika razpokanost kamnine torej močno pospeši preperevanje in tako zmanjšuje njeno obstojnost.

V **lesnobrdskem apnencu** opazujemo polja sparita, ki jih sekajo številne žilice in žile, zapolnjene z glinenimi minerali (klorit) in muskovitom ter kremenom, elementarna analiza je pokazala, da je poleg kalija, magnezija, aluminja, silicija in kisika tudi železo, ki daje kamnini barvo, z elementno analizo pa smo ugotovili tudi malo fosforja. Lahko je detritičnega ali organskega izvora. Tudi kemična analiza vzorca LBRd pokaže nekoliko povečano količino P_2O_5 (0,08 mas.%) glede na ostale vzorce. Na posameznih mestih najdemo lepe kristale apatita, velikosti 10 mm, ki je najverjetnejši vzrok za povečano količino fosforja v vzorcu. Tudi v tem vzorcu je količina magnezija v sparitu premajhna, da bi lahko ločili mesta s povečano koncentracijo magnezija od mest čistega $CaCO_3$.

Površine subhedralnih kalcitnih zrn, velikosti 5 mm, so gladke, ravne, poroznost je zelo majhna. Na posameznih mestih v lesnobrdskem apnencu opazimo zelo velike (celo več kot 500 mm) kristale kalcita, ki so praktično nepoškodovani (slika 4), mikritni deli so bolj prizadeti in gradijo nižje dele površine. Najbolj intenzivno je raztapljanje na mejah zrn, velja: čim manjši so delci, večja je specifična površina, večje je raztapljanje. Raztapljanju so močno izpostavljene razkolne razpoke in razpoke nastale zaradi tektonskih procesov (slika 5). Okrogle pore (nimajo oblike kalcitnih kristalov) so rezultat vrtanja organizmov v substrat. Raztapljanje je bolj intenzivno vzdolž že obstoječih razpok kot vzdolž razkolnih ploskev.

Relief apnenca je posledica različne velikosti kalcitnih zrn; dvignjeni deli so bolj debelozrnati in so manj prizadeti kot konkavni deli na površini vzorca. Le-ti so zgrajeni iz drobnih, navadno z nečistočami bolj bogatih kalcitnih kristalov. Nepravilnosti in primesi v kalcitni rešetki povzročajo napetosti v strukturi, kar povzroča večjo nestabilnost mineralne faze. Sistem teži k zmanjšanju te energije (WENK ET AL., 1983), torej so ta mesta bolj dovzetna za raztapljanje. Procesi raztapljanja se izmenjujejo z vmesnimi fazami precipitacije mineralov. Novonastali minerali so navadno zelo drobnozrnati, njihovi kristali so slabo razviti, saj je rast hitra, substrat pa jim predstavljajo starejša mineralna zrna (sliki 4 in 5).

Glede na velikost zrn in fosilnih ostankov ločimo dva tipa **lipiškega apnenca**: enotni in rožasti, ki pa se po kemijski in mineralni sestavi praktično ne razlikujeta med seboj. Apnenec iz Lipice je med vsemi preiskovanci najbolj čist. Vsebuje preko 99 mas.% $CaCO_3$,

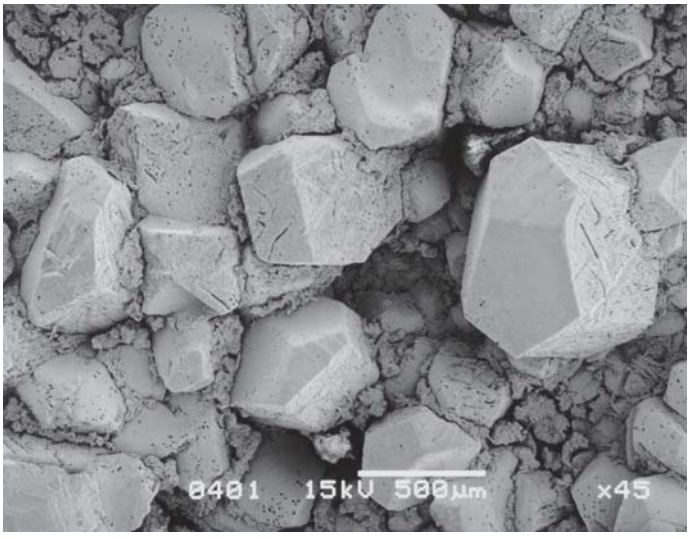

Slika 4. Na površini kalcitnih romboedrov opazujemo selektivno raztapljenje in precipitacijo sekundarnega kalcita (Vzorec LBRd).
Figure 4. The effect of selective dissolution on calcite rombohedra and the precipitation of secondary calcite at the same time.

torej je delež primesnih mineralov zelo majhen. Kljub temu smo z rentgensko difrakcijo ugotovili prisotnost glinenih mineralov iz kloritove skupine. Količina MgO je, glede na kemično analizo, v obeh strukturnih različkih okoli 0,3 mas.%, sparitni deli skoraj nimajo magnezija (pod mejo detekcije), v mikritnih delih pa je magnezija nekoliko več; včasih tudi do 0,5 mas.%.

Enotni apnenec je bolj enakomernozrnat. Poleg kalcita so posamezna zrna glinencev, gre za kalijeve in natrijeve glinence velikosti okoli 30 mm, ki se včasih tudi medsebojno preraščajo. Ugotovili smo tudi apatit, ki vsebuje malo žvepla. Redke žilice zapolnjujejo drobni kristalčki glinenih mineralov - klorita. Pore imajo obliko izpadlih kalcitnih kristalov; verjetno so nastale pri pripravi vzorca.

Mineralna sestava rožastega različka je enaka kot pri enotnem. Bistvena razlika med apnencema je v zrnavosti. Rožasti apnenec je zelo nehomogen, v njem se menjavajo veliki sparitni kristali z mikritnimi območji (5 mm). Pore so bolj pogoste kot pri enotnem različku; gre za zaprto poroznost. Majhen del por je tudi tu nastal pri pripravi vzorca.

Apnenec z Drenovega Griča je po sestavi zelo pester. S kemično analizo smo ugotovili zelo veliko primesi: baker, magnezij, aluminij, silicij, žveplo, železo... Reliefna preperela površina ni rezultat razlike v sestavi, pač pa je nastali relief posledica različne velikosti delcev. Mehansko in kemično preperevanje pospešujejo še organizmi.

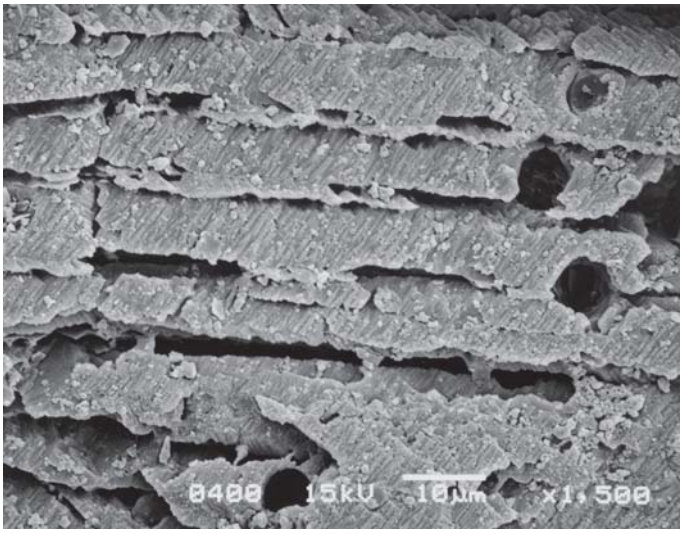

Slika 5. Močno preperela površina apnenca. Ločimo lahko tri vrste razpok: - najbolj intenzivno je raztapljanje v podolžni smeri, vzdolž že obstoječih razpok, nastalih zaradi tektonskih procesov; - razpoke vzdolž razkolnih ploskev; - okrogle pore so rezultat delovanja organizmov (vzorec LBRd).
Figure 5. Highly weathered limestone surface. Three types of fissures can be distinguished: - the dissolution along tectonic fissures is the most intensive; - fissures on the cleavage planes; - rounded fissures of biogenic origin (sample LBRd).

Pri večji povečavi opazimo, da so kristali kalcita nepravilnih oblik; gre za anhedralna zrna, velika okoli 5 mm. Površine kristalov niso ravne, nekateri robovi zrn so deloma že zaobljeni. Površine kristalov na konveksnem delu površine so bolj reliefne, njihovi robovi pa so ravni in do zaobljevanja še ni prišlo (tu je izrazitejše selektivno raztapljanje). Medtem ko so kalcitni kristali na konkavnih mestih na površini vzorca bolj zaobljeni, njihove površine pa so manj poškodovane.

Primer močno prizadetih kristalov kalcita je na sliki 6. Po sestavi gre za kalcit z malo magnezija. Na površini so že nastale manjše razpoke, ob katerih je raztapljanje intenzivnejše. Stiki med zrni so lepo vidni, zrna so tudi že dobro zaobljena. Kristalni defekti predstavljajo točke začetka raztapljanja. Kjer so kristalne ploskve pravilne, so njihove površine gladke, robovi so ostri, v nasprotju s tistimi mesti, kjer so kristalne ploskve slabše razvite ali so bile nepravilnosti v kristalni strukturi in sestavi. Kemična analiza je pokazala, da je v kristalih kalcita na takšnih mestih še magnezij, kalij, železo, titan, aluminij in silicij. Izvora teh elementov z omenjenimi metodami nismo mogli določiti, verjetno pa je bil vsaj del teh elementov vnešen v kamnino kasneje. Možno pa je, da je del kristala, ki je bolj poškodovan, imel povišano količino magnezija in železa, ki sta pospešila raztapljanje. Idealni, stehiometrijski kristal brez defektov je najbolj stabilna oblika minerala. Zaradi substitucije kationov in anionov ter mrežnih defektov se obstojnost mineralov zmanjšuje (BLATT & TRACY, 1995).

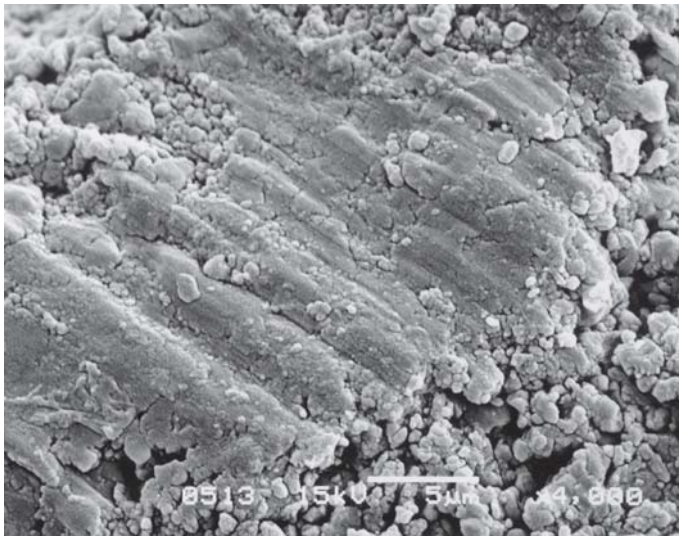

Slika 6.Močno preperel kalcit s povečano vsebnostjo magnezija (Vzorec DGC).
Figure 6. Weathered calcite with increased magnesium content (Sample DGC).

Sklepi

Obstojnost in s tem uporabna vrednost apnencev, ki se uporabljajo kot naravni kamen, je odvisna od kemične in mineralne sestave ter njihovih strukturnih značilnosti. Preiskovani slovenski apnenci, z izjemo vzorca glinenih vložkov v hotaveljskem apnencu, so kemično relativno čisti $CaCO_3$. Z izjemo apnenca z Drenovega Griča (91 mas.% $CaCO_3$) imajo preko 95 mas.% $CaCO_3$. Po sestavi so si zelo podobni, delež primesnih prvin je relativno majhen.

Z elektronskim mikroskopom lahko zelo učinkovito ločimo nekarbonatne minerale v karbonatnih kamninah. Nekarbonatni minerali nastopajo kot detritična zrna (kremen, glinenci, sljude, apatit…) ali kot kasneje nastali, diagenetski minerali (kremen, pirit, hematit, apatit, barit, anhidrit). Količina magnezija v kalcitu je premajhna, da bi lahko s pomočjo elektronskega mikroskopa točno določili lego primesi v kalcitni rešetki. Na splošno večji sparitni kristali vsebujejo manj magnezija kot mikrosparitni ali mikritni deli in tudi poroznost je v sparitnem delu bistveno manjša kot v mikritnem delu.

Predvsem velikost in habitus kristala določata njegovo odpornost. Konveksne dele preperele površine gradijo v glavnem sparitni kristali z lepo razvitimi ploskvami, kjer je navadno tudi manj magnezija v strukturi kot v mikritu, ki je raztapljanju in fizikalnim učinkom površinskega spreminjanja bolj podvržen. To ugotovitev smo lahko potrdili pri vseh preiskovanih vrstah apnenca.

Iz oblikovanosti por lahko sklepamo na njihov nastanek. Okrogle pore so biogenega nastanka, pore, nastale zaradi izpadanja kristalov, imajo obliko le-teh, pore z nepravilnimi zaobljenimi robovi pa so nastale zaradi raztapljanja mineralnih zrn. Na površini kalcitnih kristalov pa lahko ločimo tri vrste sekundarnih razpok: razpoke, ki so posledica naključnega raztapljanja, razpoke vzdolž razkolnih ploskev (z značilno usmerjenostjo) in razpoke, ki nastanejo zaradi lomljenja in drobljenja mineralnih zrn. Le-to povzroča raztapljanje in fizikalno preperevanje.

Tudi rezultati rentgenske difrakcije ne pokažejo večjih razlik med apnenci. Mineralna sestava apnencev ne more povzročiti tako velikih razlik v reaktivnosti oziroma obstojnosti kamnine. Obstojnost kamnine zaradi procesov preperevanja je odvisna predvsem od strukture apnenca, ki jo pogojuje način nastanka in vrsta diagenetskih procesov.

Summary

The weathering durability of limestones as a function of their mineral composition and texture

The effects of atmospheric weathering on some limestones from Slovenia were investigated by electron microscope. Samples were chosen from several active or temporary active limestone quarries: Hotavlje, Lesno Brdo, Drenov Grič and Lipica. Samples of fresh rock and weathered rock from abandoned parts of the quarries were taken as well. The weathered rock samples have been exposed to atmospheric conditions and effects of different organisms for about thirty years.

Investigated limestone samples are very homogenous; they are chemically relatively pure $CaCO_3$. The samples HV represent the clay layer within the Hotavlje quarry. Limestones consist of more than 95 % of $CaCO_3$. The only exception is the limestone from Drenov Grič with the 91 % $CaCO_3$. Being so alike, they are very hard to be distinguished. Some rare noncarbonate minerals represent the detritic grains (quartz, feldspars, mica, apatite...) and/or younger diagenetic minerals (quartz, pyrite, hematite, apatite, mica, anhydrite). Magnesium content in calcitic grains is also detectable. The bigger the sparite crystal is the smaller is the magnesium content. Therefore, the micritic parts have more variable chemical composition and the porosity is higher, too. The weathered surfaces display the influence of crystal size and habit on the limestone durability. The convex parts of the weathered sample consist of well shaped bigger sparitic crystals with fine developed crystal planes, whereas the concave parts are more micritic, with higher content of magnesium and other impurities.

The pores in limestone are of different origin: rounded pores are the result of biological activity, some pores have the shape of the calcitic grains and some of them have irregular shapes and are the result of selective dissolution of carbonate because of the higher impurity content in calcite lattice.

Also, the results of X-ray diffraction do not show some major differences between investigated limestones. Therefore, the high differences in weathering durability of the limestones are not caused by the chemical and mineralogical composition, rather are the result of limestone texture. The size of the calcite crystal and its habit are the most important features in durability of stone. The content of impurities in calcite lattice is also important, too.

REFERENCE

ACME (1999): ACME analytical laboratories brochure. *Acme Analytical Laboratories, Ltd.,* Vancouver; 18 p.

AMOROSO, G.G. & FASSINA, V. (1983): Stone decay and conservation, atmospheric pollution, cleaning, consolidation and protection. *Elsevier Science,* Amsterdam; 453 p.

BERNER, R.A. (1981): Kinetics of weathering and diagenesis. *Reviews in mineralogy,* 8, 111–134, Washington.

BILBIJA, N. & GRIMŠIČAR, A. (1987): Obstojnost arhitektonskega naravnega kamna iz Slovenije. *Geološki zbornik 8,* 151-160, Ljubljana.

BLATT H. & TRACY, R.J. (1995): Petrology: Igneous, sedimentary and metamorphic. W.H. *Freeman and Company,* New York; 529 p.

DREVER, J.I. (1997): The geochemistry of natural waters. *Surface and groundwater environments. Prentice Hall,* New Jersey; 436 p.

FORD, D.C. & WILLIAMS, P.W. (1994): Karst geomorphology and hydrology. *Chapman & Hall,* London; 601 p.

GAMS, I. (1974): Kras. Slovenska matica, Ljubljana; 359 p.

JARC, S. (1996): Toplotne lastnosti naravnega kamna v Sloveniji. *Diplomsko delo.* Ljubljana: Univerza v Ljubljani; 90 p.

JARC, S. (2000): Vrednotenje kemične in mineralne sestave apnencev kot naravnega kamna. *Magistrsko delo.* Ljubljana: Univerza v Ljubljani; 88 p.

KRINSLEY, D.H., PYE, K., BOGGS, S.JR., TOVEY, N.K. (1998): Backscattered scanning electron microscopy and image analysis of sediments and sedimentary rocks. *Cambridge University Press,* Cambridge; 193 p.

Mackenzie, F.T., Bischoff, W.D., Bishop, F.C., Loijens, M., Schoonmaker, J., Wollast, R. (1983): Magnesian calcites: low-temperature occurence, solubility and solid-solution behavior. *Reviews in Mineralogy,* 11, 97-144, Washington.

Meng, B. (1992): Moisture - transport - relevant characterization of pore structure. Proceedings of the *7th International congress on deterioration and conservation of stone,* 387-397, Lisboa.

Mirtič, B., Mladenovič, A., Ramovš, A., Senegačnik, A., Vesel, J., Vižintin, N. (1999): Slovenski naravni kamen. *GeoZS, ZAG, Oddelek za Geologijo NTF*, Ljubljana; 131 p.

Morse, J.W. (1983): The kinetics of calcium carbonate dissolution and precipitation. *Reviews in mineralogy,* 11, 227-264, Washington.

Morse, J.W. & Mackenzie, F.T. (1990): Geochemistry of sedimentary carbonate. *Developments in sedimetology 48*, *Elsevier,* Amsterdam; 177 p.

Ramovš, A. (1987): Triasne gradbene in okrasne kamnine v severni Sloveniji. Geološki zbornik 8, 25-35, Ljubljana.

Summerfield, M.A. (1994): Global geomorphology, an introduction to the study of landforms. *John Wiley & Sons,* New York; 537 p.

Viles, H.A. & Moses, C.A. (1998): Experimental production of weathering nanomorphologies on carbonate stone. Quarterly Journal of Engineering Geology, 31, 347-357, Oxford.

Wenk, H.R., Barber, D.J., Reeder, R.J. (1983): Microstructures in carbonates. *Reviews in Mineralogy,* 11, 301-367, Washington.

Razlikovanje apnencev s pomočjo statističnih metod

The distinction of limestone by statistical methods

Simona Jarc

Oddelek za geologijo, NTF, Univerza v Ljubljani, Aškerčeva 12, Ljubljana, Slovenija;
E-mail: simona.jarc@ntfgeo.uni-lj.si

Received: October 20, 2005 **Accepted**: November 24, 2005

Izvleček: Preiskani slovenski apnenci imajo enostavno kemično in mineralno sestavo, so razmeroma čisti; vsebujejo preko 91 mas.% $CaCO_3$. Kljub majhnim razlikam v kemični sestavi in majhni vsebnosti magnezija v kalcitni rešetki (manj kot 0,6 mas.%), pa lahko apnence z natančno kemično analizo med seboj razlikujemo. Glede na rezultate t-testa in clusterske analize se preiskovani apnenci najbolj razlikujejo glede vsebnosti SiO_2, Al_2O_3, MgO in Sr. Na osnovi detajlne kemične analize in uporabe ustreznih statističnih metod bi tako apnencem lahko celo določili njihov izvor.

Abstract: The analysed Slovenian limestones have relatively simple chemical and mineral composition. They contain above 91 wt.% $CaCO_3$, respectively. However, these small differences in composition and the very small amount of magnesium in calcite lattice (less than 0˙6 wt.%) may aid in differentiating the limestone. The results of t-test and cluster analysis are in good agreement. The content of SiO_2, Al_2O_3, MgO and Sr have the largest influence in distinction of investigated limestones. Therefore, the use of statistical methods is very helpful in their identification.

Key words: limestone, chemical composition, t-test, cluster analysis
Ključne besede: apnenec, kemična sestava, t-test, clusterska analiza

Uvod

Statistične metode nam lahko pomagajo pri identifikaciji kamnin in določanju njihovega izvora. Provenienco apnenca sem skušala določiti na osnovi njegove detajlne kemične analize in uporabo **t**-testa enakosti populacijskih povprečij ter clusterske analize. Vzorci so bili izbrani iz nekaterih aktivnih in občasno delujočih kamnolomov apnenca: iz Lipice (LiU1, LiU2, LiF1 in LiF2), Hotavelj (H1 do H7), Lesnega Brda (LB1 in LB2) in Drenovega Griča (DG1 in DG2). Mineralna sestava preiskovanih apnencev je opisana v Jarc & Mirtič (v tisku). Za primerjavo sem analizirala še dva vzorca glinenih primesi v hotaveljskem apnencu (HV1 in HV2).

Analitika

Kemična analiza je bila opravljena v laboratoriju ACME v Kanadi. Vsebnosti oksidov in prvin ter žarilne izgube (LOI – loss of ignition) so bile določene z metodo induktivno vezane plazme emisijske spektro-

Scientific paper

Tabela 1. Kemična sestava vzorcev. Količine oksidov, žarilne izgube (LOI), ogljika in žvepla so v masnih odstotkih, ostalih prvin v ppm.
Table 1. Chemical composition of investigated samples. All oxides, carbon, sulfur and loss of ignition content are in weight %, other elements are in ppm.

	SiO_2	Al_2O_3	Fe_2O_3	MgO	CaO	Na_2O	K_2O	TiO_2	P_2O_5	MnO	Cr_2O_3
LiU1	<0,02	0,12	0,07	0,35	55,63	0,02	<0,04	0,01	0,01	<0,01	0,001
LiU2	0,02	0,1	0,1	0,3	55,96	0,01	0,04	0,02	0,03	<0,01	0,01
LiF1	<0,02	0,09	0,07	0,31	55,76	0,03	<0,04	0,01	0,03	<0,01	0,004
LiF2	<0,02	0,08	0,09	0,28	56,03	0,02	<0,04	<0,01	0,02	<0,01	0,006
LB1	1,26	0,77	0,29	0,42	54,00	0,03	0,12	0,04	0,08	0,01	0,003
LB2	1,66	0,99	0,34	0,44	53,82	0,02	0,18	0,04	0,01	0,01	0,005
H1	0,21	0,17	0,05	0,91	54,91	0,03	<0,04	0,01	0,04	0,02	0,004
H1p	0,38	0,15	0,05	0,94	54,56	<0,01	<0,04	<0,01	0,02	0,02	0,004
H2	0,31	0,17	0,07	0,69	55,42	0,02	0,04	0,01	0,03	0,02	0,003
H3	1,12	0,48	0,21	0,67	53,85	0,04	0,12	0,01	0,05	0,03	0,002
H4	1,33	0,64	0,24	0,62	54,03	0,02	0,19	0,02	0,04	0,03	0,001
H5	0,58	0,31	0,59	0,52	54,24	<0,01	0,06	0,01	0,04	0,05	0,006
H6	0,84	0,42	0,75	0,45	54,08	0,04	0,12	0,01	0,03	0,05	0,006
H6p	0,95	0,42	0,72	0,46	54,16	<0,01	0,12	<0,01	0,02	0,05	0,003
H7	0,83	0,42	0,79	0,47	54,49	0,01	0,1	0,01	0,01	0,05	0,001
HV1	17,29	8,36	5,91	5,09	29,75	0,03	3,07	0,18	0,05	0,08	0,01
HV2	18,44	8,77	6,09	4,78	28,96	0,01	3,26	0,19	0,07	0,08	0,01
DG1	1,47	0,77	0,51	0,83	51,75	0,03	0,12	0,03	0,02	0,01	0,004
DG2	1,73	0,88	0,82	0,77	51,00	0,05	0,11	0,04	0,01	0,01	0,002

	Ba	Ni	Sr	Zr	Y	Nb	Sc	LOI	C/TOT	S/TOT
LiU1	<5	<20	189	<10	<10	<10	<10	43,7	11,7	0,01
LiU2	<5	<20	188	100	<10	<10	<10	43,4	11,7	0,03
LiF1	<5	<20	261	<10	<10	<10	<10	43,6	11,6	0,01
LiF2	<5	<20	220	<10	<10	<10	<10	43,4	11,7	0,04
LB1	5	<20	133	139	<10	<10	<10	42,9	11,2	0,01
LB2	9	<20	110	<10	<10	<10	<10	42,5	11,4	0,01
H1	5	<20	101	<10	<10	<10	<10	43,6	11,8	0,01
H1p	<5	<20	100	13	<10	<10	<10	43,7	11,4	0,01
H2	<5	<20	98	<10	<10	<10	<10	43,2	11,7	0,01
H3	<5	<20	96	125	<10	<10	<10	43,4	11,6	0,01
H4	5	<20	95	<10	<10	<10	<10	43	11,4	0,01
H5	8	<20	99	<10	<10	<10	<10	43,6	11,3	0,01
H6	5	<20	94	10	<10	<10	<10	43,1	11,5	0,01
H6p	7	<20	95	<10	<10	<10	<10	43,1	11,5	0,01
H7	7	<20	96	<10	<10	<10	<10	42,9	11,8	0,01
HV1	69	25	59	77	<10	<10	<10	30,2	7,61	0,01
HV2	71	24	55	95	10	<10	<10	29,4	7,07	0,03
DG1	13	<20	972	12	<10	<10	<10	44,4	13,1	0,23
DG2	13	<20	1055	29	<10	<10	<10	44,5	14,2	0,37

metrije (ICP-ES), celotni ogljik in žveplo pa z Leco (ACME, 1999). Za silikatno analizo so 0,2 g vzorca talili z 1,2 g $LiBO_2$ in raztopili v 100 ml 5 % HNO_3. Žarilno izgubo so določili glede na spremembo mase vzorca po 1 uri žganja pri temperaturi 1000 °C. Rezultati kemične analize so v tabeli 1.

Rezultati kemične analize kažejo, da so količine niklja, cirkonija, itrija, niobija in skandija v vseh vzorcih pod mejo detekcije, zato ti rezultati v nadaljevanju niso upoštevani.

Pravilnost analitike je bila ugotovljena s pomočjo standardov SO-15 in CSA, natančnost ali ponovljivost izbrane metode pa z večkratnimi analizami (vzorci označeni s **p**) istega vzorca (Swan & Sandilands, 1995, Zupančič, 1994). Pravilnost metode določanja kemične sestave je zelo dobra, saj odstopanja analitskih in priporočenih vrednosti niso večje od 6 %, v splošnem pa so analitske nekoliko nižje od priporočenih vrednosti, prav tako je natančnost metode zadovoljiva (Jarc, 2000). Slabšo natančnost zasledimo le pri tistih oksidih in prvinah, katerih količine so zelo majhne, še posebej, če je količina na meji detekcije. Pri višjih količinah (npr. CaO) je natančnost dane metode določanja kemične sestave dobra (Jarc, 2000).

Osnovne statistike, normalnost porazdelitve in korelacije

Osnovne statistike količin oksidov in prvin 19 vzorcev (N) so podane v tabeli 2. Srednje vrednosti so podane z aritmetično sredino (x), mediano (Me), geometrično sredino (x_G), razpršenost podatkov pa z razponom (razlika med najvišjo (max) in najnižjo (min) vrednostjo) ter z aritmetičnim (s) in geometrijskim (s_G) standardnim odklonom ter z aritmetično (s^2) in geometrično (s_G^2)

Tabela 2. Osnovne statistike: aritmetična (x) in geometrična (x_G) sredina, mediana (Me), razpon vrednosti (min-max), kvartilni razpon (Q_{25}-Q_{75}), aritmetični (s) in geometrični (s_G) standardni odklon, aritmetična (s^2) in geometrična (s_G^2) varianca, asimetričnost ($\sqrt{b_1}$) in sploščenost (b_2) naravnih vrednosti ter asimetričnost ($\sqrt{b_{1L}}$) in sploščenost (b_{2L}) logaritmiranih vrednosti. Število vzorcev (N) je 19.

Table 2. Basic statistics: arithmetic (x) and geometric (x_G) mean, median (Me), range (min-max), quartiles (Q_{25}-Q_{75}), arithmetic (s) and geometric (s_G) standard deviation, arithmetic (s^2) in geometric (s_G^2) variance, skewness ($\sqrt{b_1}$), kurtosis (b_2) and skewness ($\sqrt{b_{1L}}$) and kurtosis (b_{2L}) of logaritmic values. The number of samples (N) is 19.

	x	x_G	Me	min-max	Q_{25}-Q_{75}	s	s^2	s_G	s_G^2	? b_1	b_2	? b_{1L}	b_{2L}
SiO_2	2,550	0,465	0,840	0,01-18,44	0,21-1,47	5,431	29,49	9,399	88,340	2,746	6,353	0,299	1,376
Al_2O_3	1,269	0,428	0,420	0,08-8,77	0,15-0,77	2,588	6,70	3,788	14,347	2,739	6,309	10,469	10,222
Fe_2O_3	0,935	0,304	0,290	0,05-6,09	0,07-0,75	1,807	3,26	4,265	18,187	2,679	6,075	4,560	1,132
MgO	1,016	0,655	0,520	0,28-5,09	0,42-0,83	1,397	1,95	2,228	4,964	2,697	6,172	56,535	952,899
CaO	51,705	50,911	54,160	28,96-56,03	53,82-55,42	7,980	63,69	1,216	1,479	-2,669	6,030	0,002	1766453
Na_2O	0,022	0,018	0,020	0,005-0,05	0,01-0,03	0,013	0,00	2,079	4,321	0,358	0,538	0,208	4,571
K_2O	0,408	0,094	0,110	0,02-3,26	0,02-0,12	0,974	0,95	4,408	19,430	2,788	6,499	19,854	67,504
TiO_2	0,035	0,017	0,010	0,005-0,19	0,01-0,04	0,054	0,00	2,923	8,543	2,561	5,624	12,139	4,807
P_2O_5	0,032	0,027	0,030	0,01-0,08	0,02-0,04	0,020	0,00	1,920	3,685	1,002	0,689	0,641	6,499
MnO	0,028	0,012	0,020	0,0005-0,08	0,01-0,05	0,026	0,00	6,050	36,601	0,861	0,221	0,095	2,083
Cr_2O_3	0,005	0,004	0,004	0,001-0,01	0,002-0,006	0,003	0,00	2,090	4,367	0,865	0,065	0,374	3,189
Ba	12,526	6,624	5,000	3,0-71,0	3,0-9,0	20,500	420,26	2,633	6,933	2,680	6,066	39,271	148,143
Sr	216,632	141,791	100,000	55,0-1055,0	95,0-189,0	286,255	81942	2,223	4,943	2,634	5,939	44,475	294,868
LOI	41,979	41,723	43,400	29,4-44,5	42,9-43,6	4,321	18,67	1,127	1,269	-2,736	6,317	0,002	2570946
C	11,331	11,207	11,600	7,07-14,2	11,4-11,7	1,574	2,48	1,173	1,377	-1,580	4,004	0,008	79428,6
S	0,044	0,017	0,010	0,01-0,37	0,01-0,03	0,094	0,01	2,990	8,938	3,068	9,080	133,374	5490,109

varianco. Zaradi t.i. "outlierjev" (nenormalno visoke ali nizke vrednosti) je podan še kvartilni razpon (Q_{25}-Q_{75}), kjer zanemarimo 25 % najvišjih in 25 % najnižjih vrednosti (SWAN & SANDILANDS, 1995), ki daje realnejšo sliko razpršenosti podatkov. Metode parametrične statistike lahko uporabimo samo, če so podatki porazdeljeni normalno. Če porazdelitev podatkov ne ustreza normalni, jih moramo z ustrezno transformacijo prilagoditi temu pogoju (KOCH & LINK, 1970). Normalnost porazdelitve naravnih in logaritmiranih vrednosti sem ugotavljala s testi sploščenosti (b_2, b_{2L}) in asimetričnosti ($\sqrt{b_1}$, $\sqrt{b_{1L}}$). Za normalno porazdeljene podatke se vrednost asimetričnosti približije 3, vrednost sploščenosti pa 0. Iz rezultatov je razvidno, da normalni porazdelitvi bolj ustrezajo naravne vrednosti. Vsi parametri so izračunani s pomočjo računalniškega programa CSS Statistica.

Zaradi primerljivosti rezultatov (podatki so v različnih enotah) sem pri izračunu korelacijskih koeficientov uporabila logaritmirane vrednosti. S tem sem tudi zmanjša napaka zaprtega niza podatkov (vrednosti so podane v odstotkih), kjer so vrednosti že same po sebi medsebojno odvisne (SWAN & SANDILANDS, 1995). Izračunane koeficiente korelacije sem primerjala s kritično (tabelirano) vrednostjo koeficienta na 95 % ravni zaupanja, $r_{0,05;17;krit} = 0,456$ (PETZ, 1985). Korelacijska matrika (tabela 3) kaže, da je CaO z večino oksidov drugih elementov negativno koreliran. CaO je vezan predvsem na mineral kalcit, ki je kemično relativno čist. Ostale prvine so torej vezane na druge minerale, predvsem glinene minerale. To potrjuje tudi dobra korelacija SiO_2, MgO, Al_2O_3 in Fe_2O_3 ter K_2O, ki so vezani na minerale smektitove in kloritove skupine ter na muskovit (JARC & MIRTIČ, v tisku). V nekaterih

Tabela 3. Matrika korelacijskih koeficientov logaritmiranih vrednosti (N=19). * – prvini sta značilno medsebojno odvisni na 95 % ravni zaupanja.

Table 3. Matrice of correlation coefficients of logaritmic values (N=19). * – correlations are significant on 95 % confidence interval.

	SiO_2	Al_2O_3	Fe_2O_3	MgO	CaO	Na_2O	K_2O	TiO_2	P_2O_5	MnO	Cr_2O_3	Ba	Sr	LOI	C
SiO_2	1														
Al_2O_3	0,91*	1													
Fe_2O_3	0,80*	0,90*	1												
MgO	0,75*	0,81*	0,66*	1											
CaO	-0,64	-0,85*	-0,78*	-0,91*	1										
Na_2O	0,03	0,13	-0,01	0,02	-0,01	1									
K_2O	0,85*	0,97*	0,92*	0,78*	-0,87*	0,07	1								
TiO_2	0,66*	0,87*	0,71*	0,72*	-0,82*	0,28	0,84*	1							
P_2O_5	0,31	0,32	0,20	0,41	-0,41	0,07	0,38	0,33	1						
MnO	0,88*	0,66*	0,63*	0,61*	-0,43	-0,16	0,62*	0,28	0,31	1					
Cr_2O_3	0,14	0,24	0,28	0,36	-0,47*	-0,13	0,30	0,36	0,41	0,02	1				
Ba	0,77*	0,92*	0,90*	0,84*	-0,90*	0,01	0,90*	0,84*	0,22	0,54*	0,40	1			
Sr	-0,29	-0,24	-0,19	-0,32	0,34	0,39	-0,34	-0,05	-0,46*	-0,49*	-0,17	-0,14	1		
LOI	-0,58*	-0,80*	-0,73*	-0,87*	0,98*	0,05	-0,85*	-0,77*	-0,45	-0,39	-0,49*	-0,84*	0,47*	1	
C	-0,49*	-0,68*	-0,61*	-0,77*	0,90*	0,18	-0,76*	-0,64*	-0,55*	-0,37	-0,50*	-0,70*	0,66*	0,96*	1
S	0,08	0,15	0,20	0,09	-0,08	0,28	0,07	0,28	-0,28	-0,19	0,09	0,27	0,84*	0,06	0,30

primerih (n.pr. korelacija koeficienta med CaO ali MgO in Ba) je korelacijski koeficient relativno visok in je posledica posameznih nenormalno visokih ali nizkih vrednosti.

Test enakosti populacijskih povprečij

S **t**-testom enakosti populacijskih povprečij sem poskušala ugotoviti, ali lahko preiskovane apnence med seboj statistično razlikujemo.

Tabela 4. t-test enakosti populacijskih povprečij. F_{x-y} – rezultat testa populacijskih varianc posameznih skupin, t_{x-y} – rezultat testa enakosti populacijskih povprečij posameznih skupin, * – skupini se na 95 % ravni zaupanja statistično razlikujeta.

Table 4. t test of equality of population means. F_{x-y} – population variance result of individual groups, t_{x-y} – t-test of equality of population means result of individual groups, * – the groups are statistically different on 95 % confidence interval.

	F_{1-2}	t_{1-2}	F_{1-3}	t_{1-3}	F_{1-4}	t_{1-4}	F_{1-5}	t_{1-5}	F_{2-3}	t_{2-3}
SiO_2	3200,0	-11,813*	5871,78	-3,643*	26450,0	-50,698*	1352,0	-19,919*	1,835	2,509*
Al_2O_3	82,971	-11,412*	95,143	-2,991*	288,170	-67,102*	20,743	-20,189*	1,147	4,073*
Fe_2O_3	5,556	-12,238*	459,346	-1,839	72,000	-105,200*	213,556	-6,094*	82,682	-0,298
MgO	4,333	-5,237*	40,154	-3,401*	55,440	-47,459*	2,077	-17,060*	174,000	-1,503
CaO	2,076	13,059*	7,273	5,500*	9,280	95,199*	8,362	16,699*	15,101	-1,381
Na_2O	1,333	-0,730	3,135	0,071	3,000	0	3,000	-2,309	4,181	0,514
K_2O	18,000	-6,299*	32,444	-2,138	180,500	-53,532*	2,000	-11,110*	1,803	1,433
TiO_2	0,000	-6,093*	2,111	0,421	1,260	-30,889*	1,263	-4,222*	0,000	9,400*
P_2O_5	26,727	-0,995	1,758	-1,202	2,180	-3,974*	1,833	0,961	15,207	0,872
MnO	-	-	0,000	-4,804*	-	-	-	-	0,000	-2,435*
Cr_2O_3	7,125	0,432	4,071	1,258	-	-1,678	7,125	0,777	1,750	0,467
Ba	0,000	-3,266*	0,000	-2,168	-	-109,411*	-	-	2,215	1,193
Sr	4,468	3,480*	193,394	10,807*	147,710	6,102*	2,915	-22,071*	43,282	5,287*
LOI	3,556	4,961*	3,827	1,498	14,220	50,919*	4,500	-7,934*	1,076	-2,577*
C	8,000	5,222*	13,111	1,269	58,320	25,569*	242,000	-5,828*	1,639	-1,846
S	0,000	1,111	0,000	2,655*	1,130	0,195	43,556	-6,262*	-	-

	F_{2-4}	t_{2-4}	F_{2-5}	t_{2-5}	F_{3-4}	t_{3-4}	F_{3-5}	t_{3-5}	F_{4-5}	t_{4-5}
SiO_2	8,266	-26,947*	2,367	-0,587	4,505	-48,541*	4,343	3,045*	19,564	-27,591*
Al_2O_3	3,473	-33,033*	4,000	0,447	3,029	-56,963*	4,587	3,790*	13,893	-36,467*
Fe_2O_3	12,960	-60,862*	38,440	-2,229	6,380	-23,467*	2,151	1,147	2,966	-29,766*
MgO	240,250	-29,004*	9,000	-11,700*	1,381	-28,870*	19,333	1,184	26,694	-26,191*
CaO	19,262	60,611*	17,361	6,573*	1,276	63,845*	1,150	-7,799*	1,110	40,430*
Na_2O	4,000	0,447	4,000	-1,342	1,045	-0,049	1,045	1,823	1,000	1,414
K_2O	10,028	-30,263*	36,000	1,151	5,563	-56,295*	64,889	0,648	361,000	-32,061*
TiO_2	0,000	-29,000*	0,000	1,000	2,667	-47,488*	2,667	6,784*	1,000	-21,213*
P_2O_5	12,250	-0,412	49,000	0,849	1,241	-2,873*	3,222	-1,690	4,000	-4,025
MnO	-	-	-	-	0,000	-4,235*	0,000	-2,435*	-	-
Cr_2O_3	0,000	-6,000*	1,000	0,707	0,000	-4,835*	1,750	-0,233	0,000	-7,000*
Ba	4,000	-28,175*	0,000	-3,000	1,806	-44,805*	0,000	5,632*	0,000	-57,000*
Sr	33,063	5,526*	13,023	-20,713*	1,309	20,409*	563,646	59,500*	430,563	23,022*
LOI	4,000	28,845*	16,000	-8,489*	3,716	51,537*	17,222	5,349*	64,000	36,342*
C	7,290	13,754*	30,250	-4,204	4,448	25,326*	18,458	8,631*	4,150	10,299*
S	0,000	-1,000	0,000	-4,143	0,000	-2,714*	0,000	11,242*	49,000	3,960

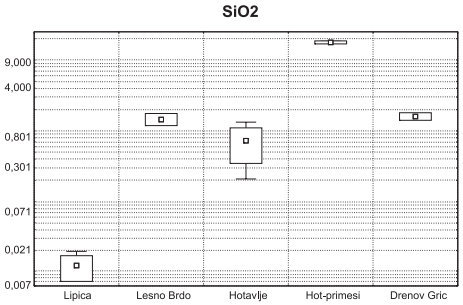
SiO2
9,000
4,000
0,801
0,301
0,071
0,021
0,007
Lipica
Lesno Brdo
Hotavlje
Hot.-primesi
Drenov Gric

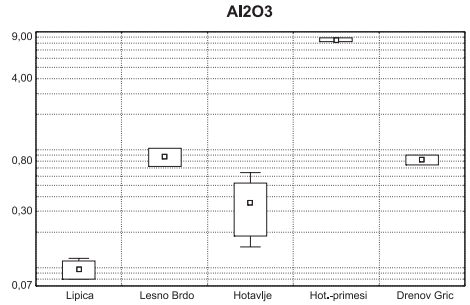
Al2O3
9,00
4,00
0,80
0,30
0,07
Lipica
Lesno Brdo
Hotavlje
Hot.-primesi
Drenov Gric

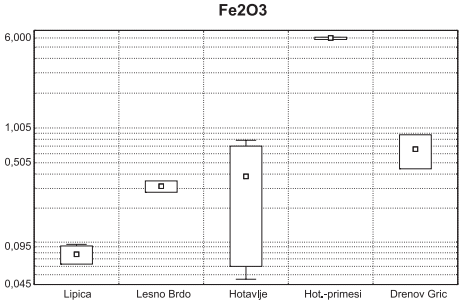
Fe2O3
6,000
1,005
0,505
0,095
0,045
Lipica
Lesno Brdo
Hotavlje
Hot.-primesi
Drenov Gric

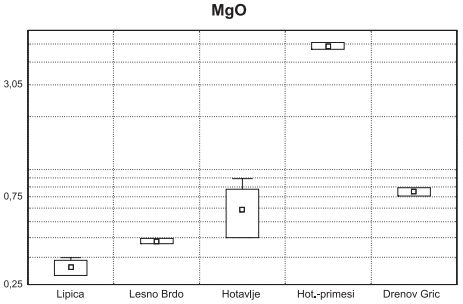
MgO
3,05
0,75
0,25
Lipica
Lesno Brdo
Hotavlje
Hot.-primesi
Drenov Gric

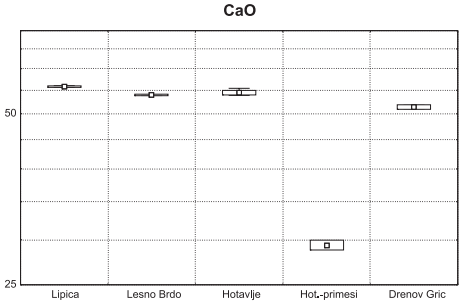
CaO
50
25
Lipica
Lesno Brdo
Hotavlje
Hot.-primesi
Drenov Gric

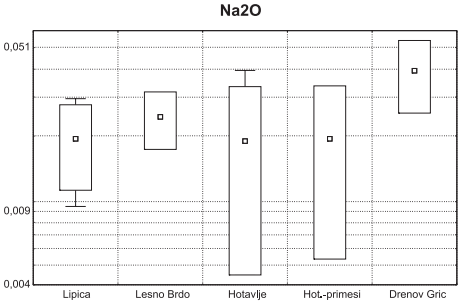
Na2O
0,051
0,009
0,004
Lipica
Lesno Brdo
Hotavlje
Hot.-primesi
Drenov Gric

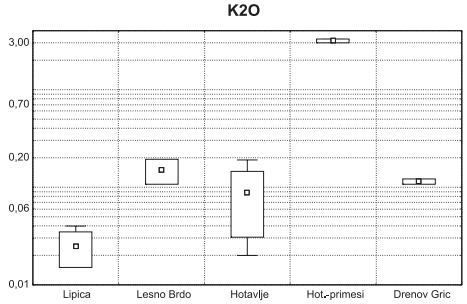
K2O
3,00
0,70
0,20
0,06
0,01
Lipica
Lesno Brdo
Hotavlje
Hot.-primesi
Drenov Gric

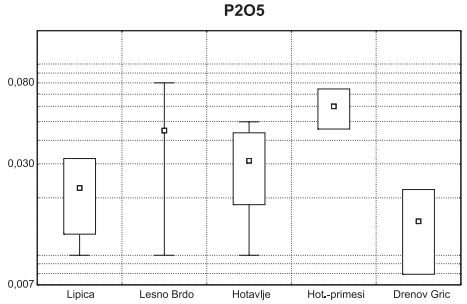
P2O5
0,080
0,030
0,007
Lipica
Lesno Brdo
Hotavlje
Hot.-primesi
Drenov Gric

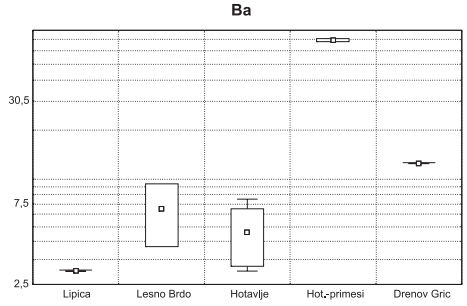
Ba
30,5
7,5
2,5
Lipica
Lesno Brdo
Hotavlje
Hot.-primesi
Drenov Gric

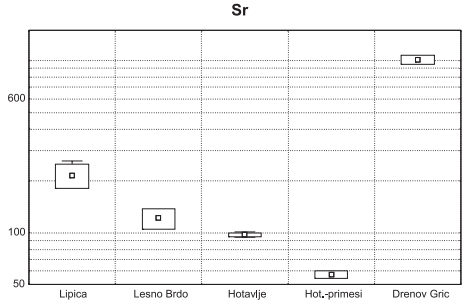
Sr
600
100
50
Lipica
Lesno Brdo
Hotavlje
Hot.-primesi
Drenov Gric

*

Vzorce sem razporedila v pet skupin glede na posamezna nahajališča. V prvi skupini so vzorci iz Lipice (LiU1, LiU2, LiF1 in LiF2), v drugi skupini je lesnobrdski apnenec (LB1 in LB2), sledi skupina hotaveljskega apnenca (H1 – H7). Vzorec HV predstavlja svojo (četrto) skupino, ker se že po sestavi močno razlikuje od vseh ostalih; gre za glinene primesi v hotaveljskem apnencu. V peto skupino sem uvrstila črni apnenec z Drenovega Griča (DG1 in DG2). Dvostranski **t**-test sem izvajala z računalniškim programom CSS z naravnimi vrednostmi. Vrednosti **t** so izračunane na podlagi izidov testa F, ki ugotavlja podobnost populacijskih varianc.

Rezultati (tabela 4) so pokazali, da se skupine med seboj statistično razlikujejo po količini večine oksidov in prvin na ravni zaupanja 95 %. Torej bi lahko že z geokemično analizo apnenca določili njegov izvor oz. nahajališče. Seveda bi bilo potrebno narediti bistveno večje število kemičnih analiz vseh apnencev iz različnih nahajališč, da bi lahko postavili statistične meje količin posameznih oskidov in prvin, na osnovi katerih bi ugotavljali izvor apnenca. Nekatere vrednosti F so zelo visoke in nam pri tako majhnem številu vzorcev kažejo na "nestabilnost" podatkov; varianca znotraj posamezne skupine je ob tako majhnem vzorcu prevelika, zato so vrednosti nezanesljive; primer apnenca iz Hotavelj, ki ima pri večini analiziranih prvin zelo širok vrednosti (slika 1). V našem primeru je bilo vzorcev apnencev vsekakor premalo, da bi lahko točno definirali kemično sestavo apnencev iz posameznih nahajališč. Kljub temu pa je test enakosti populacijskih povprečij pokazal, da se vzorec HV, ki predstavlja glinene primesi v hotaveljskem apnencu, popolnoma razlikuje od vseh ostalih (vrednosti **t** so zelo visoke). Glede na izračunane vrednosti **t** za vse prvine v dani skupini se statistično najmanj razlikujeta apnenca z Lesnega Brda in iz Hotavelj (vrednosti **t** so malo višje od kritične vrednosti **t** na ravni zaupanja 95 %), kar je tudi razumljivo, saj sta genetsko podobna (Jarc, 2000). Apnenec z Drenovega Griča se od ostalih apnencev razlikuje predvsem po povečani količini organske snovi. Posamezna nahajališča se razlikujejo predvsem po vsebnosti SiO_2, Al_2O_3, MgO in Sr, medtem ko se vrednosti Fe_2O_3 (kljub visokim vrednostim **t**), CaO, K_2O, P_2O_5, Na_2O lahko prekrivajo in jih ne moremo uporabili za identifikacijo apnencev (slika 1). Za ločevanje različnih tipov apnencev so vsekakor zanesljivejši tisti oksidi in prvine, ki nastopajo v večjih količinah, medtem ko oksidi in prvine v manjših količinah pokažejo tudi manjše statistične razlike. Kot primer lahko navedemo Na_2O, katerega vsebnost je v vseh vzorcih na meji detekcije, **t**-test pa ne da nobenih statistično značilnih razlik med izbranimi skupinami glede na njegovo količino.

*

Slika 1. Prikaz srednjih vrednosti, standardnih odklonov ter maksimalnih in minimalnih vrednosti nekaterih oksidov oz. prvin v posameznih nahajališčih. Skala je logaritemska.
Figure 1. Box-Whiskers diagrams of means, standard deviations and ranges (max-min) of some analysed oxides and elements in investigated limestone quarries. Logarithmic scale.

CLUSTERSKA ANALIZA

Cilj clusterske analize je združevanje posameznih objektov v skupine glede na podobnost med njimi. Uporabila sem clustersko analizo tipa k-mean, ki se od običajne loči po tem, da vnaprej določimo število skupin (k). Osnova izračuna te metode je "obrnjena" analiza variance. Računalniški program CSS razdeli vzorce v vnaprej določeno število skupin (k) tako, da je varianca znotraj skupine čim manjša, varianca med skupinami pa čim večja. Statistično značilnost rezultatov določi s testom F. Višja kot je vrednost F, bolj učinkovito spremenljivka vpliva na ločevanje vzorcev v skupine. Uporabljeni podatki pa morajo biti standardizirani tako, da je povprečna vrednost posamezne spremenljivke 0, standardni odklon pa 1 (ZUPANČIČ, 1994).

Ker sem poskušala ugotoviti, ali se apnenci iz posameznih nahajališč statistično razlikujejo, sem tudi clustersko analizo tipa k-mean izvedla s petimi skupinami. Rezultati so podani v tabeli 5. Čim večja je vrednost F, večji je vpliv spremenljivke na uvrstitev vzorca v določeno skupino. Na uvrstitev v posamezne skupine najbolj vplivajo spremenljivke CaO, K_2O, Sr ter SiO_2 in Al_2O_3, kar je pričakovano, saj so to oksidi in prvine, ki so vezani na karbonate in glinene minerale. Medtem ko količine Na_2O, Cr_2O_3 in P_2O_5 na uvrstitev v skupine ne vplivajo. Podobne rezultate dobimo s **t**-testom enakosti populacijskih povprečij, kjer so vrednosti SiO_2, Al_2O_3, MgO in Sr tiste, ki so najbolj značilne za posamezne apnence. Rezultati obeh statističnih metod tako potrjujejo, da na obilnost prvine vpliva predvsem prisotnost minerala v kamnini oz. vsebnost "nečistoč" v kalcitni rešetki.

Tabela 5. Rezultati analize variance clusterske analize tipa k-mean za 5 skupin.
Table 5. k-mean cluster analysis results for 5 groups.

	varianca		
	med skupinami	znotraj skupine	F
SiO_2	528,0	2,7	697,2
Al_2O_3	120,0	0,7	618,9
Fe_2O_3	58,0	0,9	226,6
MgO	35,0	0,4	332,6
CaO	1143,0	3,0	1347,2
Na_2O	0,0	0,0	1,2
K_2O	17,0	0,1	1144,7
TiO_2	0,0	0,0	154,7
P_2O_5	0,0	0,0	7,7
MnO	0,0	0,0	15,3
Cr_2O_3	0,0	0,0	3,7
Ba	7520,0	44,5	591,5
Sr	1467763,0	7195,9	713,9
LOI	334,0	1,6	713,1
C	44,0	1,0	146,2
S	0,0	0,0	48,1

V prvo skupino so uvrščeni vsi vzorci iz Lipice (LiU1, LiU2, LiF1 in LiF2), v drugo oba vzorca z Drenovega Griča (DG1 in DG2), sledi samostojen vzorec iz Lesnega Brda (LB1), četrta skupina je najbolj številčna in združuje en vzorec iz Lesnega Brda in vse vzorce apnenca iz Hotavelj (LB2, H1, H1p, H2, H3, H4, H5, H6, H6p, H7), svojo skupino pa predstavljata tudi vzorca glinenih vložkov iz Hotavelj (HV1 in HV2). Rezultati clusterske analize se ujemajo z rezulati **t**-testa enakosti populacijskih povprečij, kjer sem skupine definirala sama. Izjema je le vzorec lesnobrdskega apnenca (LB2), ki ga je clusterska analiza uvrstila v skupino apnencev iz Hotavelj. Oba tipa apnenca (iz Hotavelj in z Lesnega Brda) sta genetsko podobna (JARC, 2000) in torej glede na kemično sestavo podobna. Tudi rezultati **t**-testa enakosti populacijskih povprečij pokažejo najmanjšo statistično razliko med tema razredoma apnencev.

Rezultati in razprava

Število vzorcev je za statistično obdelavo majhno, kljub temu pa sem poskušala dobiti ocene količin oksidov in prvin, ki bi mi pomagale pri identifikaciji apnencev. Pri določanju provenience apnenca sem uporabila dve neodvisni statistični metodi: clustersko analizo in **t**-test enakosti populacijskih povprečij.

Preiskovani slovenski apnenci, z izjemo vzorca glinenih primesi v hotaveljskem apnencu, so kemično relativno čisti $CaCO_3$. Z izjemo apnenca z Drenovega Griča (91 mas.% $CaCO_3$) vsebujejo preko 95 mas.% $CaCO_3$. Po sestavi so si zelo podobni, delež primesnih prvin je relativno majhen. Kljub majhnim razlikam v sestavi, pa apnence z natančno kemično analizo in statistično obdelavo podatkov med seboj lahko razlikujemo, predvsem po vsebnosti SiO_2, Al_2O_3, MgO in Sr. Korelacija med analiziranimi oksidi in prvinami pokaže, da je CaO vezan predvsem na mineral kalcit, ki je kemično relativno čist (negativna korelacija z ostalimi oksidi in prvinami). Ostale prvine so vezane predvsem na druge minerale, gre za minerale smektitove in kloritove skupine ter na muskovit (Jarc & Mirtič, v tisku).

S pomočjo **t**-testa enakosti populacijskih povprečij sem preverila uvrščanje vzorcev v "geokemične" skupine, glede na posamezna nahajališča: Lipica, Lesno Brdo, Hotavlje - apnenci, Hotavlje - glinene primesi, Drenov Grič. Rezultati **t**-testa so pokazali, da se skupine med seboj statistično razlikujejo glede na količine večine analiziranih oksidov in prvin na 95 % ravni zaupanja. Glede na izračunane vrednosti **t** za vse prvine v dani skupini se statistično najmanj razlikujeta apnenca z Lesnega Brda in iz Hotavelj, ki sta tudi genetsko podobna. Vzorec glinenih vključkov iz Hotavelj pa se, po pričakovanjih, popolnoma razlikuje od vseh ostalih. Apnenec z Drenovega Griča se od ostalih apnencev razlikuje predvsem po povečani količini organske snovi; ta mu daje tudi značilno, črno barvo. Tudi clustersko analizo sem izvedla s petimi skupinami. V tem primeru se na podlagi uporabljenega računalniškega programa vzorci razporedijo v skupine na osnovi podobnosti med njimi. Rezultati clusterske analize se dobro ujemajo z rezultati **t**-testa enakosti populacijskih povprečij.

Apnenci se, kljub majhnim razlikam v kemični sestavi, statistično razlikujejo. Nahajališče apnenca bi torej lahko določali z detajlno kemično analizo.

Sklepi

Preiskovani apnenci so razmeroma čisti, vsebujejo preko 91 mas.% $CaCO_3$, izjema je le vzorec glinenih primesi iz Hotavelj, kjer vsebnost karbonata znatno nižja (približno 52 mas.% $CaCO_3$). CaO je z večino oksidov in prvin negativno koreliran, kar kaže na relativno čist kalcit. Dobra korelacija med SiO_2, Al_2O_3, MgO, Fe_2O_3 in K_2O torej kaže na prisotnost drugih mineralov, predvsem gre za glinene minerale.

Rezultati **t**-testa enakosti populacijskih povprečij apnencev iz 4 nahajališč so pokazali, da se apnenci med seboj statistično razlikujejo na 95 % ravni zaupanja. Največje razlike so v vsebnosti SiO_2, Al_2O_3, MgO in Sr, torej tistih prvin, ki so vezane na

prisotnost glinenih mineralov, sljud in čistost kalcita. Statistično se najmanj razlikujeta apnenca iz Hotavelj in Lesnega Brda, ki sta tudi genetsko podobna. Vzorec glinenih primesi iz Hotavelj pa se, po pričakovanjih, popolnoma razlikuje od vseh ostalih.

Clusterska analiza je potrdila rezultate **t**-testa. Največja je podobnost med apnencema iz Hotavelj in Lesnega Brda. Kljub temu da so preiskovani apnenci zelo čisti (preko 95 mas.% $CaCO_3$, apnenec z Drenovega Griča pa vsebuje le 91 mas.% $CaCO_3$) in tudi po sestavi zelo podobni, bi jih z natančno kemično analizo lahko ločevali. V tem primeru gre le za pilotske vzorce, s pomočjo katerih sem poskušala samo pokazati, da se apnenci, kljub majhnim razlikam v kemični sestavi, statistično razlikujejo.

Seveda bi bilo potrebno narediti bistveno večje število kemičnih analiz vseh apnencev iz različnih nahajališč, da bi lahko postavili statistične meje količin posameznih oksidov in prvin, na osnovi katerih bi ugotavljali provenienco apnenca.

SUMMARY

The distinction of limestone by statistical methods

The identification of limestone by two independent statistical analysis, **t**-test and cluster analysis was tested on some Slovenian samples from Lipica, Hotavlje, Lesno Brdo and Drenov Grič. The results of detailed chemical analysis are in Table 1. The accuracy and precision of the analytical technique are satisfactory (JARC, 2000). The mineral composition of investigated samples is described in JARC & MIRTIČ (in press).

The composition of the investigated limestones is very similar. The limestone from Drenov Grič contains the lowest amount of $CaCO_3$ – above 91 wt.%, whereas the others contain above 95 wt.% of $CaCO_3$. The analysis of clay layer in Hotavlje limestone (sample HV) was made for the comparison. Mineral calcite is relatively pure, as seen in the negative correlations between CaO and other oxides (Table 3). Therefore, the other elements are due to minerals like smectite or chlorite and muscovite (JARC & MIRTIČ, in press).

The **t**-test is used in testing the difference between two population means based on differences found between sample means and considering variance and number of observations. The tested groups were determined accordingly to the limestone quarry: in first group are samples from Lipica quarry (LiU1, LiU2, LiF1 and LiF2), in second group are samples from Lesno Brdo (LB1 and LB2), in third group is limestone from Hotavlje (H1 – H7), the claylayer from Hotavlje quarry (HV1 and HV2) represents the fourth group and in fifth group are samples from Drenov Grič (DG1 and DG2). Two-way **t** test was calculated by programme CSS Statistica. The results are in Table 4. The defined groups are statistically different as to almost all analysed oxides and elements on 95 % confidence interval, but the greatest differences are in content of SiO_2, Al_2O_3, MgO and Sr. Therefore, **t**-test is very helpful in the identification of the limestone regardless of their very similar chemical compositions.

Cluster analysis is a useful technique for grouping objects into unknown groups. The k-mean cluster analysis was used, where the characteristics of the groups are to be derived from the data on the basis of the smallest variance in the same group and the largest variance between the groups. For the cooperation with **t**-test the cluster analysis with five groups were performed. The largest influence on the classification of investigated samples (Table 5) have SiO_2, Al_2O_3, CaO, K_2O and Sr, whereas the content of Na_2O, Cr_2O_3 and P_2O_5 have no influence on grouping. First group represent the samples from Lipica (LiU1, LiU2, LiF1 and LiF2), in second group are samples from Drenov Grič (DG1 and DG2), in third group is the sample LB1, fourth group represent samples from Hotavlje (H1 – H2) and sample LB2 and in fifth group are both samples of clayish layer from Hotavlje (HV1 and HV2). The results of cluster analysis are in good agreement with **t**-test analysis. The only exception is sample LB2, which was classified into Hotavlje limestone group. Nevertheless, the Hotavlje and Lesno Brdo limestones are of the same origin and very similar chemical composition, which explain the result of cluster analysis and the smallest difference in **t**-test.

The origin of limestone can be determined by thorough chemical analysis and statistical analysis of the data. Limestones differ statistically significantly despite of their similar chemical composition, so the statistical methods could be useful in their identification.

Viri

ACME (1999): ACME analytical laboratories brochure. *Acme Analytical Laboratories*, Ltd., Vancouver; 18 p.

Jarc, S. (2000): Vrednotenje kemične in mineralne sestave apnencev kot naravnega kamna. *Magistrsko delo*. Ljubljana: Univerza v Ljubljani; 88 p.

Jarc, S. & Mirtič, B. (v tisku): Vpliv mineralne sestave na obstojnost apnencev kot naravnega kamna. *RMZ- Materials and Geoenvironment,* Ljubljana.

Koch, G.S. & Link, R.F. (1970): Statistical analysis of geological data. *Willey & Sons*, New York; 375 p.

Petz, B. (1985): Osnovne statističke metode za nematematičare. *SNL*, Zagreb; 409 p.

Swan, A.R.H. & Sandilands, M. (1995): Introduction to geological data analysis. *Blackwell Science,* Oxford; 446 p.

Računalniški program CSS Statistica.

Zupančič, N. (1994): Petrološke in geokemične značilnosti pohorskih magmatskih kamnin. *Doktorska disertacija.* Ljubljana: Univerza v Ljubljani; 178 p.

Ustrezne analize črpalnih poizkusov v razpoklinskih vodonosnikih

Appropriate analysis methods of pumping tests in fractured aquifers

Timotej Verbovšek

Univerza v Ljubljani, NTF, Oddelek za geologijo, Aškerčeva 12, 1000 Ljubljana, Slovenija;
E-mail: timotejverbovsek@ntfgeo.uni-lj.si
University of Ljubljana, Faculty of Natural Sciences and Engineering, Aškerčeva 12, Ljubljana, Slovenia;
E-mail: timotejverbovsek@ntfgeo.uni-lj.si

Received: June 8, 2005 **Accepted**: November 24, 2005

Izvleček: Kljub dejstvu, da so nekatere metode črpalnih poizkusov v razpoklinskih vodonosnikih že uveljavljene, se v Sloveniji za analizo razpoklinskih kamnin še vedno uporabljajo neustrezne metode, razvite za medzrnske vodonosnike. Namen prispevka je opozoriti na uporabo ustreznih postopkov, podati kratek pregled uveljavljenih metod ter na nekaj primerih analizirati rezultate črpalnih poizkusov v dolomitih predvsem z modeli dvojne poroznosti.

Abstract: Despite the fact that methods for analyzing pumping test data in fractured aquifers are at the present time developed to the practical level of use, in Slovenia they are still not used correctly. Even for the fractured aquifers the preferable analysis methods are Theis and Cooper-Jacob equations, which are applicable only to single-porosity homogenous aquifers. The purpose of this paper is to warn against erroneous applications of inappropriate methods and to give a brief summary of suitable methods. Finally few examples of pumping tests in dolomites are analyzed and interpreted with methods based on double porosity model.

Ključne besede: črpalni poizkusi, vodonosnik, razpoklinska poroznost, model dvojne poroznosti, dolomit
Key words: pumping tests, aquifer, fracture porosity, double porosity model, dolomite.

Uvod

Karbonatni vodonosniki pripadajo razpoklinskemu ali kraško-razpoklinskemu tipu. Tako pri nas kot drugod so ti vodonosniki čedalje bolj zanimivi zaradi izkoriščanja pitne vode, v tujini pa so pomembni tudi kot naftni rezervoarji. Trenutni svetovni trendi kažejo, da se raziskave razpoklinskih vodonosnikov šele začenjajo (Neuman, 2005).

Najbolj zanesljive podatke o vodonosnikih, t.j. hidravlične parametre pridobimo s pomočjo črpalnih poizkusov. Tudi za kamnine z razpoklinsko poroznostjo se uporabljajo metode črpalnih poizkusov, razvite za medzrnske vodonosnike;

Scientific paper

predvsem Theisova in Cooper-Jacobova. Te metode za razpoklinske kamnine večinoma niso primerne, zato so z njimi določeni rezultati pogosto napačni in tudi nelogični.

Namen prispevka je opozoriti na ustrezno uporabo metod v razpoklinskih vodonosnikih ter podati njihov pregled, prav tako pa na izbranih primerih podati obdelave in komentarje nekaterih metod za razpoklinske vodonosnike.

METODE

V strokovni literaturi je v primerjavi z metodami črpalnih poizkusov, razvitimi za kamnine z medzrnsko poroznostjo, metod za razpoklinske kamnine bistveno manj oz. jih nekateri celo v celoti izpuščajo (BATU, 1998). Pri prvih je namreč mogoče upoštevati popolnost vodnjakov, stacionarnost toka, anizotropnost, različno debelino vodonosnika, večplastni sistem, odprtost vodonosnikov itd. Za razpoklinske kamnine pa se uporablja precej manj metod, saj so te mlajše in še ne dovolj uveljavljene, predvsem zaradi:

- težko določljivih lastnosti razpok (terensko kartiranje, geofizikalne raziskave),
- zapletenih izračunov, ki zahtevajo precej parametrov,
- uporabe posebne tehnologije pri črpalnih poizkusih (npr. tesnil oz. 'packerjev'),
- dejstva, da so modeli dvojne poroznosti računalniško podprti šele malo časa.

Številni računalniški programi za obdelavo črpalnih poizkusov podpirajo predvsem najenostavnejše metode za medzrnske vodonosnike, le redki pa tudi za razpoklinske, npr. *Aquifer Test* (Waterloo Hydrogeologic Inc., 2001), *AQTESOLV* (HydroSOLVE, Inc., 2003) in *AquiferWin32* (RUMBAUGH & RUMBAUGH, 2003).

V prispevku je poudarek na metodah v razpoklinskih vodonosnikih in ne tudi na kraško-razpoklinskih, ker ti zahtevajo poseben pristop. Kraški vodonosniki so izredno heterogeni, saj je bilo ugotovljeno, da se lahko transmisivnost blokov matriksa kamnine in razpok razlikuje tudi za faktor 100.000 (KRIVIC, 1983).

Modeli razpoklinskih vodonosnikov

Stanje v naravi opišemo z modelom, ki predstavlja poenostavitev realnega sistema. Za razpoklinske kamnine je razvitih precej modelov, v glavnem pa jih lahko ločimo na diskretne modele, na modele kontinuuma in multikontinuuma ter na kombinirane hibridne modele (ČENČUR CURK, 2002). Pri *diskretnih modelih* moramo poznati geometrijo ter različne lastnosti razpok (položaj v prostoru, gostoto, povezanost, odprtost, hrapavost ipd.), razpoke pa nato obravnavamo deterministično, stohastično ali s fraktalnimi metodami. Pri diskretnih modelih je geometrijo razpok ponavadi zelo težko opisati, zato uporabljamo *modele kontinuuma*. Pri teh obravnavamo prostor kot ekvivalenten izotropen homogen prostor na makroskopskem nivoju tako, da upoštevamo povprečne vrednosti merjenih parametrov. Podoben pristop velja za *modele multikontinuuma*, kjer je prostor razdeljen na dva ali več prekrivajočih se homogenih podsistemov kontinuuma. Najbolj znan

model iz te skupine je model dvojne poroznosti, in je zaradi široke uporabe natančneje opisan v nadaljevanju. *Hibridni modeli* združujejo modele kontinuuma ter diskretne modele.

Model dvojne poroznosti

Pri tem modelu upoštevamo koncept dvojne poroznosti (Barenblatt et al., 1960). Zanj je značilno, da prostor ločimo na dva prekrivajoča se dela, na razpoke in na vmesne bloke matriksa, tako da tok v njih obravnavamo ločeno. Geometrija razpok je odvisna od modela, v vsakem primeru pa je zelo poenostavljena. Največkrat se uporabljata tridimenzionalni model ortogonalnih razpok, katere razdelijo prostor v kocke enakih dimenzij (Warren & Root, 1963) ali pa model med seboj vzporednih horizontalnih razpok, ki razdelijo prostor v ploščate bloke (*slab-shaped blocks*). Redkeje se uporabljajo tudi modeli dveh sistemov razpok. Ti ločijo prostor na bloke v obliki navpičnih stolpcev (npr. pri modeliranju razpok v bazaltih; Aguilera, 1987).

Za bloke matriksa je značilno, da imajo primarno poroznost ter veliko sposobnost vskladiščenja, tok v njih pa je majhen. Za razpoke velja nasprotno. Imajo namreč majhno sposobnost vskladiščenja, tok skozi vodonosnik pa teče večinoma po njih. Dodatni predpostavki sta, da je tok vode iz blokov matriksa možen le v razpoke, ter da je tok v vodnjak mogoč le iz razpok in ne iz matriksa zaradi bistveno večje prepustnosti razpok. Ločimo lahko dva režima toka. Pri *psevdo-stacionarnem toku* je prisoten tok iz matriksa v razpoke in se nivo gladine v matriksu ne spreminja. Pri *nestacionarnem toku* gladina v blokih matriksa ni stalna in se spreminja s časom. Kvantitativno opišemo tok v obeh sistemih z modificirano difuzijsko

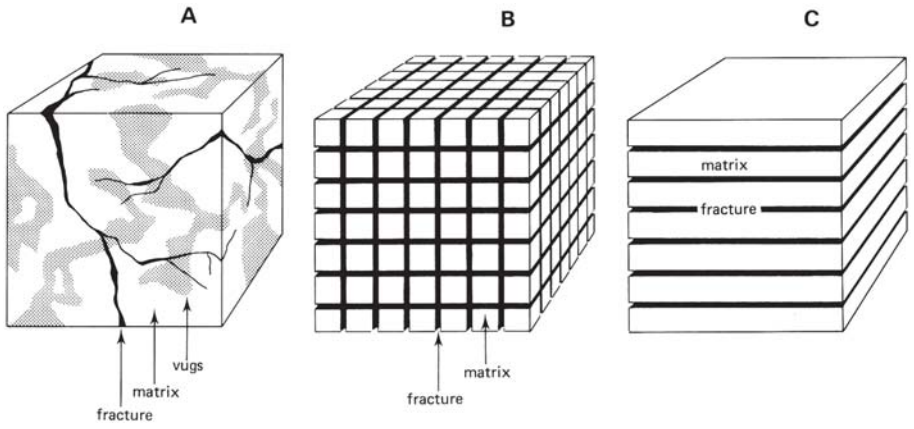

Slika 1. Razpoklinska poroznost v realni kamnini (A) ter poenostavitev z modelom dvojne poroznosti s sistemom treh pravokotnih sistemov (B) in vzporednim sistemom razpok (C) Kruseman & deRidder, 1991)
Figure 1. Fractured rock formations. (A) A naturally fractured rock formation, (B) Warren-Root's idealized three-dimensional, orthogonal fracture system, (C) Idealized horizontal fracture system (Kruseman & deRidder, 1991)

enačbo (MOENCH, 1984; DOMENICO & SCHWARTZ, 1998):

Tok v razpokah: $$K\nabla^2 h = S_s \frac{\partial h}{\partial t} + q \quad (1)$$

Tok v matriksu: $$K'\nabla^2 h = S_s' \frac{\partial h'}{\partial t} - q \quad (2)$$

q predstavlja tok iz blokov matriksa v razpoke, ki ga za psevdostacionarne razmere opišemo kot:

$$q = -\alpha K'(h' - h) \quad (3)$$

h' = prostorska povprečna vrednost hidravličnega nivoja v blokih matriksa
a = geometrijski faktor [dolžina^{-2}]

K predstavlja koeficient prepustnosti sistema razpok ($K = K_f \cdot V_f$), K' pa analogno koeficient prepustnosti sistema blokov matriksa ($K' = K_m \cdot V_m$). (4)

K_f = koeficient prepustnosti razpok
V_f = razmerje med prostornino razpok ter prostornino celotnega volumna
K_m = koeficient prepustnosti matriksa
V_m = razmerje med prostornino matriksa ter prostornino celotnega volumna

Podobno sta definirana koeficient specifičnega elastičnega vskladiščenja za sistem razpok $S_s = S_{sf} \cdot V_f$ ter za sistem blokov matriksa $S_s' = S_{sm} \cdot V_m$. (5)

Metode črpalnih poizkusov

Pri analizi rezultatov črpalnih poizkusov v razpoklinskih kamninah moramo izbrati enega od naštetih modelov razpoklinskih vodonosnikov, nato pa upoštevati še lastnosti črpalnih in opazovalnih vodnjakov ter toka v vodonosniku (popolnost vodnjaka, število opazovalnih vodnjakov, režim toka, odprtost vodonosnika itd.). Metode glede na izbrane lastnosti ločimo v več skupin:

1. Modeli z eno razpoko (horizontalna ali vertikalna razpoka). Ti primeri so v naravi precej redki, izjeme so le umetno povzročene razpoke, ki nastanejo zaradi namernega povečanja izdatnosti vodnjaka s hidravličnim razpokanjem (*hydraulic fracturing*). Tok je sprva pravokoten na ploskev razpoke, pozneje pa se spremeni v psevdoradialnega. Med metodami obdelav črpalnih poizkusov so najbolj znane (KRUSEMAN & DE RIDDER, 1991):

- metoda GRINGARTEN-WITHERSPOON (1972) za opazovalne vodnjake v homogenih izotropnih zaprtih vodonosnikih,
- metoda GRINGARTEN & RAMEY (1974) za črpalni vodnjak v homogenih izotropnih zaprtih vodonosnikih,
- metoda RAMEY-GRINGARTEN (1976) za črpalni vodnjak v homogenih izotropnih zaprtih vodonosnikih z upoštevanjem neplanarne razpoke s sposobnostjo uskladiščenja.

2. Modeli dvojne poroznosti. Med vsemi modeli za razpoklinske vodonosnike so te metode najbolj razširjene. Pri večini metod predpostavimo, da je vodonosnik izotropen, homogen, zaprt, enake debeline ter se razširja neskončno daleč. Bistvenega pomena je tudi, da je črpani pretok ves črpalni poizkus konstanten. Najbolj uveljavljene metode slonijo na naštetih predpostavkah, razlikujejo pa se predvsem v režimu toka in v številu opazovalnih vodnjakov:

- WARREN-ROOT (1963): psevdostacionaren tok (nivo gladine v matriksu se ne spreminja), velja za črpalni vodnjak,
- BOURDET & GRINGARTEN (1980): psevdostacionaren tok iz matriksa v razpoke, velja za opazovalne vodnjake,

- KAZEMI ET AL. (1969): nestacionaren tok (nivo gladine se v matriksu spreminja), velja za opazovalne vodnjake,
- BOULTON & STRELTSOVA (1977): črpalni vodnjak, vodonosnik razdeljen na porozne horizontalne bloke, ločene z razpokami,
- MOENCH (1984): psevdostacionaren in nestacionaren tok, uvedba koncepta tanke mineralne plasti.

Prve tri metode so si med seboj dokaj podobne, saj za vse veljajo naslednje matematične predpostavke. Znižanje v vodnjakih opišemo z enačbo, analogno Theisovi (KRUSEMAN & DE RIDDER, 1991):

$$s = \frac{Q}{4\pi T_f} F(u^*, \lambda, \omega) \qquad (6)$$

Theisovo funkcijo vodnjaka torej nadomešča funkcija F(u*, λ, ω), ki je odvisna od treh parametrov. Prvi, u* predstavlja modificirano vrednost Theisovega parametra u in je podan kot

$$u^* = \frac{T_f t}{(S_f + \beta S_m) r^2} \qquad (7)$$

T_f predstavlja transmisivnost razpok, S_f in S_m koeficienta elastičnega vskladiščenja v razpokah ter v blokih matriksa in β koeficient, ki je pri zgodnjih časih črpanja enak 0, pri poznih pa enak 1/3 (ortogonalni bloki) ali 1 (plasti). Dodatna parametra, s katerima opišemo tok v vodonosniku z dvojno poroznostjo, sta koeficient interporoznega toka λ, odvisen od oblike, velikosti in prepustnosti blokov matriksa, ter ω, razmerje med vskladiščenjem v razpokah ter vskladiščenjem v celotnem sistemu (oba parametra sta brez dimenzije):

$$\lambda = \alpha\, r^2 \frac{K_m}{K_f} \qquad (8)$$

$$\omega = \frac{S_f}{S_f + \beta S_m} \qquad (9)$$

α = geometrijski faktor, odvisen od odnosa med razpokami in matriksom [površina^{-1}]

Tipičen primer odziva znižanja v vodnjaku oz. v piezometrih v odvisnosti od logaritma časa je prikazan na sliki 2. Krivuljo lahko v idealnem primeru ločimo na tri dele:

- Pri zgodnjih časih črpanja (začetni del krivulje) je odvisnost *s – log t* linearna, saj je β=0 in takrat se enačba poenostavi v Theisovo enačbo, za katero lahko uporabimo Cooper-Jacobovo poenostavitev. Tok v vodnjak prihaja tedaj le iz razpok:

$$s = \frac{2{,}3Q}{4\pi T_f} \log \frac{2{,}25 T_f t}{S_f r^2} \qquad (10)$$

- Po določenem času črpanja (srednji del krivulje) se ustvari prehodno obdobje, ko začne zaradi ustvarjenega gradienta voda teči iz blokov matriksa v razpoke. Znižanje poteka tedaj počasneje, kar se odraža v manjšem naklonu krivulje oz. tudi horizontalnem poteku pri večjih prepustnostih matriksa.
- V zadnjem delu krivulje pri poznih časih črpanja priteka voda tako iz matriksa kot tudi iz razpok, krivulja se podobno poenostavi v Theisovo, le da je faktor β=1/3 oz. 1 in znižanje enako

$$s = \frac{2{,}3Q}{4\pi T_f} \log \frac{2{,}25 T_f t}{(S_f + \beta S_m) r^2} \qquad (11)$$

Moenchova metoda (1984) predstavlja nadgradnjo metod WARREN-ROOT (1963) za psevdostacionaren tok in KAZEMI ET AL. (1969) za nestacionaren tok. Z uvedbo koncepta tanke plasti na površini razpok (*angl. fracture skin*) je Moench razložil, zakaj prihaja tako do psevdostacionarnega kot tudi nestacionarnega toka. Ta plast predstavlja delno prepusten material, ki zavira tok iz matriksa v razpoke. Če je plast zelo slabo prepustna, je največji gradient hidravličnega nivoja med matriksom in razpokami prisoten na površini plasti in nestacionarni tok se poenostavi v psevdostacionarnega. Vsi računalniški programi, ki podpirajo obdelavo črpalnih poizkusov v vodonosnikih z dvojno poroznostjo, podpirajo le Moenchovo metodo, saj ta združuje koncepte vseh prej omenjenih metod. Za računalniško reševanje metode je potrebno imeti podatke o opazovalnih vodnjakih.

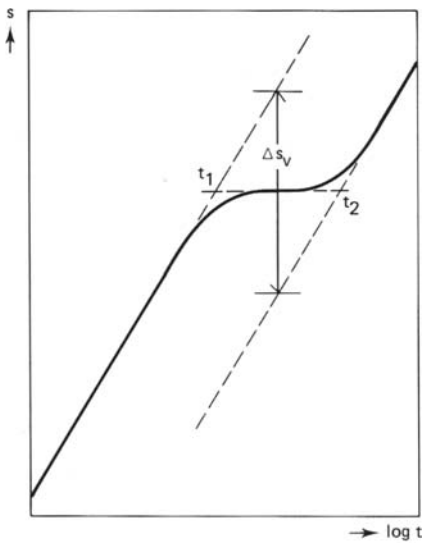

Slika 2. Odvisnost s – log t pri modelu dvojne poroznosti KRUSEMAN & DERIDDER, 1991)
Figure 2. Semi-log time-drawdown plot in a fractured rock formation of the double porosity type (KRUSEMAN & DERIDDER, 1991)

3. Diskretni oz. stohastični modeli. Za analizo črpalnih poizkusov se precej manj kot zgoraj opisani modeli uporabljajo diskretni modeli, ki temeljijo na modeliranju realne geometrije razpok z vsemi izmerjenimi razpokami (naklon, vpad, odprtost, raztezanje itd.). Hidravlične lastnosti razpoklinskega sistema se nato izračunajo s statističnimi oz. stohastičnimi metodami (National Research Council, 1996). Metode temeljijo na povezavi posameznih razpok v modele mreže razpok (DFN, *Discrete Fracture Network*) in prav tako kot fraktalne še niso širše uveljavljene.

4. Fraktalni modeli. Predvsem v zadnjih letih so za analizo črpalnih poizkusov v razpoklinskih kamninah pričeli razvijati fraktalne metode (ACUNA & YORTSOS, 1995; HAMM & BIDAUX, 1996; LEVEINEN, 2000). Metodam je skupna predpostavka, da se nek pojav pojavlja v enaki obliki v različnih merilih. Tako lahko npr. na bloku kamnin določen vzorec razpok pričakujemo v regionalnem merilu. Večina teh metod je razvitih za nestacionaren tok, rešitve pa podobno kot pri Theisovi in ostalih metodah omogoči prilagajanje podatkov tipskim krivuljam.

Pri fraktalnih metodah je lahko dimenzija toka tudi realno število *n*, ki ima vrednosti med 1 (enodimenzijski tok), 2 (cilindrični dvodimentionalni tok) ali 3 (radialni sferni tok v prostoru). Splošno difuzijsko enačbo, ki opisuje nestacionaren tok za te primere, je določil BARKER (1988) v svojem *Generalized Radial Flow* (*GRF*) modelu:

$$\frac{K_f}{r^{n-1}}\frac{\partial}{\partial r}\left(r^{n-1}\frac{\partial h}{\partial r}\right) = S_{sf}\frac{\partial h}{\partial t} + q \qquad (12)$$

Podatki iz literature kažejo, da taki primeri v naravi obstajajo, saj so rezultate črpalnih poizkusov v različnih kamninah prilagodili krivuljam z različno dimenzijo *n,* npr. n=1,8 v granitih, 1,7 v gabrih (Lods & Gouze, 2004). Za n=2 se Barkerjeve enačbe poenostavijo v znani formuli Theisa in Cooper-Jacoba za nestacionaren tok ter v Thiemovo formulo za stacionaren tok.

Rezultati in razprava

V nadaljevanju je podanih nekaj značilnih primerov rezultatov in analiz črpalnih poizkusov v dolomitih. Podobne grafe bi lahko analizirali tudi v nekaterih drugih kamninah, za katere veljajo predpostavke modela dvojne poroznosti (npr. razpokani peščenjaki, razpokane magmatske kamnine itd.). Za dolomite je značilno, da spadajo med zelo razpokane kamnine, saj so razpoke v njih precej bolj pogoste kot v peščenjakih in apnencih (Aguilera, 1980). To potrjujejo tudi opazovanja dolomitnih plasti v Sloveniji. Poroznost matriksa lahko v dolomitih niha v precej širokem razponu, od skoraj nič do nekaj odstotkov in pripada večinoma medkristalni poroznosti, nastali pri dolomitizaciji, redkeje pa poroznosti, nastali z raztapljanjem (*vugs*), ter fenestralni poroznosti, značilni za medplimske dolomite (Moore, 2001).

Na sliki 3 je prikazan graf znižanja v odvisnosti od časa pri črpalnem poizkusu v dolomitu cordevolske starosti pri konstantnem pretoku Q = 15 l/s (Verbovšek, 2003). Na njem je prikazana tridelna krivulja, značilna za model dvojne poroznosti. V začetnem delu krivulje (prvih nekaj minut) je opaznih nekaj odstopanj od premice, nato sledi položni del in kasneje (od 1000 minut dalje) spet počasno naraščanje znižanja. Podatki veljajo za črpalni vodnjak, zato je bila za analizo primerna obdelava po metodi Warren-Roota (1963), ki je dala naslednje rezultate: $T_f = 4{,}43 \cdot 10^{-3}$ m^2/s, $S_f = 1{,}85 \cdot 10^{-2}$,

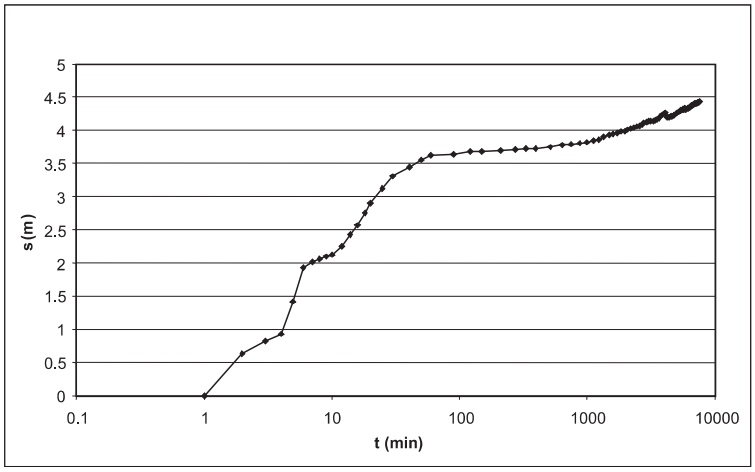

Slika 3. Diagram znižanja s v odvisnosti od časa (črpalni poizkus v dolomitu cordevolske starosti, Q=15 l/s) (Verbovšek, 2003)
Figure 3. Semi-log plot for pumping test data in dolomite (Cordevolian age, discharge Q = 15 l/s) (Verbovšek, 2003).

S_m = 0,34 in koeficienta $\lambda = 1{,}35 \cdot 10^{-6}$ ter ω = 0,05. Primerljive vrednosti smo dobili tudi pri analizi Moenchovih podatkov za črpalni vodnjak po metodi Warren-Roota (KRUSEMAN & DE RIDDER, 1991). Transmisivnosti blokov matriksa po tej metodi ni mogoče določiti. Obnašanje po modelu dvojne poroznosti je posledica dejstva, da ima dolomit cordevolske starosti veliko medkristalno poroznost, saj je nastal s pozno diagenezo.

Na drugem diagramu (sl. 4) je vidno znižanje v dolomitu zgornjetriasne starosti pri črpanju Q = 0,1 l/s (VERBOVŠEK, 2003). Črpanje je trajalo bistveno manj časa kot pri prejšnjem primeru, zato iz oblike krivulje ni jasno, kakšen bi bil nadaljni potek podatkov na grafu. Mogoče je namreč, da so meritve zajele le začetni del krivulje, ko je prisoten tok le iz razpok, saj leži večina podatkov na linearnem delu. To potrjuje nekaj zadnjih meritev, kjer se znižanje počasi izravnava v bolj položno krivuljo, ki je tipična za model dvojne poroznosti. Druga možnost pa je, da ima dolomit zelo majhno poroznost matriksa in sta tako tok kot vskladiščenje prisotna le v razpokah in ne tudi v matriksu. V tem primeru velja izračunani koeficient elastičnega vskladiščenja S = 0,31 tako za bloke matriksa kot tudi za razpoke ($S_f + \beta S_m$), zadnjih nekaj meritev pa lahko predstavlja vpliv slabše prepustne bariere ali pa manjše merske napake. Za analizo linearnega dela je lahko tedaj primerna Cooper-Jacobova metoda, kateri izračunani podatek $T = 6{,}54 \cdot 10^{-6}$ m^2/s predstavlja transmisivnost razpok T_f in ne transmisivnosti kamnine z medzrnsko poroznostjo T_m.

Na sliki 5 (VERBOVŠEK, 2003) je prikazan primer črpalnega poizkusa, kjer modela dvojne poroznosti žal zaradi prevelikih nihanj pretoka ne moremo direktno uporabiti na s-t diagramu. Zato moramo v ta namen uporabiti za pretok normirani s/Q-t diagram, na kar se često pozablja. Takih situacij je precej, saj se pogosto uporabljajo t.i. *step testi*, s katerimi

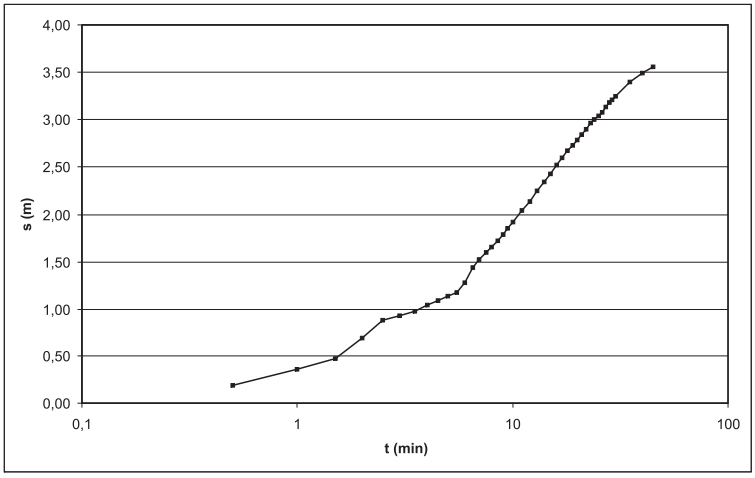

Slika 4. Diagram znižanja s v odvisnosti od časa (črpalni poizkus v dolomitu zgornjetriasne starosti, Q=0,1 l/s)
Figure 4. Semi-log plot for pumping test data in dolomite (Norian-Rhaetian age, discharge Q = 0.1 l/s) (Verbovšek, 2003)

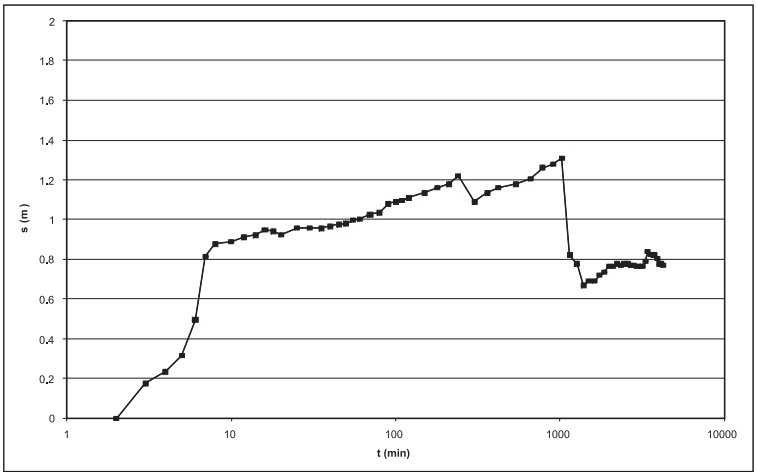

Slika 5. Diagram znižanja s v odvisnosti od časa (črpalni poizkus v "glavnem dolomitu" norijsko-retijske starosti), variabilen pretok (VERBOVŠEK, 2003)
Figure 5. Semi-log plot for pumping test data in dolomite (upper Triassic age), variable discharge (VERBOVŠEK, 2003)

določujejo učinkovitosti delovanja vodnjakov. Kadar sta v takem obravnavanem sistemu prisotni obe vrsti poroznosti, so efekti dvojne poroznosti zaradi nihanja pretokov zabrisani.

ZAKLJUČKI

Temeljna razlika med analizami črpalnih poizkusov v medzrnskih in v razpoklinskih vodonosnikih je v izračunu hidravličnih parametrov, saj dobimo v prvem primeru podatka o transmisivnosti (T) in specifičnem elastičnem vskladiščenju vodonosnika (S_s), v drugem pa ločene rezultate transmisivnosti (T_f) in specifičnega elastičnega vskladiščenja razpok (S_{sf}) ter transmisivnosti (T_m) in specifičnega elastičnega vskladiščenja blokov matriksa (S_{sm}). Razlika je opazna tudi na grafu odvisnosti znižanja od časa (*s – log t*), kjer je za medzrnske kamnine odvisnost linearna, za razpoklinske pa se kaže v obliki tridelne krivulje v obliki črke S (sl. 2 in sl. 3). Za prvi del krivulje je značilen tok le iz razpok ($T_f >> T_m$), nato pride do upočasnitve naraščanja znižanja zaradi toka iz matriksa v razpoke, na koncu pa se blažilni učinek dotoka vode iz matriksa izgubi.

V začetnem delu so zaradi kratkih merskih časovnih intervalov na krivulji mogoče manjše napake pri meritvah, prav tako pa na ta del krivulje vplivajo efekti vskladiščenja vode v vodnjaku ter "kožni" oz. *skin* efekti, zato premici (sl. 2) skoraj nikoli nista vzporedni. Tridelna krivulja je lahko zabrisana tudi, kadar je parameter λ izredno majhen, saj je tedaj transmisivnost blokov matriksa zanemarljiva in tok je v celotnem črpalnem poizkusu prisoten le v razpokah. Kamnina se tedaj obnaša podobno kot homogen vodonosnik z medzrnsko poroznostjo.

Analiza izbranih črpalnih poizkusov v dolomitnih vodonosnikih kaže, da nekatere krivulje sledijo modelu dvojne poroznosti in jih je zato potrebno tako tudi razlagati.

Rezultati samodejnega računalniškega prilagajanja rezultatov krivulj za medzrnsko poroznost skozi vse točke na sliki 3 so nelogični, dobljene vrednosti pa so napačne, saj naj bi parametre v razpokah in v matriksu obravnavali ločeno (RUMBAUGH AND RUMBAUGH, 2003).

Nekateri črpalni poizkusi v dolomitih na grafu $s - log\ t$ vseeno ne prikazujejo omenjene krivulje v treh delih, temveč le v linearni odvisnosti, podobno kot pri medzrnskih kamninah (sl. 4). Vzrokov je več. Če je črpanje prekratko, pridobimo podatke le za prvi del krivulje, saj tedaj še ne prihaja do izcejanja vode iz matriksa v razpoke. Črpalni poizkusi bi v takih primerih torej morali biti daljši (primer na sliki 2). Če so razpoke drobne in je kamnina z njimi gosto prežeta ter če zanjo veljajo pogoji laminarnega toka oz. Darcyjev zakon, potem lahko za razpoklinske vodonosnike uporabimo tudi metode, razvite za medzrnske vodonosnike (VASVARI & KRIEGL, 2003). Model dvojne poroznosti tedaj namreč izgubi pomen in se poenostavi v model z enojno poroznostjo, za katerega veljajo metode Theisa in Cooper-Jacoba. Seveda moramo upoštevati, da predstavlja izračunani podatek T transmisivnost razpok T_f hkrati pa podatek o elastičnem koeficientu vskladiščenja S velja za razpoke (S_f). Tretja razlaga za linearen potek krivulje je mogoča pri analizi podatkov iz opazovalnih vodnjakov. Tridelna krivulja je namreč značilna le za bližnjo okolico črpalnega vodnjaka, saj je na določeni oddaljenosti od vodnjaka prisoten le združen tok iz matriksa in iz razpok (KAZEMI ET AL., 1969).

Če je iz podatkov črpalnega poizkusa razvidno, da ima vodonosnik dvojno poroznost, lahko zaradi metode samodejnega računalniškega prilagajanja krivulj za medzrnsko poroznost nastanejo temeljne napake. Namesto realnih vrednosti hidravličnih parametrov dobimo prevelike ali premajhne vrednosti, kar je odvisno od načina samodejnega prilagajanja. Tako lahko npr. izračunamo večjo transmisivnost ali specifično elastično vskladiščenje vodonosnika, kot je dejanska, s tem pa precenimo sposobnost izkoriščanja vode iz vodonosnika. Napačni so lahko tudi izračuni hitrosti pretakanja vode v vodonosnikih, dejansko širjenje polutantov je lahko npr. mnogo hitrejše, kot smo izračunali, ker se polutanti v razpokah in v matriksu gibljejo s precej različno hitrostjo.

Čeprav so obdelave črpalnih poizkusov v razpoklinskih vodonosnikih bolj zapletene in manj razširjene kot metode za medzrnske kamnine, jih je vsekakor potrebno uporabljati, ko analiziramo črpalne poizkuse v razpoklinskih kamninah. Ker moramo včasih potrebne parametre določiti že med črpanjem, je za pravilne rezultate ključnega pomena predhodno poznavanje ustreznih metod.

Zahvale

Hvala izr. prof. dr. M. Veseliču za kritične pripombe pri izdelavi prispevka.

SUMMARY

Appropriate analysis methods of pumping tests in fractured aquifers

Carbonate aquifers belong to fractured or karstic-fractured type. Although the appropriate methods for analyzing pumping

test data are those developed for fractured aquifers, unsuitable methods like Theis or Cooper-Jacob are still currently used for analysis in Slovenia. Use of these methods leads to erroneous calculations of hydraulic parameters. However, even in some recent aquifer test data books the methods for fractured reservoirs are completely omitted (Batu, 1998). The reason for their absence is probably the fact that they are still "being developed" and are not widely in use, mostly because of complex mathematical theory used for analysis, hard-to-obtain fracture properties and the need for special drilling equipment.

Modeling of fractured aquifers can be divided in four categories: dicrete models, continuum, multicontinuum and hybrid models. Most aquifer test analysis methods are based on the double porosity model (Barenblatt et al., 1960), which belongs to the multicontinuum type. Characteristic for this model is that the heterogeonous space is divided into two overlapping media: the fractures and the matrix blocks (Fig. 1), both of them having their own characteristics. The fractures have high permeability and low storage capacity and the matrix blocks the opposite, low permeability and high storage capacity.

There are several aquifer test data analysis methods, which fall into different categories:

- Single vertical or horizontal fractures: methods of Gringarten-Witherspoon (1972), Gringarten & Ramey (1974) and Ramey-Gringarten (1976).
- Double porosity models: Warren-Root (1963), Bourdet & Gringarten (1980), Kazemi et al. (1969), Boulton & Streltsova (1977) and Moench (1984).
- Discrete and stochastic models: different methods, based on Discrete Fracture Network (DFN) models (National Research Council, 1996).
- Fractal analysis: most methods are based on Barker's (1988) Generalized Radial Flow (GRF) model, which allows non-integer values for flow dimension.

Most methods, used for analysis of dolomite and other fractured-type aquifers, belong to double porosity models. Drawdown in these systems can be divided in three time periods (Fig. 2): early pumping time, when all the flow comes from the storage in the fractures, medium pumping time, which represents transition period during which the matrix blocks feed the water to the fractures and late pumping times, when the water comes both from the storage in fractures and matrix blocks (Kruseman & de Ridder, 1991).

On Figure 3 is shown the semi-log plot for aquifer test data of dolomite of cordevolian age (Verbovšek, 2003). The curve follows the ideal double porosity type curve of early, middle and late pumping times. The parallel lines however do not occur, because the early time linear relationship is hidden by well-storage and skin effects. Data have been analyzed by Warren-Root (1963) method, which supports single pumping well conditions with no observation wells and it showed the following results: $T_f = 4.43 \cdot 10^{-3}$ m^2/s, $S_f = 1.85 \cdot 10^{-2}$, $S_m = 0.34$, $\lambda = 1.35 \cdot 10^{-6}$ and $\omega = 0.05$, which are comparable to those of Moench (Kruseman & De Ridder, 1991). The double porosity behaviour can be explained by large intercrystalline porosity of dolomite, which was developed by burial diagenesis. On the next figure (Fig. 4; Verbovšek, 2003) is

shown the plot which does not show the typical double porosity curve. In comparison with previous data the pumping times are much shorter, which can result in "missing" transition and late pumping times parts of the curve. Pumping test should be longer in this case. Another explanation is that dolomite has very low matrix porosity, which simplifies the double porosity model into single-porosity one, having only fracture porosity. In this case the usual Theis or Cooper-Jacob methods can be used. The last plot (Fig. 5; VERBOVŠEK, 2003) shows the data obtained by using variable discharge. Drawdown significantly deviates from the ideal three-part curve and the double porosity methods can generally not be used due to the too short later steps.

The main difference between the single porosity and double porosity models is that the last ones give the results of transmissivities and storativities of both fractures and matrix. We can also detect the double porosity behaviour on the semi-log plot of drawdown versus time, which shows two lines (usually not paralel due to well-storage and skin effects) with transition time in between (Fig. 2). Use of automatic computer-fitting linear curve to all the data in Figure 2 or Figure 3 would lead to erroneous and illogical results, as there are actually two transmissivities and storativities of the system (fracture and matrix). One can therefore calculate incorrect transmisivities and storativities, and this could lead to misinterpreted flow and pollutant velocities. The proper use of fractured aquifer methods is therefore of utmost importance.

VIRI

ACUNA, J. A. & YORTSOS, Y. C. (1995): Application of fractal geometry to the study of networks of fractures and their pressure transient.- *Water Resources Research* Vol. 31, No. 3,: pp. 527-540.

AGUILERA, R. (1980): Naturally Fractured Reservoirs.- *Pennwell Books,* 703 p.

AGUILERA, R. (1987): Well Test Analysis of Naturally Fractured Reservoirs.- *SPE Formation Evaluation,* Society of Petroleum Engineers.

BARENBLATT, G.I., ZHELTOV, IU.P., KOCHINA, I.N. (1960): Basic concepts in the theory of seepage of homogenous liquids in fissured rocks. - *Journal of Applied Mathematics and Mechanics* 24 (5): pp. 1286-1303.

BARKER, J. A. (1988): A Generalized Radial Flow Model for Hydraulic Tests in Fractured Rock.- *Water Resources Research.*: 24, No. 10, pp. 1796-1804.

BATU, V. (1998): Aquifer Hydraulics. A comprehensive guide to hydrogeologic data analysis.- *John Wiley & Sons Inc.*, 727 p.

BOULTON, N.S. & STRELSTOVA, T.D. (1977): Unsteady flow to a pumped well in a fissured water-bearing formation.- *J. Hydrol.*: 30, pp. 29-46.

BOURDET, D. & GRINGARTEN, A. C. (1980): Determination of fissure volume and block size reservoirs by type-curve analysis.- Paper SPE 9293, Presented at 1980 *SPE Annual Fall Techn. Conf. and Exhib*., Dallas

ČENČUR CURK, B. (2002): Tok in prenos snovi v kamnini s kraško in razpoklinsko poroznostjo: *Doktorska disertacija. Univerza v Ljubljani*, NTF, 253 p.

DOMENICO, P. A. AND SCHWARTZ, F. W. (1998): Physical and Chemical Hydrogeology, 2nd ed.- *Wiley,* 528 p.

GRINGARTEN, A. C. & WITHERSPOON, P. A. (1972): A method of analyzing pump test data from fractured aquifers.- *Int. Soc. Rock Mechanics and Int. Ass. Eng. Geol., Proc. Symp. Rock Mechanics,* Stuttgart, Vol. 3-B, pp.1-9.

HAMM, S-Y. & BIDAUX, P. (1996): Dual-porosity fractal models for transient flow analysis in fissured rocks.- *Water Resources Research. 32*, No. 9, pp. 2733-2745.

HYDROSOLVE INC. (2005): AQTESOLV for Windows. Version 3.5. http://www.aqtesolv.com.

Kazemi, H., Seth, M.S., Thomas, G.W. (1969): The Interpretation of Interference Tests in Naturally Fractured Reservoirs with Uniform Fracture Distribution.- Soc. of *Petrol. Engrs. J*., pp. 463-472.

Krivic, P. (1983): Študija hidrodinamike kraškega vodonosnika (Slovenski povzetek).- *Geologija.:* 26, pp. 149-186.

Kruseman, G. P. & De Ridder, N. A. (1991): Analysis and Evaluation of Pumping Test Data, 2nd ed. - International Institute for Land Reclamation and Improvement, *Wageningen, (ILRI Publication 47)*, 377 p.

Leveinen, J. (2000): Composite model with fractional flow dimensions for well test analysis in fractured rocks.- *Journal of Hydrology.* 234, pp. 116-141.

Lods, G. & Gouze, P. (2004): WTFM, software for well test analysis in fractured media combining fractional flow with double porosity and leakance approaches. *Computers & Geosciences:* 30, pp. 937-947.

Moench, A. F. (1984): Double porosity Models for a Fissured Groundwater Reservoir With Fracture Skin.- Water Resources Research. 20, No. 7, pp. 831-846.

Moore, C. H. (2001): Carbonate Reservoirs, Porosity Evolution and Diagenesis in a Sequence Stratigraphic Framework, *Elsevier Science B.V.*, Amsterdam.

National Research Council (1996): Rock fractures and fluid flow. Contemporary Understanding and Applications.- *National Academy Press*, 551 p.

Neuman, S.P. (2005): Trends, prospects and challenges in quantifying flow and transport through fractured rocks.- *Hydrogeology Journal*. 13, 124-147, DOI: 10.1007/s10040-004-0397-2

Rumbaugh, D. & Rumbaugh, J. (2003): Program AquiferWin32, Version 3.00.- *Environmental Simulations,* Inc.

Vasvári, V. & Kriegl, C. (2003): Determination of hydraulic properties in fractured aquifers in Austria.- V: Krásný, J., Zbynek, H., Bruthans, J.: I*nternational Conference on Groundwater in Fractured Rocks*, pp. 109-110, Prague.

Verbovšek, T. (2003): Izdatnost vodnjakov in vrtin v Sloveniji – skupina dolomitnih vodonosnikov.- *Diplomsko delo, Univerza v Ljubljani*, NTF, 206 p.

Warren, J.E. & Root, P.J. (1963): The Behavior of Naturally Fractured Reservoirs.- *Soc. of Petrol. Engrs. J.* 3, pp. 245-255.

Waterloo hydrogeologic inc. (2001): WHI AquiferTest, Version 3.01, Waterloo Hydrogeologic Inc., Canada (Interna pomoč programa), http://www.waterloohydrogeologic.com.

Modeliranje napajanja vodonosnika v zaledju izvira Rižane z območja Brkinov

Modelling the recharge of the aquifer in the Rižana catchment from Brkini area.

Mitja Janža

Geološki zavod Slovenije, Dimičeva 14, 1000 Ljubljana; Slovenija,
E-mail: mitja.janza@geo-zs.si

Received: June 22, 2005 **Accepted**: November 24, 2005

Izvleček: V članku je opisan dinamičen hidrološki model z distribuiranimi parametri (MIKE SHE-MIKE 11), izdelan na območju Brkinov - delu napajalnega območja vodonosnika v zaledju izvira Rižane. Rezultat modela je prostorsko in časovno porazdeljeni simulirani odtok z območja Brkinov, ki posredno napaja vodonosnik. Značilnosti odtoka, določene na podlagi simuliranih dnevnih odtokov za enajstletno obdobje (od 1.1.1983 do 31.12. 1993), so opisane s statistikami: povprečni odtok 0,970 m^3/s, standardni odklon odtokov 2,327 m^3/s, minimalni odtok 0,012 m^3/s, maksimalni odtok 30,534 m^3/s, mediana 0,288 m^3/s, petindvajseti percentil 0,129 m^3/s, petinsedemdesetini percentil 0,531 m^3/s, cenilka asimetričnosti 5,230 in cenilka sploščenosti 36,943.

Abstract: In this paper a dynamic distributed hydrological model (MIKE SHE-MIKE 11) that was developed in the area of Brkini (part of the recharge area of the aquifer of Rižana spring) is described. The result of the model is spatially distributed and temporally variable simulated outflow from the Brkini area that indirectly recharges the aquifer. Characteristics of the outflow, defined on the daily simulated outflows for eleven years period (from 1. 1. 1983 to 31. 12. 1993), are described by statistics: average outflow 0.970 m^3/s, standard deviation 2.327 m^3/s, minimum outflow 0.012 m^3/s, maximum outflow 30.534 m^3/s, median 0.288 m^3/s, 25 percentile 0.129 m^3/s, 75 percentile 0.531 m^3/s, skewness 5.230 and kurtosis 36.943.

Ključne besede: napajanje vodonosnika, hidrološki model, MIKE SHE, Brkini, izvir Rižane, Slovenija.
Key words: aquifer recharge, hydrological model, MIKE SHE, Brkini, Rižana spring, Slovenia.

Uvod

Izvir reke Rižane je najpomembnejši vir pitne vode na območju slovenske Obale. Pojavlja se na kontaktu med vodonosnimi paleogenskimi apnenci in slabo prepustnimi eocenskimi flišnimi plastmi. Po svojih značilnostih je tipični kraški izvir. Zaledje izvira je del obsežnega kraškega sistema, ki se začenja na zahodu s Krasom in na vzhodu končuje v Kvarnerskem zalivu. Sistem izvira Rižane tvori osrednji del, od koder odtekajo podzemne vode proti Tržaškemu zalivu, Kvarnerju, proti jugu pa izvirajo kot Rižana ali pa obnavljajo vodonosne plasti apnencev pod flišnim pokrovom proti Dragonji (Prestor, 1992).

Scientific paper

Vodonosnik v zaledju izvira Rižane neposredno napajajo padavine, posredno pa voda potokov, ki pritečejo z območja Brkinov in poniknejo na stiku fliša s karbonatnimi kamninami. Dotok ponikajočih voda potokov v izvir Rižane dokazujejo sledilni poskusi (KRIVIC ET AL., 1987; KRIVIC ET AL., 1989; NOVAK, 1963). Zaradi hitrega dospetja sledila iz območja ponikanja do izvira (štiri do šest dni) je to območje izjemnega pomena za varovanje vodnega vira in je uvrščeno v ožje vodovarstveno območje.

V članku je opisana ocena količine posrednega napajanja vodonosnika v zaledju izvira Rižane z območja Brkinov. Ocena temelji na hidrološkem modelu (MIKE SHE-MIKE 11), ki je bil izdelan na osnovi novo pridobljenih podatkov o pretokih v obdobju od 1. 11. 2001 do 31. 3. 2003. Prednost uporabe modela je možnost simulacije prostorske in časovne spremenljivosti napajanja. S pomočjo modela pridobljene nove informacije so bile kasneje vključene kot robni pogoj v model vodonosnika v zaledju izvira Rižane (JANŽA, 2003), s katerim so bili simulirani pretoki izvira v obdobju od 1. 1. 1983 do 31. 12. 1993.

OBRAVNAVANO OBMOČJE

Obravnavano območje Brkinov obsega severovzhodni del z varstvenimi pasovi varovanega zaledja izvira Rižane (sl. 1). Sestavljeno je iz osmih povodij s skupno površino 44,39 km^2 (sl. 2). Gradijo ga flišne kamnine in se po hidrogeoloških lastnostih

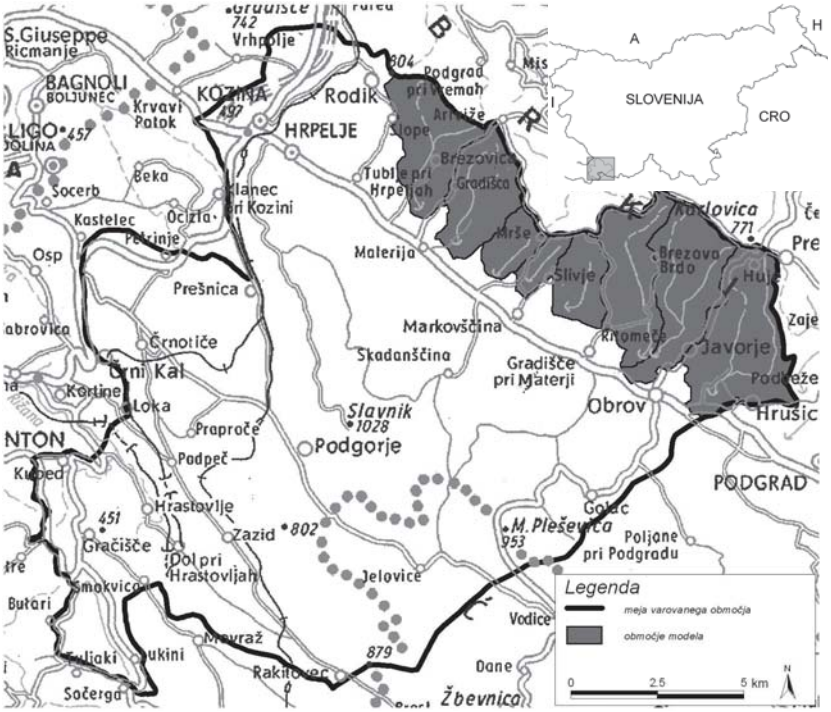

Slika 1. Obravnavano območje.
Figure 1. Study area.

Tabela 1. Osnovne reliefne značilnosti povodij.
Table 1. Basic relief characteristics of the catchments.

Oznaka povodja	**P1**	**P2**	**P3**	**P4**	**P5**	**P6**	**P7**	**P8**
Površina [km^2]	6,52	5,90	2,28	1,46	3,33	6,84	7,88	10,18
Naklon								
Povprečni [^{o}]	13,3	14,5	10,9	11,1	11,4	12,1	12,3	10,5
Standardni odklon [^{o}]	6,5	6,6	4,6	4,8	5,2	5,4	5,5	5,0
Nadmorska višina								
Povprečna [m]	632	632	632	618	604	604	612	582
Minimalna [m]	497	475	547	543	524	501	499	492
Maksimalna [m]	811	808	745	741	747	760	763	764
Standardni odklon [m]	78	81	49	52	53	58	63	57

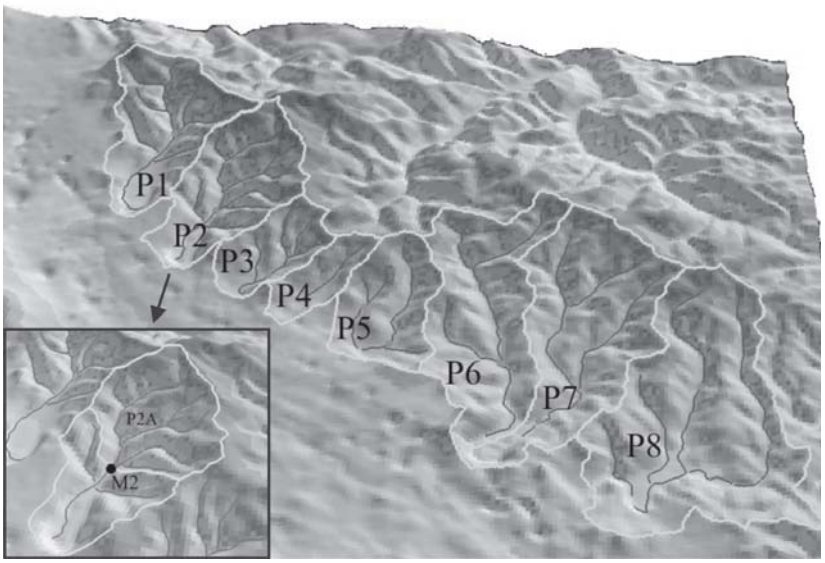

Slika 2. Digitalni model višin z območji povodij in mestom meritve M2.
Figure 2. Digital elevation model with catchments and measurement location M2.

bistveno razlikuje od pretežno karbonatnega dela zaledja. Večina vode odteče z območja Brkinov površinsko in podpovršinsko, z značilnim hitrim povečanjem odtokov po deževju. Skupna značilnost potokov je, da pritekajo iz slabo prepustnih flišnih kamnin in ponikajo na delu povodja, kjer je matična podlaga apnenec. Dno dolin na tem delu je pokrito z aluvialnimi sedimenti. Potoki se večinoma končajo s ponori. Voda potokov jih doseže le ob visokem vodostaju, drugače ponikne že v strugi.

Osnovne reliefne značilnosti povodij, ki so bile izdelane z analizo digitalnega modela višin - DMV (ZRC SAZU & Mobitel, d. d., 2000), so prikazane v tabeli 1. Zaradi različnih poimenovanj potokov na obravnavanem območju so povodja označena z oznakami od P1 do P8 (od severozahoda do jugovzhoda). Natančneje je te slepe doline morfološko analiziral MIHEVC (1991).

HIDROLOŠKI MODEL OBRAVNAVANEGA OBMOČJA

Uporabljeni podatki

Izdelava modela je zahtevala številne vhodne podatke. V nadaljevanju so na kratko opisani najpomembnejši med njimi. Natančneje je uporabljene podatke opisal JANŽA (2003).

Meritve pretokov

Za namene modeliranja so bile opravljene meritve pretokov na izbranih mestih potokov. Meritve so bile občasne, razen na merskem mestu M2, kjer je bil nameščen sistem za zvezno meritev pretoka (sl. 2). Za zvezno meritev pretoka je bilo izbrano mesto, ki po svojih značilnostih odražala lastnosti vseh povodij. Meritev je bila opravljena v umetnem kanalu, ki služi kot prepust potoka pod gozdno cesto. S tem se je izognilo vplivu spremembe merskega preseka, kar je pogosto težava pri meritvah pretoka v naravnih koritih. S konstrukcijo ob straneh kanala je bil zmanjšan njegov presek na iztoku in preoblikovan v trapezoidno obliko, ki omogoča natančnejšo meritev nizkih pretokov. Pretok je bil ocenjen posredno preko nivoja vode v kanalu, ki je bil merjen v petnajstminutnih intervalih s tlačno sondo z natančnostjo 6,2 mm. Sonda je bila postavljena na dno kanala. Privzeto je bilo, da pretoka ni, ko se gladina vode v kanalu zniža do nivoja sonde.

Za določitev odnosa med pretokom in višino vode so bile uporabljene meritve pretoka s kemijsko integracijsko metodo in takrat izmerjeni nivoji. Na podlagi teh podatkov je

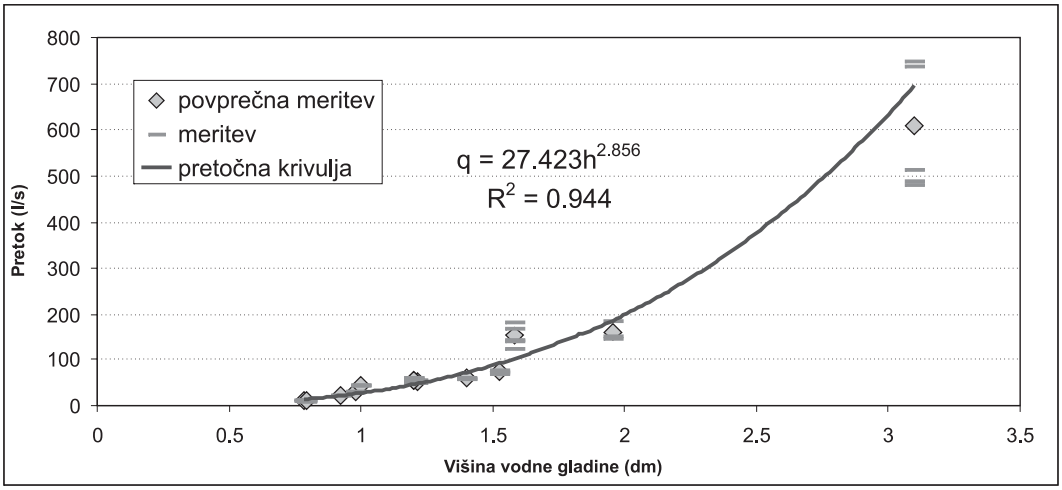

Slika 3. Pretočna krivulja.
Figure 3. Rating curve.

bila določena pretočna krivulja (sl. 3), ki ima obliko funkcije: $q = gh^u$, kjer so: (1)

q pretok;
h višina gladine vode v kanalu;
g, u umeritvena koeficienta.

Natančnost meritev, uporabljenih za določitev pretočne krivulje je prikazana na slikah 4 in 5, ki prikazujeta absolutno in relativno razliko med posameznimi meritvami in njihovim povprečjem. Na sliki 6 so prikazane razlike med modelom pretočne krivulje in povprečji merjenih pretokov.

Ustreznost uporabljenega modela pretočne krivulje je bila preverjena z analizo variance, ki temelji na razmerju med eksperimentalno napako posameznih meritev in odstopanjem modela pretočne krivulje od povprečnih meritev v posameznih točkah. V obravnavanem primeru znaša povprečni kvadrat čiste napake $MS_{PE} = 3707\ l^2/s^2$, povprečni kvadrat napake prilagajanja pa $MS_{LOF} = 5740\ l^2/s^2$. Razmerje $F^{izr.} = MS_{LOF} / MS_{PE}$ znaša 1,55, kar je manj kot tabelarična kritična vrednost porazdelitve $F_{(a,k-p,N-k)} = 2,0$ (k = 13 - število točk na katere je bil model prilagojen,

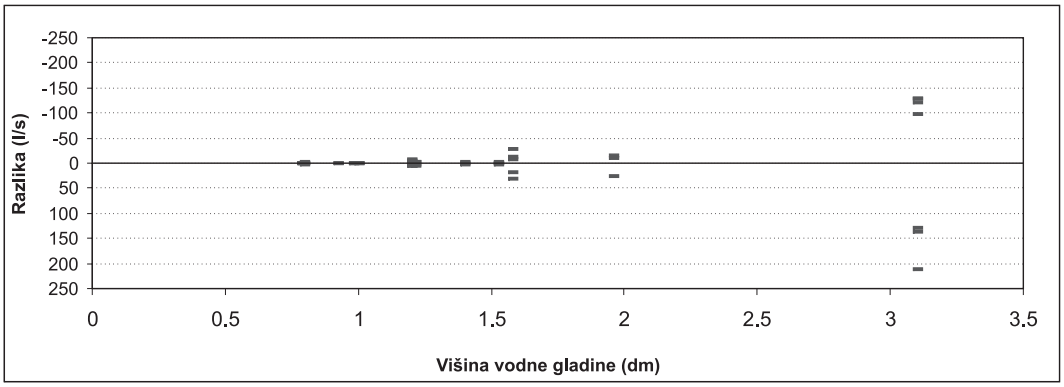

Slika 4. Razlika med posameznimi meritvami pretokov in njihovim povprečjem.
Figure 4. Difference between measured discharges and their averages.

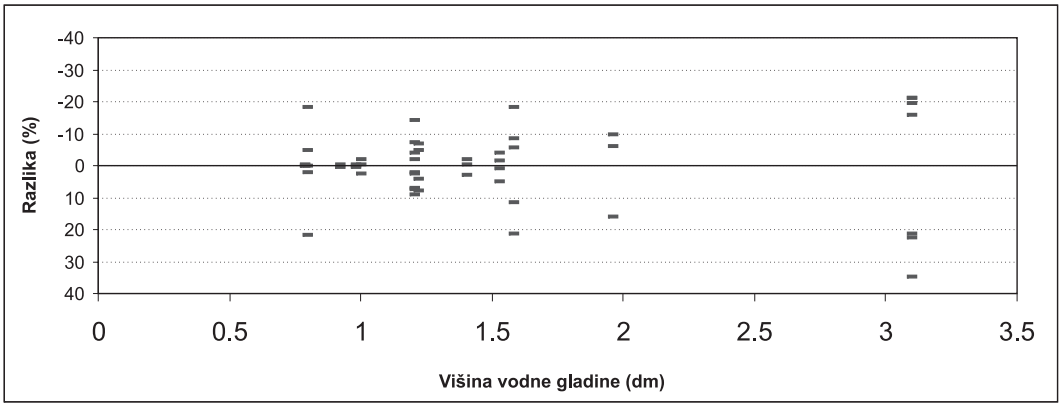

Slika 5. Relativna razlika med posameznimi meritvami pretokov in njihovim povprečjem.
Figure 5. Relative difference between measured discharges and their averages.

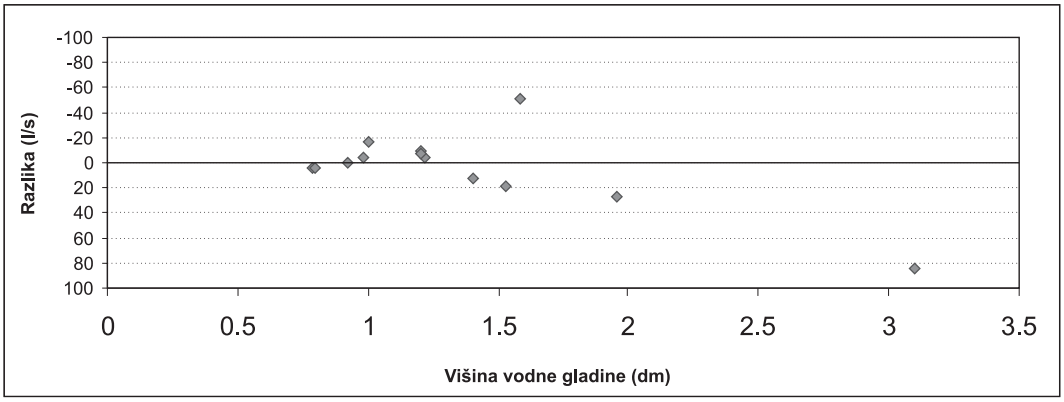

Slika 6. Razlika med modelom pretočne krivulje in povprečji merjenih pretokov.
Figure 6. Difference between the rating curve model and average discharges.

p = 1 – število parametrov modela, N = 51 – število vseh meritev) za mejo zanesljivosti a = 0,05. Z zadostitvijo pogoja: $1 < F^{izr.} < F_{(0.05,12,38)}$ je bila potrjena ustreznost modela pretočne krivulje.

Z opisanim modelom pretočne krivulje izračunani povprečni dnevni pretoki na merskem mestu M2 so prikazani na sliki 8. Zaradi tehničnih razlogov in občasno zamrznjene struge potoka meritve niso zvezne za celotno obdobje od 1. 11. 2001 do 31. 3. 2003. Okrog 20 % obravnavanega obdobja je brez podatkov. Za obdobja razpoložljivih podatkov znaša ocenjena mediana dnevnih pretokov 25 l/s.

Meritve naravnih vodotokov so podvržene številnim napakam. V opisanem primeru jih je težko ovrednotiti, so pa predvsem posledica poenostavljene izvedbe merskega mesta in omejenega števila neposrednih meritev. Zaradi manjšega števila meritev za stanja visokih vod in manjše natančnosti teh meritev (sl. 4) je zanesljivost izračuna visokih pretokov s pomočjo izdelane pretočne krivulje manjša.

Meteorološki podatki

Modeliranje je bilo izvedeno za dve obdobji. V vsakem obdobju so bili uporabljeni podatki takrat delujočih meteoroloških postaj, ki so bile najbližje obravnavanemu območju. Za prvo obdobje modeliranja (od 1. 1. 1983 do 31. 12. 1993) so bile uporabljene dnevne višine padavin iz padavinskih postaj Matavun, Kozina in Podgrad ter višine potencialne evapotranspiracije iz meteorološke postaje Ilirska Bistrica. V drugem obdobju modeliranja (od 1. 11. 2001 do 31. 3. 2003) so bile uporabljene višine padavin iz padavinskih postaj Kozina in Podgrad ter višine potencialne evapotranspiracije iz meteorološke postaje Godnje.

Za prostorsko porazdelitev padavin je bila uporabljena korigirana Thiessenova metoda (JANŽA, 2003). Vrednosti višin potencialne evapotranspiracije so bile uporabljene brez porazdelitve – enotne vrednosti na celotnem obravnavanem območju.

Digitalni model višin
Za izdelavo modela površja obravnavanega območja je bil uporabljen digitalni model višin - DMV (ZRC SAZU & Mobitel, d. d., 2000). Velikost celic DMV je 25 m, povprečna višinska natančnost okoli 2 m za ravninska območja, za zmerno razgiban relief okoli 5 m in za hribovit relief okoli 10 m (Oštir, 2000). Za potrebe modeliranja je bila spremenjena velikost celic DMV, tako da ustrezajo ostalim vhodnim prostorskim podatkom. V ta namen je bila uporabljena bilinearna interpolacija.

Pedološki podatki
Podatki za modeliranje nezasičene cone temeljijo na pedološki karti v merilu 1 : 25000 in izbranih pedoloških profilov (CPVO, 2001). Pedološka karta je poligonski informacijski sloj, sestavljen iz pedokartografskih enot (PKE), ki so osnovne kartografske enote. Posamezna PKE je sestavljena iz ene ali več pedosistemskih enot, ki v naravi značilno nastopajo skupaj in jih zaradi merila karte ni mogoče prikazati ločeno. Poligoni PKE se med seboj razlikujejo po zastopanih pedosistemskih enotah (tipih tal) in njihovem medsebojnem razmerju (Vrščaj & Tič, 1998).

Na obravnavanem območju so bile, glede na vrsto in zastopanost pedosistemskih enot v posamezni PKE, le-te združene v sedem pedoloških enot, ki so uporabljene v modelu. Hidravlične lastnosti teh enot so bile opredeljene na podlagi tipičnih pedoloških profilov (za posamezno enoto), izbranih v širši okolici obravnavanega območja. Posamezni pedološki profil je sestavljen iz različnih horizontov, ki imajo teksturne podatke (deleže peska, melja in gline). Z uporabo pedotransfer funkcij so bile na podlagi teh podatkov ocenjene hidravlične lastnosti pedoloških enot, ki so uporabljene v modelu.

Vegetacijski podatki
Porazdelitev vegetacijskih razredov oziroma raba tal v modelu je bila določena s klasifikacijo satelitske podobe LANDSAT-5 TM (Janža, 2005). Lastnosti posameznih vegetacijskih razredov so bile opredeljene s predhodno določenimi (modeliranimi) vrednostmi vegetacijskih parametrov (Kristensen et al., 2000).

Hidrološki model MIKE SHE

MIKE SHE je programski paket za modeliranje celotnega hidrološkega kroga (Abbot et al., 1986; Refsgaard & Storm, 1995). Je integriran sistem komponent ali modulov, ki omogoča modeliranje posameznih procesov hidrološkega kroga. Kompleksnost naravnega sistema oziroma njegovo konceptualno razumevanje in zahtevana zanesljivost modela pogojujeta uporabo (vključitev) različnih komponent. Hidrološki procesi so opisani z diferencialnimi enačbami, ki jih program rešuje numerično z uporabo metode končnih razlik. Ena od komponent modela MIKE SHE je MIKE 11, ki omogoča modeliranje hidrodinamičnih procesov površinskih voda. Uporablja se lahko kot samostojni model (reke, potoka, jezera) ali združen z modelom MIKE SHE, kar omogoča modeliranje celotnega hidrološkega kroga na obravnavanem območju.

Teoretične osnove modeliranja hidroloških procesov so natančneje opisane v DHI (2000a; 200b) in Janža (2003).V

nadaljevanju so podane enačbe modela za opis dinamike podzemne vode, ki je najpomembnejši del modela na obravnavanem območju. Parametri modela zasičene cone so najobčutljivejši v modelu, zato je bila kalibracija omejena na te parametre.

V modelu opisuje trodimenzionalni tok podzemne vode v zasičeni coni enačba:

$$\frac{\partial}{\partial x}\left(K_{xx}\frac{\partial h}{\partial x}\right)+\frac{\partial}{\partial y}\left(K_{yy}\frac{\partial h}{\partial y}\right)+\frac{\partial}{\partial z}\left(K_{zz}\frac{\partial h}{\partial z}\right)-Q_e=S_s\frac{\partial h}{\partial t}$$

kjer so: (2)

K_{xx}, K_{yy}, K_{zz} koeficienti prepustnosti vzdolž koordinatnih osi [m/s];

h piezometrični nivo [m];

Q_e volumski pretok na enotski volumen (dotok/iztok) [s^{-1}];

S_s specifični koeficient elastičnega uskladiščenja [m^{-1}].

Model omogoča tudi simulacijo drenažnega toka v zasičeni coni. Ta se pojavi, ko je nivo podzemne vode nad nivojem drenaže (sl. 7). Odtok je odvisen od razlike med nivojema (Δ) in časovne konstante (cdr_n), ki določa gostoto drenaž. Drenažni odtok je modeliran kot linearen rezervoar z izrazom:

$$q=(h_n-zdr_n)cdr_n \qquad (3)$$

kjer so:

q drenažni odtok [m^3]

h_n nivo podzemne vode (v n celici) [m];

zdr_n nivo drenaž [m];

cdr_n drenažna časovna konstanta [s^{-1}].

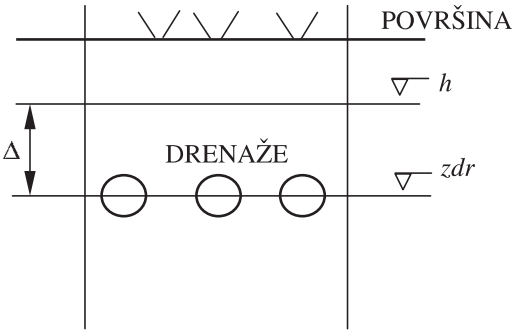

Slika 7. Shematski prikaz koncepta drenaž v modelu (po DHI, 2000a).
Figure 7. Schematic presentation of drains in the model (after DHI, 2000a).

Zasnova in parametrizacija modela na obravnavanem območju

Model na območju Brkinov je zasnovan na povodju P2A - delu povodja P2, ki leži vzvodno od merske točke M2, kjer so bile opravljene zvezne meritve pretoka (sl. 2). Enak pristop je bil uporabljen za kalibracijske parametre. Njihove vrednosti so bile določene v fazi kalibracije na povodju P2A in nato uporabljene na celotnem območju modela. Kalibracija modela je bila opravljena na podlagi vizualne primerjave merjenega (s pretočno krivuljo izračunanega) in modeliranih hidrografov. Najpomembnejša razloga za uporabo enotnega koncept na vseh povodjih sta:

- povodja imajo podobne (hidrogeološke, topografske, vegetacijske) značilnosti;
- pomanjkanje ustreznih merskih podatkov na ostalih povodjih, ki bi omogočili kalibracijo vsakega povodja posamezno.

Modeliranje je bilo izvedeno za dve ločeni obdobji:

- prvo obdobje modeliranja, od 1. 1. 1983 do 31. 12. 1993;
- drugo obdobje modeliranja, od 1. 11. 2001 do 31. 3. 2003.

Postopek modeliranja je bil razdeljen na več faz:

1. Modeliranje pretoka na merskem mestu M2 – odtoka iz povodja P2A. Ta model je bil izdelan za obdobje izvedenih meritev pretokov (od 1. 11. 2001 do 31. 3. 2003).
2. Vrednosti parametrov, ki so bile določene v procesu kalibracije tega modela, so bile nato uporabljene pri izdelavi modela za vsa povodja potokov na celotnem obravnavanem območju.
3. Ta skupni model povodij je bil nato uporabljen za modeliranje količine ponikajočih vod potokov v obdobju med 1983 in 1993, ki ustreza obdobju, uporabljenem v modelu vodonosnika v zaledju izvira Rižane (JANŽA, 2003).

Za potoke na območju Brkinov je značilno hitro povečanje pretokov po deževju. Večina vode odteče površinsko in podpovršinsko. Ta tokova sta v modelu simuliran z uporabo funkcije drenaž. Nivo drenaž je bil postavljen 0,5 m pod površino. Predpostavljeno je bilo, da je to globina manjših kanalov, ki delujejo kot drenažni sistem in niso ustrezno opisani z uporabljenim DMV (zaradi njegove premajhne natančnosti). Model deluje tako, da v primeru, ko podzemna voda v računski celici naraste nad nivo drenaž, odvede presežek vode do sosednje celice z nižjim nivojem. Postopek se nadaljuje, dokler ni dosežen vodotok. V manjšem delu povodij (predvsem njihovem nižjem delu), kjer se pojavljajo lokalne depresije, je bila uporabljena funkcija drenaže, ki ne upošteva naklona drenažnega nivoja in odvaja drenirano vodo neposredno do najbližjega vodotoka. Dinamika odvajanja vode je definirana s časovno konstanto, ki je bila določena v fazi kalibracije in ima v modelu vrednost $6x10^{-6}$ s^{-1}.

Tako odvedena (drenirana) voda tvori skupaj z osnovnim (baznim) tokom, ki je modeliran kot medzrnski tok v zasičenem delu računske (geološke) plasti, vhodne podatke za model odtoka po strugi potokov.

Območje Brkinov je sestavljeno iz slabo prepustnih flišnih plasti, zato so hidrološki procesi, ki vplivajo na odtok z območja omejeni na zgornji del teh plasti. V modelu so njihove lastnosti opredeljene z eno računsko plastjo, ki ustreza geološki plasti debeline 5 m. S kalibracijo določena vrednost koeficienta prepustnosti plasti v horizontalni smeri je 10^{-7} m/s, v vertikalni pa 10^{-8} m/s. Spodnji meji plasti je pripisana zelo nizka vertikalna prepustnost (10^{-9} m/s) in deluje praktično kot neprepustna plast. Horizontalna velikost računske celice modela je 90 x 90 m.

Odtok po strugi potokov je modeliran s programskim orodjem MIKE 11, ki je integrirano z modelom MIKE SHE. Položaj strug potokov v modelu (sl. 2) je določen z digitalizacijo rečne mreže topografske osnove 1 : 5000 (Geodetska uprava RS). Korita potokov so definirana poenostavljeno s trikotnimi preseki. Na začetku potokov (v najvišjem delu) je nastavljen robni pogoj ni dotokov. Za modeliranje toka v koritih je uporabljena metoda enostavnega hidravličnega izračuna (ang. kinematic routing), kjer temelji postopek izračuna hidrografa v določeni točki na dotoku in hidrografih vzvodno ležečih pritokov (DHI, 2000b). Prednost metode je stabilnost in nezahtevnost glede vhodnih parametrov, ki v obravnavanem primeru niso bili na razpolago.

REZULTATI IN RAZPRAVA

Povprečni simulirani dnevni pretok za celotno drugo obdobje modeliranja (1. 11. 2001 do 31. 3. 2003) na merskem mestu M2 znaša 71 l/s (P50 = 29 l/s). Grafična primerjava modeliranih povprečnih dnevnih pretokov na merilnem mestu M2 (sl. 9) z neposrednimi in z modelom pretočne krivulje izračunanimi zveznimi meritvami pretoka

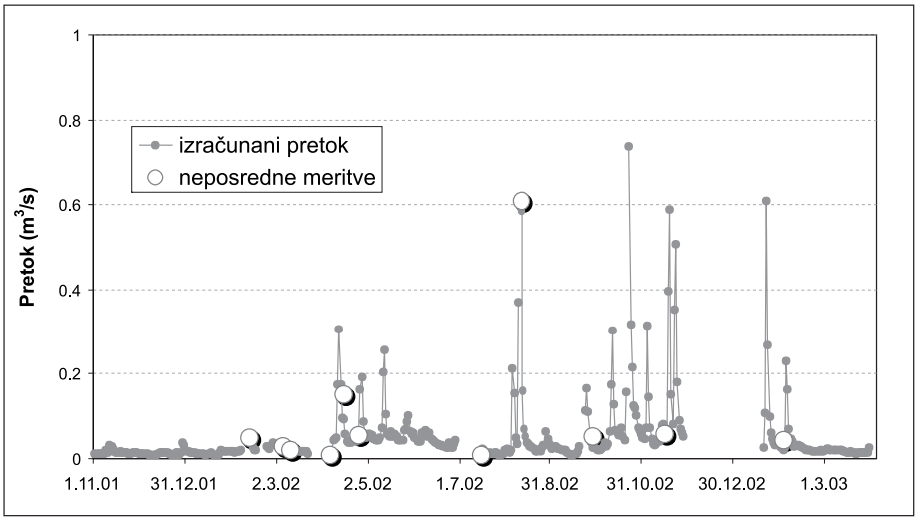

Slika 8. Neposredne meritve pretoka in izračunani povprečni dnevni pretoki (s pretočno krivuljo) na merskem mestu M2 (od 1. 11. 2001 do 31. 3. 2003).
Figure 8. Direct discharge measurements and calculated average daily discharges (with rating curve) on measurement location M2 (from 1. 11. 2001 to 31. 3. 2003).

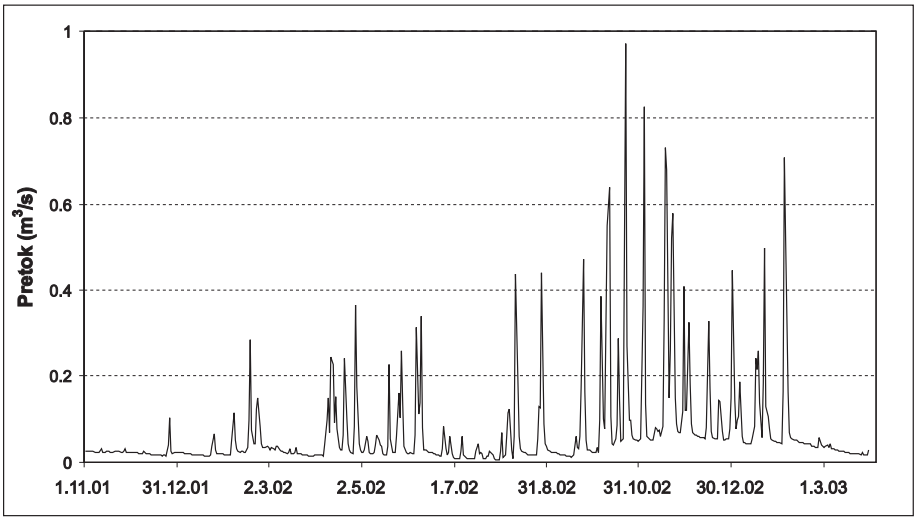

Slika 9. Simulirani povprečni dnevni pretoki na merskem mestu M2 (od 1. 11. 2001 do 31. 3. 2003).
Figure 9. Simulated average daily discharges on measurement location M2 (from 1. 11. 2001 to 31. 3. 2003).

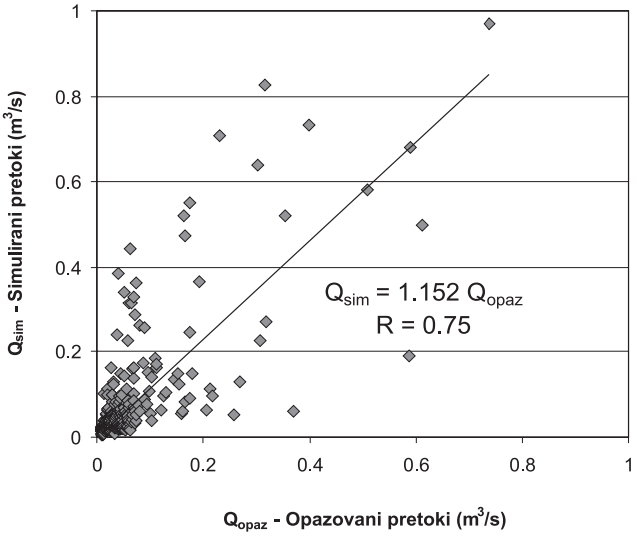

Slika 10. Korelacija med opazovanimi in simulirani povprečni dnevni pretoki na merskem mestu M2 (od 1. 11. 2001 do 31. 3. 2003).
Figure 10. Correlation between observed and simulated average daily discharges on measurement location M2 (from 1. 11. 2001 to 31. 3. 2003).

(sl. 8) kaže zmožnost modeliranja nizkih pretokov, kakor tudi dinamiko povečanja in upadanja pretoka. Vendar pa se določeni pretoki (vrhovi) hidrografov ne ujemajo. To odstopanje bi se lahko pripisalo predvsem vhodnim padavinskim podatkom, ki so najpomembnejša vhodna spremenljivka v modelu. Relativno majhno območje povodja P2A (3,6 km^2) je podvrženo lokalnim vremenskim razmeram, ki se težko opišejo z oddaljenimi padavinskimi postajami.

Korelacija med simuliranimi in opazovanimi (merjenimi) pretoki na merskem mestu M2 je prikazana na sliki 10. Smerni koeficient za linearno odvisnost pri kateri nastopa simulirani pretok kot odvisna, opazovani pretok pa kot neodvisna spremenljivka znaša 1,152, koeficient korelacije med primerjanima pretokoma pa 0,75.

Glavne bilančne komponente modela vseh povodij za enoletno obdobje (od 30. 3. 2002 do 30. 3. 2003) so prikazane na sliki 11. V modelu je polovica padavinske vode prenesena nazaj v ozračje kot posledica evapotranspiracije. Preostala voda iz povodij odteče do potokov predvsem v obliki površinskega in podpovršinskega hitrega odtoka, ki je v modelu simuliran s funkcijo drenaž. Približno trikrat manjši je počasen osnovni – bazni odtok.

Hidrograf simuliranih skupnih odtokov s celotnega območja modela za prvo obdobje modeliranja in statistike odtokov po povodjih in skupno so prikazane na sliki 12 ter v tabelah 2 in 3.

Krivulja trajanja simuliranih povprečnih dnevnih skupnih odtokov iz vseh povodij v prvem obdobju modeliranja je prikazana na sliki 13. Celoten razpon pretokov je bil razdeljen na trideset enakih intervalov. Iz grafa je razvidno, da močno prevladujejo nizki odtoki. Le okrog 15 % simuliranih

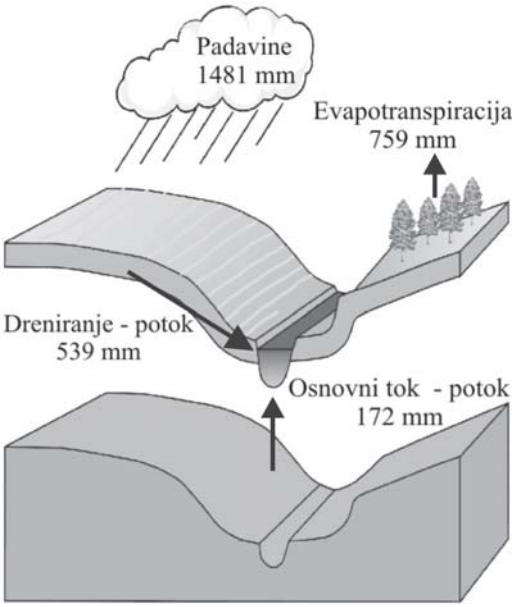

Slika 11. Glavne bilančne komponente modela vseh povodij (skupno) za obdobje od 30. 3. 2002 do 30. 3. 2003 (1mm ustreza 1,4 l/s).
Figure 11. Main water balance components of the model of all catchments for the period from 30. 3. 2002 to 30. 3. 2003 (1mm corresponds to 1.4 l/s).

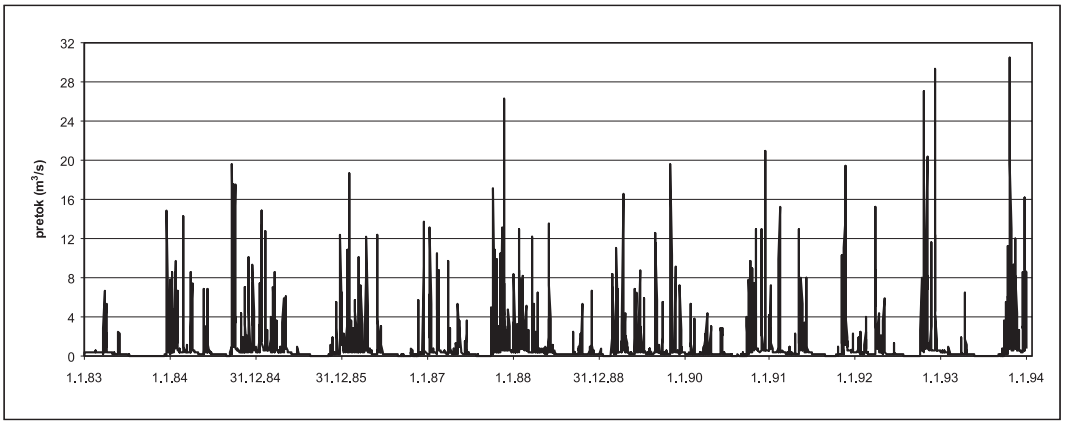

Slika 12. Hidrograf simuliranih skupnih odtokov s celotnega območja modela (od 1. 1. 1983 do 31. 12. 1993).
Figure 12. Hydrograph of simulated average daily total outflows from all catchments (from 1. 1. 1983 to 31. 12. 1993).

dnevnih odtokov preseže 1 m^3/s, okrog 5 % odtokov 5 m^3/s, 1,5 % odtokov 10 m^3/s in manj kot 0,5 % odtokov 15 m^3/s. Slika 14 prikazuje natančneje frekvenčno porazdelitev odtokov do 1 m^3/s. Iz grafa je razvidno, da najnižja razreda (do 0,1 m^3/s in 0,2 m^3/s) skupno tvorita skoraj 40 % simuliranih dnevnih odtokov. Frekvenca višjih pretokov enakomerno upada do vrednosti 1 m^3/s.

Tabela 2. Statistike simuliranih povprečnih dnevnih odtokov iz posameznih povodij (od 1. 1. 1983 do 31. 12. 1993).
Table 2. Statistics of simulated average daily outflows from single catchments (from 1. 1. 1983 to 31. 12. 1993).

Oznaka povodja	P1	P2	P3	P4	P5	P6	P7	P8
$\overline{Q}$ [m^3/s]	0,134	0,132	0,052	0,036	0,076	0,148	0,176	0,215
s [m^3/s]	0,282	0,270	0,115	0,103	0,174	0,397	0,485	0,549
Q_{min} [m^3/s]	0,002	0,002	0,001	0,000	0,002	0,001	0,001	0,003
Q_{max} [m^3/s]	3,989	3,700	1,515	1,331	2,255	5,184	6,333	7,119
P50 [m^3/s]	0,050	0,053	0,020	0,006	0,027	0,035	0,036	0,057
P25 [m^3/s]	0,022	0,023	0,008	0,002	0,018	0.015	0,014	0,025
P75 [m^3/s]	0,091	0,099	0,037	0,013	0,042	0,066	0,070	0,105
$\sqrt{b_1}$	4,954	5,114	5,250	5,440	5,363	5,415	5,368	5,337
b_2	34,597	36,949	37,526	39,506	38,341	39,082	38,221	37,930

$\overline{Q}$ – povprečni odtok, s – standardni odklon, Q_{min} – minimalni odtok, Q_{max} – maksimalni odtok, P50 – mediana, P25 – petindvajseti percentil, P75 – petinsedemdeseti percentil, $\sqrt{b_1}$ – cenilka asimetričnosti, b_2 – cenilka sploščenosti.

Tabela 3. Statistike simuliranih povprečnih dnevnih skupnih odtokov iz vseh povodij (simuliranih od 1. 1. 1983 do 31. 12. 1993).
Table 3. Statistics of simulated average daily total outflows from all catchments (from 1. 1. 1983 to 31. 12. 1993).

$\overline{Q}$ [m^3/s]	s [m^3/s]	Q_{min} [m^3/s]	Q_{max} [m^3/s]	P50 [m^3/s]	P25 [m^3/s]	P75 [m^3/s]	$\sqrt{b_1}$	b_2
0,970	2,327	0,012	30,534	0,288	0,129	0,531	5,230	36,943

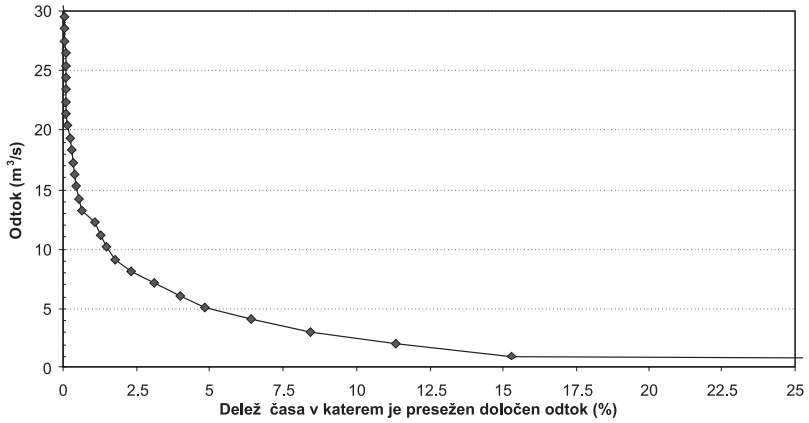

Slika 13. Krivulja trajanja simuliranih povprečnih dnevnih skupnih odtokov iz vseh povodij (od 1. 1. 1983 do 31. 12. 1993).
Figure 13. Flow duration curve of simulated average daily total outflows from all catchments (from 1. 1. 1983 to 31. 12. 1993).

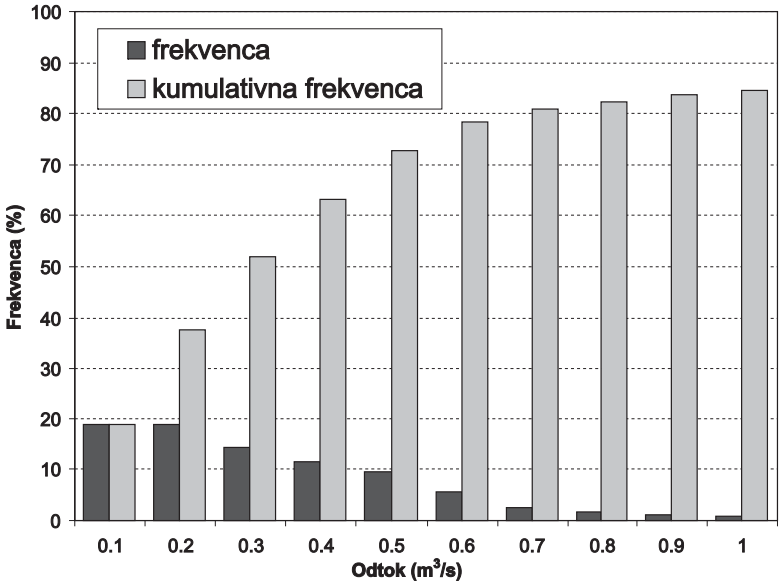

Slika 14. Frekvenčna porazdelitev simuliranih povprečnih dnevnih skupnih odtokov iz vseh povodij do 1 m^3/s (simuliranih od 1. 1. 1983 do 31. 12. 1993).
Figure 14. Frequency distribution of simulated average daily total outflows from all catchments up to 1 m^3/s (from 1. 1. 1983 to 31. 12. 1993).

SKLEPI

Izdelani dinamični matematični model z distribuiranimi parametri omogoča modeliranje hidrološkega kroga na obravnavanem območju Brkinov - severovzhodnem delu varovanega zaledja izvira Rižane. Z modelom in izvedenimi meritvami pretokov so pridobljene nove informacije o vodni bilanci obravnavanega območja in posrednem napajanju vodonosnika v zaledju izvira Rižane. Novost je predvsem vključitev prostorske in dinamične komponente procesov, ki vplivajo na napajanje vodonosnika, kar bo prispevalo k boljšemu razumevanju celotnega vodonosnega sistema v zaledju izvira Rižane.

Z modelom simulirani odtoki z obravnavanega območja kažejo na izrazito hudourniško naravo potokov, ki drenirajo obravnavano območje. Povečanja odtoka so zelo hitra in pogojena z obilnejšim deževjem. Trajanje visokih odtokov je relativno kratko. V simuliranem enajstletnem obdobju (od 1. 1. 1983 do 31. 12. 1993) je le okrog 15 % simuliranih skupnih povprečnih dnevnih odtokov iz vseh povodij višjih od 1 m^3/s, okrog 40 % odtokov pa je nižjih od 0,2 m^3/s. Povprečni simulirani odtok za navedeno obdobje znaša 0,97 m^3/s, mediana odtokov pa 0,288 m^3/s.

Negotovost rezultatov modela je pogojena z več dejavniki. Eden pomembnejših je povezan z vhodnimi padavinski podatki, ki so najpomembnejša vhodna spremenljivka modela. Relativno majhno območje zasnove modela P2A (3,6 km^2) je del reliefno razgibanega območja in je podvrženo lokalnim vremenskim razmeram, ki jih je težko opisati z oddaljenimi padavinskimi

postajami. Prav tako pomemben razlog negotovosti v modelu je natančnost meritev, uporabljenih za izdelavo modela pretočne krivulje. Zaradi omejenega števila meritev visokih pretokov je izračun le-teh z umeritveno krivuljo (še posebej pa ekstrapolacija izven območja meritev) lahko pomemben vir napake. Nepreverjeni možni vir napake ostaja zasnova modela, ki je bila izdelana na povodju P2A in uporabljena na ostalih povodjih obravnavanega območja. Za potrditev uporabljenega pristopa in predpostavke o podobnih lastnostih zaledij bi bila potrebna izvedba dodatnih zveznih meritev pretokov na ostalih povodjih.

Summary

Modelling the recharge of the aquifer in the Rižana catchment from Brkini area

In the paper a dynamic distributed hydrological model (MIKE SHE-MIKE 11) that was developed in the area of Brkini is described. The model area is a part of the recharge area of the aquifer of Rižana spring. With the model new information regarding water balance of the area and indirect recharge of the aquifer is obtained. Of great importance is the temporal variability of the aquifer recharge, which will contribute to the better understanding of the processes in the aquifer system and which will help to more efficiently manage this important water resource. Characteristics of the outflow, defined on the daily simulated outflows for eleven years period (from 1. 1. 1983 to 31. 12. 1993), are described with statistics: average outflow 0.970 m^3/s, standard deviation 2.327 m^3/s, minimum outflow 0.012 m^3/s, maximum outflow 30.534 m^3/s, median 0.288 m^3/s, 25 percentile 0.129 m^3/s, 75 percentile 0.531 m^3/s, skewness 5.230 and kurtosis 36.943. Frequency distribution of the simulated average daily total outflows from the model area (with the interval step size 0.1 m^3/s) shows the domination of low outflows. Almost 40 % of simulated outflows are lower than 0.2 m^3/s. Frequency of higher outflows gradually decreases to 1 m^3/s. Higher than 1 m^3/s is only about 15 % of outflows.

Viri

Abbot, M. B., Bathurst, J. C., Cunge, J. A., O'connell, P. E., Rasmussen, J. (1986): An Introduction to the European Hydrological System-Systeme Hydrologique Euopeen, "SHE", 2: structure of a physically-based, distributed modelling system. *Journal of Hydrology*; Vol. 87, pp. 61–77.

CPVO (2001): Digitalna pedološka karta 1 : 25000 [za obravnavano območje].: Center za pedologijo in varstvo okolja, Biotehniška fakulteta, Univerza v Ljubljani, Ljubljana.

DHI. (2000a): MIKE SHE WM – User Manual, Edition 1.2., DHI Water & Environment, Horsholm.

DHI (2000b): MIKE 11 A Modelling System for Rivers and Channels – Reference manual, DHI Water & Environment, Horsholm, 335 p.

Janža, M. (2003): Modeliranje napajanja regionalnega vodonosnika z uporabo metod daljinskega zaznavanja: doktorska disertacija. Univerza v Ljubljani, NTF, Ljubljana, 139 p.

Janža, m. (2005): Določitev rabe tal s klasifikacijo satelitske podobe za namene hidrološkega modeliranja na območju zaledja izvira Rižane. *Geologija*; Vol. 48/1, v tisku.

Kristensen, M., Andersson, U., Sřrensen, H. R., Refsgaard, A. (2000): Water Resources Management Model for Ljubljansko Polje and Ljubljansko Barje, Model report. DHI, Horsholm, 79 p.

KRIVIC, P., BRICELJ, M., ZUPAN, M. (1989): Podzemne vodne zveze na področju Čičarije in osrednjega dela Istre. *Acta Carsologica*, Vol. 17, pp. 265–295.

KRIVIC, P., BRICELJ, M., TRIŠIČ, N., ZUPAN, M. (1987): Sledenje podzemnih vod v zaledju izvira Rižane. *Acta Carsologica*; Vol. 16, pp. 83–104.

MIHEVC, A. (1991): Morfološke značilnosti ponornega kontaktnega krasa: izbrani primeri s slovenskega krasa: *magistrsko delo. Univerza v Ljubljani,* Ljubljana, 206 p.

NOVAK, D. (1963): Slovenski kras. A. Primorski kras. Hidrogeološko raziskovanje Primorskega krasa. *Geološki zavod Slovenije,* Ljubljana, 96 p.

OŠTIR, K. (2000): Analiza vpliva združevanja radarskih interferogramov na natančnost modelov višin in premikov zemeljskega površja: *doktorska disertacija. Univerza v Ljubljani*, Ljubljana, 175 p.

PRESTOR, J. (1992): Prispevek k preučevanju odnosov med padavinami in odtokom iz kraškega vodonosnika: *magistrsko delo. Univerza v Ljubljani,* NTF, Ljubljana, 44 p.

REFSGAARD, J. C. & STORM, B. (1995): MIKE SHE. In: SINGH, V. P. (ed.). *Computer Models of Watershed Hydrology*. *Water Resources Publications*; pp. 809–846.

VRŠČAJ, B. & TIČ, I. (1998): Digitalni podatki tal Slovenije; Gradivo kot pomoč pri uporabi digitalnih pedoloških podatkov, verzija 1.0. Center za pedologijo in varstvo okolja, *Biotehniška fakulteta, Univerza v Ljubljani,* Ljubljana, 25 p.

ZRC SAZU & Mobitel (2000): InSAR DMV 25 (Digitalni model višin). ZRC SAZU, Ljubljana.

Toplo stiskanje jekla za poboljšanje CF53

Hot compression of CF53 tempering steel

Milan Terčelj[1], Iztok Peruš[2], Goran Kugler[1], Rado Turk[1]

[1]Oddelek za materiale in metalurgijo, Univerza v Ljubljani,
Aškerčeva cesta 12, 1000 Ljubljana, Slovenija;
E-mail: milan.trcelj@ ntf.uni-lj.si, goran.kugler@ ntf.uni-lj.si, rado.turk@ntf.uni-lj.si
[2]FAGG, Univerza v Ljubljani, Jamova 2, 1000 Ljubljana, Slovenjia;
E-mail: iperus@siol.net

Received: June 1, 2005 **Accepted:** November 24, 2005

Povzetek: Na fizikalnemu simulatorju termomehanskih metalurških stanj Gleeble 1500 je bilo izvedeno toplo stiskanje cilindričnih vzorcev iz jekla za poboljšanje (CF53). Za potrebe optimiranja tehnologij toplega preoblikovanja je napovedovanje krivulj tečenja z empiričnimi in fenomenološkimi modeli premajhne natančnosti, zato se v zadnjem času za njihovo napovedovanje vključujejo metode umetne inteligence, med katerimi pogosto opazimo uporabo nevronskih mrež. Uspešnost metode je povezana s težavami glede izbire optimalne arhitekture plasti nevronskih mrež, omejitve števila vhodnih parametrov, itd. Z namenom, da te postopke racionaliziramo, smo eksperimentalno bazo krivulj tečenja uporabili za napovedovanje s CAE NN (angl. "Conditional Average Estimator Neural Network"), ki so sposobne modeliranja fizikalnih zakonov tudi v področjih velikih gradientov. Natančnost napovedovanja je praktično v območju 0-3 %. Za dano bazo toplih krivulj tečenja CF53 jekla je bila izračunana tudi aktivacijska energija.

Abstract: By means of hot compression tests carried out on a Gleeble 1500 thermomechanical simulator the deformation behaviour of CF53 tempering steel was investigated over a wide range of temperatures (900-1200 °C) and with a strain rate of 0.1-8 s^{-1} and true strains of 0-0.6. Due to the poor accuracy in predicting flow stress curves for the needs of optimizing hot forming technologies by empirical and phenomenological models, it is nowadays current practice to employ neural networks for their prediction. This approach is justified only in the case of predicting ability on the entire area of testing and not only the measured data. This study confirmed the good predictive power of CAE NN (Conditional Average Estimator Neural Network) to predict flow stress curves since it can model physical laws in areas of high gradients. The accuracies achieved are practically within 3 %; an average is error of 1 %. We also calculated the activation energy for deformed steel.

Ključne besede: CF53 jeklo za poboljšanje, toplo stiskanje, krivulje tečenja, CAE nevronske mreže, aktivacijska energija.
Key words: CF53, hot compression, flow stress, CAE neural network, activation energy.

Scientific paper

UVOD

Na krivulje tečenja med toplo deformacijo jekel vpliva veliko faktorjev (slika 1), katerih vplivi so zelo kompleksni. Zato so zveze med temi faktorji in krivuljami tečenja nelinearne in prostorsko zelo razgibane (predvsem v prostoru napetost - deformacija – hitrost deformacije) [1-2]. Posledično so tudi opisi krivulj tečenja med toplo deformacijo z empiričnimi, kot tudi fenomenološkimi modeli velikokrat premalo natančni. Fizikalni modeli so že zelo izpopolnjeni, so pa bolj ali manj še vedno omejeni na dokaj čiste kovine in jih za namene industrijskih aplikacij še ne uporabljamo [3]. Razvoj konstitutivnih enačb od čistih empiričnih do bolj fizikalno podprtih še vedno ostaja cilj znanstvenih raziskav. Kljub vedno novim konstitutivnim modelom za opis krivulj tečenja pa v natančnosti napovedovanja ni prišlo do vidnega napredka, saj je le-ta za aplikativne namene še vedno nezadovoljiva in se giblje v območju običajnega variiranja testnih parametrov vroče predelave med 2 in 60 %. Iskanje novih poti zato ostaja še naprej predmet intenzivnih študij [4-11]. V zadnjem času se kot učinkovito sredstvo ponujajo BP nevronske mreže (BP NN), vendar tudi tu nastopajo težave glede izbire optimalne arhitekture plasti, vključevanja števila vhodnih vplivnih parametrov, unifikacije vrednosti parametrov, itd. Natančnost interpolacijskega napovedovanja z BP nevronskimi mrežami je sicer boljša kot v primeru empiričnih funkcijkih zapisov in se v giblje v mejah npr. med 0 – 7 % za hitrorezna jekla in 0 – 9 % za ogljikova jekla [3,11-12].

Hodgson and Kong [13-14] poročata o potrebni natančnosti znotraj 5 % pri napovedovanju napetosti tečenja za učinkovito optimiranje tehnologij toplega valjanja. To med drugim zahteva povsem kontrolirano izvajanje nastavljenih parametrov preiskusa, na kar med drugim precej vpliva zadostna togost samega eksperimentalnega sistema. Iz izkušenj vemo, da so experimentalni podatki, posebno starejšega

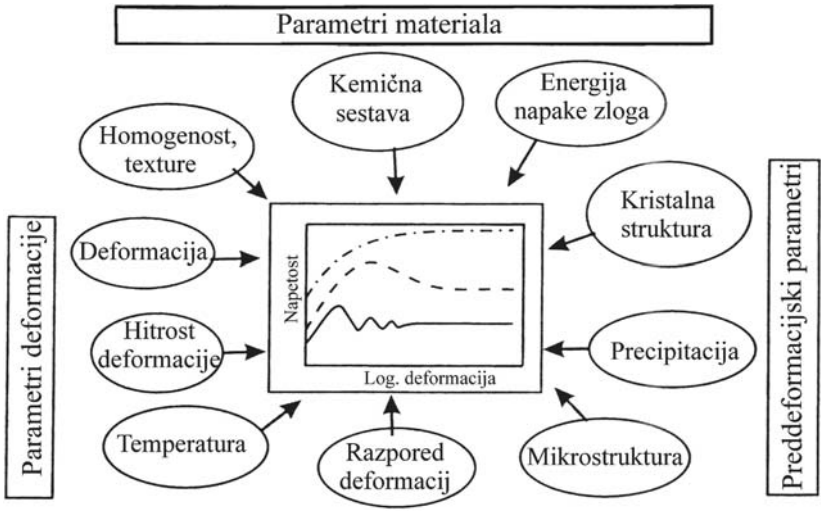

Slika 1. Parametri, ki vplivajo na krivulje tečenja [2].

datuma, premalo zanesljivi za današnje zahteve napovedovanja. Žal so velikokrat še naprej osnova za namene računalniškega simuliranja procesov vročega preoblikovanja, ko je potrebno npr. opisati tok snovi, prenos toplote, maksimalne obremenitve na preoblikovalnem stroju ter lokalne obremenitve (mehanske, termične, tribološke, itd.) na preoblikovalnem orodju. Zato določevanje zanesljivih krivulj tečenja ostaja še nadalje predmet intenzivnih študij [8,15].

Eno takšnih področij, ki zahteva zanesljivo poznavanje krivulj tečenja, so tudi jekla za poboljšanje, in to ne-le v fazi njihove metalurške izdelave (npr. valjanje polizdelkov), pač pa tudi kasneje pri študiju obnašanja materiala med izdelavo izdelka npr. toplo utopno kovanje). CF53 jeklo za poboljšanje uporabljamo za izdelavo konstrukcijskih delov, ki so pri uporabi izpostavljeni velikim in časovno spreminjajočim obremenitvam (npr. vzmeti, sorniki, pogonske gredi, vretena, odmične gredi, večji zobniki, itd). V študijo vključeno jeklo izdelujemo po konvecionalni poti t.j. najprej vlivamo v bloke, nato valjamo na valjalnem stroju do gredic dimenzijskega območja kvadrat 50 - 90 mm. Tako dobljene gredice, razrezane na določene dolžine, lahko služijo tudi kot vhodni material za utopno kovanje. Optimiranje plastičnega preoblikovanja omenjenega jekla je usmerjeno v zmanjšanje števila dogrevanj med toplim preoblikovanjem (valjanjem) na manjše dimenzije, za kar moramo maksimalno izkoristiti preoblikovalne lastnosti jekla pri intenziviranju plana valjanja (optimalno razporediti redukcije presekov glede na energetsko-obremenitvene zmožnosti samega valjalnega stroja ter trdnostne karakteristike valjev).

V dostopni literaturi se karakterizacije preoblikovalnih lastnosti jekel za poboljšanje nanašajo predvsem na torzijske preizkuse [16-17], podatki na osnovi tlačnih preizkusov pa so redkejši. V tem prispevku podajamo krivulje tečenja, dobljene s pomočjo toplega stiskanja cilindričnih vzorcev, iz jekla za poboljšanje CF53, deformiranega pri različnih temperaturah in hitrostih deformacije. S pomočjo te baze so nato krivulje tečenja napovedovane s pomočjo CAE nevronskih mrež. Pri tem sta bila uporabljena tako konstantni, kot tudi nekonstantni parametra gladkosti.

EXPERIMENT

Vzorci in material

Kemična sestava jekla za poboljšanje je podana v tabeli 1. Cilindrični vzorci tipa Rastegew in dimenzij ϕ = 8 mm x 12 mm so bili izdelini iz okrogle palice ϕ = 60 mm, ki je bila predhodno valjana iz gredice 250 mm x 250 mm. Vhodno mikrostrukturo uporabljenih vzorcev podaja slika 2**,** iz katere so razvidna zrna lamelarnega perlita in zrna ferita.

Tabela 1. Kemična sestava cilindričnih vzorcev iz CF53 (wt %).

C	S	Si	Cr	Ni	Al	Cu	Mn	Mo	P	Sn
0,55	0,042	0,24	0,22	0,05	0,034	0,14	0,69	0,02	0,027	0,010

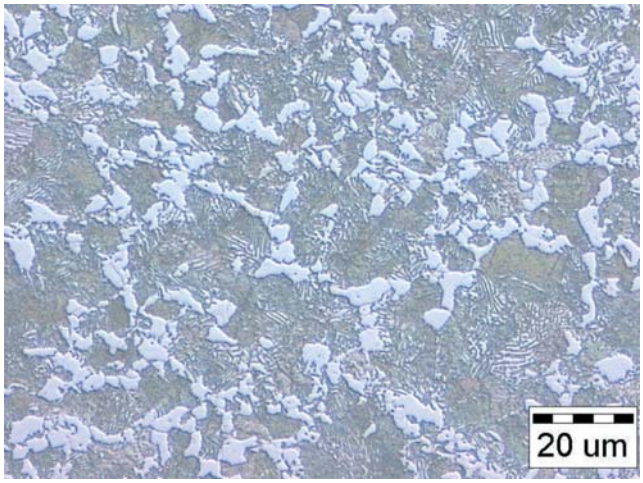

Slika 2. Začetna mikrostruktura cilindričnih vzorcev iz CF53, (zrna lamelarnega perlita in zrna ferita).

Testna naprava in testni pogoji

Tople stiskalne preizkuse smo izvedli na Gleeble 1500 testni napravi, ki omogoča fizikalno simulacijo želenih termomehanskih metalurških stanj. Slika 3 prikazuje ureditev testne celice za toplo stiskanje. Za zmanjšanje trenja med stiskanim cilindričnim vzorcem in orodjem ter preprečevanje njunega medsebojnega zvarjanja smo uporabili grafitno mazivo.

Testni pogoji toplega stiskanja cilindričnih vzorcev so podani v tabeli 2. Izvedeno je bilo v temperaturnem območju med 900 - 1200 °C, pri treh različnih hitrostih deformacije

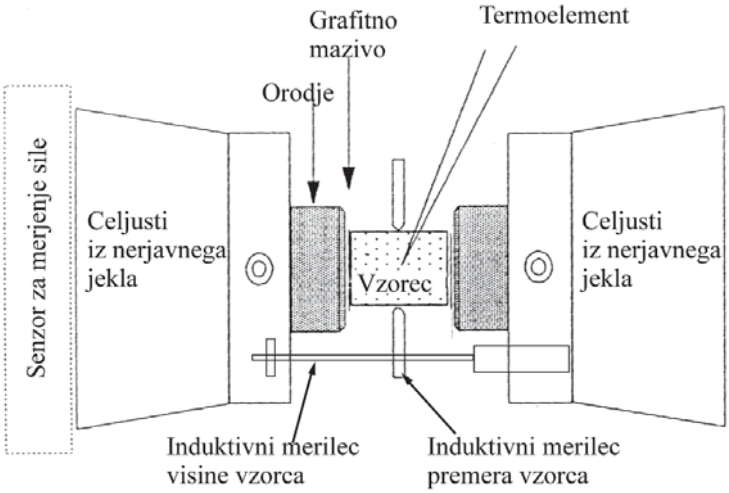

Slika 3. Shematičen prikaz izvedbe tlačnega preizkusa na simulatorju termomehanskih stanj Gleeble 1500.

Tabela 2. Vrednosti glavnih parametrov testiranja.

Jeklo	Ta [°C]	Temperaturno območje [°C]	Hitrost deformacije s^{-1}
CF53	1200	900 -1200	0,1 , 1 , 8

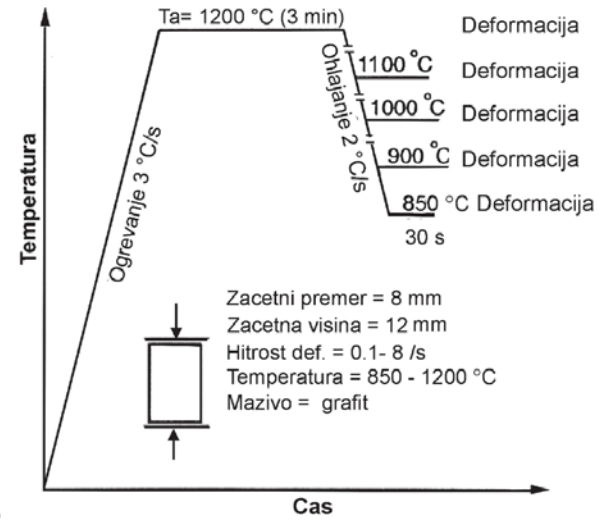

Slika 4. Shematski prikaz poteka temperature testiranih cilindričnih vzorcev.

(0,1, 1, 8 s^{-1}) in ob predhodnem ogrevanju cilindričnih vzorcev (slika 4). Hitrost ogrevanja je znašala 3 °C/s, čemur je sledilo triminutno zadrževanje na temperaturi (Ta) 1200 °C, nato ohlajanje s hitrostjo 2 °C/s na temperaturo deformacije ter ponovno 30 sekundno zadrževanje na načrtovani temperaturi deformacije. Po deformaciji so bili vzorci naglo gašeni z vodo.

Uporaba CAE nevronskih mrež pri napovedi krivulj tečenja

Teoretične osnove in izrazi

V članku obravnavamo problem, kako oceniti/napovedati krivulje tečenja v odvisnosti od znanih vplivnih parametrov kot so temperatura, deformacija in hitrost deformacije. Prvo spremenljivko - eno točko krivulje tečenja - običajno imenujemo izhodni parameter, znane vplivne parametre pa vhodne parametre problema.

Za določitev neznanega izhodnega parametra (npr. za eno točko krivulje tečenja) s CAE nevronsko mrežo je potrebna baza podatkov, ki vsebuje zadostno število zanesljivih in primerno razporejenih empiričnih podatkov. Baza podatkov vsebuje empirične podatke, ki ustrezajo vhodnim in izhodnim parametrom opazovanega pojava. Vsako posamično opazovanje poljubnega fizikalnega pojava tako matematično predstavimo z *modelnim vektorjem*, pri čemer vhodni in izhodni parametri pojava ustrezajo komponentam tega vektorja. Na primer, če je pri temperaturi T = 950 °C, deformaciji 0,3 in hitrosti deformacije 5 s^{-1}

izmerjena napetost 350 MPa, lahko modelni vektor zapišemo kot *{950, 0,3, 5; 350}*. Baza podatkov vsebuje končno število takšnih modelnih vektorjev.

Tipično shemo strukture CAE nevronske mreže lahko najdemo v literaturi [18-19]. Po tem pristopu lahko vsak izhodni parameter oz. komponento obravnavanega modelnega vektorja (t.j. vektorja z znanimi vhodnimi parametri in neznanimi izhodnimi parametri) napovemo s pomočjo izraza:

$$\hat{r}_k = \sum_{n=1}^{N} C_n \cdot r_{nk} \qquad (1),$$

kjer je

$$C_n = \frac{c_n}{\sum_{j=1}^{N} c_j} \qquad (2)$$

in

$$c_n = \exp\left[\frac{-\sum_{i=1}^{L}\left(p_i - p_{ni}\right)^2}{2w^2}\right] \qquad (3).$$

Pri tem je $\hat{r}_k$ napovedan (ocenjen) *k*-ti izhodni parameter (npr. *napetost*), r_{nk} je enak izhodni parameter, ki ustreza *n*-temu modelnemu vektorju iz baze podatkov, *N* je število modelnih vektorjev v bazi podatkov, p_{ni} je *i*-ti vhodni parameter *n*-tega modelnega vektorja v bazi podatkov (npr. *temperatura, deformacija, hitrost deformacije*), p_i je *i*-ti vhodni parameter obravnavanega modelnega vektorja in *L* je število vhodnih parametrov obravnavanega pojava.

Enačba 1 kaže, da se napoved izhodnega parametra določi kot kombinacija vseh izhodnih parametrov iz baze podatkov. Posamezne uteži so odvisne od podobnosti med vhodnimi parametri p_i obravnavanega modelnega vektorja in enakimi vhodnimi parametri p_{ni} modelnih vektorjev iz baze podatkov. C_k je merilo podobnosti. Neznana vrednost izhodnega parametra je torej izračunana tako, da je modelni vektor, sestavljen iz znanih (vhodnih) in neznanih (izhodnih) parametrov, maksimalno konsistenten z modelnimi vektorji iz celotne baze podatkov.

Parameter *w* predstavlja širino Gaussove funkcije in ga imenujemo parameter gladkosti, saj določa gladkost rešitve. V splošnem velja, da manjša kot je vrednost *w*, slabše je posploševanje metode, in obratno, večja kot je vrednost *w*, boljše je posploševanje metode, vendar na račun zmanjšanja natančnosti. V praksi se zato primerna vrednost *w* določa z iteracijskim postopkom, kjer najboljši *w* ustreza primerno gladkim rešitvam problema ob istočasni minimizaciji napake napovedi. Potrebno je poznavanje obravnavanega pojava, nekaj izkušenj in logično-tehničnega razmisleka.

Izbira konstatnega *w* ustreza najbolj osnovnemu pristopu uporabe metode. V praksi pa se v nekaterih primerih izkaže, da nekonstantna vrednost *w* pogosto daje boljše rezultate. Pri uporabi nekonstatnega *w* lahko še vedno uporabimo enačbo 1, vendar ob izbiri primerne, lokalno ocenjene vrednosti w_i , pri čemer indeks *i* označuje *i*-ti vhodni parameter. Izraz za c_n (glej enačbo 1) se lahko zapiše kot

$$c_n = \exp\left[-\sum_{i=1}^{L}\frac{\left(p_i - p_{ni}\right)^2}{2w_i^2}\right] \qquad (4).$$

Važno je omeniti, da so izrazi enačb 1-3 izpeljani povsem teoretično [18-20] ob predpostavki konstantne (ne)zanesljivosti empiričnih podatkov. Razširitev te metode z uporabo nekonstantnega *w* (enačba 4) pa temelji na fizikalnih razmišljanjih. Medtem ko konstanten *w* ustreza krogli v *L*-dimenzionalnem hiperprostoru (*L* je število vhodnih parametrov), ustreza nekonstanten w večosnemu elipsoidu v istem prostoru [21-22].

Proces učenja

Originalen predlog CAE metode [18] sestoji iz dveh delov. Prvi del ustreza tako imenovanemu procesu samoorganizacije nevronov. V primeru uporabe relativno majhnih baz podatkov lahko ta del brez večjih težav opustimo. Drugi del ustreza matematičnemu opisu obravnavanega pojava z uporabo optimalne cenilke, opisanem v prejšnjem poglavju. Iz tega vidika ustreza proces učenja enostavni predstavitvi baze podatkov CAE nevronskih mrež. Še več, v primerjavi s klasičnimi nevronskimi mrežami (BP NN), je testiranje uspešnosti modela bistveno enostavnejše. Namesto uporabe približno 70 % podatkov za učenje in preostalih 30 % za testiranje, je uporabljen drugačen pristop. Izhodni parameter, npr. napetost v krivulji *napetost-temperatura-deformacija-hitrost deformacije*, je napovedan za vsako točko krivulje iz baze podatkov, pri tem pa je obravnavan modelni vektor začasno izvzet iz baze podatkov. Z nekaj takšnimi poskusi se določi optimalna vrednost parametra gladkosti.

Da bi kvantitativno ocenili natančnost CAE metode pri napovedovanju krivulj tečenja, smo uporabili naslednjo enačbo, ki računa kvadratni koren vsote kvadratov odstopanj za vsako deformacijsko opazovanje:

$$RMSSD = \sqrt{\frac{\sum_{i=1}^{N} (\hat{r}_k - r_k)^2}{N}} \qquad (5).$$

Napoved se smatra kot dobra, če je RMSSD vrednost znotraj 5 % povprečne krivulje tečenja za obravnavano stanje [11], pri čemer se povprečna krivulja tečenja s_{mfs} izračuna kot

$$\sigma_{mfs} = \frac{1}{\varepsilon}\int \sigma \, d\varepsilon \qquad (6)$$

Krivulje tečenja in CAE napovedi pri uporabi konstatnega parametra gladkosti

Krivulje tečenja za jeklo CF53 pri različnih temperaturah in različnih hitrostih deformacije so prikazane na Sliki 5. Krivulje tečenja najprej hitro naraščajo z deformacijo do neke konstatne vrednosti, potem pa padejo do neke konstantne vrednosti pri višjih deformacijah. Ta oblika toplih krivulj tečenja je tipična za materiale, kjer med plastično deformacijo poteka tudi dinamična rekristalizacija. Rezultati za jeklo CF53 kažejo na relativno dobro ujemanje med eksperimentalnimi in napovedanimi vrednostmi krivulj tečenja. To je posledica dejstva, da so relacije med vhodnimi in izhodnimi parametri relativno enostavne. Uporaba konstantnega *w* je smiselna (enačba 3).

Slike kažejo relacije *napetost-deformacija* za različne temperature med 850 °C in 1200 °C, pri treh različnih hitrostih deformacij: 0,1 s^{-1}, 1 s^{-1} in 8 s^{-1}. Večja odstopanja lahko opazimo le pri manjših deformacijah kjer so večji gradienti krivulj tečenja. Omeniti velja, da bi

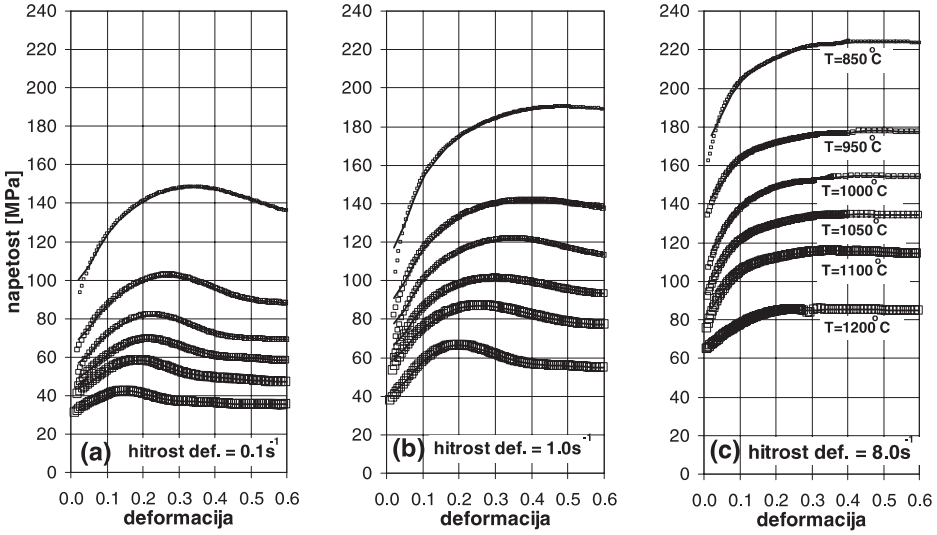

Slika 5. Krivulje tečenja za jeklo CF53 – eksperimentalne in napovedane vrednosti pri uporabi konstatnega parametra gladkosti (w=0.03).

načeloma lahko uporabili manjše vrednosti w, s čimer bi izboljšali rezultate na tem območju, vendar bi potem poslabšali rezultati na drugih območjih. Dosežena natančnost pri učnih podatkih je od 0,5 % do 1,1 %, s povprečno napako okoli 0,8 %. Natančnost napovedi na testnih podatkih je 0,6 % do 1,3 %, s povprečno napako okoli 1 %. Dobljene napake so v povprečju znotraj meja zahtevanih natančnosti.

Krivulje tečenja in CAE napovedi pri uporabi nekonstatnega parametra gladkosti

Slika 6 jasno kaže bistveno izboljšanje rezultatov krivulj tečenja v območju deformacij med 0,02 in 0,1. Rezultati nakazujejo, da lahko modeliranje krivulj tečenja izboljšamo z uporabo nekonstatnega parametra gladkosti (enačba 4).

Dosežena natančnost pri učnih podatkih je od 0,1 % do 0,3 %, s povprečno napako okoli 0,2 %. Natančnost napovedi na testnih podatkih je 0,2 % do 0,6 %, s povprečno napako okoli 0,5 %. Dobljene napake so v povprečju precej bolj znotraj meja zahtevanih natančnosti kot jih navajajo različni avtorji pri uporabi klasičnih nevronskih mrež z uporabo BP algoritma. Večja natančnost v obravnavanem primeru je tudi posledica večje razpoložljive gostote podatkov.

Sposobnost CAE nevronskim mrež za interpolacijo je potrjena s prikazom napovedanih krivulj tečenja preko celega območja na katerem je bila trenirana. Slika 7 kaže tridimenzionalno sliko krivulj tečenja kot funkcijo temperatur in deformacij pri različnih hitrostih deformacij. Pri hitrosti deformacije 0,1 s^{-1} je razvidno rahlo progresivno naraščanje preoblikovalne trdnosti s padanjem temperature deformacije. Ta trend je pri hitrosti deformacije 1 s^{-1} in 8 s^{-1} še manj izrazit.

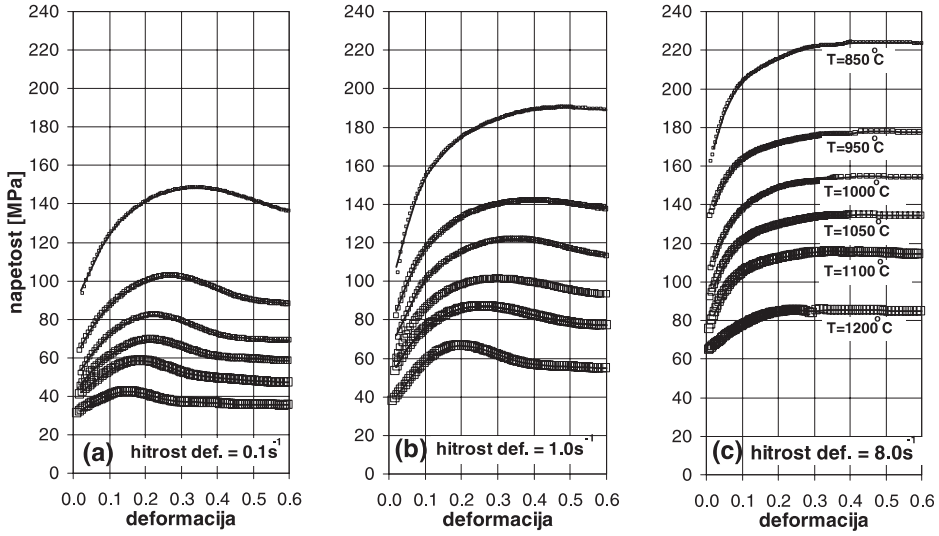

Slika 6. Krivulje tečenja za jeklo CF53 - eksperimentalne in napovedane vrednosti pri uporabi nekonstatnega parametra gladkosti ($w_e = w_T = 0{,}03$, $w_{e(e=0.02)} = 0{,}01$, $w_{e(e=0.60)} = 0.03$).

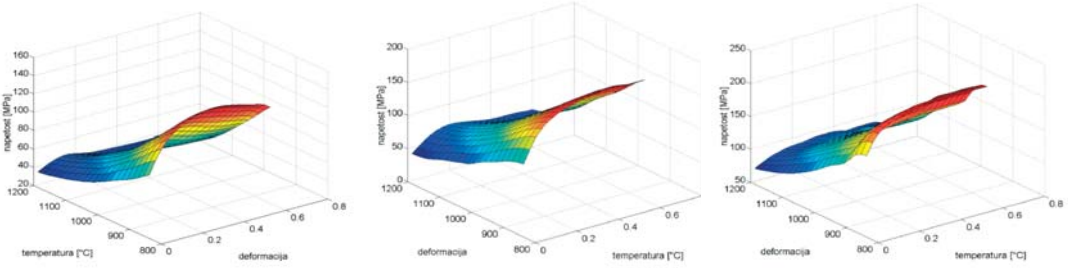

Slika 7. Prostorska predstavitev krivulj tečenja za jeklo CF53 – eksperimentalne in napovedane vrednosti pri uporabi nekonstatnega parametra gladkosti ($w_e = 0{,}03$, $w_T = 0{,}10$, $w_{e(e=0.02)} = 0{,}01$, $w_{e(e=0.60)} = 0{,}03$) .

Diskusija

Iz maksimalnih napetosti tečenja za različne temperature in hitrosti deformacije smo izračunali konstante hiperbolične sinusne enačbe 7 [26].

$$Z = \dot{\varepsilon}\exp(Q/RT) = A(\sinh \alpha\sigma)^n \qquad (7)$$

To enačbo najprej logaritmiramo in takole preuredimo

$$\ln(\sinh(\alpha\sigma)) = \frac{1}{n}\ln(\dot{\varepsilon}) + \frac{Q}{RnT} - \frac{1}{n}\ln(A), \quad (8)$$

nato pa definiramo funkcijo c^2, ki minimizira razliko med izračunanimi in izmerjenimi vrednostmi napetosti tečenja [25]

$$\chi^2 = \sum_{i=1}^{N} \frac{(z_i - a_1 x_i - a_2 y_i - a_3)^2}{e_i^2}, \qquad (9)$$

kjer je N število meritev, $z_i = \ln(\sinh\alpha\sigma_i)$, $x_i = \ln\dot{\varepsilon}_i$ in $y_i = 10^4 T^{-1}$. Ostale oznake so $a_1 = n^{-1}$, $a_2 = 10^{-4} Q n^{-1} R^{-1}$ in $a_3 = n^{-1}\ln A$. Pri napaki upoštevamo samo napako napetosti z_i, ki jo lahko izrazimo kot

$e_i = \alpha\, e_i^{\sigma}\, \coth\alpha\sigma_i$, kjer so e_i^{σ} napake izmerjenih napetosti. Podrobnosti postopka minimizacije zgornje enačbe 9 najdemo v [23]. Funkcija c^2 ima minimum pri Q = 316,86 kJ mol^{-1}, α = 0,00945 MPa^{-1}, n = 5,3 in A = 1,88·10^{12} s^{-1}. Ta vrednost je primerljiva z območjem vrednosti (Q = 280 - 330 kJ mol^{-1}) sorodnih jekel za poboljšanje, ki so bile dobljene po tangentni metodi na osnovi rezultatov, dobljenih iz torzijskih preizkusov [16-17].

Primerjavo odvisnosti maksimalne napetosti tečenja od temperature, med izračunanimi in izmerjenimi vrednostmi za tri različne hitrosti deformacije, prikazuje slika 8a. Na sliki 8b pa je podana primerjava med izračunanimi in izmerjenimi maksimalnimi napetostmi tečenja. Iz obeh slik je razvidno, da za obravnavano jeklo izbrana empirična enačba 8 odlično opiše zvezo med hitrostjo deformacije, temperaturo in maksimalno napetostjo tečenja.

Kemična sestava jekel od šarže do šarže, čeprav v dovoljenih mejah, stalno niha. Vpliv kemične sestave (posebno karbidotvornih elementov) na napetost tečenja avtorji pri njihovem napovedovanju rešujejo z vpeljavo ogljikovega ekvivalenta, saj pri uporabi BP nevronskih mrež veliko število vhodnih vplivnih parametrov vpliva na natančnost napovedovanja. V primeru uporabe CAE nevronske mreže pa teh težav nimamo, saj lahko uporabimo poljubno število vhodnih parametrov, torej lahko upoštevamo tudi vsak legirni element posebej [24-25].

Pri uporabi običajnih BP nevronskih mrež moramo najprej določiti optimalno arhitekturo nevronske mreže, t.j. določiti število plasti in število nevronov v teh plasteh, saj doslej še ni jasnih navodil za izbiro teh parametrov. Pri uporabi CAE nevronske mreže imamo fiksno število skritih plasti, število nevronov v plasti pa je odvisno od števila modelnih vektorjev. Inženir se lahko posveti modeliranju pojava in ne izgublja časa z določanjem abstraktnih parametrov nevronske mreže. Bistvena prednost CAE metode v prikazanem primeru je enostavnost in relativno dobra natančnost predlaganih modelov. Pomembno dejstvo, ki dodatno opravičuje uporabo CAE nevronskih

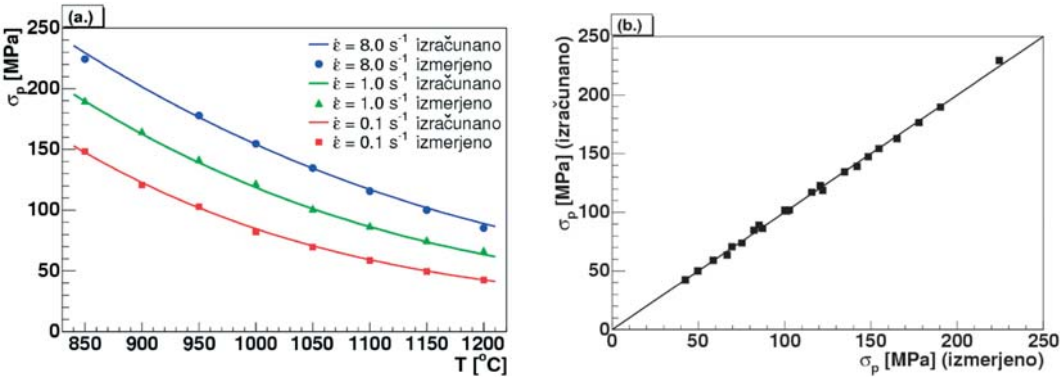

Slika 8. Primerjava med izmerjeno in izračunano odvisnostjo maksimalne napetosti tečenja od temperature za tri različne hitrosti 0,1 s^{-1}, 1 s^{-1}, 8 s^{-1} (a.) in primerjava med izmerjenimi in izračunanimi maksimalnimi napetostmi (b.).

mrež je, da se parametri med preizkusom spreminjajo; CAE nevronske mreže so namreč na osnovi tako dobljene baze podatkov sposobne določiti realne krivulje tečenja pri konstantnih pogojih.

V obravnavanem primeru so bile pri meritvah upoštevane samo tri različne hitrosti deformacij. Znano je, da je mogoče skozi tri točke v najboljšem primeru napeljati kvadratno krivuljo oz. polinom drugega reda, ki opisuje pojav. Brez vnaprej znane zakonitosti, ki bi jo upoštevali v CAE modelu, je opisovanje pojava v smeri hitrosti deformacij relativno slabo. Predvidevamo, da bomo v prihodnjih raziskavah CAE metodo lahko dopolnili tako, da bo v primeru premajhnega števila podatkov za katerikoli vhodni parameter pojava (v opisanem primeru hitrosti deformacije) mogoče upoštevati vnaprej predpostavljeno oz. poznano zakonitost. To dejstvo se namreč s pridom izkorišča pri optimizaciji experimentalnega dela, težje pa ga je upoštevati v matematičnih modelih krivulj tečenja brez a-priori predpostavk.

5. Zaključki

Za potrebe optimiranja tehnologije toplega preoblikovanja jekla za poboljšanje CF53, namenjenega predvsem za strojne dele, ki so lahko izpostavljeni visokim mehanskim obremenitvam, smo na Gleeble 1500 izvedli tople stiskalne preizkuse. Temperaturno, deformacijsko in hitrostno deformacijsko območje ustreza območju toplega valjanja. Preizkusili smo metodo napovedovanja krivulj tečenja s pomočjo umetne inteligence (CAE NN). Oblike krivulj tečenja kažejo na procese dinamične rekristalizacije med toplo deformacijo.

Študija je potrdila odlično napovedno sposobnost CAE nevronske mreže za napovedovanje krivulj tečenja Pri tem smo uporabili dva pristopa in sicer metodo konstantnega parametra gladkosti ter metodo nekonstantnega parametra gladkosti. Slednji daje boljše rezultate predvsem zaradi boljše sposobnosti modeliranja fizikalnih zakonitosti v področjih velikih gradientov. Dosežene natančnosti so praktično znotraj območja 5 %, v povprečju znaša napaka 3 %. Pri uporabi CAE nevronske mreže ne potrebujemo določevanja optimalne arhitekture plasti mreže, s »poskus-napaka« postopkom pa enostavno določamo optimalne vrednosti parametra gladkosti pri razpoložljivi bazi podatkov. Postopek napovedovanja z CAE NN je enostavnejši v primerjavi BP NN, natančnost napovedovanja pa je na isti ravni. Izračunali smo tudi aktivacijsko energijo za CF53, ki znaša $Q = 316{,}86$ kJ mol^{-1}.

Zahvala

Avtorji se zahvaljujejo Unior-u Zreče za izdelavo vzorcev.

LITERATURA

[1] KOOP, R., LUCE, R., LEISTEN, B., WOLSKE, M., TSCHIRNICH, M., REHRMANN, T., VOLLES, R., (2001): Flow stress measuring by use of cylindrical compression test and special application to meta forming processes, *Steel Research,* 72, 394-401.

[2] SCHOTEN, K., BLECK, W., DAHL, W. (1998): Modelling of flow curves for hot deformation, *Steel Research*, 69, 193-197.

[3] KUGLER, G., TURK, R. (2004): Modeling the dynamic recrystalization under multi-stage hot deformation, *Acta Materialia*, 52/16, 4659-4668.

[4] LIU, J., CHANG, H., HSU, T.Y., RUAN, X. (2000): Prediction of the flow stress of high speed steel during hot deformation using a BP artificial neural network, *Journal of Materials Processing Technology*, 103, 200-205.

[5] HATA, N., KAKADO, J.I., KIKUCHI, S., TAKUDA, H. (1985): Modelling on flow stress of plain carbon steel at elevated temperatures, *Steel research*, 56/11, 575-582.

[6] RAO, K.P., HAWBOLT, E.B. (1992): Development of constitutive relationships using compression testing of medium carbon steel, *Trans. ASME* 114, 116-123.

[7] KLIBER, J., SCHINDLER, I. (1997): Matematical description of stress-strain curve in metal forming processes, *Metalurgija*, 36/1, 9-13.

[8] DAVENPORT, S.B., SILK, N.J., SPARKS, C.N., SELLARS, C.M., (2000): Development of constitutive equations for modelling of hot rolling, *Materials Science and Technology*, 16, 539-546.

[9] LIU, J., CHANG, H., WU, R., HSU, T.Y., RUAN, X. (2000): Investigation on hot deformation behaviour of AISI T1 high-speed steel, *Materials characterization*, 45, 175-186.

[10] MCQUEEN, H.J., RYAN, N.D. (2002): Constitutive analysis in hot working, *Materials Science and Engineering A*, 322, 43-63.

[11] PHANIRAJ, M.P., LAHIRI, A.K. (2003): The applicability of neural network to predict flow stress for carbon steels, *Journal of Materials Processing Technology*, 141, 219-227.

[12] RAO, K.P., PRASAD, Y.K.D.V. (1995): Neural network approach to flow stress evaluation in hot deformation, *Journal of Materials Processing Technology*, 53, 552-566.

[13] HODGSON, P.D., KONG, L.X., DAVIES, C.H.J. (1999): The prediction of the hot strength of steels with an integrated phenomenological and artificial neural network model, *Journal of Materials Processing Technology*, 87, 131-138.

[14] KONG, L.X., HODGSON, P.D. (1999): The application of constituitive and artificial neural network model to predict the hot strength of steels, *ISIJ Int.* 39/10, 991-998.

[15] CHENG, Y.W., TOBLER, R.L., FILLA, B.J., COAKLEY, K.J. (1999: Constitutive behaviour modeling of steels under hot rolling conditions, NIST Technical Note 1500-6, *Materials Reliability Series*, 39-49.

[16] MCQUEEN, H.J., RYAN, N.D. (2002): Constitutive analysis in hot working, *Materials Science and Engineering A*, 322, 42-63.

[17] MCQUEEN, H.J., YUE, S., RYAN, N.D., FRY, E. (1995): Hot working characteristics of steels in austenitic state, *Journal of Materials Processing Technology*, 53, 293-310.

[18] GRABEC, I., SACHSE, W. (1997): Synergetics of Measurement, Prediction and Control. ISBN 3-540-57048-9, *Springer-Verlag*.

[19] GRABEC, I. (1990): Self-Organization of Neurons Described by the Maximum-Entropy Principle. *Biol.Cybern*, 63, 403.

[20] PERUŠ, I., FAJFAR, P., GRABEC, I. (1994): Prediction of the seismic capacity of RC structural walls by non-parametric multidimensional regression, *Earthquake Eng. Struct. Dyn*. 23, 1139-1155.

[21] FAJFAR, P., PERUŠ, I. (1997): A non-parametric approach to attenuation relations. *Journal of Earthquake Engineering*, 1(2), 319.

[22] PERUŠ, I., FAJFAR, P. (1997): A non-parametric aproach for empirical modelling of engineering problems, *Engineering Modelling*, 10(1-4), 7.

[23] KUGLER, G., KNAP, M., PALKOVSKI, H., TURK, R. (2004): Estimation of activation energy for calculating the hot workability properties of metals, Metalurgia, 43/4, 267-272.

[24] TERČELJ, M., PERUŠ, I., TURK, R. (2003): Suitability of CAE neural network and FEM for predicting of wear on die radii in hot forging, *Tribology International*, 36, 573-583.

[25] TURK, R., PERUŠ, I., TERČELJ, M. (2004): New starting points for prediction of tool wear in hot forging, *Int. J. of Machine Tools & Manufacture*, 44/12-13, 1319-1331.

[26] SELLARS, C.M., MCG. TEGART, W.J. (1972): *Int. Metall. Rev*., 17, 1-24.

Feeding behaviour of graphite containing material

Heinz-Josef Wojtas

Fakultät für Ingenieurwissenschaften, Institut für Angewandte Materialtechnik,
Universität Duisburg-Essen, Lotharstr. 65, D-47057 Duisburg;
E-mail: hk225wo@uni-duisburg.de

Received: June 30, 2005 **Accepted**: November 24, 2005

Abstract: On casting and cooling of metals in a mould energy in form of heat will be transferred from the liquid metal to the moulding material. The mechanism of energy transfer and the corresponding capture capacity of the moulding material define the energy transfer in form of heat by cooling of the metal at contemporaneous heating of the moulding material. Only the exact knowledge of the temporary and quantitative process of heat flow will lead a solidification simulation to correct results. According to second law of thermodynamics energy in the form of heat may only be transferred from a colder to a warmer material if this is forced by mechanical work. Self-transfer of heat is only possible from an area of higher temperature in direction to areas with lower temperature. Only on the premises of a temperature drop a self-transfer of heat is possible. The energy transfer between materials of different temperatures is finished when an energetic balance is reached, i.e. when after the heat transfer there is the same temperature at all materials. Energy in the form of heat is transferred by means of heat conductivity, heat transfer (heat convection) or heat radiation.

Key words: metal/mould material, graphite, heat transfer, conductivity, energy balance, feeding

Part 1: Definition of various influencing variables

Physical values defining the solidification process

Density (ρ)

The density of a substance is the relation of mass to volume, some times called "specific mass". Although most of the solid bodies and liquids expand on heating, these volume changes are relatively small and nearly independent of temperature and pressure.

Thermal conductivity (λ)

Thermal conductivity means the energy transport inside a substance by interaction of atoms and molecules, which are not transported themselves (for example within the single silica grain, the solidified crystal or the convection-free melt). The energy transport is done in the way, that quicker and larger swinging molecules of a more heated substance area continue to transfer energy to adjoining and less heated substance regions, until – after energy transfer is

Scientific paper

finished – the same average swinging condition and the same temperature is set.

Thermal conductivity of various materials is different. It is expressed by thermal conductivity λ. Thermal conductivity of different materials is experimentally investigated and depends on temperature.

Heat transfer (sometimes called "heat convection")

Under the term "heat transfer" is to be understood an energy transport between several materials (for example between two touching silicate grains or the solidified casting surface and the mould material) with different temperature and without material transport. Energy transfer is done in the touching area of both substances and implies a temperature drop. After heat transfer is finished both substances have the same temperature T within the touching area.

Real heat convection is combined with a material transfer. This materials transfer is called forth within liquid and gaseous materials by a thermal change of volumes and density. Heat convection within liquid metals is detectable only at an early stage of mould filling. Heat convection of air has not been detected within a mould. The pressure build-up within pore volume of the mould by means of evaporation or combustion processes does not belong to the physical values, but to the variable moulding material values defining the solidification process.

Heat transition

If liquids or gases of different temperatures are separated by a solid wall, an energy transfer will take place, consisting of heat conduction and heat transfer. This combined form of heat transfer is called heat transition.

Heat radiation

Between bodies of different temperatures heat is not only transferred by means of thermal conductivity or heat convection but also at same time by means of heat radiation (for example across the gap between the silicate grains). Everywhere at heat transfer processes the kinetic energy of the molecules is partially transferred into radiation energy and radiated. The percentage of radiation energy at complete energy transfer is small at low temperatures.

Heat radiation belongs to electro-magnetic waves and they are within visible frequency range only at higher temperatures. Frequency range, diffusion, reflection and refraction follow the valid regularities of luminous radiation.

The radiation energy impacting a radiated body may be absorbed reflected or transmitted. The absorbed part of the radiation energy will be transferred again into kinetic energy of the molecules and will heat the radiated body which therefore becomes source of own radiation.

A body absorbing all impacting radiation energy is called an absolute black body. Absorption and emission are on highest level.

The heat Q radiated from an absolute black body with a surface A within a time t depends on the body temperature T and results from the law of Stefan Boltzmann.

Amount of heat

The amount of heat Q is the quantity of energy in the form of heat, which can be feed to a material or taken away. On thermo-technical calculation there is often a reference to material quantity of 1 kg. The amount of heat referring to 1 kg is called specific heat q.

Specific heat capacity (c_p)

The specific heat capacity (c_p) characterizes the various heating-up of materials. It indicates the amount of energy in the form of heat, which is necessary to heat a material quantity with a mass of 1 kg for 1 K (or 1°C) by keeping the respective aggregate state.
If a material quantity with the mass m_1 and the temperature T_1 shall be heated to a temperature T_2 by supply of heat this adding heat results of:

$$Q = mc_p (T_2 - T_1) \qquad (1)$$

Those materials that extend noticeable during heating is to differ between heat capacities at constant pressure and constant volume respectively. This is irrelevant for liquids and solid bodies due to the unimportant volume modification. Although it is normally calculated with heat capacity at constant pressure.

Variable moulding material values defining the solidification process

Density, bulk density, packing density (ρ)

At production of moulds a loose, granular material conglomerate is compacted on machines. The voids fraction between the grains decreases. Generally you have to assume considerable density fluctuation for all moulds. The density fluctuation varies with type and sort of sand, binder, moulding box and method of compacting. By this the voids fraction fluctuates, too, and – as a result

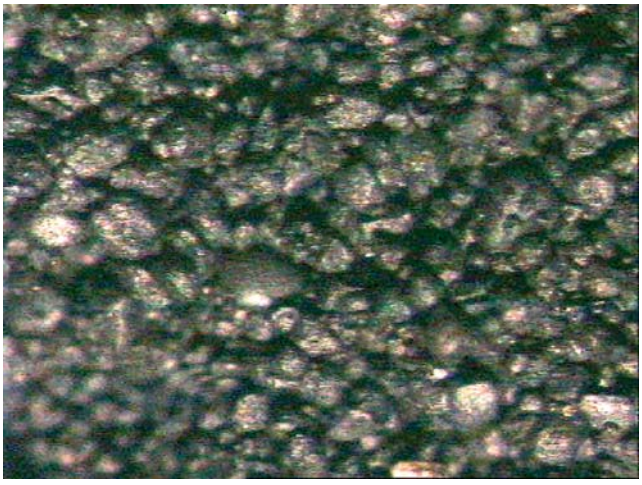

Figure 1. View of a mould wall

– the density of the material conglomerate. This "packing density" significantly influences the energy transport through the mould (Fig. 1). Therefore the average density of the mould should be considered at least.

The movement of the mould wall is mainly caused by the thermal expansion of the mould sand. But this expansion is only approx. 1 % within relevant temperature range, so that the amendment of packing density caused by this may be neglected on further calculation of heat flow.

Heat capacity "apparent heat capacity" (c)

The heat capacity, that enters into the equations 2 in this case, is the heat capacity of a granular material conglomerate of mould basis material and binder system (Fig. 1). It is an "apparent heat capacity" applying at first only to the volume element with a certain voids fraction and a certain packing density, which underlies the measurement.

$$\rho c(T)\frac{\partial T}{\partial t} = div\left[\lambda(T)\, grad T\right] + \dot{W}(T,\vec{r},t) \quad (2)$$

The influence of the inorganic binder to the heat capacity of this volume element may be neglected, as their portion is small and as there is not a big difference within heat capacity between mould basis material and binder.

The portion of organic binders within mould material systems is even smaller and their contribution to the heat capacity of the system, in which an oxygen deficiency inside of the pore volume avoids the complete combustion of the binders, results from required energy for disintegration and the energy set-free from combustion. This energy contribution in the form of a heat source within the volume element might be negligible.

The enthalpy for the α–β allotrope change of the quartz is 10.5 kJ/kg and – compared with the heat capacity of the mould – is consequently negligible small too.

Inside wet sand the vaporization, the condensation and the migration of the condensation zone goes through the volume element at low temperatures at the beginning of the solidification. Therefore, at first a heat source (releasing condensation heat) goes through the volume element followed by a heat lowering (depriving heat of vaporization). These effects enter into the apparent heat capacity and there is no need to consider them specially.

This apparent specific heat or heat capacity respectively would be independent from T but would depend on the temperature at transition point metal / mould material and considers the heat absorbed from the mould completely.

Thermal conductivity "apparent thermal conductivity" λ

In the same meaning as at heat capacity there results an "apparent thermal conductivity". These "apparent thermal conductivities" would be different at the same sand and different casting alloys, such as aluminium, cast iron and steel. It results in a dependence of the apparent thermal conductivity from packing density and from the melting temperature of the alloy. The apparent thermal conductivity decreases on increasing voids fracture.

Within a lot of papers the specific thermal conductivity is defined as apparent specific thermal conductivity between room temperature and transition temperature at transition point metal / mould. But here the above-mentioned definition is used, as it considers the heat absorbed from the mould.

Variable material values, which define the solidification process

Average carbon activity

The average carbon activity of cast iron is mainly defined by the content of carbon graphite or carbide stabilizers as well as of the actual temperature. Within a certain range the degree of saturation and the carbon equivalent are rules for it.

Local carbon activity

This means the carbon activity directly at the place of solidification. It is defined by the local composition which is defined by separation processes, liquation and undercooling.

Diffusion coefficient

The diffusion coefficient of a cast iron is defined by the content of carbon, graphite and carbide stabilizers as well as by the actual temperature. There is no simple term like the degree of saturation to describe this value, but it defines the separation process of the two phases austenite and graphite during the eutectic solidification.

Diffusion path length

The diffusion path length during the separation of the eutectic melt to austenite and graphite is arranged by the number of nuclei forming and able to growth. The diffusion path length only depends on the number of nuclei and not on their formation (theory of nuclei formation).

Growth of austenite and graphite

The growth is defined by the thermodynamic values volume energy and interfacial tension.

Influence of material values

Material values and their definable structure

If – in a first step – the shrinkage volume resulting from a mould wall movement are regarded as constant and not influenceable by the material, the total shrinkage volume results as additive sum of contraction volume of the hypoeutectic austenite the eutectic austenite and the volume increase of graphite at its precipitation.

The size of the hypoeutectic solidification contraction is mainly defined by the chemical composition, especially by the carbon and silicon content and values like the degree of saturation or the carbon equivalent respectively, in which further elements are considered. They are a degree how much the actual composition differs from the eutectic one (Fig. 2). Therefore the quantity of hypoeutectic solidification may be fixed by

the thermal analysis by means of the temperatures, which define the beginning and the end of the hypoeutectic solidification. A contraction volume can be derived from the weight or volume of the predictable hypoeutectic solidification. This contraction volume can be equalized either by feeding or can be minimized by changing the chemical composition. The minimization of the contraction volume may be done by

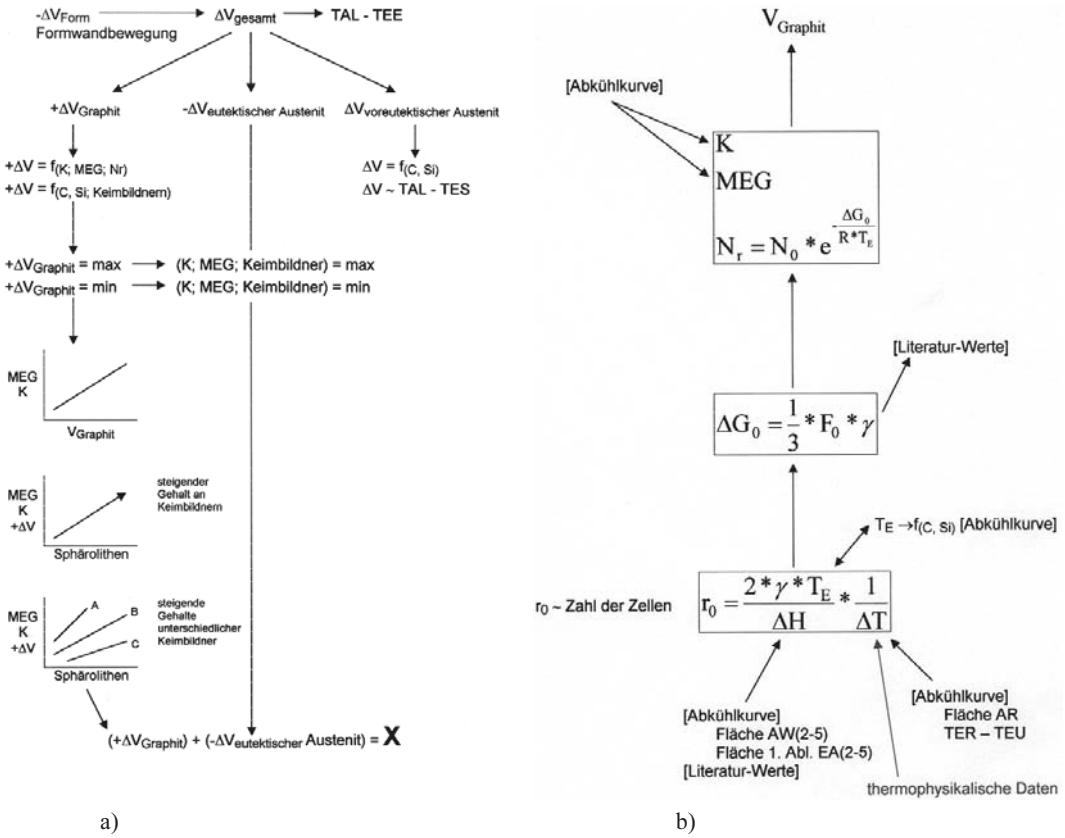

ΔT:	Unterkühlung der Schmelze
ΔH:	Enthalpie
T_E:	Temperatur der stabilen eutektischen Erstarrung
γ:	Oberflächenspannung
r_0:	Keimradius
F_0:	Oberfläche des Keims
ΔG_0:	Freie Enthalpie des Keims
N_r:	Zahl der kugelförmigen Cluster
MEG:	Menge des eutektischen Graphits
K:	Graphitisierungstendenz

Figure 2. Influence of the solidification manipulation for controlling the solidification contraction.

addition of carbon or silicon or by an amended inoculation modus.

The hypoeutectic solidification portion, defined by this way, fixes the quantity of the eutectic solidification as a complementary sum to the total volume or to the weight considered. The eutectic solidification consists of the eutectic austenite with a volume contraction and the graphite with a volume dilatation. Eutectic austenite and graphite are fixed in their mutual relationship according to the multiple component system. By this the contraction sum of the eutectic austenite becomes a calculable value (Fig. 2a).

The only value, which is now decisive for the decrease of the eutectic shrinkage volume, is the quantity of the precipitated graphite with the corresponding volume increase. At first you have to avoid the possibility of the meta-stable solidification of eutectic that would be combined with a non-compensation of the eutectic austenite contraction. As a rule this is done by adjustment of the carbon and silicon contents to the wall thickness and by adding inoculants that initiate the precipitation of graphite. The quantity of eutectic graphite and consequently the size of volume increase is a function of carbon and silicon contents. The number of spheroids is a question of the number of nuclei, as the same graphite volume may divide to one great spheroid or to any number of small ones. The efficient number of nuclei results of the content of inoculants and the combination of efficient components within inoculants (Fig. 2a).

Without entering nucleation theories it is possible – by means of known data from literature of surface tension and enthalpy of fusion – to make calculations, which may lead by support of the thermal analyse to statements about number of nuclei and the approximate graphite volume (Fig. 2b).

Influence of moulding material values

The real feeding demand of a casting consists of:

- volume deficit of the hypoeutectic contraction,
- volume deficit of the eutectic contraction,
- volume increase of the eutectic graphite precipitation and
- "apparent shrinkage".

The "apparent shrinkage" is a value that is only found within a few reflections for feeding calculations so far. To carry out this paper it was consequently necessary to define the possible influence factors of the "apparent shrinkage" exactly.

The "apparent shrinkage" is a magnification or enlargement of the mould cavity due to the casting process, the solidification behaviour of the cast iron and the attributes of the mould material (mould wall movement). These influences may increase the feeding demand of the casting.

The "apparent shrinkage" consists of two main influence factors:

- the load defining the pressure onto the mould wall produced by the casting process and the solidification behaviour of the cast iron (graphite precipitation),
- the enlargement of the mould cavity or the stability of the mould that withstands the pressure (mould wall movement).

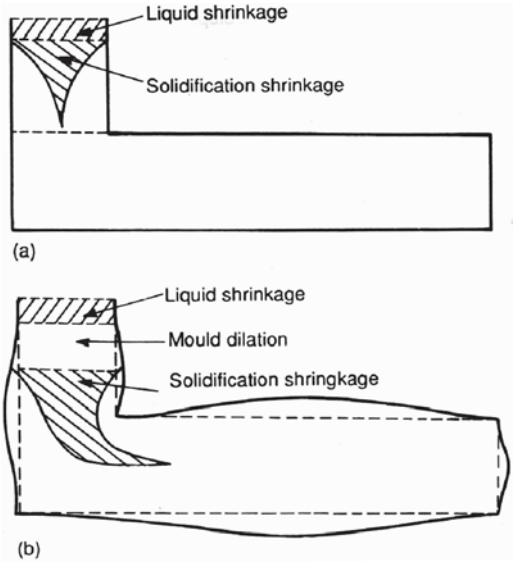

Figure 3. Interaction between solidification and shrinkage in a mould:
a) the apparent shrinkage does not appear,
b) the apparent shrinkage appears.

Figure 3 shows shrinkage cavities appears when the feeder does not have enough liquid iron for compensation of apparent shrinkage, a) no mould wall movement, shrink-free casting, exactly according to pattern, sufficient feeding volume b) great mould wall movement, casting larger than pattern, shrinkage within casting, insufficient feeding volume.

The graphite precipitation or the solidification behaviour of cast iron with spherical graphite is not the only parameter that defines the pressure onto the mould wall. Other loads developing on casting and solidification process are big figures too.

These loads result of:
- the ferrostatic pressure,
- the casting heat,
- the composition of alloy.

The second main influence factor defining the apparent shrinkage is the mould movement or the mould attributes respectively. The dependences of the mould wall movement result of:
- the type of mould material,
- the composition of mould material,
- the compaction,
- the geometry of the mould,
- the attributes of the mould box.

Part 2: Solidification structure of cast iron and efficiency of feeders

Thermal Analysis

From the 1st derivative of the cooling curve results the gradient of the cooling rate over the complete solidification process. The point where the cooling rate (the first derivate) shows the first maximum and starts to decrease again corresponds to the liquidus temperature TL. The following first minimum is the temperature for the beginning eutectic solidification, the eutectic start temperature TES. The TES following point of intersection of the 1st derivative and the zero line marks TE_{low}. At this point the dissipated heat and the released latent heat are in balance. From this point the released latent heat of graphite precipitation prevail and this leads to temperature increase. After a now following maximum of the first derivative the cooling rate decreases again and shows a zero value corresponding to TE_{high}. After this the ongoing eutectic solidi-

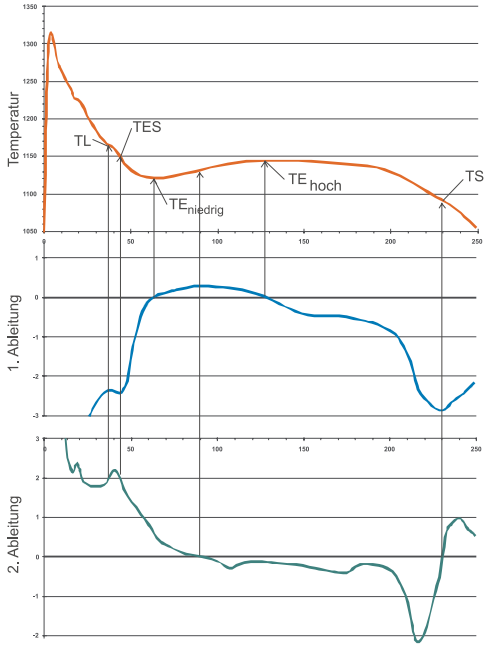

0	TL	1	Liquid temperature, it is the temperature where the first solid particles appear, normally austenite as a consequence of cooling in the cast iron
2	TES	3	Start temperature of beginning eutectic solidification
4	TE_{LOW}	5	The minimum eutectic temperature after that temperature increases as a result of released latent heat
6	TE_{HIGH}	7	The maximum eutectic temperature as a result of the released latent heat
8	TS	9	Solidus temperature, the temperature when the solidification process is finished
10	T_{METAST}	11	Temperature of metastable eutectic solidification
12	R	13	Recalescence - difference of temperatures TE_{LOW} and TE_{HIGH}

Figure 4. Significant points within cooling curve of cast iron

fication ends at point TS, indicated by a minimum at the first derivative.

The first derivative is also in a position to define the periods of solidification. The period of hypoeutectic austenite solidification results up to the first minimum, which is marked by the length growth of the dendrites. The first minimum represents the moment when the eutectic solidification begins and between minimum and crossing zero-line the austenite dendrites are growing thicker instead of growing in length. This process is coupled with a eutectic solidification at the same time. This pure eutectic solidification is defined by this zero crossing and the zero crossing of the second derivative at the end of solidification.

The possibility of metastable eutectic solidification is marked by the metastable eutectic temperature, which can be calculated with different factors. If TE_{low} falls below this specific temperature, which is strongly influenced by Si and elements stabilizing carbide, this may lead to a metastable solidification with a corresponding higher volume deficit. Due to carbide decomposition during further solidification process this chill must not be positively recognizable at room temperature. Therefore T_{metast} should be lower than TE_{low}.

Likewise there can arise a shift to metastable solidification at the end of the solidification process by an enrichment of alloying elements within remaining melt. The final temperature of the eutectic solidification should be above those of the metastable eutectic temperature.

The height of (TL) liquidus temperature as well as the period of time until temperature TE_{low} will be reached are a degree for the quantity of hypoeutectic austenite solidification and – proportional to this – for a feeding demand. This feeding demand can only be equalized by a feeder. This volume

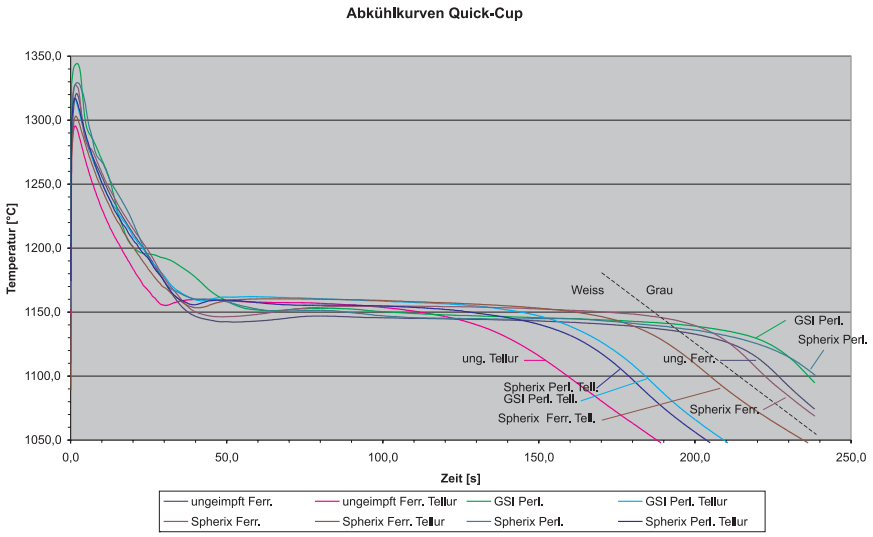

Figure 5. Some real cooling curves.

deficit of solidification cannot be reduced by the following graphite precipitation. Within this phase – after the austenite dendrites have built a spongy network structure and thereby have defined the future surface resp. wall structure – there is at first the diameter growth of the dendrites and the beginning precipitation of graphite between the dendrites with a corresponding volume increase. In this connection exists the possibility resp. the danger of an enlargement (growth) of casting areas with an increasing inner volume deficit. Therefore TL should be as low as possible and the period between TL and TE_{low} should be as short as possible.

The recalescence R is the difference between TE_{low} and TE_{high}. It represents the released latent heat of the eutectic solidification. The recalescence should be as low as possible, and TE_{low} as well as TE_{high} should be clearly above T_{metast}. Steady and good graphite precipitation can be expected then that would correspond to the conditions for self-feeding or riserless pouring technique.

Real cooling curves show characteristic differences with regard to their nucleation condition and the cooling conditions (Fig. 5).

From reflections on solidification and solidification morphology the different significant temperatures and time periods of the cooling curves have to point out, which structure as well as which volume deficit have to be expected (Fig. 6). With today's computer facilities it is possible to define the single periods of time and temperature also by a 1st and 2nd derivative of curve already during recording the solidification curve and to

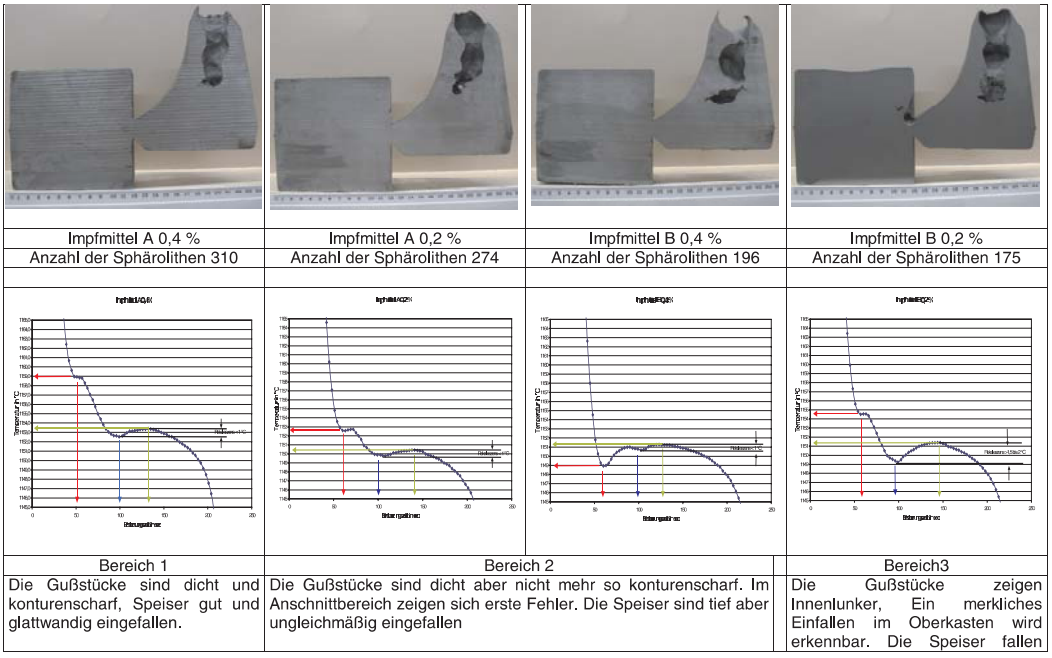

Figure 6. Real cooling curves in comparison to casting results.

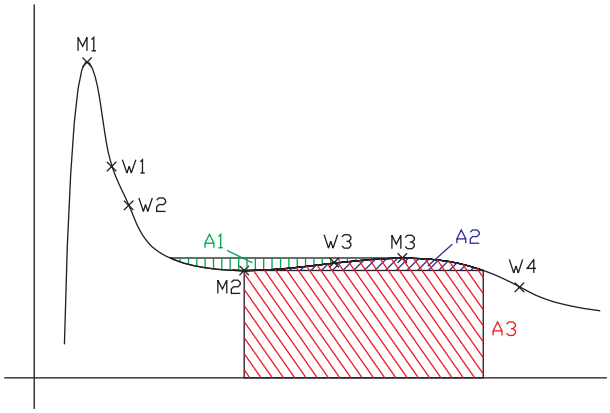

Figure 7. Scheme of points and areas of evaluation in comparison with structure evaluation

transfer them to a analysis of variance, from which a correction measure has to be derived.

According to Figure 7 evaluation programmes have been made for the melts in question, and it was tried to state dependences.

TIME FRAME OF FEEDER EFFICIENCY

Feeding is a transport phenomenon

Feeding is founded on transport processes of flowable material from the feeder into the contraction areas of the casting to compensate there the arising volume deficit. This means that in the casting, too, corresponding transport processes have to take place. These necessary transport processes are restricted by the solidification morphology of the alloys. At a cast iron with spheroidal graphite several crystallization processes with different morphologies take place one after the other.

The primary solidification of cast iron is always exogenous spongy up to mushy. Already at an early stage a dendrite network passes through the casting wall and builds a spongy plaiting, in which the remaining eutectic melt solidifies.

Spheroidal eutectic solidify endogenous mushy. The graphite spheroids will be enclosed by growing austenite and will be isolated from remaining melt. By diffusing carbon through the austenite to the graphite spheroid this spheroids can grow and can affect a strong pressure to their surroundings. This effect will be stronger and for a longer period of time the longer the solidification time is or the longer the wall / casting remains in liquid condition.

Feeding types differ according to:

- mass feeding,
- interdendritic feeding,
- feeding by sucking solidified shells inwards (surface sinks),
- self-feeding – compensation of the metallic solidification contraction by the volume increase of precipitating graphite.

Mass feeding is the movement of a mixture of crystals and melt from the feeder into the casting due to gravity. This process come to an end as soon as the crystals hinder each other in their movement, hook or jam, this is the so-called "pour point". There are a direct coherence between feeding capacity and solidification morphology. The mass feeding is mainly responsible for the formation of macro-shrinkage within feeder.

Interdendritic feeding is the movement of melt through a crystal network. With their quantity portion at feeding it is defined by the ramification degree of the crystals and the resulting flow channels. Within interdendritic area conditions are to assume like within a filter, at which the size of flow channels at a point of time X is defined by volume relation between crystal network and melt. Portion of interdendritic feeding at total volume of a macro-shrinkage has to be estimated as small.

Feeding by sucking solidified shells inwards (surface sinks), as movement of two opposite surfaces to each other, can only avoid the formation of an inner deficit and for the present it has no perceptible influence to the formation of macro-shrinkage within feeder. Surface sinks often are not macroscopic perceptible offhand.

Self-feeding as a compensation of metallic volume contraction by volume increase of self-precipitating graphite within a melt has to be regarded in a direct coherence between the quantity of self-precipitating graphite and the quantity of hypoeutectic and eutectic austenite, so that the contraction of austenite can partially or completely be compensated by the volume increase of graphite, or may be even exceeded. The latter is known as a swelling or growing of castings combined with a volume increase of the castings.

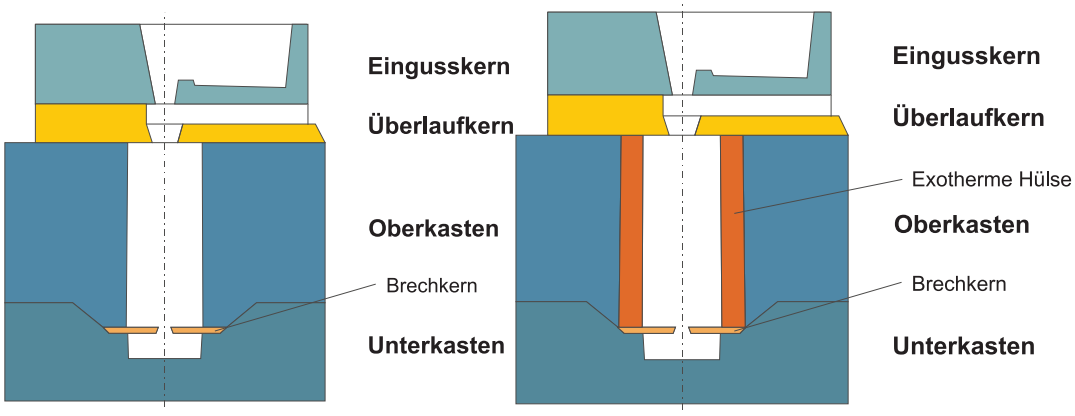

Figure 8. The assembly – pour point investigation.

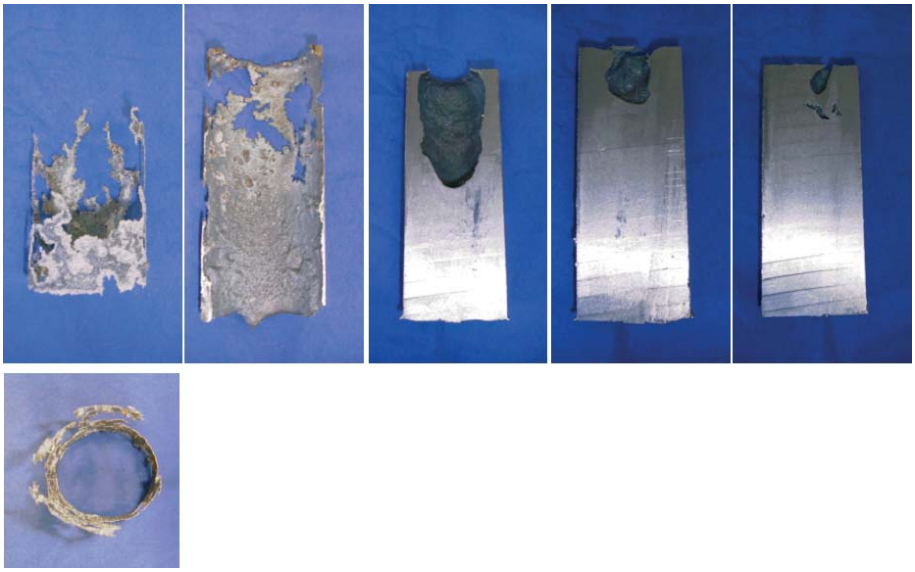

Figure 9. Several Points of time during solidification.

Pour point

Figure 8 schematically shows the experimental set-up. This set-up was oriented on an experimental arrangement, which already has been used in a similar way. The test-piece, in principle representing the feeder, was arranged within a cope box, a cam with separating core were arranged within a drag box. Sprue-core and flow-off core are set on the cope box. The sprue-core, flow-off-core and separating-core were made of CO_2 sand or furan resin sand. There were used common production resins without additives. The sprue-core had the function to enable a uniform filling of the test-piece and to position the flow-off-core above the test-piece. The flow-off-core took care for a constant filling level of the test-piece. Surplus material from the sprue-core flew-off over the rear side of cope box after effected filling of the test-piece. This led to uniform test conditions (no feeding effects). The cam and the test-piece heat the separating core (principle of a breaker core below a feeder) and thereby decrease the cooling speed at the bottom side of the test-piece. In this area the test-piece solidifies more slowly. Now it is guaranteed that material which is still being moveable inside the feeder will flow-out by taking off the feeder. Figure 9 shows several points of time during solidification.

Conclusions of the results of the pour point test (Fig. 10)

Under same conditions pearlitic and ferritic iron become immovable approx. at the same time. For both cast iron qualities the possibility of a mass feeding is finished already before the beginning of eutectic solidification. The volume deficit occurring during further solidification of metallic

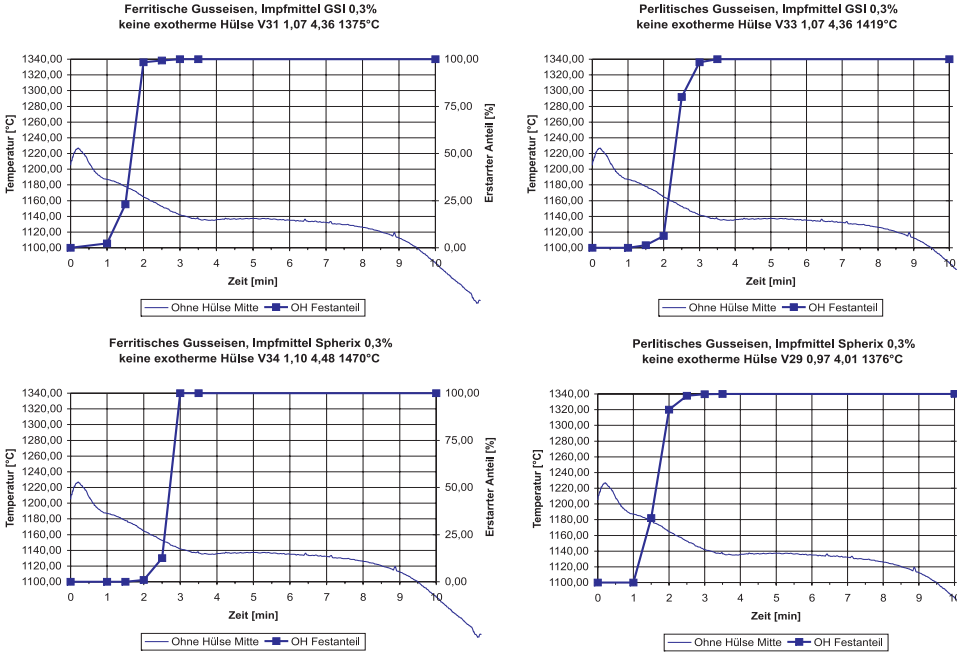

a) without exothermic sleeve

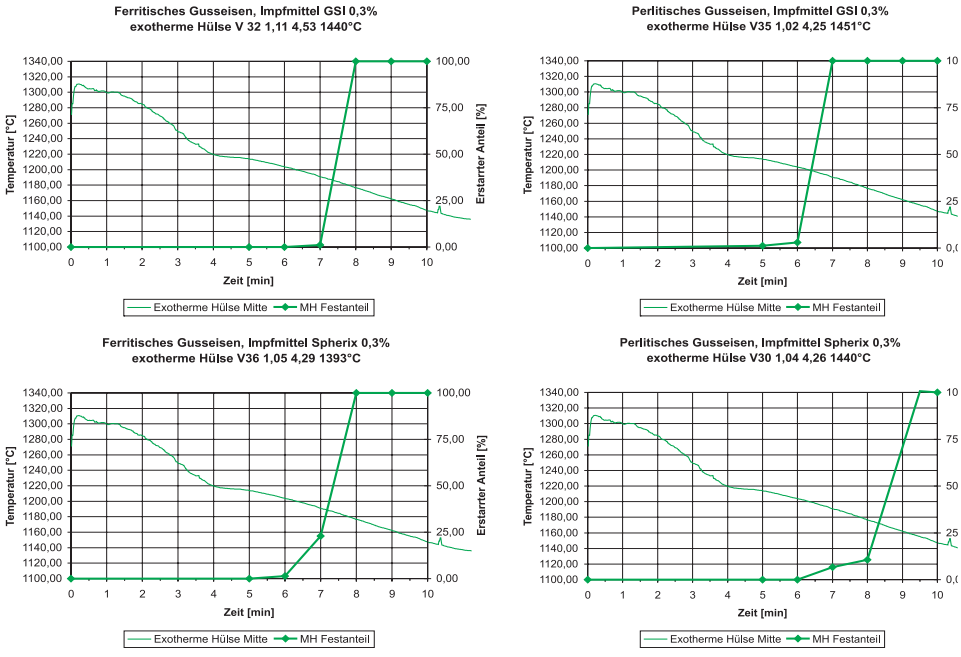

b) with exothermic sleeve

Figure 10. Quantity of the solidified portion a) without and b) with using an exothermic sleeve, registered in the solidification curve.

matrix may then only be compensated by
- interdendritic feeding,
- feeding by surface sinks,
- self-feeding,

i.e. by volume increase of the eutectic self-precipitating graphite. This should have the main influence with regard to the density of a casting, because the feeding possibility within interdendritic area for longer distances is not possible without corresponding pressure differences (analogy to filter), and a sinking of the walls should become impossible, too, with a dendrite self-supporting network existing all over the complete cross-section of the wall.

So a feeder at cast iron with spheroidal graphite can only compensate the liquid contraction from casting temperature up to the beginning of solidification as well as a part of the volume contraction of the hypoeutectic austenite solidification. After starting eutectic solidification there is no moveable metal in the feeder. The main rest of volume contraction of the solidifying metallic matrix has to be compensated by the volume increase of the self-precipitating graphite. This quantity may – among others – be controlled by composition, graphitization potential and cooling speed.

With regard to the solidification simulation it results that the early immovability of the mass within feeder has to be considered, as it is only possible to give an accurate prediction when it is known how long a feeder can supply movable material at different iron qualities. Resulting change of shifting thermal centres due to gravity ends at this time. The principle of directional solidification and it's corresponding simulative translation cannot be maintained for cast iron after this point of time, this means approx. 20 – 30 % of the total solidification time at both ferritic and pearlitic cast iron. Thermal centre still existing or still arising at this point of time have to be criticized with the consideration of volume increase of graphite at a controllable eutectic graphitization potential. This must be different to the eutectoid graphitization potential with the consequence of ferritic and pearlitic cast iron.

Part 3: Influence of cooling conditions as well as of inoculation to the solidification structure

Casting method

The hot-wire method as a measuring method to analyse thermo-physical data of refractory material is only conditionally suitable to analyse thermo-physical data of the moulding material, as the values analysed by this method do not reflect the conditions within the mould during casting. The long heating times, necessary for this method due to the necessity of a temperature balance, lead to modifications within mould material. At each measurement at more than 100 °C or even at nearly 100 °C the moulding material will be completely dried. At higher temperatures the lustrous carbon former pyrolyse, and the bentonite, too, changes due to loss of chemically combined water. These processes, which may have effects to the heat transfer within the mould, do not take place within the mould in this way, at least not at a greater distance to the casting or within the time between pouring and formation of a rigid outer shell.

Furthermore, it is hardly possible to effect measurements under operation conditions according to the hot-wire method. Due to the fact that the thermo-physical data also depend on the packing density of the mould material and therefore depend on its compaction, the mould – as a consequence - has to be produced by a moulding machine under operation conditions. Afterwards, the hot wire would have to be built into the mould, and the complete mould box would have to be put into the furnace for analyse of the temperature dependence.

An alternative to analyse thermo-physical data – especially under operation conditions – is the casting method. This method is useful for analysis of thermal diffusivity.

$$a = \frac{\chi}{\rho c_p} \tag{3}$$

This value describes the speed, by which a temperature modification spreads within mould material.

The analysis of the thermal diffusivity is made by the casting method by measuring the spreading of a temperature front within mould material. Although in general an analytic solution of the heat conductivity equation is not possible a solution can be found for simple special cases, especially for one- or two-dimensional problems. These cases can be approached to a test by using a geometrical simple body – for example a cube, a plate or a cylinder. Such a mould is poured and during solidification and cooling process the temperature is measured at different distances to the casting wall within mould material. Design and size of the test body are chosen in such a way to achieve a temperature distribution within mould material, which will be easily to describe. This will only take place if the distance between measuring position and casting wall will be small compared with the expansion of the casting wall releasing heat. If a one-dimensional temperature distribution is achieved (i.e. the temperature only depends on the distance from measuring position to

the casting wall) it is possible – by laying down the heat balance – to calculate thermal diffusivity according to

$$a = \frac{(T_{2b} - T_{2a}) \cdot \left(\left(\frac{r_2 + r_3}{2} \right)^2 - \left(\frac{r_1 + r_2}{2} \right)^2 \right)}{2 \cdot \Delta t \cdot \left(\frac{T_1 - T_2}{\ln\left(\frac{r_2}{r_1} \right)} - \frac{T_2 - T_3}{\ln\left(\frac{r_3}{r_2} \right)} \right)} \qquad (4)$$

At which r_1, r_2, r_3 are radii of the three measuring positions, Δt is the relevant period of time, T_1, T_2, T_3 are the average temperatures of the three measuring points within this section, and T_{2a} and T_{2b} are the temperatures of the middle measuring point at the beginning and at the end of this period of time.

There are possible measuring points within mould material in front of the middle of a plate or a cube surface; easier measuring conditions are given at a cylindrical test body. By using a rotation symmetry several measuring points may be arranged around the test body (Fig. 11), and by taking the average of measured curves it is possible to reduce the effects of insecurities of measuring positions and other faults of measuring. The figured test arrangement represents the optimum.

Due to mould technical reasons the test body cannot be a perfect cylinder, as a certain inclination of mould is necessary to remove the pattern from the produced mould. For measuring the temperature distribution within mould material there are used thermo couples without protection covering, which are set into boreholes of less than 2 mm diameter within mould material. Due to the small mass of these thermo couples they can quickly follow up modifications of mould material temperature.

The thermo couples are set into blind holes, which are cut into the mould material from the mould joint by using a strickle. As the thermo couples are led from the measuring point (tip of the thermo element) up to the mould joint at a parallel way to the casting

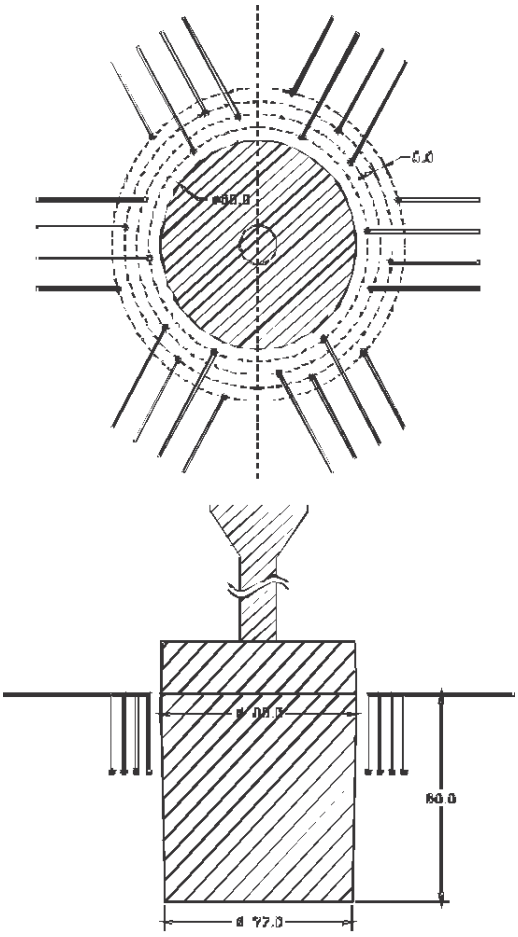

Figure 11. Arrangement of measuring positions at a rotationally symmetrical experimental set-up.

wall and by that alongside the isothermal line, a falsification of the measuring values by the heat conduction of the thermoelectric wire can be avoided. The lead-in wire of the thermo couples are led to the outside alongside the mould joint and are connected with a multichannel data logger (Fig. 12). Due to the grain structure of the mould material as well as due to its rather low strength the positioning of the thermo couples cannot be done as accurate as desired. This is the reason for using 6 trial equipments (each 4 thermo couples) equally placed around the test pattern (it was measured at a distance of 5, 10, 15 and 20 mm from mould wall).

The average of these 6 temperature curves achieved by this method was taken, whereby the highest as well as the lowest measuring value have been ignored. Within mould material result the following temperature curves (Fig. 13).

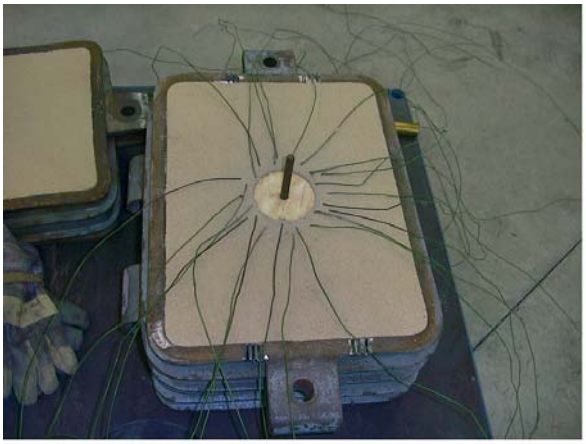

Figure 12. Design of experiments.

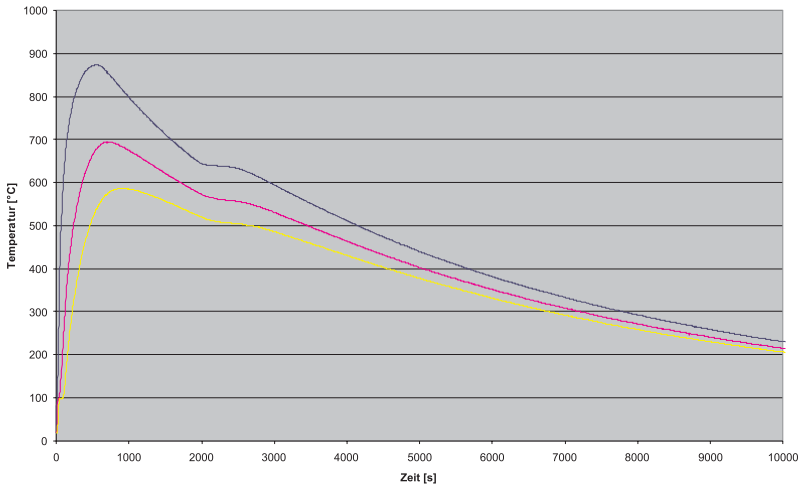

Figure 13. Average temperature curves within mould material.

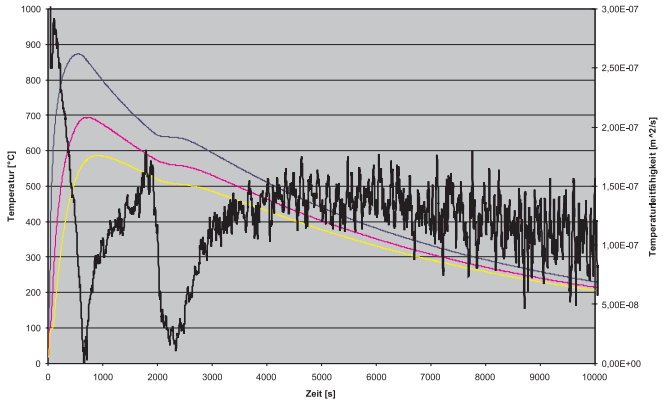

Figure 14. Calculated temperature diffusivity during test phase.

From this temperature curves the thermal diffusivity during test phase can be continuously calculated. Only the area of cooling phase has been evaluated, because after pouring the liquid metal into the mould there are further processes, which influence the measurement and the evaluation. So an arrest point of 100 °C can clearly be recognized at the beginning of all temperature curves, after that the temperature rises again and shows a course, which corresponds to a heat transfer by means of thermal conductivity. The arrest point is caused by the displacement of water, which was used for bonding purposes. This is the reason for not using this area within the calculation of thermal diffusivity. A second area at which the measurement cannot be evaluated is within figure 14 approx. 2000 up to 2400 seconds. During this time period a latent heat that compensates the cooling for a certain period of time is set free within the casting. During the further course of the measurement temperature differences become smaller and smaller, so that the relative measuring error continuously rises, until at least, at low temperatures, no more evaluation will be possible.

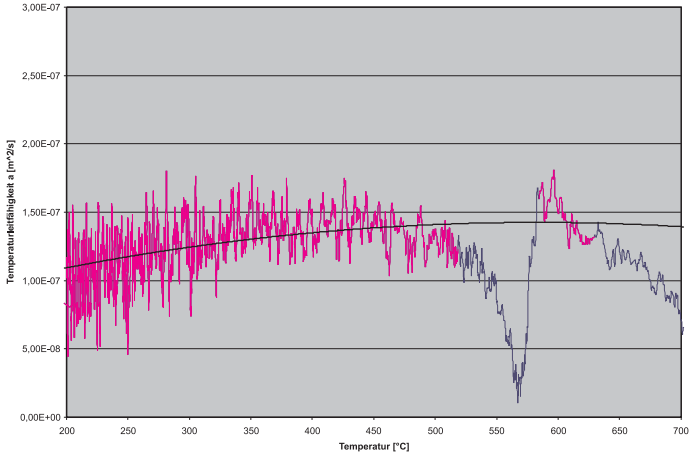

Figure 15. Calculated temperature dependence of temperature diffusivity

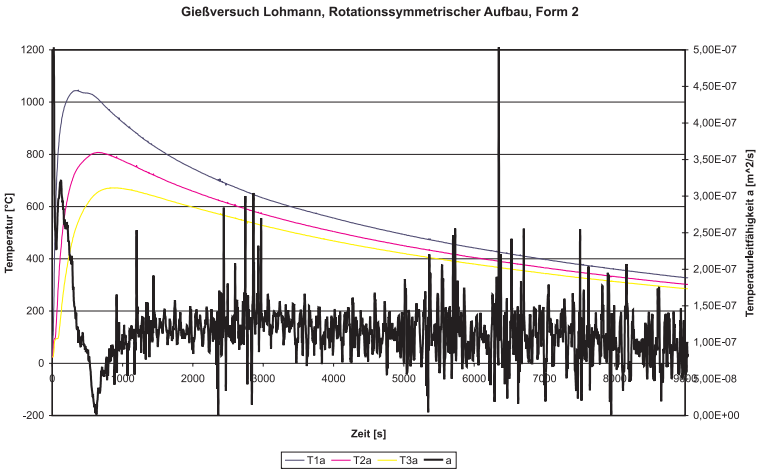

Figure 16. Temperature curves of steel

If the calculated temperature diffusivity is figured above the average temperature taken within mould material (in the area of measurement points) it results to Figure 14.

The gap, within calculated temperature diffusivity curve, corresponds to the above explained arrest point due to set-free latent heat. But it is easily possible to define a compensation curve that bridges this area (Fig. 15).

By using a single test it is possible to define the thermal diffusivity of mould material for a large temperature range (here: 200 up to 700 °C). Nevertheless the evaluation of the used mould material – consisting of silica sand with 8 % bentonite and adjusted to a compactability of 45 % - shows a rather small temperature dependence of thermal diffusivity. Similar results have been achieved on further tests, among other things with production mould materials of participating foundries.

As expected, the steel tests do not show the described arrest point of temperature curves. The reason is the different solidification behaviour of steel.

At each participating foundry two measurements had been done (Fig. 16).

It is conspicuous that at each second measurement were always analysed higher thermal diffusivity in the three foundries for all test runs. This may eventually refer to the fact, that the moulds were produced directly one after the other, i.e. with an interval of several minutes, according to machine cycle time. But the positioning of the thermo couples and the connection to the data logging device took approx. 30 minutes per mould, so that – although the second mould had been immediately covered – a drying resp. modification of mould material by souring effect could not be excluded in the course of time.

Influence of different cooling conditions to solidification

The different thermal diffusivities of the mould material, i.e. its different cooling effect and by that a different cooling rate

within casted metal – even at same conditions – may cause different structures and by that different shrinkage sensitivities. The effects, which may have even small differences within cooling rate, are shown in Figure 17. In this diagram the relationship is shown between the volume contraction and the degree of saturation. It should be noted that a volume expansion can only take place in a small range of the degree of saturation, defined by Si-contents, and this only for the stable eutectic solidification, i.e. for low cooling rate. At higher cooling rates the curves rise up, so that no more volume expansion can take place within short time, even not at an optimum degree of saturation of 1. Therefore a limitation of cooling rate is necessary to secure a self-feeding.

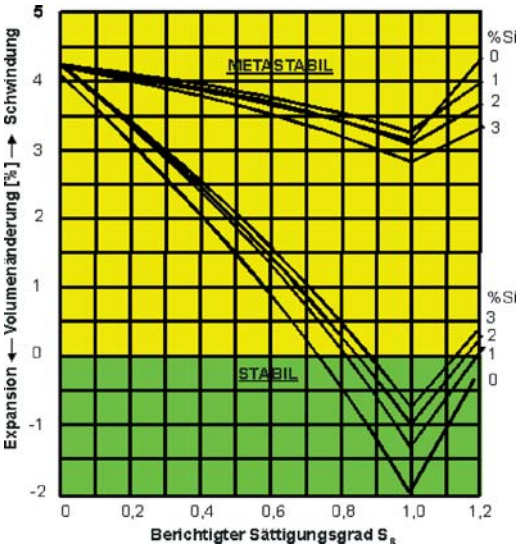

Figure 17. Theoretic volume modification of cast iron

It is apparent that the concept of the degree of saturation is not only sufficient for description of volume modification and by that for the formation of shrinkage, i.e. the figure of carbon with regard to the graphite precipitation cannot be replaced for example by silicon, as it has been done at corresponding calculations of CE and Sc values.

But it also shows that at same chemical composition in a first step there cannot be differences between a pearlitic and a ferritic cast iron with regard to structure, volume modification and thereby shrinkage behaviour. Ferritic and pearlitic amount will not be fixed before eutectoid transformation in solid condition.

Between the group of curves of stable and metastable solidification there is the area in which the structure will be defined by the cooling rates thereby the shrinkage behaviour, and that will be the result of thermal diffusivity of mould material and the set-free heat quantity of the test piece.

But this process is – at same carbon activity within the melts - highly defined by diffusion, diffusion length and the growth rate, because in opposite to the ledeburite formation the graphite precipitation is a kinetic problem. The lower group of curves shows the optimum of an inoculated stable solidification with the effect of self-feeding.

A continuous transition is possible between both groups of curves, which may be expressed at the castings in form of hard spots or carbides within structure. Each part of carbide or ledeburite within the structure increases the feeding demand in opposite to the optimum. Due to the following transformation and precipitation processes in solid it might be these processes during cooling will not be recognized within metallographic evaluations at room temperature.

The adjustment of different cooling rates by variation of thermal diffusivity of mould material - for example by different compactibilities or mould material compositions - is only hardly to realize in practice. A pattern plate with test castings had been made to control the dependences. By one pouring there could be casted plates with a thickness of 10, 20, 30 and 40 mm, a cube with module 1.6 as well as a transverse link for cars (Fig. 18).

Figure 18. Cluster with test castings

Figure 19. Stepped wedge

The different plate thicknesses led to different moduli and by that to different reproducible cooling rates. The transverse links for cars were sawed, and the shrinkage was compared with known fault protocols of the foundry, but the results will not be shown at this place. Parallel to this stepped wedges were casted and compared (Fig. 19).

During the tests there were casted:
- ferritic and pearlitic adjusted cast iron,
- with each 2 different inoculants.

By these it was varied:
- carbon activity,
- diffusion coefficient,
- diffusion length,
- austenite resp. graphite growth.

Whereby further parameter were hold on a constant level for example degree of saturation, mould material composition etc..

Three test pieces were taken from each cube or plate, each one of the top (near mould joint), from the bottom and from the middle.

These test pieces were polished and they were evaluated by using a image analysis program with regard to the parameter:
- number of spheroids (recognized spheroids per mm^2) and
- graphite quantity (percentage at surface).

As an example, Figures 20 and 21 show the influence of different wall thicknesses (and by that different cooling rates) to the formation of spheroids.

There are remarkable differences within the single structures. By increasing wall thickness and by that by decreasing cooling

speed the number of spheroids decreases, but their diameter increases. Especially inoculant B seems to have its optimum effect at a wall thickness of 30 mm.

CASTING IN PLATE DESIGN

At left side the Figure 22 shows pearlitic cast iron and in comparison ferritic cast iron at right side. The upper diagram shows the

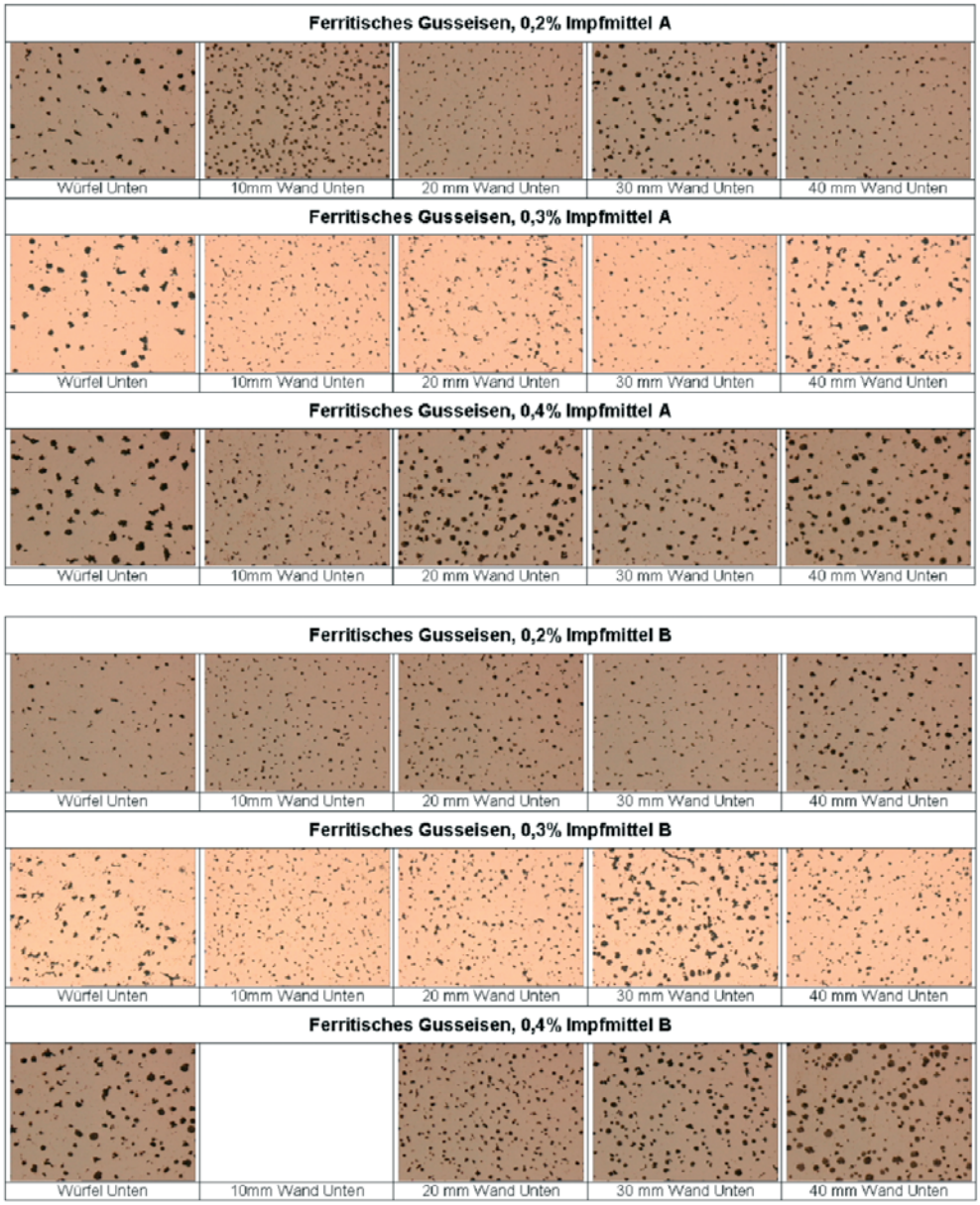

Figure 20. Ferritic ductile, inoculated with inoculants A and B

number of spheroids, the lower diagram shows the surface component of spheroids in percentage. Within each diagram inoculants A and B are shown in comparison.

At pearlitic cast iron it is clearly to see, that at same type and concentration of inoculant a higher cooling speed (at lower wall thickness) leads to an increase of the number of spheroids. The evaluation of surface component does not show a uniform tendency.

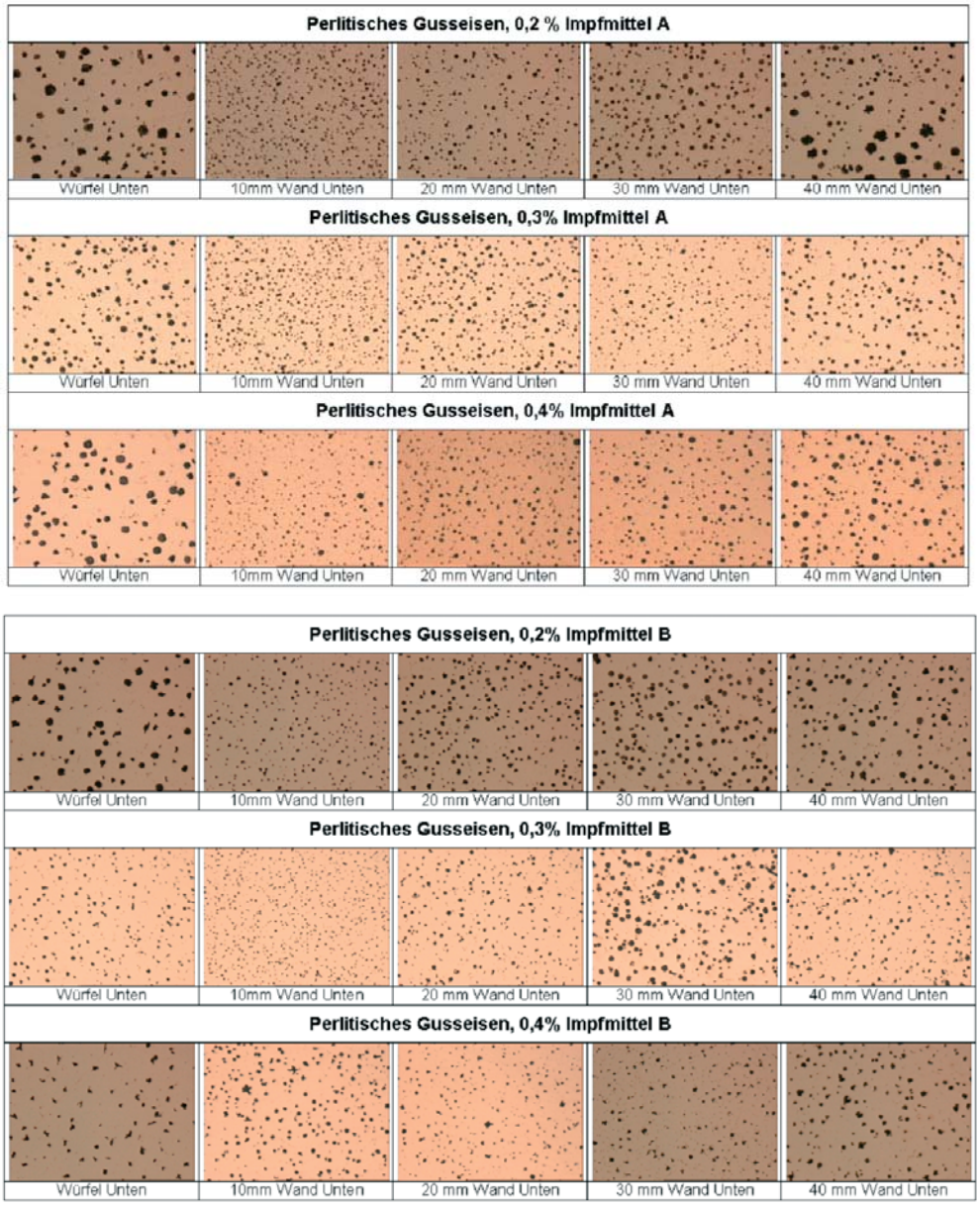

Figure 21. Pearlitic ductile iron, inoculated with inoculants A and B

At ferritic cast iron the dependence of the number of spheroids from cooling rate is remarkably lower. Here, too, the surface component does not show a uniform relationship between wall thickness or concentration of inoculant.

At both types of iron an inoculant concentration of 0.3 % results to an optimum number of spheroids. At higher inoculant concentration the number of spheroids decreases again.

STEPPED WEDGE

Giving same inoculant at same concentrations the quicker type of cooling shows a remarkable higher number of spheroids (Fig. 23). Beginning at a wall thickness of 30 mm this tendencies efface a little and are not longer clearly. No basic difference is to recognize between inoculant A and B. Inoculant B tends a little to a lower number of spheroids.

On increasing addition of inoculant the number of spheroids decreases at pearlitic cast iron. At ferritic cast iron inoculant A shows the same tendencies like pearlitic cast iron, but at a remarkable lower number of spheroids. At ferritic cast iron and at different inoculant additions inoculant B shows contrary behaviour to the use with pearlitic cast iron. The number of spheroids increases with increasing inoculant quantity.

On increasing inoculant addition the surface component of spheroids decreases at both inoculants. For inoculant A there is no difference to recognize for all wall thicknesses with an inoculant addition of 0.4 %, and for inoculant B the surface component decreases even more. For both inoculant quantities the influence of wall thickness is shown. The lowest wall thickness has the highest surface component,

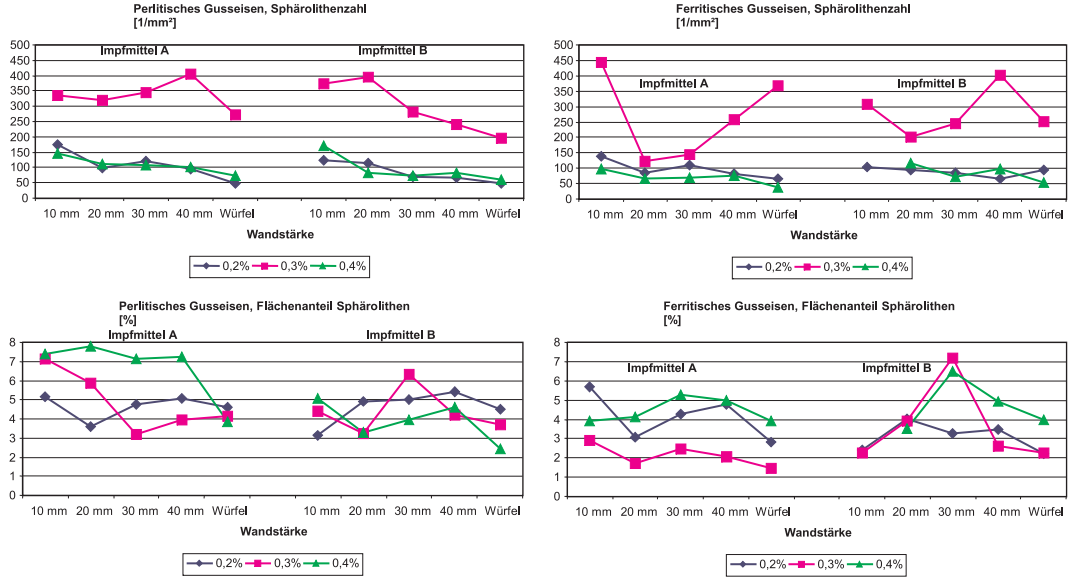

Figure 22. Graphite formation at test castings in plate design.

which equally lowers down above 30 mm up to 50 mm.

On ferritic cast iron the relation within wall thicknesses are not as unequivocally as at pearlitic cast iron, and the wall thickness of 30 mm seems to have a special position.
The effect of inoculant A and B clearly differs on pearlitic and ferritic cast iron.
It has been shown that the thermal diffusivity as a value for cooling of a casting is very different within the different foundries, and by that it has to be clearly defined at each foundry as a decisive value for the solidification simulation. Variations of more than 30 % between the values of the different foundries are the rule.

At the tests for definition of the influence of different variable material values to the graphite precipitation in form of:
- number of spheroids,
- graphite quantity.

It has been shown that these values cannot alone give sufficient information about the quantity of eutectic graphite and by that about volume deficits or a shrinkage volume to be expected at solidification.

To be able to predict shrinkage volume by means of:
- physical values which define the solidification process,
- variable mould material values which define the solidification process,
- variable material values which define the solidification process.

It is necessary to get – on the side of material – one or more new quantitative parameter, which have to result from thermodynamic criterions of solidification.

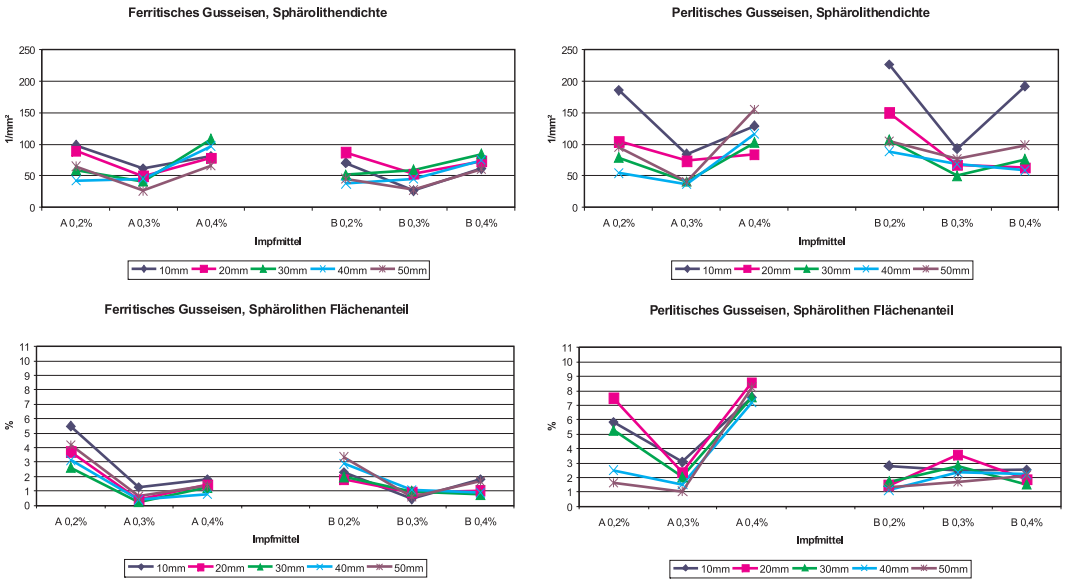

Figure 23. Graphite formation on casting of stepped wedges.

PART 4: INFLUENCE OF MOULD AND MOULD MATERIAL

Besides the metal wall movement (Part 2) the mould wall movement (the attributes of the mould) is the second main influence factor that has an effect on "apparent shrinkage". The dependence of the mould wall movement results of:

- type of mould material,
- composition of mould material,
- compaction,
- mould box attributes.

Influence of mould box attributes

Four test cubes were positioned on a square pattern plate, each two of them with a modulus of 1.7 and 1.6 (Fig. 24). Each cube was equipped with the corresponding exothermic feeder.

By using this pattern equipment there were formed and cast three moulds, under simulation of different mould box attributes.

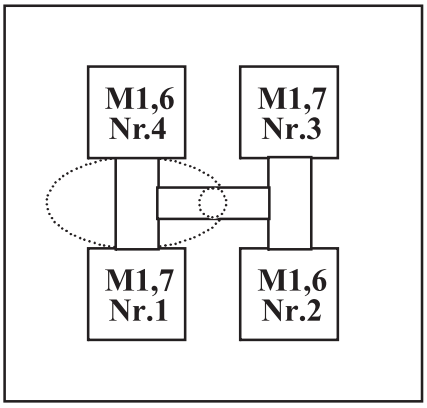

Figure 24. Construction of pattern plate

All the moulds were made of a clay bonded mould material (sand F32, 8 % bentonite A and ~ 2 % water) and compacted with a pneumatic

a) Without mould box

b) Filled in with resin bonded mould material

c) With mould box and charged

Figure 25. Simulation of mould box attributes

hand rammer. There was used spheroidal graphite cast iron $S_R = 1$ as casting material:

- The first mould was poured **without mould box** (Fig. 25a). There was used a conical wooden frame during ramming. The frame was removed after compaction of the mould.
- The second mould was compacted by means of wooden frame, too. After removing this wooden frame there was set a metal frame around the mould. To increase the stability of the mould **resin bonded mould material was filled in between mould and metal frame** (Fig. 25b).
- To achieve an even higher mould stability it was chosen a rigid mould box for the third mould and the mould was charged (Fig. 25c).

There were taken photos from the castings with sprue, runner and feeder as well as from the actual cubes. The mass of feeders and castings (cubes) were graphically evaluated, just as the surface of the cubes, sawed through the midst.

The evaluation of the surfaces should document the size of the enlargement of the three different moulds. For the purpose of comparison the contours of the sawed cubes were copied on a sheet of paper, scanned into the computer and calculated. The surfaces shown above were defined by means of the average values of the two indentic cubes of a mould.

Figure 26 shows the changes of the sawed cube surfaces for the three cast moulds in dependence of the "mould box stability". The surfaces decrease on increasing stability of the mould, and there is to remark no difference within their behaviour between both moduli.

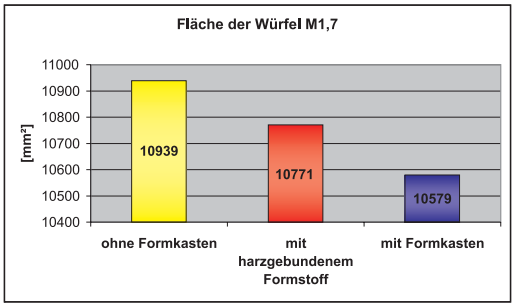

Surface of cubes M1,7

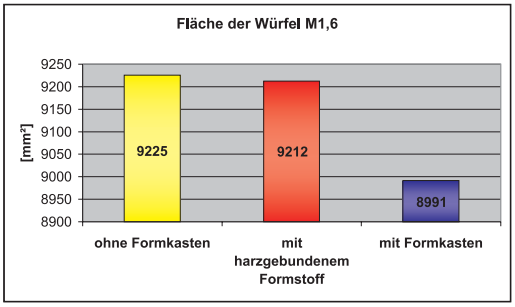

Surface of cubes M1,6

Figure 26. Surface of the cubes (M1,6 and M1,7)

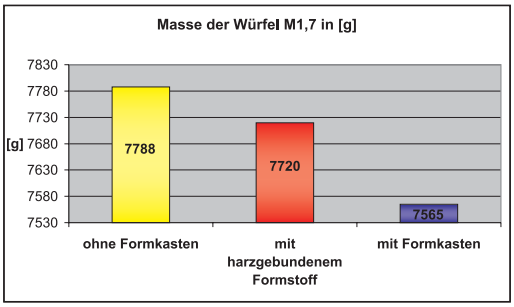

Mass of cubes M1,7 (g)

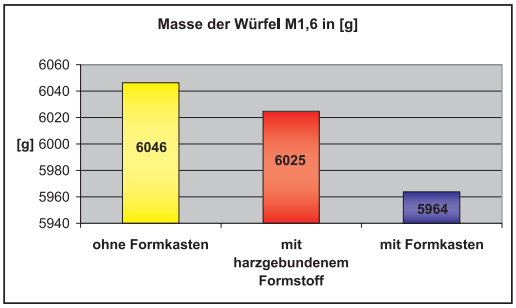

Mass of cubes M1,6 (g)

Figure 27. Mass of the cubes (M1,6 and M1,7)

By evaluating the mass of cubes and feeders there should also be defined the size of the enlargement of the three moulds. For the purpose of comparison the feeders were sawed off, and feeders and cubes were separately weighed.

Figure 27 shows the mass of the cubes (M1.6 and 1.7) and Figure 28 shows the total masses (M1.6 and 1.7) of the three cast moulds. Just like the evaluation of the surfaces the masses shown in the figures were defined by means of the average values of the two identic cubes of a mould. On the X-axle there are shown the three moulds with the different box attributes, on the Y-axle there are shown the masses (g).

The mass of the cubes decreases on increasing stability of the mould, and there is to remark no difference within their behaviour between both moduli.

The evaluation of the mass of cubes clearly shows, that the mass of the cube or the enlargement of mould is the smallest one by using a rigid mould box. The difference of enlargement is much less between the moulds without any mould box and the one with resin bonded mould material filled in between mould and metal frame.

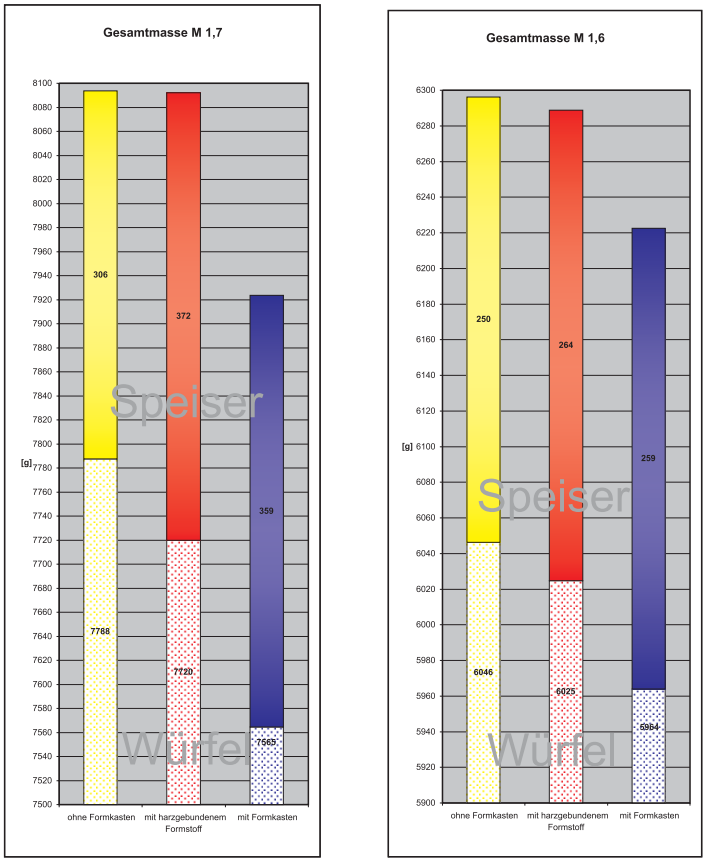

Figure 28. Mass of the cubes and feeders

First of all, you would assume that the cast quantity of iron or the total mass is identical for all the three moulds. But the representation of total mass (Fig. 28) shows that the mould enlarges already while pouring the cast iron into the mould. In this connection it becomes clear, that the enlargement is the smallest one by using a rigid mould box.

This test makes clear that the mould box attributes have influence on the mould wall movement. By comparing the differences between the masses extending of mould wall movement it is obviously mould wall movement can unequivocally define the feeding behaviour or the quality of a casting. The mould box attributes tested in this experiment are relative easy to stabilize in practice or should always be constant on a plant.

The influence of type of bentonite / type of mould material

The pattern equipment or the arrangement of the cubes and the pouring system of the preceding tests have been taken over, and the cubes and the pouring system have been fixed

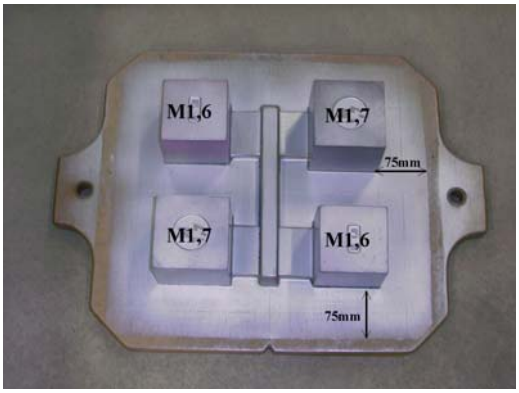

Figure 29. Pattern equipment

on a pattern plate, which could be installed in a moulding machine. As the distance of the cubes to the box border is important for the valuation of the influence of the mould wall movement, this distance has been the same at each cube (75 mm) (Fig. 29).

Three different types of bentonite were used. The relevant mould material attributes were measured and stated for each mixture, but they are not shown in this short version. There were produced four moulds with different contents of bentonite (5, 7, 9, 11 %) from each type of bentonite. There was added coal dust to each mould material

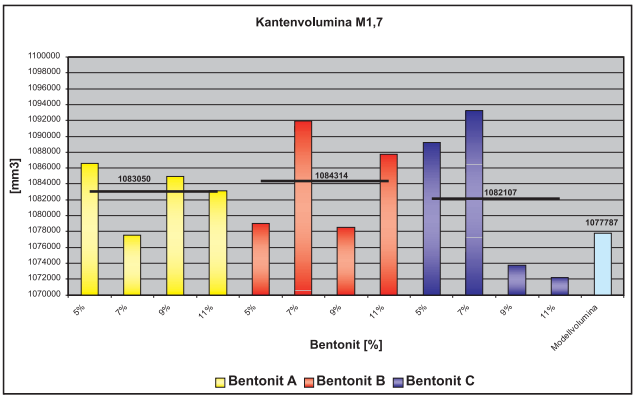

Figure 30. Edge volumes

mixture, the quantity was half of bentonites's content.

Just like the preceding tests silica sand F32 was prepared with the different bentonite types in a turbo-mixer. The cast iron ($S_R = 1$) was melted in a medium frequency coreless crucible induction furnace.

In opposite to the preceding tests the cubes were not sawed and their surfaces were not evaluated, but the cube-edges were measured and the volume was calculated.

The evaluation of the edge-volume (Fig. 30) shows that for the three types of bentonite the average values of volume of the cast cubes was bigger than those of the original pattern volume, whereby there was no large difference between the three average values of edge-volume.

It can be assumed that the enlargement of a mould is not only defined by bulge of surfaces, but also by the enlargement of the "edge-frame" of the mould.

Influence of the type of bentonite

The influence of the type of bentonite to the enlargement of the mould cavity is clearly to recognize in the evaluation of the mass of cubes (Fig. 31). The enlargement of mould cavity is the biggest one at type A and the smallest one at type C, whereby the difference of enlargemet of mould cavity is not as large between bentonite type B and C as to bentonite type A.

The unequal behaviour of the three types of bentonite (Fig. 31) is hardly to interpret by means of the methylene blue value, as a comparison of these values is only possible for clay-types of the same origin. To give reasons for this behaviour an exact analysis of the attributes of the three bentonite-types would be necessary.

Influence of bentonite content

The influence of the bentonite content to the enlargement of mould cavity is not easy to interpret for the three tests (Fig. 31-33).

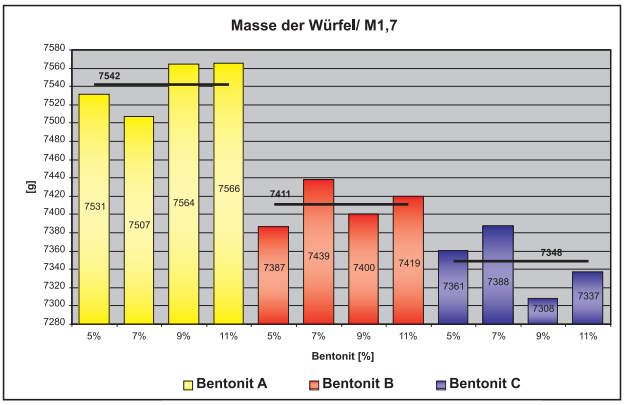

Figure 31. Masses of cubes with M 1.7

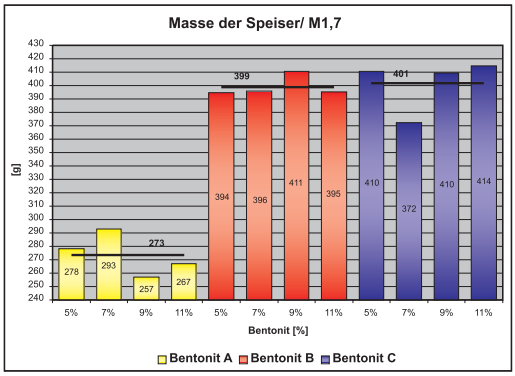

Figure 32. Masses of feders

An important influence of the bentonite content to the enlargement of the mould cavity is not recognizable at the three cast tests.

But it has to be considered that the mechanical properties increase, too, with increasing bentonite content. But on all cast tests this overservation could not be connected with the enlargement of mould cavity.

To achieve the respective mould condition of each mixture at different bentonite contents each of the mould material mixtures need a different quantity of water. This observation is easy to recognize, too, within the mould material analysis, and it directs to the fact that – besides the influence of the type of bentonite – the compactability (water content) seems to be the determining parameter for the size of the mould wall movement.

"Apparent shrinkage"

The graphic evaluation of the total masses (Fig. 33) and the mass of the feeders (Fig. 32) shows that already while pouring, the moulds enlarge in different ways due to the ferrostatic pressure and the casting heat. Dependent bentonite-type the mass of the mould of bentonite-type C is a little smaller than those of bentonite-types A and B.

The enlargement of mould cavity and – as a consequence – an increase of cube mass is mainly marked at bentonite-type A. Here it flows the most material from feeder for compensation of mould space enlargement, whereby at type of bentonite B at approx. same total mass (Fig. 33) the mass of the cubes are clearly less, but therefore the mass

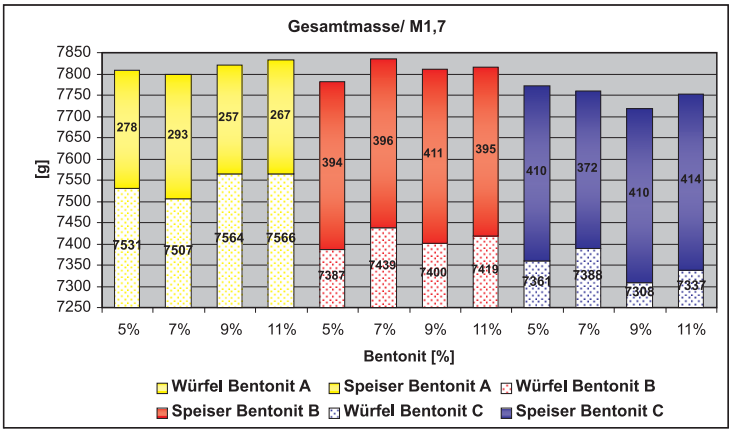

Figure 33. Total mass and partition to feeder and cube.

of the feeders are clearly larger than it is at bentonite type A. The mould space enlargement was smaller at this type of bentonite B with the consequence that less material from feeder was necessary for compensation of mould space enlargement. At same type of feeder bentonite B has a greater security against "apparent shrinkage".

The enlargement of mould cavity at each type of bentonite does not show any tendency on change of bentonite contents.

As the influence of bentonite contents to the mould wall movement is not so important, it was taken an average value of eight cubes (M1.7) of each type of bentonites, which were produced with different contents of bentonite. At same time it was taken an average value of the corresponding eight compactabilities measured of the mould sand mixtures. Figure 34 shows the average value of the mass of the cubes (M1.7) for each type of bentonite above the average value of the compactabilities.

The influence of the type of bentonite to the enlargement of mould cavity is clearly to see by means on Figure 34. By comparing the mass of cubes of the bentonite-types B and C the difference of masses is more than 60 g. Between type A and C there is even a difference of nearly 200 g. This is approx. 3 % of the cube-volume, this value could absolutely define the quality of a casting.

As a consequence of this test it becomes clear, that the type of bentonite and the compactability (water content) are two important parameters that define the enlargement of mould cavity and thereby define the "apparent shrinkage".

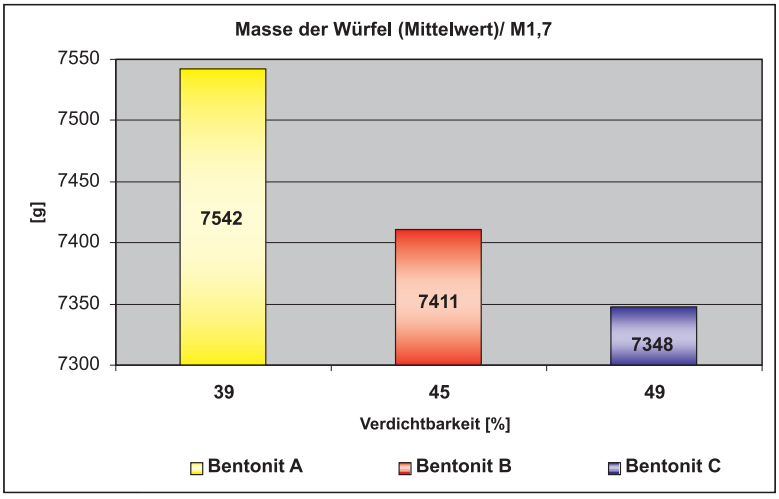

Figure 34. Average values of mass of cubes as function of average values of compactabilities of moulds

Summary

At first several physical values defining the solidification process are collected. These physical values are characterised as variable moulding material values after that.

Material values defining the solidification process are afterwards described and than their influence on feeding behaviour by chemical composition explained. The real feeding demand of a casting is described by influence of the mould and than the idea of the "apparent shrinkage" is explained. With thermal analysis results an assessment tool for quality and solidification structure of cast iron. Feeding behaviour of a melt can be specified by this method.

Feeding is a transport phenomenon and there are several different feeding mechanisms during solidification time. It is shown that feeders are only active till 20 – 30 % of the solidification time.

This report will be continued.

References

Koppe, W.; Engler, S. (1962): *Giesserei* 49, Nr. 10/11, S. pp. 265-306.

Engler, S.; Dette, M. (1974): *Giesserei* 61, Nr. 26, S. pp. 769-774.

Engler, S.; Wojtas, H. J.(1979): *Giessereiforschung* 31, Nr. 1, S. pp. 37-44.

Feichtinger, H. K.(1980): VSE-Tagung 22.01.1980 „Methoden der Qualitätsprüfung von Grauguss-Schmelzen" (Institut für Metallurgie der ETH Zürich).

Autor's Index, Vol. 52, No. 4

Autor's Index, Vol. 52

(NEW) INSTRUCTIONS TO AUTHORS (from Sep. 2003)

RMZ-MATERIALS & GEOENVIRONMENT (RMZ- Materiali in geookolje) is a periodical publication with four issues per year (established 1952 and renamed to RMZ-M&G in 1998). The main topics of contents are Mining and Geotechnology, Metallurgy and Materials, Geology and Geoenvironment.
RMZ-M&G publishes original Scientific articles, Review papers, Technical and Expert contributions (also as short papers or letters) **in English**. In addition, evaluations of other publications (books, monographs, …), short letters and comments are welcome. A short summary of the contents in Slovene will be included at the end of each paper. It can be included by the author(s) or will be provided by the referee or the Editorial Office.
Additional information and remarks for Slovenian authors:
English version with extended "Povzetek", and additional roles (in Template for Slovenian authors) ***can*** *be written. Only exceptionally the articles in the Slovenian language with summary in English will be published. The contributions in English will be considered with priority over those in the Slovenian language in the review process.*

Authorship and originality of the contributions. Authors are responsible for originality of presented data, ideas and conclusions as well as for correct citation of data adopted from other sources. The publication in RMZ-M&G obligate authors that the article will not be published anywhere else in the same form.

Specification of Contributions

Optimal number of pages of full papers is 7 to 15, longer articles should be discussed with Editor, but 20 pages is limit.
Scientific papers represent unpublished results of original research.
Review papers summarize previously published scientific, research and/or expertise articles on the new scientific level and can contain also other cited sources, which are not mainly result of author(s).
Technical and Expert papers are the result of technological research achievements, application research results and information about achievements in practice and industry.
Short papers (Letters) are the contributions that contain mostly very new short reports of advanced investigation. They should be approximately 2 pages long but should not exceed 4 pages.
Evaluations or critics contain author's opinion on new published books, monographs, textbooks, exhibitions …(up to 2 pages, figure of cover page is expected).
In memoriam (up to 2 pages, a photo is expected).
Professional remarks (Comments) cannot exceed 1 page, and only professional disagreements can be discussed. Normally the source author(s) reply the remarks in the same issue.

Supervision and review of manuscripts. All manuscripts will be supervised. The referees evaluate manuscripts and can ask authors to change particular segments, and propose to the Editor the acceptability of submitted articles. Authors can suggest the referee but Editor has a right to choose another. **The name of the referee remains anonymous**. The technical corrections will be done too and authors can be asked to correct missing items. The final decision whether the manuscript will be published is made by the Editor in Chief.

The Form of the Manuscript

The manuscript should be submitted as a complete hard copy including figures and tables. The figures should also be enclosed separately, both charts and photos in the original version. In addition, all material should also be provided in electronic form on a diskette or a CD. The necessary information can conveniently also be delivered by E-mail.

Composition of manuscript is defined in the attached Template

The original file of Template is temporarily available on E-mail addresses:
joze.pezdic@ntfgeo.uni-lj.si, joze.pezdic@guest.arnes.si
barbara.bohar@ntfgeo.uni-lj.si

References – can be arranged in two ways:
- first possibility: alphabetic arrangement of first authors – in text: (Borgne, 1955),
or
- second possibility: [1] numerated in the same order as cited in the text: example[1]

Format of papers in journals:

Le Borgne, E. (1955): Susceptibilite magnetic anomale du sol superficiel. *Annales de Geophysique*, 11, pp. 399-419.

Format of books:

Roberts, J. L. (1989): Geological structures, *MacMillan, London*, 250 p.

Text on the hard print copy can be prepared with any text-processor. The electronic version on the diskette, CD or E-mail transfer should be in MS Word or ASCII format.
Captions of figures and tables should be enclosed separately. **Figures (graphs and photos)** and tables should be original and sent separately in addition to text. They can be prepared on paper or computer designed (MSExcel, Corel, Acad)
Format. Electronic figures are recommended to be in CDR, AI, EPS, TIF or JPG formats. Resolution of bitmap graphics (TIF, JPG) should be at least 300 dpi. Text in vector graphics (CDR, AI, EPS) must be in MSWord Times typography or converted in curves.
Color prints. Authors will be charged for color prints of figures and photos.
Labeling of the additionally provided material for the manuscript should be very clear and must contain at least the lead author's name, address, the beginning of the title and the date of delivery of the manuscript. In case of an E-mail transfer the exact message with above asked data must accompany the attachment with the file containing the manuscript.
Information about RMZ-M&G:
Editor in Chief prof. dr. Jože Pezdič (tel. ++386 1 4704-633) or
Secretary Barbara Bohar Bobnar, un. dipl. ing. geol. (++386 1 4704-630),
Aškerčeva 12, Ljubljana, Slovenia

or at E-mail addresses:
joze.pezdic@ntfgeo.uni-lj.si, joze.pezdic@guest.arnes.si
barbara.bohar@ntfgeo.uni-lj.si

Sending of manuscripts. Manuscripts can be sent by mail to the **Editorial Office** address:
- RMZ-Materials & Geoenvironment
  Aškerčeva 12,
  1001 Ljubljana, Slovenia

or delivered to:
- **Reception** of the Faculty of Natural Sciences and Engineering (for RMZ-M&G)
  Aškerčeva 12, Ljubljana
- E-mail – addresses of Editor and Secretary
- You can also contact them on their phone numbers.

These instructions are valid from September 2003

TEMPLATE

The title of the manuscript should be written in bold letters (Times New Roman, 14, Center

Name Surname[1], …. , & Name Surname[X] (Times New Roman, 12, Center)

[x]Faculty of ... , University of ... , Address…, Country, e-mail: ... (Times New Roman, 12, Center)

THE LENGTH OF FULL PAPER SHOULD NOT EXCEED TWENTY (20, INCLUDING FIGURES AND TABLES) PAGES (OPTIMAL 7 TO 15), SHORT PAPER FOUR (4) AND OTHER TWO (2) WITHOUT TEXT FLOWING BY GRAPHICS AND TABLES.

Abstract(Times New Roman, Bold/Normal, 11): The text of the abstract is placed here. The abstract should be concise and should present the aim of the work, essential results and conclusion. It should be typed in font size 11, single-spaced. Except for the first line, the text should be indented from the left margin by 10 mm. The length should not exceed fifteen (15) lines (10 are recommended).

Key words: a list of up to 5 key words (3 to 5) that will be useful for indexing or searching. Use the same styling as for abstract.

Introduction (Times New Roman, Bold, 12)

Two lines below the keywords begin the introduction. Use Times New Roman, font size 12, Justify alignment.

There are two (2) admissible methods of citing references:

1. by stating the first author and the year of publication of the reference in the parenthesis at the appropriate place in the text and arranging the reference list in the alphabetic order of first authors; e.g.:
   "Detailed information about geohistorical development of this zone can be found in: Antonijević (1957), Grubić (1962), ..."
   "… the method was described previously (Hoefs, 1996)"
2. by consecutive Arabic numerals in square brackets, superscripted at the appropriate place in the text and arranging the reference list at the end of the text in the like manner; e.g.:
   "... while the portal was made in Zope[3] environment."

Results and discussion (Times New Roman, Bold, 12)

Tables, figures, pictures, and schemes should be incorporated (inserted, not pasted) in the text at the appropriate place and should fit on one page. Break larger schemes and tables into smaller parts to prevent extending over more than one page.

Conclusions (Times New Roman, Bold, 12)

This paragraph summarizes the results and draws conclusions.

Acknowledgements (Times New Roman, Bold, 12, Center - optional)

This work was supported by the ****.

References (Times New Roman, Bold, 12)

Regardless of the method used, in the reference list, the styling, punctuation and capitalization should conform to the following:

FIRST OPTION – in alphabetical order

Casati, P., Jadoul, F., Nicora, A., Marinelli, M., Fantini-Sestini, N. & Fois, E. (1981): Geologia della Valle del'Anisici e dei gruppi M. Popera – Tre Cime di Lavaredo (Dolomiti Orientali). *Riv. Ital. Paleont.*; Vol. 87, No. 3, pp. 391-400, Milano.

Folk, R. L. (1959): Practical petrographic classification of limestones. *Amer. Ass. Petrol. Geol. Bull.;* Vol. 43, No. 1, pp. 1-38, Tulsa.

SECOND OPTION – in numerical order

[1] Trček, B. (2001): *Solute transport monitoring in the unsaturated zone of the karst aquifer by natural tracers.* Ph.D. Thesis. Ljubljana: University of Ljubljana 2001; 125 p.

[2] Higashitani, K., Iseri, H., Okuhara, K., Hatade, S. (1995): Magnetic Effects on Zeta Potential and Diffusivity of Nonmagnetic Particles. *Journal of Colloid and Interface Science 172*, pp. 383-388.

Citing the Internet site:

CASREACT-Chemical reactions database [online]. Chemical Abstracts Service, 2000, updated 2.2.2000 [cited 3.2.2000]. Accessible on Internet:<http://www.cas.org/CASFILES/casreact.html>.

Povzetek (Times New Roman, 12)

A short summary of the contents in Slovene (up to 400 characters) can be written by the author(s) or will be provided by the referee or by the Editorial Board.

TEMPLATE for Slovenian Authors

The title of the manuscript should be written in bold letters (Times New Roman, 14, Center)

Naslov članka (Times New Roman, 14, Center)

Name Surname[1], …. , & Name Surname[X] (Times New Roman, 12, Center)
Ime Priimek[1], …, Ime Priimek[X] (Times New Roman, 12, Center)

[x]Faculty of ... , University of ... , Address…, Country; e-mail: ... (Times New Roman, 12, Center)
[X]Fakulteta…, Univerza…, Naslov…, Država; e-mail: … (Times New Roman, 12, Center)

THE LENGTH OF ORIGINAL SCIENTIFIC PAPER SHOULD NOT EXCEED TWENTY (20, INCLUDING FIGURES AND TABLES) PAGES (OPTIMAL 7 TO 15), SHORT PAPER FOUR (4) AND OTHER TWO (2) WITHOUT TEXT FLOWING BY GRAPHICS AND TABLES.
DOLŽINA IZVIRNEGA ZNANSTVENEGA ČLANKA NE SME PRESEGATI DVAJSET (20, VKLJUČNO S SLIKAMI IN TABELAMI), STROKOVNEGA ČLANKA ŠTIRI (4) IN OSTALIH PRISPEVKOV DVE (2) STRANI.

Abstract(Times New Roman, Bold/Normal, 11): The text of the abstract is placed here. The abstract should be concise and should present the aim of the work, essential results and conclusion. It should be typed in font size 11, single-spaced. Except for the first line, the text should be indented from the left margin by 10 mm. The length should not exceed fifteen (15) lines (10 are recommended).

Izvleček(TNR, B/N, 11): Kratek izvleček namena članka ter ključnih rezultatov in ugotovitev. Razen prve vrstice naj bo tekst zamaknjen z levega roba za 10 mm. Dolžina naj ne presega petnajst (15) vrstic (10 je priporočeno).

Key words: a list of up to 5 key words (3 to 5) that will be useful for indexing or searching. Use the same styling as for abstract.

Ključne besede: seznam največ 5 ključnih besed (3-5) za pomoč pri indeksiranju ali iskanju. Uporabite enako obliko kot za izvleček.

Introduction – Uvod (Times New Roman, Bold, 12)

Two lines below the keywords begin the introduction. Use Times New Roman, font size 12, Justify alignment. All captions of text and tables as well as the text in graphics must be prepared in English and Slovenian language.

Dve vrstici pod ključnimi besedami se začne Uvod. Uporabite pisavo Times New Roman, velikost črk 12, z obojestransko poravnavo. Naslovi slik in tabel (vključno z besedilom v slikah) morajo biti pripravljeni v slovenskem in angleškem jeziku.

There are two (2) admissible methods of citing references – obstajata dve sprejemljivi metodi navajanja referenc:

1. by stating the first author and the year of publication of the reference in the parenthesis at the appropriate place in the text and arranging the reference list in the alphabetic order of first authors; e.g.:
1. z navedbo prvega avtorja in letnice objave reference v oklepaju na ustreznem mestu v tekstu in z ureditvijo seznama referenc po abecednem zaporedju prvih avtorjev; npr.:
   "Detailed information about geohistorical development of this zone can be found in: Antonijević (1957), Grubić (1962), ..."
   "… the method was described previously (Hoefs, 1996)"
2. by consecutive Arabic numerals in square brackets, superscripted at the appropriate place in the text and arranging the reference list at the end of the text in the like manner; e.g.:
2. z zaporednimi arabskimi številkami v oglatih oklepajih na ustreznem mestu v tekstu in z ureditvijo seznama referenc v številčnem zaporedju navajanja; npr.;
   "... while the portal was made in Zope[3] environment."

Results and discussion – Rezultati in razprava (Times New Roman, Bold, 12)

Tables, figures, pictures, and schemes should be incorporated (inserted, not pasted) in the text at the appropriate place and should fit on one page. Break larger schemes and tables into smaller parts to prevent extending over more than one page.

Tabele, sheme in slike je potrebno vnesti (z ukazom Insert, ne Paste) v tekst na ustreznem mestu. Večje sheme in tabele je potrebno ločiti na manjše dele, da ne presegajo ene strani.

Conclusions – Sklepi (Times New Roman, Bold, 12)

This paragraph summarizes the results and draws conclusions.
Povzetek rezultatov in zaključki.

Acknowledgements – Zahvale (Times New Roman, Bold, 12, Center - optional)

This work was supported by the ****.

References - Viri (Times New Roman, Bold, 12)

Regardless of the method used, in the reference list, the styling, punctuation and capitalization should conform to the following:
Ne glede na uporabljeno metodo pri seznamu citiranih referenc upoštevajte naslednjo obliko:

FIRST OPTION – in alphabetical order (v abecednem zaporedju)

Casati, P., Jadoul, F., Nicora, A., Marinelli, M., Fantini-Sestini, N. & Fois, E. (1981): Geologia della Valle del'Anisici e dei gruppi M. Popera – Tre Cime di Lavaredo (Dolomiti Orientali). *Riv. Ital. Paleont.*; Vol. 87, No. 3, pp. 391-400, Milano.

Folk, R. L. (1959): Practical petrographic classification of limestones. *Amer. Ass. Petrol. Geol. Bull.;* Vol. 43, No. 1, pp. 1-38, Tulsa.

SECOND OPTION – in numerical order (v numeričnem zaporedju)

[1] Trček, B. (2001): *Solute transport monitoring in the unsaturated zone of the karst aquifer by natural tracers.* Ph.D. Thesis. Ljubljana: University of Ljubljana 2001; 125 p.

[2] Higashitani, K., Iseri, H., Okuhara, K., Hatade, S. (1995): Magnetic Effects on Zeta Potential and Diffusivity of Nonmagnetic Particles. *Journal of Colloid and Interface Science 172*, pp. 383-388.

Citing the Internet site:

CASREACT-Chemical reactions database [online]. Chemical Abstracts Service, 2000, updated 2.2.2000 [cited 3.2.2000]. Accessible on Internet:<http://www.cas.org/CASFILES/casreact.html>.

Citiranje internetne strani:

CASREACT-Chemical reactions database [online]. Chemical Abstracts Service, 2000, obnovljeno 2.2.2000 [citirano 3.2.2000]. Dostopno na svetovnem spletu: <http://www.cas.org/CASFILES/casreact.html>.

Povzetek – Summary (Times New Roman, 12)

An extended summary of the contents in Slovene (from one page to approximately 1/3 of the original article length).
Razširjeni povzetek vsebine prispevka v Angleščini (od ene strani do približno 1/3 dolžine izvirnega članka).

Number of SCI search (število SCI citatov) 185

Number of paper indexing in different bases
(Število indeksiranih člankov v posameznih bazah)

CA SEARCH – Chemical Abstracts (1967 – present) 375
METADEX: Metal Science 135
GeoRef 125
Inside Conferences 76
PASCAL 30
Energy Science and Technology 27
Aluminium Industry Abstracts 18
Ei Compendex 13
EngineeredMaterials Abstracts 3
Analytical Abstracts 1
FLUIDEX (Fluid Engineering Abstracts) 1
TULSA™ (Petroleum Abstracts) 1

Indexing also in (number of indexing not yet available)
(Indeksiran tudi v (števila vpisov še nimamo)

Alloys Index, Bibliography and Index of Geology, Chemical Titles, IMM Abstracts and Index (Institution of Minimg and Metallurgy), INIS Atomindex, Metals abstracts Index, Nonferrous Metals Alert, Polimers, Ceramics, Composites Alert, Steel Alerty